ALLOSTERIC REGULATION AND FUNCTION OF GTPASES

DYLAN GIRODAT
Bachelor of Science, University of Lethbridge, 2012

A thesis/project submitted
in partial fulfilment of the requirements for the degree of

DOCTOR OF PHILOSOPHY

in

BIOMOLECULAR SCIENCE

Department of Chemistry and Biochemistry
University of Lethbridge
LETHBRIDGE, ALBERTA, CANADA

ALLOSTERIC REGULATION AND FUNCTION OF GTPASES

DYLAN GIRODAT

Date of Defence: June 17, 2019

Dr. Hans-Joachim Wieden Thesis Supervisor	Professor	Ph.D.
Dr. Marc Roussel Thesis Examination Committee Member	Professor	Ph.D.
Dr. Wade Abbott Thesis Examination Committee Member Agriculture and Agri-Food Canada	Research Scientist	Ph.D.
Dr. Borries Demeler Internal External Examiner Department of Chemistry and Biochemistry Faculty of Arts and Science	Professor	Ph.D.
Dr. Oliver P. Ernst External Examiner University of Toronto Toronto, Ontario	Professor	Ph.D.
Dr. Michael Gerken Chair, Thesis Examination Committee	Professor	Ph.D.

Abstract

Guanosine triphosphatases (GTPases) are some of the most vital and versatile molecular switches found in all domains of life. For proper functionality these enzymes require allosteric regulation mediated by ligand binding. This thesis highlights three key problems in allosteric regulation: equilibrium, transmission, and transition, investigating how GTPases address each problem. The free energy equilibrium upon nucleotide binding to Elongation Factor (EF)-Tu was investigated to describe how GTPases tackle the equilibrium problem of allostery. Additionally, the mechanism of how the ribosome allosterically regulates the GTPase activity of EF-Tu was investigated to describe how GTPases can solve the transmission problem of allostery. Lastly, the D2 dopamine receptor conformational ensemble revealed how the transition problem of allostery can be addressed in guanosine nucleotide exchange factors. Altogether this thesis provides a framework which can be used to study the three problems of allostery in any protein, highlighting strategies utilized by GTPases.

Acknowledgements

I would like to acknowledge Dr. Evan Mercier, Katherine E. Gzyl, and Darren Gemmill, who helped in obtaining data presented here. Dr. Evan Mercier aided in concept development and stopped flow experiments in Chapter 2 as well as the Cα covariance analysis presented in Chapter 3 and 4. Katherine E. Gzyl aided in stopped-flow experiments in Chapter 2. Darren Gemmill helped in the D2R model development in Chapter 3.

Additionally, I would like to acknowledge Dr. Karissa Y. Sanbonmatsu and Dr. Scott C. Blanchard for aiding in concept development for Chapter 4 of this thesis. Dr. Karissa Y. Sanbonmatsu also provided computational resources at Los Alamos National Laboratory (LANL) allowing for simulations of the 70S ribosome.

This work was funded by the Natural Sciences and Engineering Research Council of Canada, Alberta Innovates Technology Futures, Canada Foundation for Innovation, and the University of Lethbridge. Computational resources were provided by WestGrid, Compute Canada, and Los Alamos National Laboratory.

I appreciate all of the time and effort that my Ph.D. committee took in aiding me through graduate studies through constructive comments and feedback.

Special thank you to my family who have always supported me during my academic pursuits. Especially Stephanie who made my graduate studies easier everyday through her love and support.

Thank you to H.J. who worked side-by-side with me throughout my entire graduate studies. I will always remember how you encouraged me to pursue a scientific career and how you made me believe that I was capable of contributing to the scientific community.

To all of the members of the Wieden, Kothe, and Patel labs past and present I would like to thank you for always being open to scientific and non-scientific conversations, helping me solve problems and keep my sanity.

I would also like to thank all of my friends that have assisted me through the years. The ones that I've made in and outside of graduate studies, you all have helped me more than you know throughout the years.

Table of Contents

Content Page

Thesis Examination Committee ii

Abstract iii

Acknowledgements iv

List of Tables viii

List of Figures ix

List of Abbreviations xi

Chapter 1. Introduction

1.1 Guanosine 5’ triphosphatases 2
1.2 Translation 7
1.3 G-protein coupled receptors 22
1.4 Allostery 26
1.5 Hypothesis and Summary 36

Chapter 2. Elongation Factor Tu’s Nucleotide Binding is Governed by a Thermodynamic Landscape Unique Among Bacterial Translation Factors

2.1 Forward 38
2.2 Abstract 40
2.3 Introduction 41
2.4 Materials and Methods 46
2.5 Results 51
2.6 Discussion 65
2.7 Conclusion 72

Chapter 3. Sampling the Pre-activation Conformations of the D2 Dopamine Receptor Reveals a GPCR Allosteric Pathway

3.1 Forward 74
3.2 Abstract 76
3.3 Introduction 78
3.4 Materials and Methods 82
3.5 Results 87
3.6 Discussion 102

Chapter 4. Near-cognate aminoacyl-tRNA accommodation proceeds through an alternative pathway

4.1 Forward 112
4.2 Abstract 113
4.3 Introduction 114
4.4 Materials and Methods 119
4.5 Results 124

4.6 Discussion 139
4.7 Conclusion 146

Chapter 5. Summary and Conclusion 147

References 158

Appendix 1. Supplemental Material to Chapter 2 173

Appendix 2. Supplemental Material to Chapter 3 199

Appendix 3. Supplemental Material to Chapter 4 212

List of Tables

2.1 Thermodynamic parameters of nucleotide binding in EF-Tu and other proteins of the trGTPase family 59

A1.1 Temperature dependent rates of nucleotide association and dissociation to EF-Tu 162

A1.2 Transition state thermodynamic properties governing nucleotide binding in EF-Tu compared to equilibrium determined thermodynamic properties 163

A1.3 Entropic contributions summary of the EF-Tu•GTP and EF-Tu•GDP conformations 164

A1.4 Differences in transition state thermodynamic properties governing nucleotide dissociation for EF-Tu variants compared to wild type 165

A1.5 Location of waters that are resident (within 4.0Å of EF-Tu) in a single location in the EF-Tu•GTP or EF-Tu•GDP simulations during more than 50% of frames 166

A1.6 Summary of hydrogen bonds formed by the peptidyl backbone carboxylic acid oxygen (O) to a peptidyl backbone amide (N-H) of EF-TU 167

A1.7 The modulation of *E. coli* EF-TU nucleotide binding affinities by antibiotics 174

A2.1 Relative activity and ligand affinity of variants compared to wild type D2R as reported in Sung *et al.*(2016) 184

A3.1 Average number of times steps required for accommodation of the CCA end of A-site tRNA 198

List of Figures

Figure Page

1.1 The canonical cycle of GTPases 3
1.2 Structural representation of a G-domain 4
1.3 Structural representation of *E. coli* 70S ribosome 8
1.4 Schematic outline of the translational cycle 11
1.5 Antibiotics that impact accommodation of aa-tRNA 14
1.6 Structural representation of the decoding center of the *E. coli* ribosome 14
1.7 Structural representations of the conformations of EF-Tu 16
1.8 EF-Tu ribosome contact points for GTP hydrolysis stimulation 19
1.9 The active and inactive conformations of a GPCR 25
1.10 The equilibrium problem represented in free energy landscape 28
1.11 MWC and KNF models 30
2.1 Nucleotide-dependent conformations of EF-Tu and minimal kinetic mechanism of EF-Tu nucleotide binding 44
2.2 Pre-steady state kinetics of Ef-Tu nucleotide association and dissociation 52
2.3 Temperature-dependent kinetic properties of nucleotide binding for determination of entropic and enthalpic activation barriers 53
2.4 Energy landscapes for EF-Tu nucleotide binding 58
2.5 EF-Tu structural and dynamic contributions favoring the EF-Tu•GDP conformation 60
2.6 The entropic contributions of water coordination and protein flexibility 64
2.7 Features that enable the thermodynamic fine-tuning of the nucleotide bound states of EF-Tu 70
3.1 Dynamics of the wild type and variants of D2R 89
3.2 Markov State Modelled (MSM) identified conformations of D2R and the probability of transitions between them 91
3.3 Structural features of the D2R clusters identified by Maxcluster 96
3.4 The shortest communication paths between the ligand binding pocket and G-protein interface 99
3.5 Dynamics of the V154I D2R variant which is linked to Myoclonus Dystonia 101
3.6 Conformational dynamics and signaling of D2R prior to activation 104
3.7 Cα covariance communication pathway displayed on the structure of D2R 108
4.1 The conformations of 70S•EF-Tu•aa-tRNA complex 125
4.2 The accommodation pathway of cognate and near-cognate tRNA-mRNA interactions 128
4.3 Aminoglycosides preventing the alternative pathway of near-cognate aa-tRNA accommodation 131
4.4 EVN prevents proper accommodation of cognate aa-tRNA 133
4.5 Impact of HGR on the accommodation of cognate and near-cognate aa-tRNA 135
4.6 Correlated amino acid and nucleic acid dynamics of EF-Tu bound to the ribosome 138
4.7 Model of cognate and near-cognate tRNA accommodation and the molecular dynamic mechanisms by which antibiotics disrupt accommodation 141

4.8 Most likely paths for Cα covariance to be propagated to EF-Tu GTP binding site 144
A1.1 LIGPLOT view of EF-Tu interactions with GTP and GDP 175
A1.2 EF-Tu simulation deviations and flexibility 176
A1.3 Hydrogen bonding network of EF-Tu•GDP 177
A1.4 Hydrogen bonding network of EF-Tu•GTP 178
A1.5 Number of backbone oxygens that are involved in hydrogen bonds in the EF-Tu• and EF-Tu•GDP simulations separated by each domain 179
A1.6 Water coordination of EF-Tu•GTP and EF-Tu•GDP during 100ns of simulation 180
A1.7 Eyring plot of nucleotide dissociation for EF-Tu variants H22G and M112L 181
A1.8 Analysis of 100ns EF-Tu H22G and M112L MD simulations 182
A2.1 Stability and dynamics of D2R simulations 185
A2.2 Principle component analysis (PCA) of wild type and variant D2R 186
A2.3 Time independent component analysis (tICA) and kmeans clustering of wild type and variant D2R 187
A2.4 Correlated Cα protein structure networks 188
A2.5 Extracellular TM helix distances 189
A2.6 Intracellular TM helix distances 190
A2.7 Representative distributions of θ 191
A2.8 Molecular dynamic properties of D2R clusters 192
A2.9 Enthalpy contributions to the clusters of D2R 193
A2.10 PC1 of low-activity D2R variants 194
A2.11 PC2 of low-activity D2R variants 195
A3.1 Convergence of tRNA accommodation simulations 199
A3.2 Description of the angles and distances used in MD analysis 200
A3.3 Time dependence of R_3 during cognate and near-cognate accommodation in the presence and absence of antibiotics 201
A3.4 1D free energy landscape of cognate and near-cognate tRNA accommodation in the presence of gentamicin and neomycin 202
A3.5 1D free energy landscape of cognate tRNA accommodation in the presence and absence of antibiotics 203
A3.6 1D free energy landscape of near-cognate tRNA accommodation in the presence and absence of antibiotics 204
A3.7 The free energy landscape of cognate CCA end accommodation 205
A3.8 The free energy landscape of near-cognate CCA end accommodation 206

List of Abbreviations

aa-tRNA	aminoacyl-tRNA
ASL	anticodon stem loop
β2AR	β2-adrenergic receptor
ccPSN	Cα covariance protein structure network
CHARMM	chemistry at Harvard molecular mechanics
D2R	D2 dopamine receptor
D3R	D3 dopamine receptor
ECL	extracellular loop
EF	Elongation Factor
EVN	evernimicin
FRET	fluorescence resonance energy transfer
GA	GTPase activated state
GAF	GTPase activating factor
GEN	gentamycin
GEF	guanosine nucleotide exchange factor
GTPase	guanosine 5'-triphosphatases
GPCR	G-protein coupled receptor
HGR	hygromycin A
IC	initiation complex
ICL	intracellular loop
IF	initiation factor
KNF	Koshland, Nemethy, and Filmer
LSU	large ribosomal subunit
MD	molecular dynamics
MSM	Markov state modelling
MWC	Monod, Wyman, and Changeux
NAMD	nanoscale molecular dynamics
NEO	neomycin
PC	principle component
PCA	principle component analysis
PCPM	protein characterization for personalized medicine
PIC	pre-initiation complex
POPC	phosphatidylcholine
PTC	peptidyl transferase center
RF	release factor
RMSD	root-mean-squared deviation
RMSF	root-mean-squared fluctuation
RRF	ribosome recycling factor
SASA	solvent accesable surface area
SelB	selenocysteine-specific elongation factor
smFRET	single molecule FRET
SNP	single nucleotide polymorphism
SP	shortest path
SRL	sarcin ricin loop
SSU	small ribosomal subunit

tICA	time independent component analysis
TM	transmembrane helix
trGTPase	translational GTPases
UTR	untranslated region
VMD	visual molecular dynamics

Chapter 1

Introduction

1.1 Guanosine 5'-triphosphatases

Cellular homeostasis is maintained by a suite of biomolecular factors all with specific functions, the disruption of which can lead to disadvantageous phenotypes, diseases, or cell death. One of the most critical families of proteins for cellular homeostasis is the guanosine 5'-triphosphatases (GTPases). These proteins are found in all domains of life and dysregulation of their function can lead to diseases, such as cancer in the case of the ras superfamily as one example (Bos, 1989; Goodsell, 1999). GTPases are required for several cellular functions and often regulate gene expression, either through signal transduction pathways or by fine-tuning translation. Critical to their function is the ability to bind to and hydrolyze guanosine triphosphate (GTP) into guanosine diphosphate (GDP) and inorganic phosphate (Pi), a process which is coupled by a conformational change in the protein often creating a signal for downstream processes.

GTPases function as molecular switches, coupling GTP hydrolysis with turning on or off biological processes (Verstraeten, Fauvart, Versees, & Michiels, 2011; Wittinghofer & Vetter, 2011). Canonically, GTPases are considered in their 'active' or 'on' state when bound to GTP, where the protein can interact with a GTPase activating factor (GAF) triggering a response at a downstream effector (Fig 1.1). The intrinsic rate of GTP hydrolysis of GTPases is slow, on the order of minutes to hours, requiring interactions with a GAF to stimulate GTP hydrolysis and subsequent Pi release (Neal, Eccleston, Hall, & Webb, 1998). If the intrinsic rate was faster, many GTPases would be considered constitutively 'on', interfering with their function as molecular switches which could be detrimental to the cell, as is the case for ras where constitutively 'on' variants lead to cancer (Karnoub & Weinberg, 2008). GAFs enhance GTP hydrolysis by coordinating a catalytic

water molecule for in-line nucleophilic attack on the γ-phosphate of GTP (Feuerstein, Goody, & Webb, 1989; Grigorenko, Shadrina, Topol, Collins, & Nemukhin, 2008). GTP hydrolysis and subsequent Pi release results in a conformational change of the GTPase where it adopts the 'inactive' or 'off' state bound to GDP. The affinity that GTPases have for GDP can often be higher than that for GTP, and therefore, exchange of GDP for GTP or recycling of the GTPase to its active form is often facilitated by a guanosine nucleotide exchange factor (GEF) (Fig 1.1). Therefore, the regulation of GTPase activity is executed by two factors, their respective GAF and the GEF.

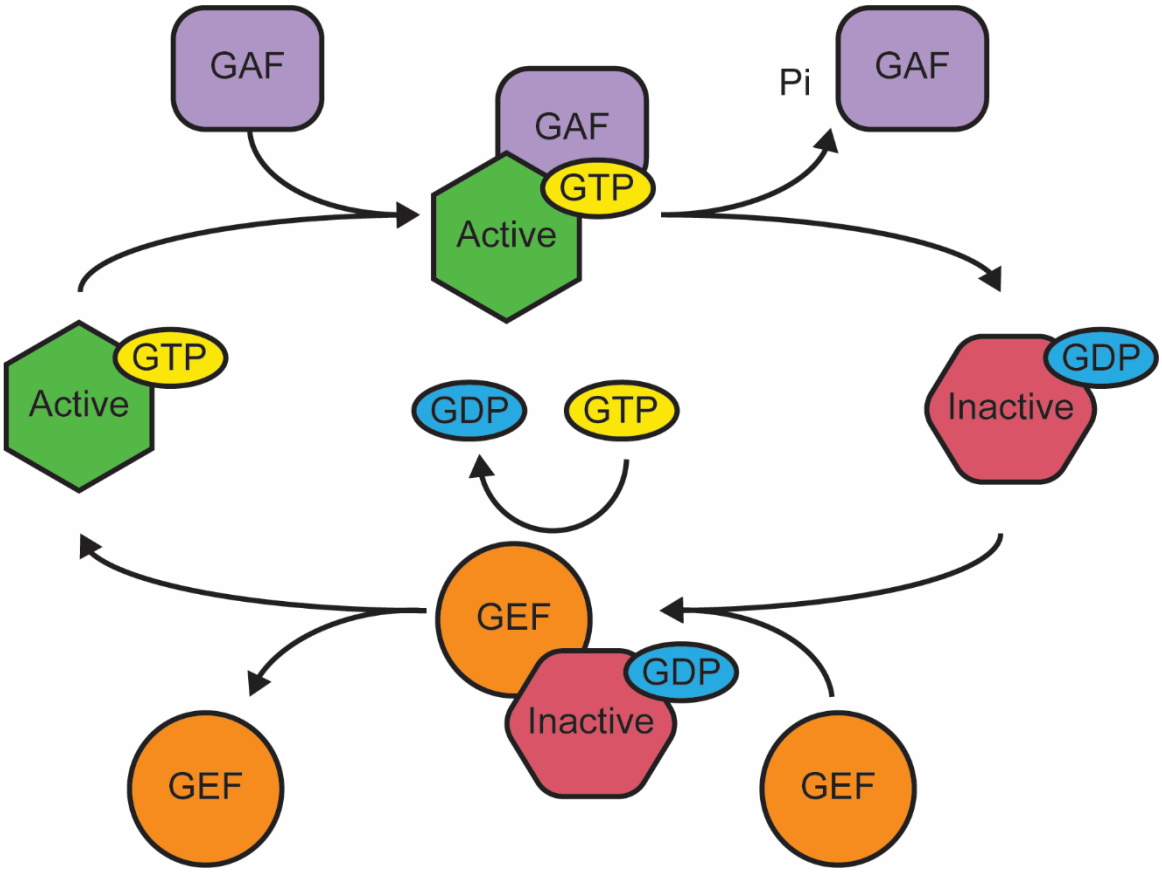

Figure 1.1 The canonical GTPase cycle. The GTP-bound 'active' conformation of the GTPase interacts with a GAF where the hydrolysis activity of the GTPase is induced. Pi is released leading to the inactive state of the GTPase bound to GDP. GDP is exchanged for GTP by the GTPase interacting with its respective GEF where the GTPase returns to the active form.

All translational GTPases (trGTPases) contain an N-terminal G-domain with a Rossmann fold (six β-sheets and two pairs of α-helices) where GTP binding and hydrolysis occur. The G-domain contains five G-motifs (G1-G5) which are critical to GTP binding (Fig 1.2). G-1, also known as the P-loop or Walker A motif, is defined by the sequence GXXXXGK(S/T) and directly interacts with the phosphates of GTP or GDP (Bourne, Sanders, & McCormick, 1991). The next two G-motifs, G-2 and G-3, known as switch I and switch II, respectively, define the conformation of the GTPase. The switch I sequence is less conserved amongst GTPases, whereas switch II is defined by the DXXG motif. In this motif, the D coordinates water molecules interacting with the phosphates of GTP and GDP (Bourne et al., 1991). Lastly, G-4 and G-5 coordinate the nucleoside and define specificity for GTP through the (N/T)(K/Q)XD and SA(K/L) sequence motifs, respectively (Bourne et al., 1991).

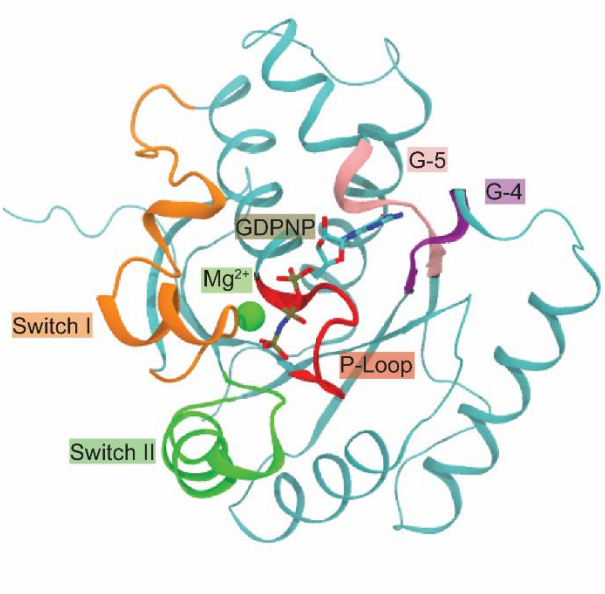

Figure 1.2 Structural representation of a G-domain. G-domain of EF-Tu (PDB ID: 1EFT) bound to GDPNP and Mg^{2+} with G-1 – red (P-loop), G-2 – orange (switch I), G-3 – green (switch II), G-4 – purple and G-5 –pink motifs highlighted.

GEFs can play critical roles in integrating signals, such as binding of a small molecular ligand, coupling these events to downstream signalling cascades. The GEFs of signal-transduction pathways are G-protein-coupled receptors (GPCRs), a family of transmembrane proteins that have specificity for particular ligands. These proteins are activated by binding to their particular ligand, upon which they catalyze the exchange of GDP for GTP in the bound small GTPase, releasing it into the cytosol. From here the GTPase can interact with a variety of GAFs to stimulate or repress gene expression, such as in the cyclic adenosine monophosphate (cAMP) pathway (Sassone-Corsi, 2012). The central GAF during translation is the ribosome; this is true in eukaryotes and prokaryotes. The GEF in these systems is often an additional protein factor, as is the case for the bacterial protein Elongation Factor (EF) Tu, EF-Ts is the GEF (Weissbach, Miller, & Hachmann, 1970). However, translational GTPases can also function without a specific GEF, such as EF-G where nucleotide exchange is a spontaneous process driven by higher cellular concentration of GTP compared to GDP (~10-fold higher in mid-log phase in *E. coli*) (Buckstein, He, & Rubin, 2008).

GTPases are required to process the information provided through effector binding (either the GAF or GEF) distal to the GTP-binding pocket into a functional response at a distal site, a process known as allostery. Guanosine nucleotides can also be considered effectors of GTPases as the bound nucleotide defines the conformation and state of the GTPase. This is not unique to GTPases as GPCRs also undergo allosteric regulation where ligand binding induces a response at the GTPase or G-protein interface. Therefore, a detailed comprehension of the GTPase cycle requires an understanding of how both GTPases and their effectors can propagate binding information throughout their protein

scaffolds. This thesis will explore the role of allostery in GTPases during nucleotide binding, translation, and in GPCRs during signal transduction.

1.2 Translation

Translation overview

Protein synthesis is the essential process by which the genetic information, transcribed into messenger RNA (mRNA), is converted into the corresponding polypeptides. This process is performed by the ribosome, a massive ribonucleoprotein (RNP) complex. The ribosomal RNA (rRNA) catalyzes the formation of peptide bonds between two amino acids which are conjugated to a transfer RNA (tRNA). To maintain translational fidelity the mRNA is decoded in nucleotide triplets by codon-anticodon interactions between the mRNA and tRNA, respectively. Base pairing rules ensure that cognate aminoacyl (aa)-tRNA are incorporated, maintaining the integrity of the genetic information in the resulting peptide chain. After peptide-bond formation occurs, the ribosome ratchets, translocating the tRNA bound through the ribosome, thus allowing for another round of tRNA decoding and translation. Once the ribosome reaches a stop codon in the mRNA, the growing peptide is released, and the ribosome recycled.

The prokaryotic 70S ribosome consists of core structural features, such as the 50S and 30S subunit; the peptidyl transferase center (PTC), which is the site of peptide bond formation; the A-, P-, and E-sites for tRNA binding; the decoding center; and the mRNA channel (Fig 1.3). The PTC-containing 50S large ribosomal subunit (LSU) is composed of the 23S and 5S rRNA and 34 proteins, while the 30S small ribosomal subunit (SSU) is composed of the 16S rRNA and 21 proteins. The 23S rRNA and LSU ribosomal proteins at the core of the ribosome adjacent to the P-site make up the PTC and are involved in peptide bond formation (Fig 1.3). Peptide bond formation is facilitated through proper positioning of the tRNA, rRNA, water molecules, and electrostatic shielding, allowing for

nucleophilic attack from the A-site amino acid on the growing peptide chain (Sharma, Xiang, Kato, & Warshel, 2005) (Wallin & Aqvist, 2010). The A-site is the point of aminoacyl-tRNA entry, the P-site is where peptidyl tRNA is bound, and the E-site is the location of deacylated-tRNA release from the ribosome (Fig 1.3). The tRNA binding sites include regions of the 30S and 50S, spanning the mRNA channel. Altogether, these elements of the ribosome work in conjunction with one another to facilitate the four phases of peptide synthesis. The decoding center, which is part of the 30S at the A-site, is the site of codon-anticodon interactions between the mRNA and aa-tRNA (Fig 1.3). Residues A1492, A1493, G530 of the 16S rRNA are critical to the decoding center, proposed to influence the incorporation of cognate over near-cognate aa-tRNA (single nucleotide codon-anticodon mismatch, excluding wobble base pairing) (Ogle et al., 2001).

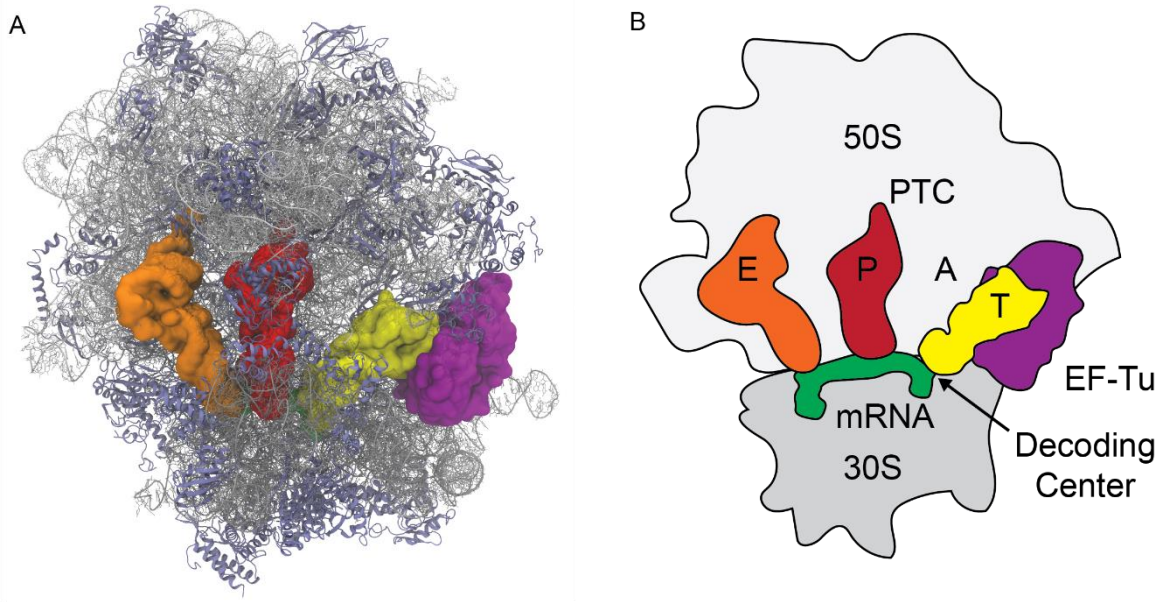

Figure 1.3 Structural representation of *E. coli* 70S ribosome. (A) Cryo-EM structure of the *E. coli* 70S ribosome (PDB ID: 5AFI) bound to EF-Tu•Phe-tRNA^{Phe}•GDP ternary complex with kirromycin to stabilize EF-Tu in the GTP conformation (Fischer et al., 2015). EF-Tu, A/T- Phe-tRNA^{Phe}, P- fMet-tRNA^{fMet}, and E-site Phe-tRNA^{Phe} are in purple, yellow, red, and orange respectively. (B) Cartoon of the 70S ribosome with tRNA binding site, mRNA channel, PTC, and EF-Tu highlighted.

The four sequential phases of translation are initiation, elongation, termination, and recycling, each requiring specific auxiliary protein factors (Fig 1.4). In prokaryotes, initiation is triggered when the 5' untranslated region (UTR) of the mRNA, encoding a ribosomal binding site, recruits the SSU. Initiation factor (IF) 1, 2, and 3 facilitate initiation where IF2 delivers fmet-$tRNA^{fmet}$ to the P-site, IF1 prevents aa-tRNA binding to the A-site, and IF3 maintains subunit separation (Anderson, Bretscher, Clark, & Marcker, 1967; Antoun, Pavlov, Andersson, Tenson, & Ehrenberg, 2003; Gualerzi & Pon, 2015). The binding of these three factors in combination with mRNA forms the 30S pre-initiation complex (PIC). After codon-anticodon interactions have formed in the P-site, the LSU is recruited to the 30S PIC to form the 70S initiation complex (IC) (Milon, Konevega, Gualerzi, & Rodnina, 2008; Milon, Maracci, Filonava, Gualerzi, & Rodnina, 2012). The IC is competent to enter into elongation where Elongation Factor (EF) Tu delivers aa-tRNA to the ribosomal A-site in a guanosine 5'-triphosphate (GTP) hydrolysis-dependent manner. Binding of EF-Tu to the ribosome positions the aa-tRNA in the A/T state, denoting the location of the anticodon stem loop (ASL)/acceptor stem of the tRNA in the ribosome (Fig 1.1) (Schmeing et al., 2009). Codon-anticodon interactions are rapidly formed at the decoding center, stimulating 30S subunit closure and docking EF-Tu onto the Sarcin Ricin Loop (SRL), an element of the 23S rRNA critical for GTP hydrolysis in EF-Tu (Fislage et al., 2018; Loveland, Demo, Grigorieff, & Korostelev, 2017). Once engaged with the SRL, EF-Tu adopts the GTPase-activated (GA) state where the rate of GTP hydrolysis is enhanced 10^5-fold, enabling Pi release and triggering EF-Tu conformational change (Kothe & Rodnina, 2006; Pape, Wintermeyer, & Rodnina, 1998). EF-Tu bound to GDP dissociates

from the ribosome coupled with aa-tRNA accommodation into the A/A site, where both the ASL and the acceptor stem are in the A-site. With a filled A/A and P/P site, the ribosome is in the so-called 'normal' configuration; however, it can undergo spontaneous 30S rotation relative to the 50S, causing the tRNA to adopt the A/P and P/E hybrid conformations, or 'rotated' configuration (Bock et al., 2013; Frank, Gao, Sengupta, Gao, & Taylor, 2007; Moazed & Noller, 1989; Zhang, Dunkle, & Cate, 2009). Either the 'rotated' or 'normal' conformation of the ribosome is recognized by EF-G, which catalyzes the translocation of tRNA from the A- and P-sites to the P- and E-sites. Binding of EF-G to the ribosome causes the opening of the mRNA channel, allowing the translocation of the mRNA and tRNA through steric barriers imposed by the ribosome, which act as molecular pawls to maintain the codon frame (Rodnina, 2018; Zhou, Lancaster, Donohue, & Noller, 2013). Rounds of aa-tRNA delivery and translocation are repeated until the ribosome reaches a stop-codon (UAG, UAA, or UGA) which recruits Release Factor (RF) 1 or 2 to bind to the ribosome (Capecchi, 1967; Scolnick, Tompkins, Caskey, & Nirenberg, 1968). Either of these RFs can stimulate hydrolysis of the ester bond between the growing peptide chain and P-site tRNA (Capecchi, 1967). RF3 recognizes the complex with RF1/2 bound after peptide release, binding to the A-site and triggering dissociation of either RF1 or RF2. After RF3 dissociation, the ribosomal particles are recycled by a complex of Ribosomal Release Factor (RRF) and EF-G. This recycling complex binds to the ribosome and induces subunit separation, allowing the ribosomal particles to enter into another round of translation (Hirashima & Kaji, 1970, 1973).

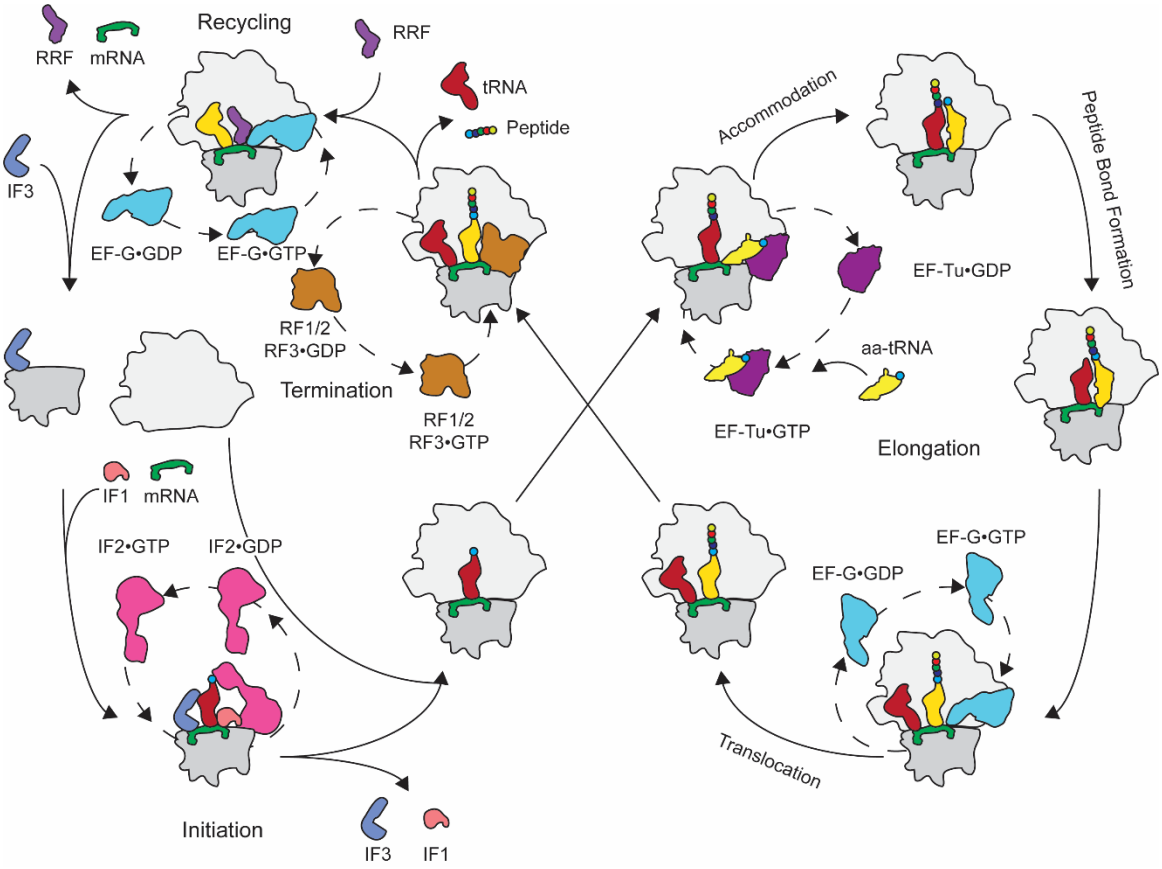

Figure 1.4 Schematic outline of the translational cycle (adapted from Wilson *et al*. 2009).

In prokaryotes, trGTPases are essential to every phase of translation and include IF2, EF-Tu, EF-G, and RF3. Several additional non-essential GTPases are required for specific functions during translation, including selenocysteine-specific elongation factor (SelB), LepA, BipA, TetM, and TetO. The function of some of the non-essential GTPases has been studied in detail, such as SelB which delivers sec-tRNA^{sec} to the ribosome during elongation, or TetM and TetO which confer tetracycline resistance (Burdett, 1986, 1996; Connell et al., 2003; Forchhammer, Leinfelder, & Bock, 1989; Manavathu, Fernandez, Cooperman, & Taylor, 1990). However, the cellular function of BipA and LepA are still under debate. BipA has been proposed to function as a ribosome biogenesis factor and has

also been implicated in virulence (Choudhury & Flower, 2015; Scott, Diggle, & Clarke, 2003). The proposed functions of LepA are more diverse, being implicated in back-translocation, ribosome sequestering, ribosome biogenesis, or involved in translation initiation (Heller, Kamalampeta, & Wieden, 2017). Despite the functional differences of these proteins they all retain features that define them as GTPases.

Accommodation

Elongation can be subdivided into two different processes, accommodation and translocation, the former being regulated by EF-Tu and the latter by EF-G. Accommodation defines the fidelity of translation, ensuring that cognate aa-tRNA is incorporated into the ribosomal A-site. The process begins with the binding of a ternary complex of EF-Tu•aa-tRNA•GTP to the A-site of the ribosome after initiation is completed, or after translocation has occurred (Fig 1.5). A competent ribosome for ternary complex binding consists of an open 70S where the 30S and 50S are separated at the A-site due to movements of the SSU (Fig 1.5) (Ogle, Murphy, Tarry, & Ramakrishnan, 2002). Initial contacts between domain II of the ternary complex and helix 5 (h5) of the 30S ribosomal subunit are formed prior to base-pairing between the mRNA-tRNA codon-anticodons (Fislage et al., 2018; Loveland et al., 2017). The tRNA anticodon searches for the codon of the mRNA and forms base pairs, positioning the tRNA into the A/T conformation and triggering the closure of the 30S subunit (Fig 1.5). Domain closure causes A1492, A1493, and G530 of the 16S rRNA decoding site to enter into a 'flipped-out' conformation where they interact with the mini-helix formed by the base pairs between the codon and anti-codon (Loveland et al., 2017; Ogle et al., 2001) (Fig 1.6). The 'flipped-out' conformation of these nucleotides is proposed to stabilize the codon-anticodon interactions, yet they seem not to distinguish cognate from

near-cognate as they adopt this conformation regardless of which tRNA is present (Demeshkina, Jenner, Westhof, Yusupov, & Yusupova, 2012). Closure of the 30S also docks EF-Tu onto the SRL of the 23S rRNA, triggering the GTPase activity of the protein (Loveland et al., 2017). A mechanistic description for the 10^5-fold stimulation of EF-Tu GTP hydrolysis in the presence of cognate compared to near-cognate aa-tRNA is still lacking (Pape et al., 1998). Pi release after GTP hydrolysis occurs before the conformational change of EF-Tu resulting in domain separation (Kothe & Rodnina, 2006). As resolved by molecular dynamics (MD) simulations there are three unique pathways that the aa-tRNA can take as it moves from the A/T to A/A conformations (Whitford et al., 2010). These pathways are defined by helix 89 (H89) (nucleotides 2454 to 2498 of the 23S), the major steric barrier for aa-tRNA accommodation (Noel & Whitford, 2016; Whitford et al., 2010). The acceptor stem of the tRNA resolves this barrier by transitioning through the major groove of H89, passing over the A-loop (nucleotides G2545-C2563 of the 23S rRNA), or moving between H89 and the A-loop. After the tRNA proceeds through one of these pathways and the CCA-end of the tRNA carrying the incoming aminoacyl is in position for peptide bond formation, it is considered accommodated into the A/A state.

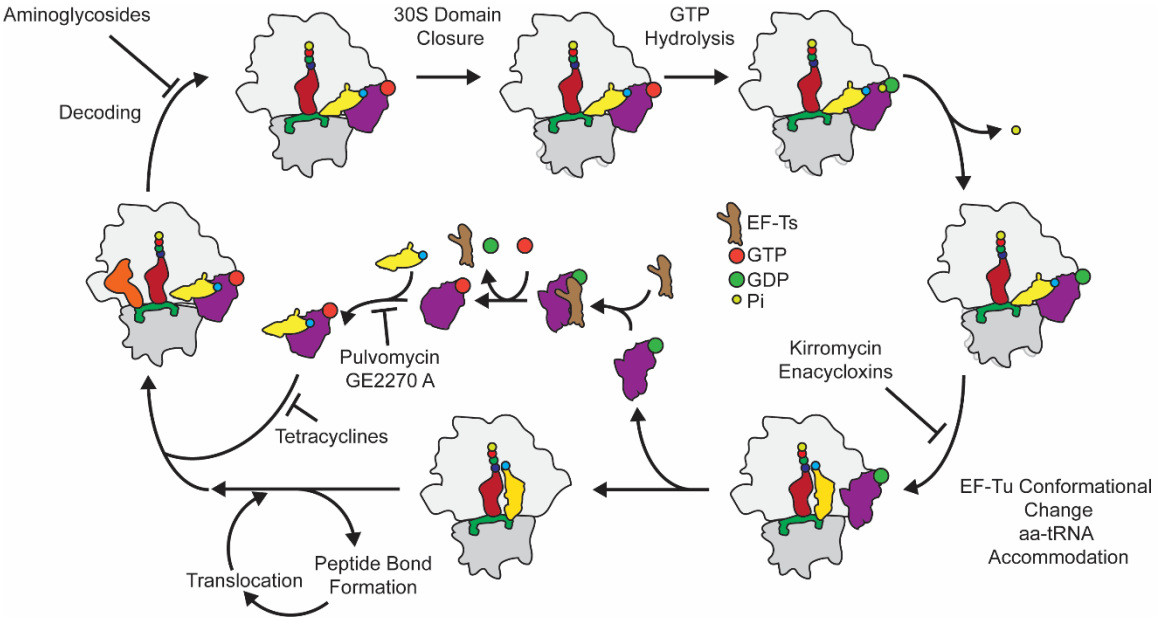

Figure 1.5 Antibiotics that impact accommodation of aa-tRNA. Accommodation occurs through several sequential steps that can be inhibited or modulated by antibiotics such as aminoglycosides, kirromycin, enacycloxins, pulvomycin, GE2270A, and tetracyclines (Wilson, 2009). Aminoglycosides induce misreading of the mRNA, kirromycin and enacycloxins prevent EF-Tu conformational change, pulvomycin and GE2270A prevent EF-Tu•aa-tRNA•GTP ternary complex formation, and tetracyclines prevent the ternary complex from binding to the A-site.

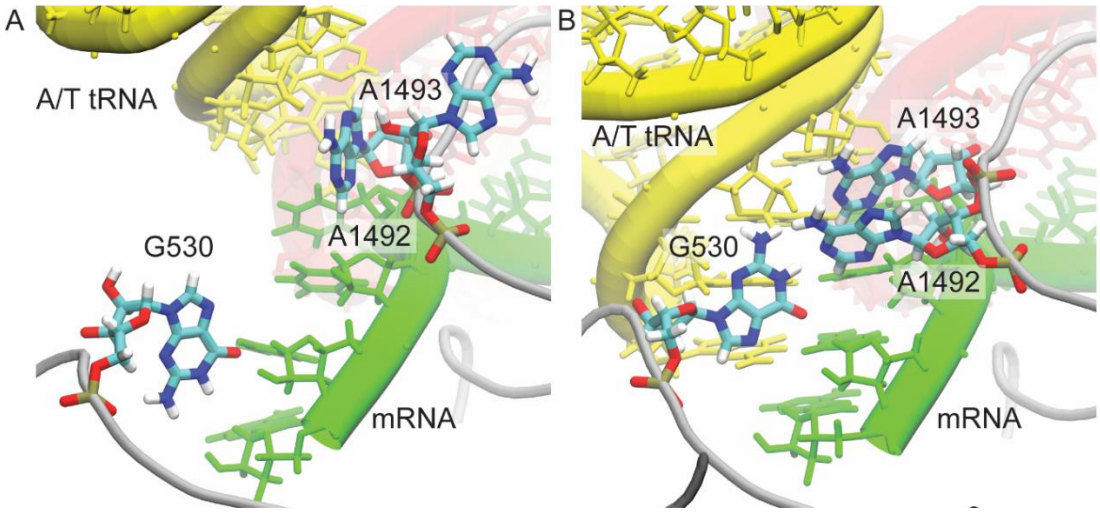

Figure 1.6 Structural representation of the decoding center of the *E. coli* ribosome (Loveland et al., 2017). (A) The decoding center before codon-anticodon interactions have formed G530 in the cis orientation and A1492 and A1493 in canonical conformation. (B) The decoding center when cognate codon-anticodon interactions have formed, G530 is in the syn orientation and A1492 and A1493 are considered 'flipped-out' capable of interacting with the helix formed between the codon and anticodon.

Elongation Factor Tu

EF-Tu is present in all domains of life, highly conserved (~70 – 82% identity), one of the most abundant proteins in the *E. coli* cytosol, and is indispensable for translation (De Laurentiis, 2009; Ishihama et al., 2008). EF-Tu is responsible for delivering aa-tRNA to the A-site of the translating ribosome by binding to all elongator aa-tRNAs, with nearly the same affinity (Louie, Ribeiro, Reid, & Jurnak, 1984). EF-Tu in the GTP conformation binds to aa-tRNA, forming a ternary complex which is considered the active state of the protein (Fig 1.7A). After binding to and delivering the aa-tRNA, EF-Tu releases Pi and changes its conformation into the canonical GDP conformation (Fig 1.7C). In the GDP conformation, EF-Tu dissociates from both aa-tRNA and the 70S ribosome, allowing for EF-G to bind and translocation to occur (Pape et al., 1998). Interestingly, EF-Tu has a 60-fold higher affinity for GDP over GTP, a unique feature among the translational GTPases; therefore, it is the only bacterial GTPase with a GEF, EF-Ts (Gromadski, Wieden, & Rodnina, 2002). EF-Ts binds to EF-Tu in the GDP conformation and stimulates the dissociation of GDP by 60 000-fold. EF-Tu can then bind to GTP due to the 10-fold higher cellular GTP concentration in *E. coli* compared to GDP (Bochner & Ames, 1982).

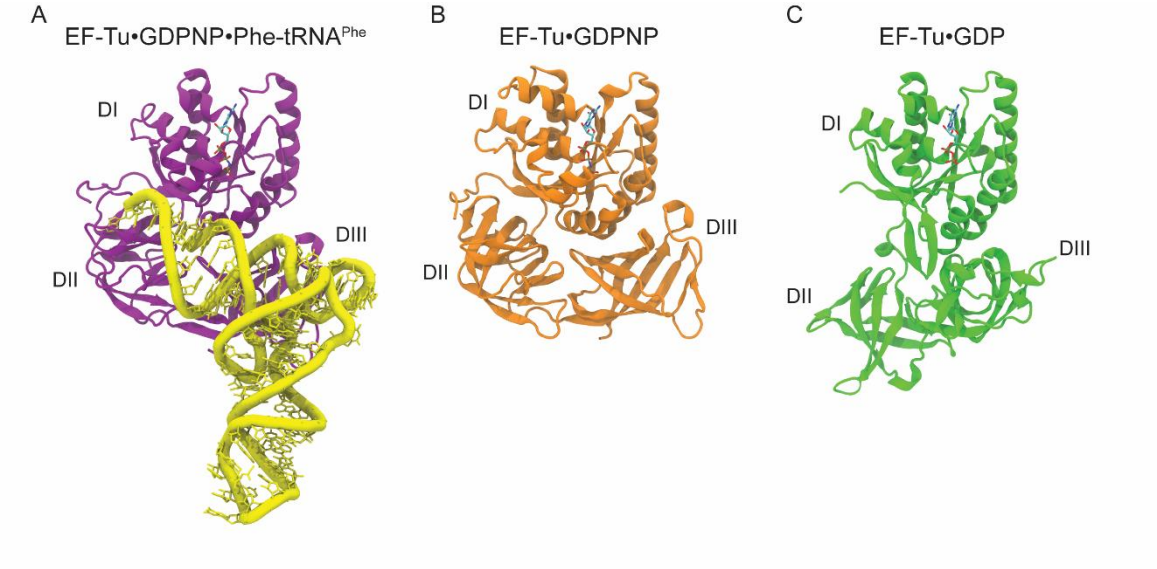

Figure 1.7 Structural representations of the conformations of EF-Tu. (A) Ternary complex of EF-Tu (purple)•GDPNP•Phe-tRNA^{Phe}(yellow). EF-Tu from *E. coli* and Phe-tRNA^{Phe} from *S. cerivisiae* (PDB ID: 10B2). (B) EF-Tu (orange) in the GTP or 'closed' conformation bound to GDPNP from *T. aquaticus* (PDB ID: 1EFT). (C) EF-Tu (green) in the GDP or 'open' conformation bound to GDP from *E. coli* (PDB ID: 1EFC) (Kjeldgaard, Nissen, Thirup, & Nyborg, 1993; Song, Parsons, Rowsell, Leonard, & Phillips, 1999).

EF-Tu is a three-domain protein where the N-terminal or G-domain binds to and hydrolyzes GTP, while the other two are both β-barrels. The GDP conformation of EF-Tu is more open where domain I has separated from domains II and III (Fig 1.7C) (Song et al., 1999). In the more compact canonical GTP conformation of EF-Tu, numerous inter-domain interactions between domains I and II are formed (Fig 1.7B) (Berchtold et al., 1993; Kjeldgaard et al., 1993). With respect to domain II and III, the G-domain in the GDP conformation undergoes a 90° rotation which is accompanied by a rotation of domain III about the axis of the β-barrel relative to the GTP conformation (Berchtold et al., 1993).

The conformational differences between the GTP and GDP conformation are proposed to be controlled by switch I and II of EF-Tu (Berchtold et al., 1993; Kjeldgaard

et al., 1993). In the GDP conformation, switch I adopts two parallel β-strands that interact with domain III of EF-Tu. When EF-Tu binds to GTP, switch I undergoes rearrangement into two α-helices (A' and A'') that can directly interact with and coordinate a bound magnesium ion via T61. The function of the two β-strand conformation of switch I in EF-Tu is unclear as, for other trGTPases such as EF-G and RF3, switch I adopts the α-helical form in the GTP conformation and is unstructured in the GDP conformation (Czworkowskil, Wang, Steitz, & Moore, 1994; Kihira et al., 2012; Zhou et al., 2013). Unlike switch I, switch II (helix B) of EF-Tu is an α-helix in both the GTP and GDP conformation (Kjeldgaard et al., 1993; Song et al., 1999). Switch II packs with the G-domain when bound to GTP and rotates 42°, extending towards domain III when bound to GDP. As EF-Tu transitions from the GTP to the GDP conformation, the helix of switch II decreases by two and increases by four amino acids at the C- and N-terminal ends, respectively. Since G83 of switch II interacts directly with the γ-phosphate of GTP it is likely that this interaction senses the phosphorylation state of the nucleotide bound to EF-Tu and facilitates the conformational change of the helical element.

Ribosome-stimulated hydrolysis of GTP by EF-Tu is an enigmatic process whereby interaction surfaces with multiple points on the ribosome contribute to the overall stimulation. In the absence of the ribosome, the intrinsic rate of GTP hydrolysis by EF-Tu is slow (~10^{-4} s^{-1}). However, this is stimulated 10^5-fold by the ribosome (Maracci, Peske, Dannies, Pohl, & Rodnina, 2014; Pape, Wintermeyer, & Rodnina, 2000). The mechanism of how EF-Tu hydrolyzes GTP was investigated through the single amino acid substitution variant H84A, which exhibits a 10^6 fold reduction in GTP hydrolysis on the ribosome, yet ribosome and aa-tRNA binding were not affected (Daviter, Wieden, & Rodnina, 2003).

Structural data supports the essential role of H84 as docking of EF-Tu onto the SRL positions H84 so that it can coordinate a catalytic water molecule (Voorhees, Schmeing, Kelley, & Ramakrishnan, 2010). However, deleting the nucleotides U2653-C2667 from the SRL does not impact the GTP hydrolysis activity of EF-Tu, suggesting it is not directly involved in the GTP hydrolysis mechanism (Shi, Khade, Sanbonmatsu, & Joseph, 2012). There is also evidence that it is not only the SRL that affects the GTP hydrolysis rate of EF-Tu, because cognate codon-anticodon interactions are required for efficient GTP hydrolysis. In the presence of non-cognate tRNA, EF-Tu hydrolysis is similar to the intrinsic rate of GTP hydrolysis ($\sim 10^{-4}\ s^{-1}$) (Rodnina, Pape, Fricke, Kuhn, & Wintermeyer, 1996). A mechanism in which cognate aa-tRNA–mRNA interactions lead to a position of the aa-tRNA in the A/T site allowing for proper GTP hydrolysis has been proposed but not biochemically validated (Sanbonmatsu, 2006). Lastly it has been proposed that ribosome-induced GTP hydrolysis by EF-Tu is dependent on interactions between EF-Tu and the 30S SSU (Schmeing et al., 2009). This hypothesis is based on the G222D variant of EF-Tu, a substitution in domain II that inhibits ribosome-stimulated GTP hydrolysis (Vorstenbosch, Pape, Rodnina, Kraal, & Wintermeyer, 1996). Structural studies of EF-Tu on the ribosome have revealed that G222D is in close proximity to helix 5 (h5) of the 16S rRNA and it is proposed that these interactions are required for efficient GTP hydrolysis (Schmeing et al., 2009). Altogether these data make it difficult to pinpoint the structural mechanism of EF-Tu's ribosome-induced GTP hydrolysis activity.

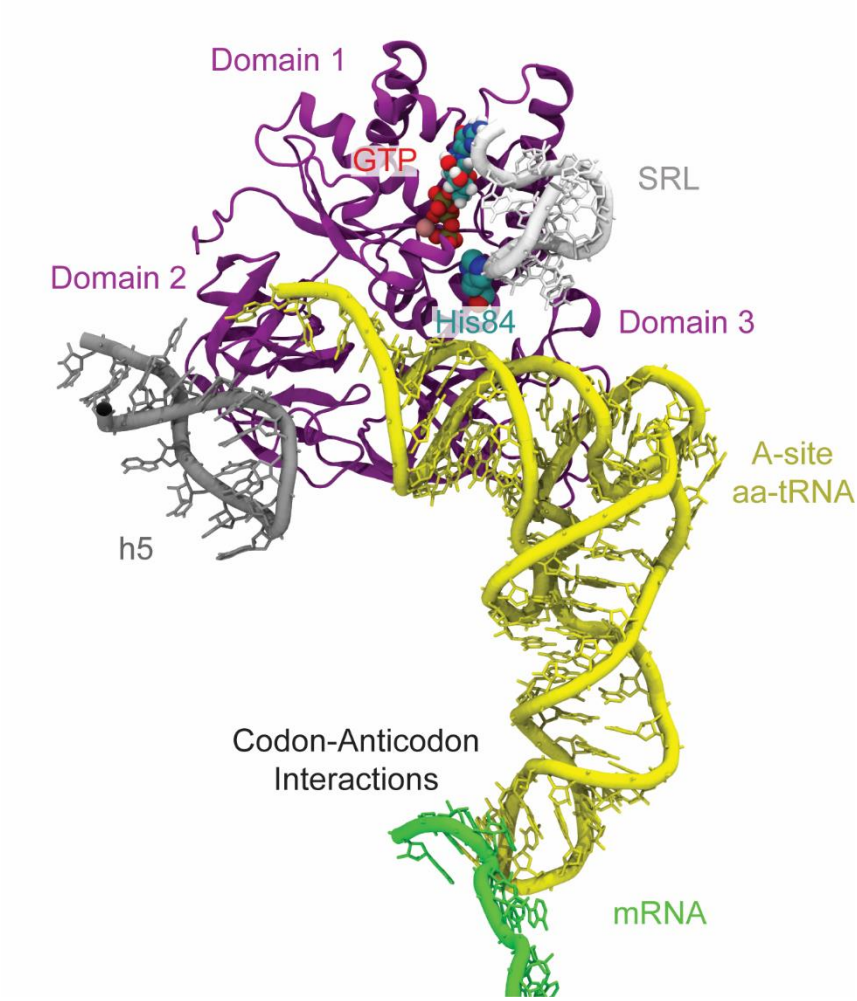

Figure 1.8 EF-Tu ribosome contact points for GTP hydrolysis stimulation. SRL binding to domain 1 of EF-Tu is predicted to coordinate H84 required for coordination of a catalytic water molecule. Interactions between domain 2 of EF-Tu and h5 of the 16S rRNA predicted to be required for GTP hydrolysis as G222D variant prohibits GTP hydrolysis. Cognate codon-anticodon interactions formed between the mRNA and aa-tRNA are required for GTP hydrolysis.

Antibiotics that affect accommodation

An ideal antibiotic would be a small molecule that is not easily metabolized, that can easily be taken up by bacteria, and selectively targets an essential prokaryotic process. One essential prokaryotic process often targeted by conventional antibiotics is protein synthesis by the 70S ribosome. Despite performing the same cellular function in prokaryotes and eukaryotes, the components of the ribosome differ considerably.

Eukaryotic ribosomes, composed of four rRNAs and eighty-two proteins, have a higher protein content then the prokaryotic counterpart, comprised of three rRNAs and fifty-two proteins (Voet & Voet, 2010). These differences in ribosomal architecture, in combination with rRNA sequence diversity between kingdoms, make translation an ideal target for antibiotics as they can selectively target prokaryotic translation without adverse effects on the host ribosomes. Antibiotics have been shown to target each phase of translation as bacteriostatic effectors or to promote miscoding (Wilson, 2009, 2014). Among these phases the elongation cycle is the most frequently targeted by antibiotics (Wilson, 2009). Six known families of antibiotics impair the delivery of aa-tRNA to the ribosome; aminoglycosides, tetracyclines, kirromycin, enacycloxins, pulvomycin, and GE2770A. The first structural data of antibiotics bound to the ribosome came shortly after the structures of the ribosome itself (Brodersen et al., 2000; Carter et al., 2000; Schlunzen et al., 2001). With structural data of antibiotics bound to the ribosome, the mechanism of translation inhibition could be described. Aminoglycosides induce misreading of the mRNA allowing incorporation of incorrect amino acids (Fig 1.5) (Karimi & Ehrenberg, 1994; Pape et al., 2000). Misreading is induced, for example, by binding of aminoglycosides to helix 44 (h44) of the 16S rRNA near the decoding center at the A-site of the ribosome (Becker & Cooper, 2013). Binding of these antibiotics induces a 'flipping out' of the universally conserved nucleotides A1492 and A1493 of the 16S rRNA which have been shown to interact with the minor groove formed between mRNA-tRNA base-pairs, stabilizing the tRNA in the A-site (Fig 1.5, 1.6) (Ogle et al., 2001). Tetracyclines prevent the association of aa-tRNA•EF-Tu•GTP ternary complex with the 70S and subsequent accommodation of aa-tRNA into the A-site of the ribosome by binding to the 16S rRNA at the A-site (Fig 1.5) (Blanchard, Gonzalez, Kim, Chu, & Puglisi, 2004; Brodersen et al., 2000). Kirromycin and

enacycloxins bind between domain I and III of EF-Tu instead of the ribosome, stalling EF-Tu in a conformation similar to EF-Tu bound to GTP (Fig 1.5) (Parmeggiani, Krab, Watanabe, et al., 2006; Schmeing et al., 2009; Valle et al., 2002). These antibiotics prevent the conformational changes of EF-Tu on the ribosome that is required for efficient aa-tRNA accommodation and dissociation of EF-Tu from the ribosome (Parmeggiani & Nissen, 2006). Pulvomycin and GE2270A are similar to kirromycin in that they bind to EF-Tu; however, these antibiotics prevent aa-tRNA binding to EF-Tu by binding to domain II of EF-Tu (Hogg, Mesters, & Hilgenfeld, 2002; Parmeggiani, Krab, Okamura, et al., 2006).

Although structural data is available for these antibiotics, there are several questions that still remain regarding their detailed function, particularly regarding to how they impact the dynamics of the system. Aminoglycosides 'flip-out' nucleotides A1492 and A1493 but it is unclear on how this induces misreading by the ribosome; are the nucleotides flipped-out prior to codon-anticodon interactions and how do the antibiotics alter the accommodation pathway? Additionally, it is unclear how certain antibiotics that have been resolved by structural data, such as evernimicin, impair accommodation (Arenz et al., 2016). It has been proposed that evernimicin blocks aa-tRNA accommodation sterically, yet the tRNA in the structure is in the A/T site not contacting the antibiotic; therefore, it is not clear if it blocks accommodation or increases the energy barrier for accommodation. To resolve how antibiotics like aminoglycosides and evernimicin impact accommodation, a detailed atomic description of the dynamics of the system is required.

1.3 G-protein-coupled receptors

Signal transduction is the process by which signalling molecules bind factors on the extracellular surface of a cell, triggering a cascade of enzymatic processes leading to a cellular response. Often GPCRs on the extracellular surface are the proteins that bind to signalling molecules responsible for triggering the cascade. These proteins are bound to a GTPase (G-protein) and upon effector binding to the GPCR act as the GEF for the GTPases. Once the GTPase is bound to GTP it dissociates from the GPCR to regulate cellular processes such as the cAMP or phosphatidylinositol signalling pathways (Hanlon & Andrew, 2015). Since GPCRs are on the extracellular surface and are easily accessible they constitute roughly one third of all current drug targets (Hauser, Attwood, Rask-Andersen, Schioth, & Gloriam, 2017; Hauser et al., 2018; Rask-Andersen, Masuram, & Schioth, 2014; Santos et al., 2017). GPCRs are encoded by 810 human genes making up 4% of the human protein-coding genome (Bjarnadottir et al., 2006). Despite the pharmacological and regulatory importance of these proteins the structural mechanism of their activation facilitating their GEF activity is unclear.

Evolution has produced six classes of GPCRs, yet all form a seven transmembrane helical bundle (Baldwin, 1993). Class A, the rhodopsin family, is the largest constituting ~85% of all GPCRs, the majority of which are olfactory (Fredriksson, Lagerstrom, Lundin, & Schioth, 2003). Members of this family commonly bind to hormones, signalling proteins, or nucleotides, to induce intracellular signalling (Joost & Methner, 2002). The secretin family, or class B, primarily binds to hormones and is only found in the animal kingdom (Harmar, 2001). Metabotropic glutamate receptors (class C) bind to amino acid neurotransmitters. Fungal mating pheromone receptors (class D) are only found in fungi

and bind to small peptide sequences. Cyclic AMP receptors (class E) bind to cAMP, while frizzled or smoothed receptors (class F) are part of the Wnt signalling pathway (Huang & Klein, 2004; Jones Jr. & Bennett, 2011; Willard & Koochekpour, 2013). Intriguingly, these classes of receptors form the same seven transmembrane helical architecture yet have little to no sequence similarity or a common ancestor, which has led to the theory that they reached this structural arrangement through convergent evolution (Bockaert & Pin, 1999). Therefore, the seven transmembrane helical arrangement is a versatile and flexible solution to produce signalling modules that evolution has invoked several times.

The seven transmembrane helix (TM 1-7) composition perpendicular to the membrane allows for protein incorporation into the cellular membrane (Fig 1.8). An additional helix (H8) is found on the intracellular surface of the cell and is parallel to the membrane (Fig 1.8). Tying together each of the TM helices are three intracellular and three extracellular loops (ICL and ECL). ECL2, between TM4 and 5, is the longest extracellular loop and contains an essential disulfide bridge in class A receptors like the β2 adrenergic receptor (β2AR), forming part of the ligand-binding pocket for GPCRs (Fraser, 1989; Wheatley et al., 2012). X-ray crystal structures of GPCRs bound to their G-protein have shown that ICL2 and ICL3 form the G-protein interface with TM3, TM5, TM6 and TM7 (Rasmussen, DeVree, et al., 2011). TM6 and TM7 have the conserved motifs $E(D)^{3.49}RY$, and $NP^{7.50}xxY$ (Balesteros-Weinstein numbering, first number denoting the helix it belongs to, the second is the position relative to the most conserved residue) motifs that are critical for interactions with the G-protein (Balesteros & Weinstein, 1995; Weis & Kobilka, 2018).

Structural data of GPCRs bound to G-proteins also revealed a 14Å movement of TM6 for β2AR upon activation of the receptor, a finding that supports a long-standing

mechanism of TM6 rigid body movements proposed by NMR (Fig 1.8) (Farrens, Altenbach, Yang, Hubbell, & Khorana, 1996; Rasmussen, DeVree, et al., 2011). This movement allows for the formation of a pocket where the α5 helix of the bound G-protein can interact with the GPCR. Additionally, activation of GPCRs also involves breaking of a conserved salt bridge known as the 'ionic lock' between $R^{3.50}$ and $E^{6.30}$ (Fig 1.8) (Vogel et al., 2008). These rearrangements are accompanied by a suite of molecular switches in the protein, all undergoing conformational change upon GPCR binding to an agonist (Trzaskowski et al., 2012). The first molecular switch is the 'ionic lock' (described above). The second is the '3-7 lock', which forms a link between TM3 and 7 through residues $Y^{7.43}$ and $D^{3.32}$ (Fig 1.8). Upon activation the 3-7 lock is broken similarly to the 'ionic lock'. The transmission switch involves the outward rotation of TM6 by one helical turn. This is induced by movement of $W^{6.48}$ and $F^{6.44}$ upon agonist binding, allowing TM6 to move towards $L^{5.51}$ and $P^{5.50}$ (Fig 1.8). The 'tyrosine toggle switch' involves a change in the hydrophobic barrier of GPCRs which is composed of $L^{2.43}$, $L^{2.46}$, $L^{3.43}$, $L^{3.46}$, $M^{6.36}$, and $M^{6.40}$ in the inactive conformation (Fig 1.8). Upon activation TM6 rotates and breaks the hydrophobic barrier allowing $Y^{5.58}$ and $Y^{5.53}$ along with $Y^{7.53}$ to swing into the core of the protein forming interactions with the E(D)RY motif to form a new hydrophobic gate (Fig 1.8). Lastly, the 'global toggle switch' is the bending of TM6 at $P^{6.50}$ upon activation by an agonist binding, the classical indication of an activated GPCR (Fig 1.8).

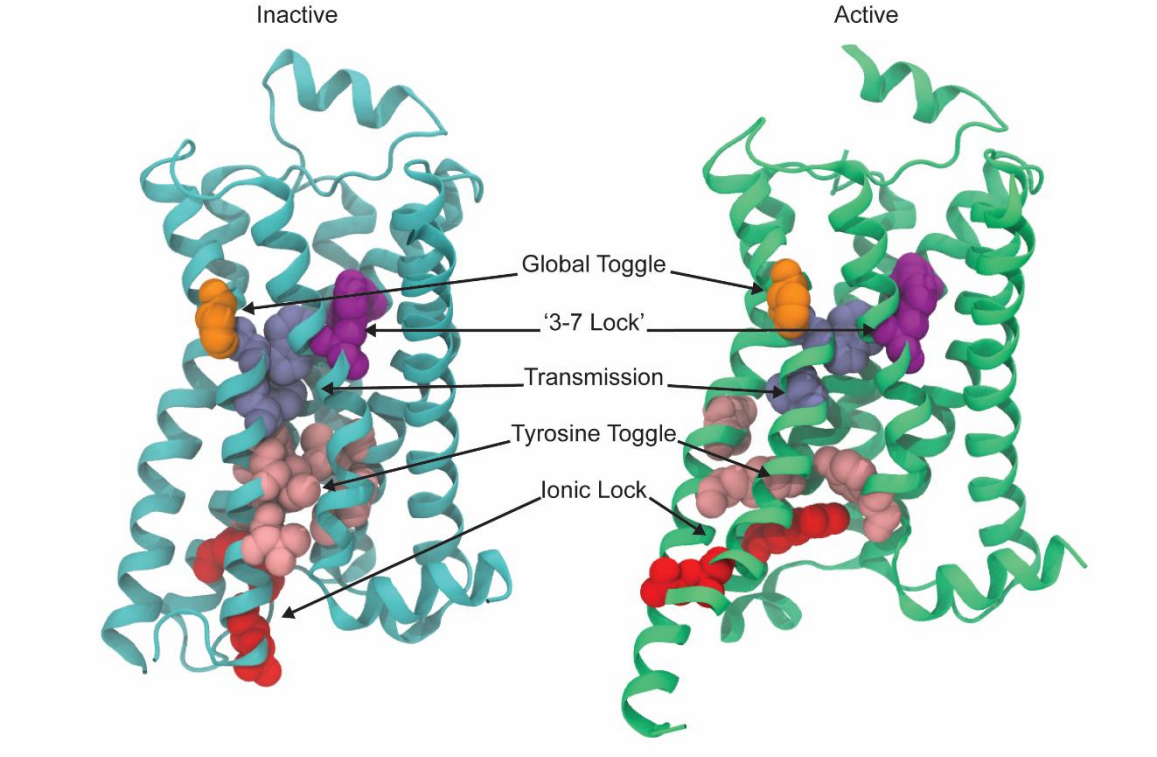

Figure 1.8 The active and inactive conformations of a GPCR. Cartoon representation of β2-adrenergic receptor in the inactive (left) and active (right) conformations. Highlighted are the 5 different switches separating the active and inactive conformations. PDBID: 3D4S – inactive, and 3SN6 – active.

Although plenty of structural data exists for GPCRs in the active and inactive conformation there are still several questions that need to be addressed concerning how GPCRs are activated, such as how agonist binding induces conformational rearrangement of the molecular switches? This is a fascinating question as GPCRs bind to a variety of different ligands to induce activation, and the ligand-binding pocket of GPCRs are dramatically different, yet conformational rearrangement of GPCRs occur in similar fashions.

1.4 Allostery

The function of many proteins is regulated by the binding of effector molecules to sites distal to the orthosteric site, a process known as allostery. How proteins mediate allostery has been a fundamental question of biochemistry even before the term was coined by Monod and Jacob in 1961 (Monod & Jacob, 1961). Three unique problems to allostery described by Tsai, Nussinov, Guo, and Zhou have arisen over the years that have been addressed with different models (Guo & Zhou, 2016; Tsai & Nussinov, 2014). The first problem, denoted as the equilibrium problem here, is how effector binding alters the conformational equilibrium of the protein. Does it shift the equilibrium from on conformation to another, or does it broaden a specific minimum of an equilibrium? Second, the transition problem, is how does effector binding change the equilibrium; are different conformations available prior to or only after effector binding has occurred? Lastly, the transmission problem is how information of effector binding is propagated to the orthosteric site through communication pathways. Multiple models can be used to describe allostery, indicating that evolution has found several solutions to each of these problems.

The equilibrium problem

Generally, it has been considered that effector binding alters the thermodynamics of the protein, especially at the orthosteric site, shifting the equilibrium from one conformation to another (Fig 1.9) (Guo & Zhou, 2016; Monod, Wyman, & Changeux, 1965; Nussinov & Tsai, 2015). The first allosteric protein studied, hemoglobin, displays these features transitioning from the tense (T) to the relaxed (R) conformation upon oxygen binding (Monod et al., 1965; Perutz, 1970). This idea is often conceived as the enthalpic view of allostery, as a conformational change would coincide with alterations in hydrogen

bonds or salt bridges, therefore promoting alterations to the activity at the orthosteric site (Tsai, del Sol, & Nussinov, 2008). However, an additional view has been proposed by Dryden and Cooper, where instead of shifting the conformational equilibrium from one minimum to another, effector binding broadens the minimum of a conformation (Fig 1.9) (Cooper & Dryden, 1984). This description would grant more conformational flexibility to the protein as the minimum is broadened and therefore this view is often termed 'dynamic allostery' (Cooper & Dryden, 1984; Guo & Zhou, 2016). The dominant factor in the changes to the thermodynamic landscape would be a less negative entropy term of the system upon effector binding. Support for this mechanism is provided by the regulation of PDZ domain from PSD-95/SAP90 (PDZ3) by α-helix 3 (α-3) binding to the protein CRIPT. The loss of α-3 increases the flexibility of PDZ3 as resolved by NMR; as CRIPT binds, this flexibility is lost, causing an entropic penalty for CRIPT binding and decreasing the affinity for the protein by ~20-fold (Petit, Zhang, Sapienza, Fuentes, & Lee, 2009). Therefore, the function of α-3 is to regulate CRIPT binding by modulating the flexibility of PDZ3 so there is no entropy loss when CRIPT binds. More recently, Chung-Jung Tsai, Antonia del Sol, and Ruth Nussinov have provided support for this theory that allostery can occur without large conformational change (Tsai et al., 2008). They argue for three types of allostery: Type I involves a change in dynamics and is regulated by entropy, Type II where allostery is regulated by both entropy and enthalpy and involves a change in conformation and dynamics, and Type III where allostery involves a conformational change and is driven by enthalpy (Fig 1.9) (Tsai et al., 2008). However, they also state that although conformational change is not observed by structural studies it does not mean that it cannot occur (Nussinov & Tsai, 2015). They suggest that conformational changes are not observed due to: crystal packing or conditions, inherent flexibility, lack of oligomer, an effector is missing, or that

the activation requires a gradient of conformations (Nussinov & Tsai, 2015). More common today is the idea that we should not limit our concept of allostery to one mechanism over the other. Usually allostery falls under Type II where both enthalpic and entropic contributions change the free energy landscape of the conformational equilibrium (Liu & Nussinov, 2017).

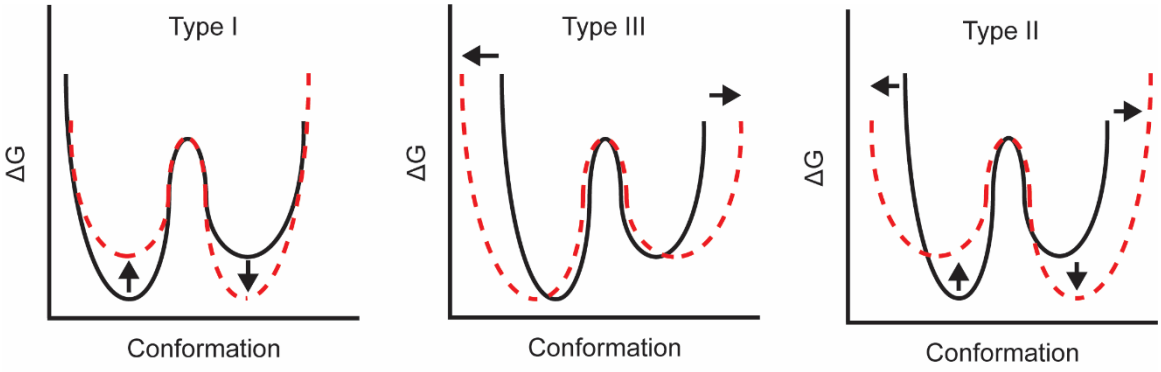

Figure 1.9 The equilibrium problem represented in free energy landscape. Type I equilibrium where effector binding induces a changing which equilibrium minimum is favored. Type III equilibrium where effector binding expands the width of the minimum indicating the protein is more dynamic. Type II equilibrium effector binding induces a combination of effects of type I and type III.

The transition problem

The transition problem addresses how effector binding at a distal site alters the conformational equilibrium of a protein. The two classical views to this problem are the Monod, Wyman, and Changeux (MWC) or the Koshland, Nemethy, and Filmer (KNF) models, often referred to as the concerted or sequential models, respectively (Koshland, Nemethy, & Filmer, 1966; Monod et al., 1965). In brief, the MWC or concerted model describes an allosteric protein that has an ensemble of states including the active or inactive (active and inactive refer to effector bound-like or *apo*-like, respectively) (Fig 1.10). Under any conditions, the protein will be able to adopt the active or inactive states as there will be

intrinsic transitions between them forming an equilibrium; however, effector binding to the protein will stabilize the active state. This model suggests that conformational change of the protein from inactive to active can occur before or at the same time as effector binding, hence the concerted model. Considering oligomeric complexes, the MWC model describes that the binding of effector to one subunit, stabilizing it in the active state, will induce the active state of the other monomers in a symmetrical fashion. The KNF or sequential model suggests that effector binding follows an induced-fit model where effector binding causes the protein to adopt the active state (Fig 1.10). Under this model the active state of the protein is not sampled in the absence of the effector. For an oligomeric complex, effector binding induces the active state of one subunit, but does not induce the active state of the other monomers, yet it may impact their conformations. These two models have been debated for over 50 years, and it seems that proteins can utilize either the MWC or KNF model to achieve allosteric regulation as there are examples of both.

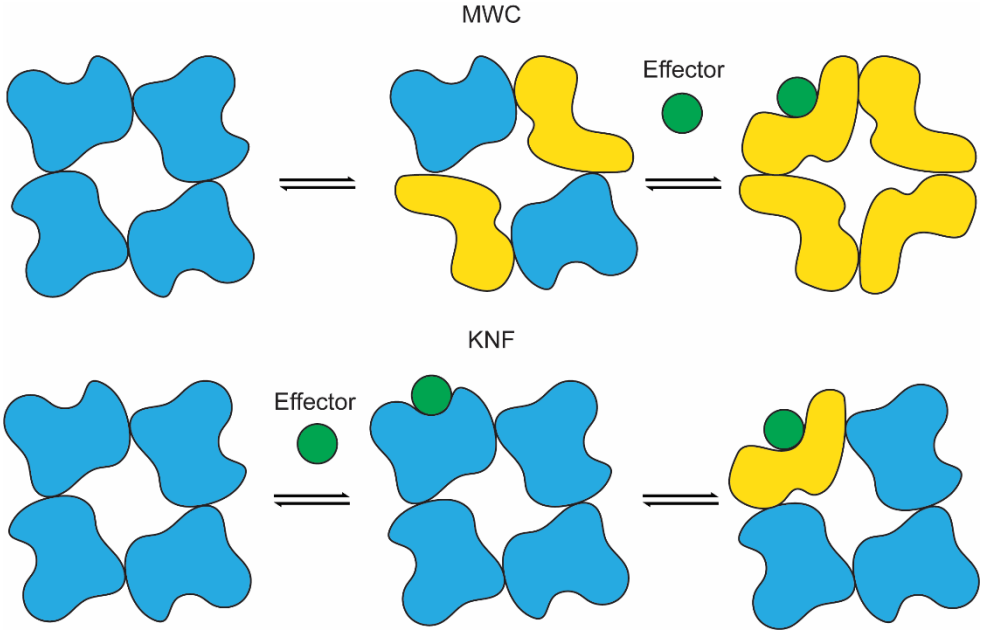

Figure 1.10 MWC and KNF models. The MWC model where monomers of each oligomer can adopt the active (yellow) or inactive (blue) conformation before effector binding, yet effector binding causes all monomers to adopt the active conformation. The KNF model describes how each monomer of an oligomer can only adopt one conformation before effector binding which induces a conformational change of only one of the monomer.

The transmission problem

The transmission problem is concerned with how information of effector binding is propagated to the orthosteric site through structural rearrangements. Although this issue has come into focus in the allosteric field due to advances in MD simulations and NMR approaches, the problem was initially addressed by Perutz on how oxygen binding induces structural rearrangements in hemoglobin (Perutz, 1970). In this seminal work he showed how salt bridges constrain the oxygen-free or inactive form of hemoglobin; however, in the oxygen-bound conformation, these salt bridges were absent. This was the first structural description of how effector binding regulates specific structural elements of a protein. It is considered that allostery can be transmitted from the effector site to the orthosteric site

through structural or dynamic changes in the amino acids of the protein, leading to pathways of amino acids that propagate allostery called allosteric communication pathways (Guo & Zhou, 2016).

A common approach to investigating the transmission problem has been looking at changes in residue-residue contacts between the active and the inactive states of a protein using network theory (Atilgan, Akan, & Baysal, 2004; Flock et al., 2015). Several research groups have started to incorporate dynamic information into their networks, analyzing residue-residue contact networks in MD simulations (Doshi, Holliday, Eisenmesser, & Hamelberg, 2016). Coupling correlated dynamics of amino acids from MD simulations with contact information has provided an even more in depth look at possible allosteric communication pathways (Rivalta et al., 2012; Sethi, Eargle, Black, & Luthey-Schulten, 2009; Shukla, Meng, Roux, & Pande, 2014). To reduce the complexity of the residue-residue networks in order to reveal the most likely allosteric communication pathway, community analysis has been employed (Guo & Zhou, 2016; Sethi et al., 2009). Often the Girvan-Newman approach to cluster amino acids into communities is used, whereby the edge betweenness for each edge in the network is measured and the edges with the highest betweenness are eliminated (Girvan & Newman, 2002). Edge betweenness is a summation of how many shortest paths pass through a specific edge, if the shortest path between each node pair was determined. Therefore, removing the edge with the highest edge betweenness value will separate amino acids into clusters based on edges that are bottlenecks in the possible communication pathway.

The transmission problem has also been addressed by NMR where changes in spectra and chemical shift are measured by relaxation dispersion experiments on the

backbone of labelled amino acids (^{15}N) in the presence or absence of an effector (Grutsch, Brüschweiler, & Tollinger, 2016; Holliday, Camilloni, Armstrong, Vendruscolo, & Eisenmesser, 2017; Popovych, Sun, Ebright, & Kalodimos, 2006). NMR studies are advantageous because they provide an *in vitro* approach to study the transmission problem of allostery; however, the ability to provide an atomic description of the allosteric communication pathway is limited.

EF-Tu allostery

EF-Tu binds to the ribosome as a ternary complex in complex with aa-tRNA and GTP, and in doing so, its GTP hydrolysis activity is stimulated by the ribosome. The enhancement of the GTP hydrolysis activity of EF-Tu is fundamentally an allosteric process, as it requires binding to the ribosome (effector) to alter the orthosteric site (GTP binding site) to induce GTP hydrolysis. Structural studies have suggested that the 30S domain closure docking EF-Tu onto the SRL leads to coordination of H84 of EF-Tu and a catalytic water by the phosphate backbone of the SRL (Schmeing et al., 2009). The variant H84A of EF-Tu has been shown to be inactive in GTP hydrolysis, supporting this theory. However, ribosomes depleted of SRL are still capable of stimulating the GTPase activity of EF-Tu (Daviter et al., 2003; Shi et al., 2012). Additionally, cognate codon-anticodon interactions between the tRNA and mRNA on the 30S ribosomal subunit stimulate the GTP hydrolysis of EF-Tu by 10^5-fold (Pape et al., 1998; Rodnina et al., 1996). The decoding center where mRNA and tRNA recognition occur is ~80Å away from the GTP binding site of EF-Tu, suggesting that the stimulation from these interactions is an allosteric effect. It has been hypothesized that cognate aa-tRNA-mRNA interactions, unlike near- or non-cognate, lead to proper positioning of the tRNA in the A-site, allowing for stimulation of

GTP hydrolysis (Sanbonmatsu, 2006). However, this has yet to be experimentally validated. Lastly, interactions between EF-Tu and h5 of the 16S rRNA, an interaction surface ~40Å from the GTP binding site, has been shown to stimulate GTP hydrolysis (Vorstenbosch et al., 1996). Altogether this suggests that the GTP hydrolysis activity of EF-Tu is regulated by three distinct interaction surfaces with the ribosome: (1) SRL, (2) decoding center, and (3) h5.

The conformation of EF-Tu is defined by which ligand it is bound to, ultimately determining if EF-Tu is in an active (GTP-bound) or inactive (GDP-bound) conformation. This again resembles allosteric regulation, as the conformation is determined by the binding of an effector. However, it is unclear how ligand binding induces the structural rearrangement of EF-Tu, therefore, the transmission problem is unclear. Additionally, the impact that ligand binding has on the free energy landscape of EF-Tu is unknown. Tavelera *et al* have shown that GTP binding to EF-Tu is entropically favoured whereas GDP binding is both enthalpically and entropically favoured (Talavera et al., 2018). However, the free energy landscape changes due to ligand binding have not been resolved nor has any comparison to the *apo* conformational ensemble been performed. Therefore, the equilibrium and transmission problems for EF-Tu nucleotide binding have not been solved. There is evidence that EF-Tu follows a KNF type model, as the rate limiting step in EF-Tu for the conformational change from GTP to GDP is the release of the formed Pi (Kothe & Rodnina, 2006). This suggests that it is the change in ligand that alters the conformation of EF-Tu. However, it cannot completely rule out that EF-Tu follows a MWC model, because EF-Tu has been shown by structural studies to adopt the GDP conformation even when bound to GDPNP, a non-hydrolysable analogue of GTP (Johansen et al., 2018). Johansen

et al. also show that EF-Tu can adopt both the GTP-bound (closed) or GDP-bound (open) conformations in the presence of either ligand by using FRET dye pairs attached to domain I and III of EF-Tu (Johansen et al., 2018).

The three interaction surfaces between EF-Tu and the ribosome that lead to the allosteric regulation of GTP hydrolysis makes solving the three problems of allostery for EF-Tu a complicated yet fundamentally fascinating problem. How are all three of the signals from these interaction surfaces integrated into a single signal that leads to effective GTP hydrolysis? What makes this problem even more intriguing is that EF-Tu, which is known to undergo a conformational change from an active GTP to an inactive GDP conformation, does not appear to undergo structural rearrangements upon binding to the ribosome (Schmeing et al., 2009). Therefore, EF-Tu is likely a protein that undergoes Type III allostery where by the allostery is mediated by a change in the dynamics of the protein. Additionally, since the conformational change only occurs after GTP hydrolysis and Pi release, describing allosteric regulation of EF-Tu using the MWC or KNF models is difficult (Kothe & Rodnina, 2006). Therefore, the problem that should be addressed to describe the allosteric regulation of EF-Tu in the most detail would be the transmission problem, ultimately answering the question, how do alterations in the EF-Tu ternary complex dynamics on the ribosome lead to the stimulation of GTP hydrolysis activity of EF-Tu?

GPCR allostery

GPCRs bind to ligands (effectors) on the extracellular surface of the cell and induce a response at their G-protein interface (orthosteric site) on the intracellular surface, and as such are classified as allosteric proteins. Prior to ligand binding, GPCRs can adopt a

number of different conformations, some of which are similar to the activated conformation (Kobilka & Deupi, 2007; Lee, Choi, & Hyeon, 2015; Nygaard et al., 2013; Weis & Kobilka, 2008). This dynamic feature of GPCRs indicate that they solve the transition problem through the MWC model, where both the active and the inactive conformations are available to the protein before ligand binding. Although there is evidence provided by NMR that an ensemble of conformations exists in GPCRs prior to ligand binding, there is little to no structural detail at the atomic scale describing them. The differences between the inactive and the active conformations of GPCRs are defined by rearrangements of internal switches, described above, all of which sense the bound effector. The rearrangement of the internal switches suggests that GPCRs follow a type I solution to the equilibrium problem where the protein enters into a new conformation on ligand binding. However, during activation TM6 becomes more dynamic, indicating that along with the rearrangement of internal switches GPCRs follow a type II solution to the equilibrium problem (Bhattacharya, Salomon-Ferrer, Lee, & Vaidehi, 2016). Despite several studies observing the conformational change in TM6 there has been little to no description for the transmission problem of how ligand binding induces the movements of TM6. Lee *et al.* (2015) describe the likely order of the internal switches changing from the inactive to active conformations using μs simulations. However, they never looked at the direct communication from ligand binding to these regions. Altogether, there is a lack of understanding for the conformations that GPCRs can adopt prior to activation at the atomic scale, as well as how ligand binding transmits information to distal regions of the protein. Answering these two questions will provide critical insight into the mechanism of GPCR's function.

1.5 Hypothesis and Objective

This thesis aims to address the allosteric regulation of GTPases by their respective GAFs or GEFs. Chapter 2 will describe how nucleotide binding of EF-Tu is thermodynamically regulated and give insights into the structural dynamics that respond to nucleotide binding, facilitating conformational change of EF-Tu. Chapter 3 will describe the application of a molecular dynamics simulation toolset that can analyze allosteric communication pathways on the GPCR D2 dopamine receptor (D2R), utilizing existing biochemical data. Given the availability of the biochemical information, D2R is a perfect model to analyze the equilibrium and transmission problem of allostery in GPCRs. Lastly, Chapter 4 will investigate the structural dynamics of EF-Tu on the ribosome that lead to efficient accommodation of cognate over near-cognate aa-tRNA, and how antibiotics affect this process. Additionally, the approach verified for D2R in chapter 3 will be used on EF-Tu bound to the ribosome to investigate the transmission problem of allostery as binding information is passed from the ribosome to EF-Tu during decoding to stimulate GTP hydrolysis. Altogether this thesis will give information on how GTPases are allosterically regulated using model systems such as GPCRs for GEFs, the ribosome as a GAF, and how nucleotide binding defines the conformation of EF-Tu.

Chapter 2

Elongation Factor Tu's Nucleotide Binding is Governed by a Thermodynamic Landscape Unique Amongst Bacterial Translation Factors

2.1 Forward

This chapter is presented in the manuscript form that was published in the Journal of the American Chemical Society (JACS) (Girodat, Mercier, Gzyl, & Wieden, 2019). As co-first author, with Evan Mercier, I wrote the majority of the manuscript, performed temperature dependence of mant-GDP dissociation as well as nucleotide association/dissociation in the presence of 5μM kirromycin stopped-flow experiments, MD simulations and subsequent analysis. Evan Mercier performed temperature dependence of mant-GTP dissociation stopped-flow experiments, established models for MD simulation, and aided in writing of the manuscript. Katherine Gzyl performed temperature dependence of mant-GDP and mant-GTP association stopped-flow experiments, and Hans-Joachim Wieden aided in concept development and writing.

In this chapter, thermodynamic properties governing nucleotide binding to EF-Tu and the structural dynamic elements of the protein that stabilize each nucleotide bound state were investigated. Therefore, I report how EF-Tu responds to nucleotide binding through conformational or structural dynamic changes, describing the equilibrium problem for the enzyme. This study aims at understanding how EF-Tu has evolved into the only bacterial translational GTPase known to have a 60-fold higher affinity for GDP than GTP. As such, this study provides insights into why EF-Tu requires a GEF (EF-Ts).

By employing the Eyring-Polani equation for pre-steady state stopped-flow experiments of mant-nucleotide association and dissociation at varying temperatures the activation barriers of each reaction are revealed. These activation barriers chart the enthalpic, entropic, and free energy landscapes for both mant-GTP and mant-GDP binding to EF-Tu. The thermodynamic landscape supports the hypothesis from De Laurentiis *et al.*

that EF-Tu does not discriminate which nucleotide it is binding to during its initial encounter, but does so during dissociation (De Laurentiis, Mercier, & Wieden, 2016). Additionally, the transition states for both nucleotide binding events are similar, thermodynamically speaking. Altogether our data support EF-Tu•GDP being enthalpically and entropically stabilized compared to the *apo* state, indicating a type II solution to the equilibrium problem. A type III solution to the equilibrium problem describes GTP binding as EF-Tu•GTP is entropically stabilized compared to both the GDP and *apo* state. However, since the thermodynamic landscape reveals that the *apo* state is likely a unique conformation it would seem that GTP binding follows a type II solution to the equilibrium problem where GTP induces a conformational change with similar enthalpy.

MD simulations reveal that EF-Tu•GTP is entropically stabilized by a decreased water coordination shell and that EF-Tu•GDP is enthalpically stabilized due to an increased number of hydrogen bonds. To validate that the structural dynamics features identified in MD give rise to the thermodynamic landscape of EF-Tu, they were targeted with point mutations and antibiotics. Kirromycin, which prevents the conformational change in EF-Tu, shows that nucleotide dissociation rates are in an inverted order compared to EF-T in the absence of antibiotic, indicating that the conformation of EF-Tu defines the rate of nucleotide dissociation. EF-Tu variants designed to target helix A of EF-Tu, which enthalpically stabilizes the GDP conformation and entropically stabilizes the GTP conformation, disrupt the respective thermodynamic properties involved in binding of both nucleotides. Altogether, this chapter provides insight into how EF-Tu and evolution has solved the 60-fold higher affinity for GDP in the context of the canonical G-domain architecture.

2.2 Abstract

Molecular switches such as GTPases are powerful devices turning ‘on’ or ‘off’ biomolecular processes at the core of critical biological pathways. To develop molecular switches *de novo,* an intimate understanding of how they function is required. Here the thermodynamic parameters that define the nucleotide-dependent switch mechanism of EF-Tu as a prototypical molecular switch were investigated. EF-Tu alternates between GTP- and GDP-bound conformations during its functional cycle, representing the ‘on’ and ‘off’ states, respectively. For the first time the activation barriers for nucleotide association are reported as the same for both nucleotides, suggesting a guanosine nucleoside or ribose first mechanism for nucleotide association. Additionally, MD simulations indicate that enthalpic stabilization of GDP binding compared to GTP binding originates in the backbone hydrogen bonding network of EF-Tu. In contrast, binding of GTP to EF-Tu is entropically driven by the liberation of bound water during the GDP- to GTP-bound transition. GDP binding to the *apo* conformation of EF-Tu is both enthalpically and entropically favored, a feature unique amongst translational GTPases. This indicates that the *apo* conformation does not resemble the GDP-bound state. Finally, antibiotics and single amino acid substitutions are used to target specific structural elements in EF-Tu to re-design the thermodynamic landscape. These findings demonstrate how, through evolution, EF-Tu has fine-tuned the structural and dynamic features that define nucleotide binding, providing insight into how altering these properties could be exploited for protein engineering.

2.3 Introduction

Molecular switches are critical components of the cellular machinery, regulating a vast number of essential biological processes including protein synthesis and signal transduction. As such, they have been the targets of a large number of antibiotics (Savelsbergh, Rodnina, & Wintermeyer, 2009; Wolf, Chinali, & Parmeggiani, 1977). Molecular switches are also of great interest for synthetic biology applications, in particular for protein engineering. In the past, protein engineers have successfully constructed small globular proteins that resemble naturally occurring proteins through rational design (Hosseinzadeh et al., 2017; Lin, Koga, Vorobiev, & Baker, 2017; Strauch et al., 2017) and novel proteins through directed evolution (Butterfield et al., 2017). In contrast to their fundamental role in biology and potential in synthetic biology, a detailed understanding of the biomolecular design principles and biophysical parameters underlying their switching-mechanism is lacking.

Due to their essential role in gene expression and abundance in nature, we focused here on trGTPases as model molecular switches with a broad biological impact. Translational GTPases are required for protein synthesis and are essential for each step of translation. To facilitate their role in translation, GTPases hydrolyze GTP into GDP and Pi. After hydrolysis, these proteins undergo a conformational change which defines their switching behavior. All translational GTPases contain similar conserved elements such as switch I, switch II, the G4, G5, and P-loop nucleotide recognition motifs (Maracci & Rodnina, 2016). Despite these similarities, the translational GTPase EF-Tu has a 60-fold higher affinity for GDP than it does for GTP (Gromadski et al., 2002). The higher affinity for GDP is a unique characteristic of EF-Tu, as the other translational GTPases EF-G, RF3,

and IF2 have similar affinities for both nucleotides (Hauryliuk et al., 2009; Peske, Kuhlenkoetter, Rodnina, & Wintermeyer, 2013; Wilden, Savelsbergh, Rodnina, & Wintermeyer, 2006). As a result of the high affinity EF-Tu has for GDP, it is the only known bacterial translational GTPase with a guanosine nucleotide exchange factor, EF-Ts, which enhances the rate of GDP dissociation by more than 10^6-fold (Gromadski et al., 2002). The unique differential binding affinity that EF-Tu has towards the two nucleotides is eliminated upon deletion of domains II and III (Parmeggiani et al., 1987). This indicates that these domains have a critical role in defining the nucleotide affinity, although they do not directly interact with the nucleotide. Structural studies of EF-Tu have failed to elucidate how these domains can fine-tune the preferential nucleotide binding. The cellular function of EF-Tu is to deliver aa-tRNA to the A-site of the 70S ribosome during the elongation phase of protein synthesis. The aa-tRNA delivery mechanism requires GTP binding and hydrolysis, a process that is dependent upon cognate codon-anticodon interactions between the aa-tRNA and the mRNA (Pingoud, Gast, Block, & Peters, 1983). GTP hydrolysis is followed by Pi release and conformational change of EF-Tu into the GDP-bound conformation (Kothe & Rodnina, 2006; Mohr, Wintermeyer, & Rodnina, 2002; Rodnina & Wintermeyer, 2001; Vorstenbosch et al., 1996). EF-Tu•GDP then dissociates from the 70S ribosome which allows for subsequent rounds of elongation (Pape et al., 1998). Therefore, the switching mechanism of EF-Tu is defined by the two functional states that it alternates between, GTP- and GDP-bound (Fig 2.1A).

Recently, Talavera *et al*. deduced the thermodynamics of nucleotide binding to EF-Tu using isothermal titration calorimetry (Talavera et al., 2018). They showed that binding of GTPγS is entropically driven rather than enthalpically. In general, an enthalpically

driven biomolecular process results in additional interactions being formed (such as hydrogen bonds, ionic interactions, or covalent bonds), whereas, an entropically driven process results in a greater number of microstates through increased structural fluctuations or the release of bound molecules. With this in mind, the finding that GTPγS binding is entropically driven is counter intuitive as EF-Tu forms more interactions with the bound GTP than the bound GDP (Fig A1.1), as well as more inter-domain interactions, when in the GTP-bound conformation compared to the GDP-bound conformation (Fig 2.1A, Fig A1.1) (Berchtold et al., 1993; Kjeldgaard et al., 1993; Nissen et al., 1995; Schmeing et al., 2009). Interestingly, support for EF-Tu•GTP being entropically stabilized is provided by the recent studies from Johansen *et al.* and Kavliauskas *et al.* where EF-Tu•GTP was observed in both the classical GTP-like and GDP-like conformations, although the thermodynamic contributions of the observed conformational dynamics have yet to be determined (Johansen et al., 2018; Kavaliauskas et al., 2018). Talavera and co-workers also show that GDP binding is both entropically and enthalpically favored, a feature which is unique among translational GTPases. For IF-2, SelB, and EF-G, GDP binding is only enthalpically driven (Table 2.1), suggesting that EF-Tu has evolved an additional entropic parameter for GDP binding (Hauryliuk et al., 2009; Hauryliuk et al., 2008; Paleskava, Konevega, & Rodnina, 2012). To understand the underlying biomolecular design strategy, it is critical to obtain thermodynamic information on the intermediate states of nucleotide binding, in particular how the thermodynamics of nucleotide association or dissociation regulate nucleotide binding, information that currently is unknown. Furthermore, there is no clear understanding of the evolutionary design features of EF-Tu that are responsible for its unique thermodynamic landscape of nucleotide binding. Understanding how these features of EF-Tu, using the common translational GTPase scaffold, give rise to the unique

thermodynamic landscape of nucleotide binding will aid in identifying generalizable strategies for the rational design of novel molecular switches.

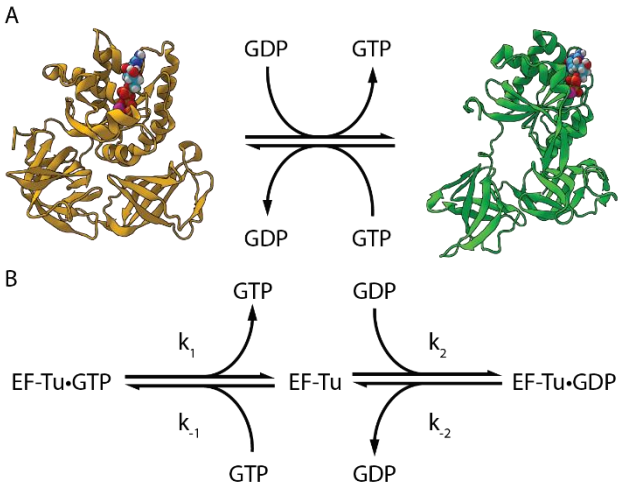

Figure 2.1 Nucleotide-dependent conformations of EF-Tu and minimal kinetic mechanism of EF-Tu nucleotide binding. (A) Guanosine nucleotide-dependent conformations of: EF-Tu•GTP in orange (left) and EF-Tu•GDP in green (right) (PDB ID: 1EFT and 1EFC) (Kjeldgaard et al., 1993; Song et al., 1999). Guanosine nucleotides are represented in cyan, red, blue, and white spheres. (B) Kinetic mechanism of EF-Ts-independent EF-Tu guanosine nucleotide exchange.

Here we report for the first time the activation energies and transient structural dynamic properties of EF-Tu that lead to the 60-fold higher affinity for GDP compared to GTP and provide critical and previously missing mechanistic description of EF-Tu's thermodynamic landscape of nucleotide binding. Overall, we use a work flow involving: (1) solving the kinetic mechanism for nucleotide binding, (2) calculating the entropic and enthalpic contributions to the thermodynamic landscape, and (3) molecular dynamics simulations to identify the transient structural elements contributing to the thermodynamic barriers. The entropy, enthalpy, and free energy activation barriers reveal that EF-Tu has fine-tuned the binding affinity for GDP and GTP by altering the activation barrier of dissociation rather than association. In addition, we find that the transition states of EF-Tu

binding to GTP and GDP are very similar. We also report that the compact EF-Tu•GTP conformation is entropically favored, relative to the *apo* and GDP state, due to a reduced hydration shell, while EF-Tu•GDP is enthalpically favored as a result of an increased number of backbone hydrogen bonds. Both of these structural features require conformational changes within domains II and III of EF-Tu which explains how the deletion of these domains abolishes the 60-fold higher affinity EF-Tu has for GDP over GTP. Since the free energy change associated with the switch from the 'off' to the 'on' conformation for a molecular switch sets the limits on the interaction with downstream effectors, the ability to modulate or fine-tune this free energy landscape provides the potential to engineer molecular switches with a weak, strong, or inverted preference for the 'on' or 'off' conformation. To demonstrate this, we show how single amino acid substitutions outside of the nucleotide binding pocket, as well as antibiotic binding, can alter the thermodynamic landscape of the 'on' to 'off' transition.

2.4 Materials and methods

EF-Tu overexpression and purification

EF-Tu purification was performed as described in De Laurentiis *et al* (De Laurentiis, 2011). In brief, a C-terminal polyhistidine-tagged EF-Tu was overexpressed in *E. coli* (cell line BL21 (DE3)) containing pKECAHIS encoding the full-length *E. coli tufA* gene. *E. coli* cultures were grown in 100 µg/mL ampicillin and EF-Tu expression was induced by the addition of Isopropyl β-D-1-thiogalactopyranoside to a final concentration of 1 mM at an OD_{600} of 0.6. The cells were lysed with 1 mg/mL lysozyme and 2 mg/mL sodium deoxycholate which was followed by sonication in Buffer A (50 mM Tris-HCl pH 8.0 @ 4.0°C, 60 mM NH_4Cl, 7 mM $MgCl_2$, 7 mM β-mercaptoethanol, 1 mM phenylmethylsulfonyl fluoride, 50 µM GDP, 300 mM KCl, 10 mM Imidazole, and 15% Glycerol). EF-Tu was purified from cellular lysate by Ni^{2+} nitrolotriacetic acid affinity chromatography (GE Healthcare). Proteins that bound to the column nonspecifically were washed off the column with Buffer A, followed by Buffer B (50 mM Tris-HCl pH 8.0 @ 4.0°C, 60 mM NH_4Cl, 7 mM $MgCl_2$, 7 mM β-mercaptoethanol, 1 mM PMSF, 50 µM GDP, 300 mM KCl, 20 mM Imidazole, 15% glycerol). Bound protein was eluted from the column using Buffer C (50 mM Tris-HCl pH 8.0 @ 4.0°C, 60 mM NH_4Cl, 7 mM $MgCl_2$, 7 mM β-mercaptoethanol, 1 mM PMSF, 50 µM GDP, 300 mM KCl, 250 mM Imidazole, 15% glycerol). EF-Tu was further purified using Superdex 75 size exclusion chromatography (GE Healthcare) using Buffer D (50 mM Tris-HCl pH 7.5 @ 4.0°C, 70 mM NH_4Cl, 30 mM KCl, 7 mM $MgCl_2$). EF-Tu purity (>95%) and concentration were determined by 12% sodium dodecyl sulfate-polyacrylamide gel electrophoresis (SDS-PAGE) stained with Coomassie Brilliant blue.

Nucleotide-free EF-Tu

As outlined in Wieden *et al*. (2002) purified EF-Tu was incubated in Buffer E (25 mM Tris-HCl pH 7.5, 50 mM NH_4Cl, 10 mM EDTA) for 10 minutes at 37°C (Wieden, Gromadski, Rodnin, & Rodnina, 2002). EF-Tu and nucleotide were separated with Superdex 75 (GE Healthcare) chromatography using Buffer F (25 mM Tris-HCl pH 7.5, 50 mM NH_4Cl). Concentration of nucleotide-free EF-Tu was determined by UV spectroscopy at 280 nm using a molar extinction coefficient of 32 900 M^{-1} cm^{-1}.

Rapid kinetic measurements

All kinetic measurements were performed with a KinTek SF-2004 stopped-flow instrument. Mant-nucleotide (Jena Bioscience) fluorescence was measured by first exciting W184 which in turn excited the mant group attached to the respective nucleotide through fluorescence resonant energy transfer (FRET) (Gromadski et al., 2002; Wagner, Simon, Sprinzl, & Goody, 1995).

The fluorescence signal from mant-nucleotide was measured after passing a LG-400-F long-pass filter. EF-Tu•mant-nucleotide dissociation was observed by rapidly mixing 25 µL of 0.3 µM EF-Tu•mant-nucleotide with 25 µL of 30 µM unlabeled nucleotide. A decrease in FRET signal was observed due to the dissociation of mant-nucleotide. Association was measured by rapidly mixing 25 µL of 0.3 µM nucleotide-free EF-Tu with 25 µL with varying concentrations of mant-nucleotide. Association and dissociation experiments were repeated at different temperatures ranging from 4°C to 37°C.

The fluorescent signals from the stopped-flow experiments were fit with equation 2.1 using TableCurve software (Jandel Scientific).

$$F = F_{\infty} + Ae^{-k_{app}t} \quad (2.1)$$

Since the rate of nucleotide dissociation does not depend on the concentration of any components the k_{app} is equivalent to the k_{off} (Gromadski et al., 2002). The association rate constants k_1 and k_2 (Fig 2.1B) were determined from the linear regression derived from the concentration dependence of the apparent rate constant (k_{app}) for EF-Tu•mant-nucleotide complex formation.

$\Delta H°^{‡}$, and $\Delta S°^{‡}$ were extracted from Eyring-Polani plots of the temperature dependence (1/T) of the rate constants ($\ln(k_{on/off}/T)$). The Eyring-Polani equations (equation 2.2) were transformed to a linear regression (equation 2.3) which was used to determine the thermodynamic parameters.

$$k = \frac{k_B T}{h} e^{\frac{\Delta S^{‡}}{R}} e^{-\frac{\Delta H^{‡}}{RT}} \quad (2.2)$$

$$\ln\left(\frac{k_{on/off}}{T}\right) = \frac{-\Delta H^{0‡}}{R}\left(\frac{1}{T}\right) + \frac{\Delta S^{0‡}}{R} + \ln\frac{k_B}{h} \quad (2.3)$$

Where R is the ideal gas constant (8.3145 J K^{-1} mol^{-1}), k_B is the Boltzmann constant (1.3907 x 10^{-23} J K^{-1}), h is Planck`s constant (6.6261 x 10^{-34} J s), $\Delta H^{‡}$ and $\Delta S^{‡}$ are, respectively, the enthalpy and entropy of activation for mant-nucleotide association or dissociation. Thermodynamic parameters for the overall binding reaction ($\Delta G°_B$, $\Delta H°_B$, and $\Delta S°_B$) were computed from the individual half reaction ($\Delta G°_B = \Delta G^{‡}_a - \Delta G^{‡}_d$).

Molecular dynamics simulations

MD simulations were performed as described in Wieden *et al.* (Wieden, Mercier, Gray, Steed, & Yawney, 2010). An *E. coli* homology model of EF-Tu•GTP was constructed from the crystal structure of EF-Tu•GDPNP from *Thermus aquaticus* (PDB ID: 1EFT)

using the SWISS-MODEL server (Arnold, Bordoli, Kopp, & Schwede, 2006; Biasini et al., 2014; Guex, Peitsch, & Schwede, 2009; Kiefer, Arnold, Kunzli, Bordoli, & Schwede, 2009; Kjeldgaard et al., 1993). The GDPNP was transformed to GTP by manual conversion. A model for *E. coli* EF-Tu•GDP was derived from the PDB ID: 1EFC, in which the first seven amino acids of EF-Tu are missing; they were added from the homology model created from 1EFT (Song et al., 1999). Hydrogen atoms were added to both models using the psfgen package within the NAMD software (only the ε nitrogen of histidine sidechains were protonated) (Phillips et al., 2005). Water molecules were then added to the model using the solvate package in NAMD (water molecules from the crystal structure were retained). Both models were minimized by a two time iterative process of freezing all non-water atoms, then by freezing all water molecules followed by a full system minimization. Sodium ions were added using the autoionize package of NAMD to neutralize the system (Humphrey, Dalke, & Schulten, 1996). A final relaxation of the system was performed for 100 000 steps. Each of the minimized models was equilibrated at constant pressure and a temperature of 300°K or 350°K for 150 ps. The coordinates of the 300°K and the velocities of the 350°K equilibrations were combined as initial conditions for the production runs of EF-Tu•GTP and EF-Tu•GDP. Production runs were performed using CHARMM 27 force fields with NAMD software until 100 ns of simulation time was achieved (Humphrey et al., 1996).

Molecular dynamics analysis

The backbone hydrogen bond network of EF-Tu was determined by calculating the number of frames in which hydrogen bond donors or acceptors were within 3.0 Å and 150-210° of each other (Steiner, 2002). Salt bridges in the EF-Tu simulations were determined

with the Salt Bridges plugin in Visual Molecular Dynamics (VMD) software (Humphrey et al., 1996). A salt bridge was defined as an oxygen-nitrogen pair within the cutoff distance of 3.2 Å. Solvent accessible surface area (SASA) of EF-Tu was calculated with the measure sasa package in VMD (Humphrey et al., 1996). This package extends the radius of an atom by 1.4Å to probe for the solvent accessible surface area. Water molecules within 2.5, 3.0, or 4.0 Å of EF-Tu were determined as coordinated water molecules. Simulation results plotted in a histogram were fit with a one or two Gaussian functions (equation 2.4 and 2.5).

$$\text{counts} = \text{A}e^{\frac{-(x-\bar{x}_a)}{2\sigma_a^2}} \tag{2.4}$$

$$\text{counts} = \text{A}e^{\frac{-(x-\bar{x}_a)}{2\sigma_a^2}} + \text{B}e^{\frac{-(x-\bar{x}_b)}{2\sigma_b^2}} \tag{2.5}$$

2.5 Results

Kinetics of guanosine nucleotide binding to EF-Tu

To gain an understanding of the thermodynamic parameters that govern nucleotide binding in EF-Tu, we solved the kinetic scheme outlined in figure 2.1B at temperatures ranging from 4 to 37°C. We used the stopped-flow technique to determine the rate of mant-GTP and mant-GDP association (k_1 and k_2 respectively) as well as dissociation (k_{-1} and k_{-2} respectively) described previously (Gromadski et al., 2002; Wieden et al., 2010). Nucleotide association showed a mant-emission increase due to an increase in FRET between mant and the tryptophan in position 184 (Fig 2.2A), whereas nucleotide dissociation showed a decrease in mant-emission from a reduction in FRET (Fig 2.2B). Fluorescent traces from the association and dissociation stopped-flow experiments (Fig 2.2A, B respectively) were fitted with a single-exponential equation (eq 2.1) to determine apparent rates (k_{app}) (Table A1.1). Association and dissociation kinetics of mant-GTP and mant-GDP at 22°C are in good agreement with previously reported rates (Table A1.1) (Gromadski et al., 2002). The rate of mant-nucleotide binding to EF-Tu is concentration-dependent and therefore was titrated using varying concentrations ranging from 0.5-5 μM mant-nucleotide (Fig 2.2A, Table A1.1). The apparent rates at each concentration were then plotted as a function of mant-nucleotide concentration (Fig 2.3A). The slope describing the concentration dependence shown in figure 2.3A is equal to the k_{on} at the respective temperature.

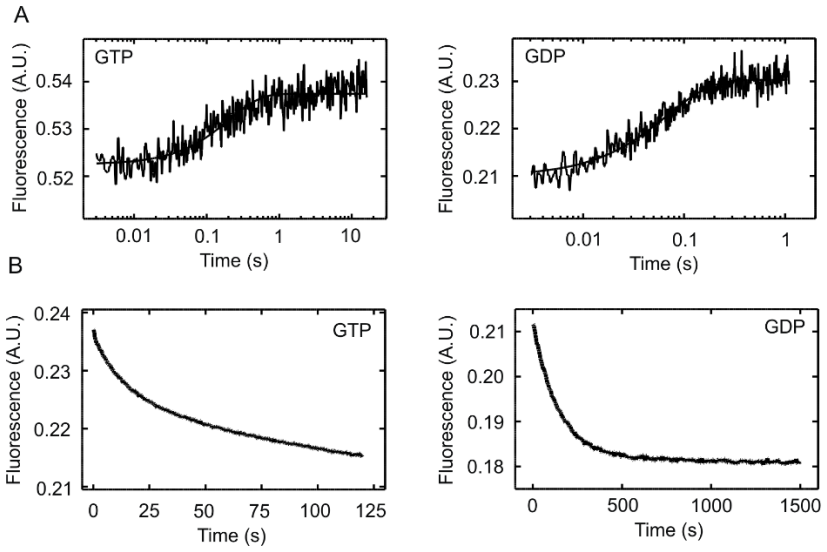

Figure 2.2 Pre-steady state kinetics of EF-Tu nucleotide association and dissociation. Tryptophan 184 was excited at 280 nm and mant fluorescence was measured using a 400 nm long-pass filter. All concentrations are given after mixing. (A) Association time course of 10 μM mant-GTP to EF-Tu (0.25 μM) at 37°C (left) and association of 10 μM mant-GDP to EF-Tu (0.25 μM) at 37°C (right). (B) Dissociation of 1.5 μM mant-GTP from EF-Tu (0.15 μM) in the presence of 25 μM GTP at 37°C (left) and dissociation of 1.5 μM mant-GDP from EF-Tu (0.15 μM) in the presence of 25 μM GDP at 37 °C (right).

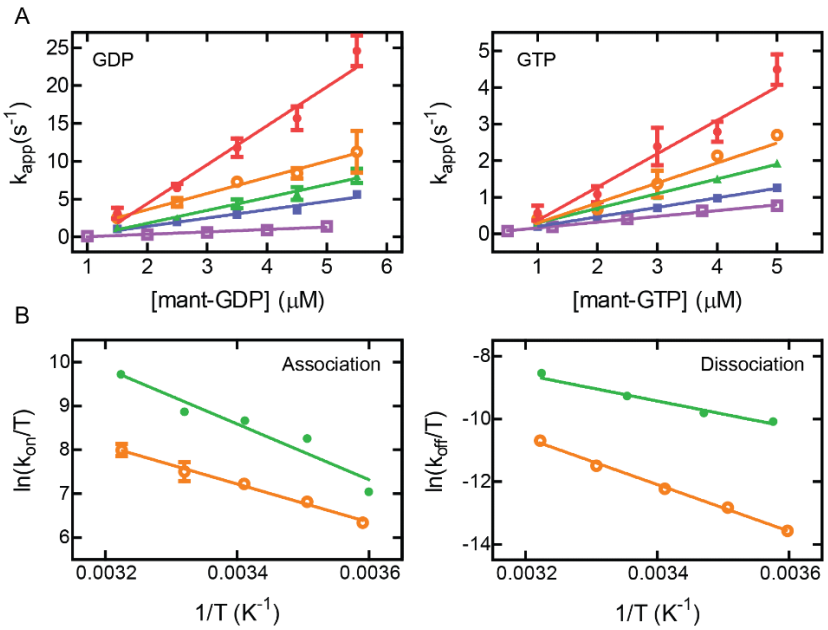

Figure 2.3. Temperature-dependent kinetic properties of nucleotide binding for determination of entropic and enthalpic activation barriers. (A) Concentration dependence of k_{app} values for mant-GDP (left) and mant-GTP (right) association to EF-Tu (4°C–purple open squares, 12°C–blue closed squares, 20°C–green triangles, 29°C–orange open circles, 37°C–red closed circles). (B) Eyring plot of mant-nucleotide association (left) and mant-nucleotide dissociation (right) to EF-Tu (GDP–green, GTP–orange)

Thermodynamic landscape of EF-Tu nucleotide binding

To determine the enthalpic and entropic activation barriers ($\Delta H^{\ddagger}$ and $\Delta S^{\ddagger}$) for nucleotide association (k_1 and k_2) and dissociation (k_{-1} and k_{-2}) we plotted the relationship of ln(k/T) with respect to 1/T (Fig 2.3B). By using a transformation of the Eyring-Polani equation (equation 3) we determined the $\Delta H^{\ddagger}$ from the slope and $\Delta S^{\ddagger}$ from the y-intercept of the linear fit in figure 2.4B (Table A1.2). The $\Delta H^{\ddagger}$ and $\Delta S^{\ddagger}$ for association and dissociation of both GTP and GDP allowed us to plot an enthalpic and entropic landscape for EF-Tu nucleotide binding (Fig 2.4B, C). From the $\Delta H^{\ddagger}$ and $\Delta S^{\ddagger}$, we calculated the $\Delta G^{\ddagger}$ for nucleotide association and dissociation, as well as the $\Delta G°$, $\Delta H°$ and $T\Delta S°$ of binding ($\Delta G°_B$, $\Delta H°_B$ and $T\Delta S°_B$) (T=22°C) (Table A1.2). These calculated values are in agreement

with Talavera *et al* (Talavera et al., 2018). Gromadski *et al.* reported a K_D of 1 nM and 60 nM for EF-Tu binding to GDP and GTP respectively, which is equivalent to a $\Delta G°_B$ of -51 kJ/mol and -41 kJ/mol (Gromadski et al., 2002). These values are in excellent agreement with our measured $\Delta G°_B$ values of -50 ± 10 kJ/mol and -41 ± 6 kJ/mol for GDP and GTP binding. Surprisingly, the $\Delta G^‡$ of association ($\Delta G^‡_a$) for both nucleotides were statistically indistinguishable (GDP=37±7 kJ/mol, GTP=40±4 kJ/mol). However, the $\Delta G^‡$ of dissociation ($\Delta G^‡_d$) was significantly different (GTP=81±2 kJ/mol, GDP=88±3 kJ/mol). The similar $\Delta G^‡_a$ leads to a similar energy for the transition state of GTP and GDP binding to EF-Tu (Fig 2.4A). Together these data suggest that EF-Tu does not discriminate between the two nucleotides upon association but rather does so during the dissociation event. Interestingly, the $\Delta H°_B$ and $T\Delta S°_B$ landscapes reveal no enthalpic or entropic preference for association of one nucleotide over the other, as the $\Delta H^‡$ and $T\Delta S^‡$ of association ($\Delta H^‡_a$ and $T\Delta S^‡_a$) were indistinguishable for GDP and GTP (Fig 2.4B, C and Table A1.2). These data have implications for the mechanism of nucleotide binding and support the model from De Laurentiis *et al*. in which nucleotide association occurs base side first by interacting with the G4 (NKCD) and G5 (SAL) motifs of EF-Tu (De Laurentiis et al., 2016), as opposed to a phosphate-first binding mechanism. If the phosphate moiety of GTP or GDP was recognized first by EF-Tu the differences in the phosphates (di-phosphate vs. tri-phosphate) would likely result in different association barriers due to differences in the hydrogen bonding. The activation barriers also aid in our understanding of the transition states for nucleotide binding (Table A1.2). The transition states of GTP and GDP binding have relatively similar energy level in terms of free energy, enthalpy, and entropy (Fig 2.4).

Directly comparing the energy level of the different states of EF-Tu (Fig 2.4) reveals how these are thermodynamically stabilized relative to each other. In doing so we notice that EF-Tu•GDP is enthalpically stabilized by a large $\Delta H^{\ddagger}$ for dissociation ($\Delta H^{\ddagger}_{d}$) which is 2-fold larger than the $\Delta H^{\ddagger}_{a}$ for GDP (Fig 2.4B, Table A1.2). As a result, EF-Tu•GDP is more stable enthalpically in comparison to the *apo* and the EF-Tu•GTP state. Additionally, the EF-Tu•GTP conformation has a net zero ΔH°_{B} when compared to the *apo* conformation (Fig 2.4B). The $T\Delta S^{\ddagger}$ of dissociation ($T\Delta S^{\ddagger}_{d}$) for both the EF-Tu•GTP and EF-Tu•GDP states are stabilizing compared to *apo* EF-Tu. Intriguingly, the $T\Delta S^{\ddagger}_{a}$ for GTP and GDP is negligible when compared to $T\Delta S^{\ddagger}_{d}$ (Table A1.2). A negligible $T\Delta S^{\ddagger}_{a}$ suggests that there is no loss in available microstates (or thermal fluctuations) upon nucleotide binding. However, a significant increase in available microstates occurs after passing though the transition state, consistent with accommodation into a different conformation (Fig 2.4C). The $T\Delta S^{\ddagger}_{d}$ of GTP is 2-fold larger than that of GDP being -46 ± 1 kJ/mol and -27 ± 1 kJ/mol, respectively (Table A1.2). Therefore, EF-Tu•GTP is entropically favored compared to the GDP and *apo* state.

Structural and dynamic contributions to EF-Tu's thermodynamic landscape

Some interesting structural insight into the plasticity of the thermodynamic landscape of nucleotide binding is provided in Talavera *et al* (Talavera et al., 2018), reporting that phosphorylation at T382 stabilizes the open GDP-like conformation and alters GTPγS binding to be enthalpically rather than entropically favored. This indicates that enthalpic stabilization during nucleotide binding is a feature of the open (GDP-like) conformation. Therefore, for a detailed structural interpretation of the complete thermodynamic landscape, we studied features of the crystal structures of EF-Tu

representing the primary *on* and *off* states (PDB ID: 1EFC, 6EZE, and 1EFT) (Johansen et al., 2018; Kjeldgaard et al., 1993; Song et al., 1999). To this end, we considered hydrogen bonds and electrostatic interactions such as salt bridges to explain the enthalpic contributions to nucleotide binding of each state. Surprisingly, we could not explain the enthalpic stabilization of EF-Tu•GDP using these. EF-Tu makes 10 more intramolecular hydrogen bonds and 8 more salt bridges when bound to GTP compared to GDP (Fig A1.1). This is inconsistent with the greater enthalpic stabilization measured for EF-Tu•GDP. Additionally, it is difficult to ascertain what contributes to the entropic stability of the nucleotide bound state of EF-Tu, as structural studies do not resolve the available microstates or dynamics of the protein. In order to investigate the stability of the hydrogen bonds and salt bridges, as well as to gain insight into available microstates, we performed explicit-solvent MD simulations.

EF-Tu•GDP is enthalpically favored by extra hydrogen bonding potential in the peptide backbone

The EF-Tu•GDP state is enthalpically favored with a $\Delta H°_B$ = 27 ± 5 kJ/mol compared to the EF-Tu•GTP with a $\Delta H°_B$ = 1 ± 3 kJ/mol. We considered that the enthalpic contributions for the EF-Tu•GDP conformation could arise from intramolecular salt bridges or hydrogen bonds. Therefore, we calculated the total intramolecular salt bridges available in EF-Tu•GDP and EF-Tu•GTP for 100ns of simulation time (Fig 2.5A). The mean number of salt bridges for EF-Tu•GTP and EF-Tu•GDP are 5.8 and 5.9 per frame respectively, indicating that there is no significant difference between the two conformations (Fig 2.5A) excluding differences in the number of salt bridges as the source of this preferential stabilization.

Next, we considered hydrogen bonds within EF-Tu. To this end we determined all the potential hydrogen bond donors and acceptors within EF-Tu for both the GTP and GDP states (Fig 2.5 B-E). For this, hydrogen bond donors and acceptors had to be within a distance of 3.0 Å and an angle of 150° to 210° with a potential acceptor or donor, respectively. If we consider the hydrogen bonds formed between amino acid sidechains of EF-Tu, we observed that EF-Tu•GTP forms, on average, slightly more hydrogen bonds (222:100, donors:acceptors) per frame compared to EF-Tu•GDP (216:97) (Fig 2.5 B, D). When we further consider the backbone hydrogen bonds, however, EF-Tu•GDP is favored (166:92) over EF-Tu•GTP (158:89) (Fig 2.5 C, E). Together, the sidechain and backbone hydrogen bonds in EF-Tu•GDP, on average, provide two additional hydrogen bond donors when compared to EF-Tu•GTP. Since the measured hydrogen bonds fit the criteria of a weak hydrogen bond (dissociation energy of <16.7 kJ/mol), the expected energy contribution (<33.4 kJ/mol) of these 2 extra hydrogen bonds formed in EF-Tu•GDP can account for the experimentally observed 26 kJ/mol difference (Steiner, 2002). Most of the hydrogen bonds that preferentially form (engaged in >30% of frames) in EF-Tu•GDP are located in domain I of EF-Tu (Figure 2.5F, Table A1.5) and are a result of the conformational change that occurs within switch I and switch II of EF-Tu. In the EF-Tu•GTP conformation, switch I forms an α-helix which changes to β-strands in the EF-Tu•GDP conformation (Abel, Yoder, Hilgenfeld, & Jurnak, 1996). The formation of the β-strands increases the backbone hydrogen bonding potential for amino acids 46, 47, 55, 60, and 62 (Table A1.5). Additionally, residues 80, 84, 85, 86, and 87 of switch II also form additional hydrogen bonds, enthalpically favoring the EF-Tu•GDP conformation over the EF-Tu•GTP conformation (Table A1.5). To get an understanding for the dynamics of the backbone hydrogen bonds of EF-Tu, we determined the backbone hydrogen bonding

network in our MD simulations (Fig A1.3 and A1.4). Two clusters of hydrogen bonds appear in the EF-Tu•GDP network at helix A (amino acids 23-35) and switch II (amino acids 84-89) where on average these hydrogen bonds are formed for ~20% more simulation time in EF-Tu•GDP compared to EF-Tu•GTP (Figure 2.5F, G, Table A1.5). In the EF-Tu•GTP simulation, helix A is less rigid and a breathing motion of the helix can be observed (Video 1, 2). Altogether this suggests that helix A and switch II are able to modulate the switching behavior of EF-Tu by serving as enthalpic stabilizing modules in EF-Tu•GDP, whereas in EF-Tu•GTP, helix A serves as an entropic stabilizing module amplifying the effect of the bound nucleotide.

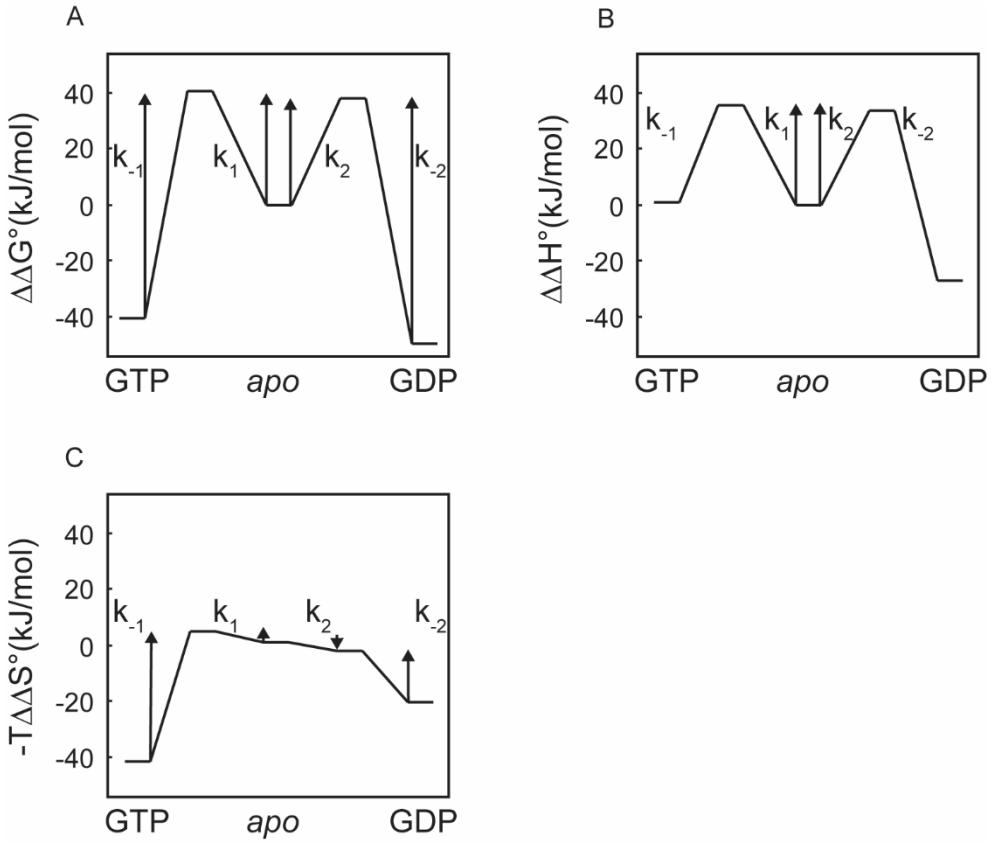

Figure 2.4. Energy landscapes for EF-Tu nucleotide binding. (A) ΔG° landscape of nucleotide binding. (B) ΔH° landscape of EF-Tu nucleotide binding. (C) –TΔS° landscape of nucleotide binding. Rates association with transition state are highlighted. k_1 = GDP binding and k_2 = GTP binding

Table 2.1 Thermodynamic parameters of nucleotide binding in EF-Tu and other proteins of the trGTPase family. ¥-Measured at 22°C, *- Measured at 20°C, χ-$\Delta G^{\circ\ddagger}_B$, $\Delta H^{\circ\ddagger}_B$, $T\Delta S^{\circ\ddagger}_B$.

GTPase	Ligand	ΔG°_B (kJ/mol)	ΔH°_B (kJ/mol)	$T\Delta S^{\circ}_B$ (kJ/mol)	K_D(M)
EF-Tu¥χ	GTP	-41 ± 6	-1 ± 3	42 ± 5	6.0×10^{-8}
	GDP	-50 ± 10	-27 ± 5	24 ± 5	1.0×10^{-9}
EF-G*(Hauryliuk et al., 2008; Wilden et al., 2006)	GTP	-29	-7	22	7.0×10^{-6}
	GDP	-28	-26	2	1.7×10^{-5}
IF2*(Hauryliuk et al., 2009)	GTP	-29	-62	-33	7.1×10^{-6}
	GDP	-33	-40	-7	1.4×10^{-6}
SelB*(Paleskava et al., 2012; Thanbichler, Bock, & Goody, 2000)	GTP	-33	-64	-31	7.4×10^{-7}
	GDP	-28	-24	4	1.3×10^{-5}

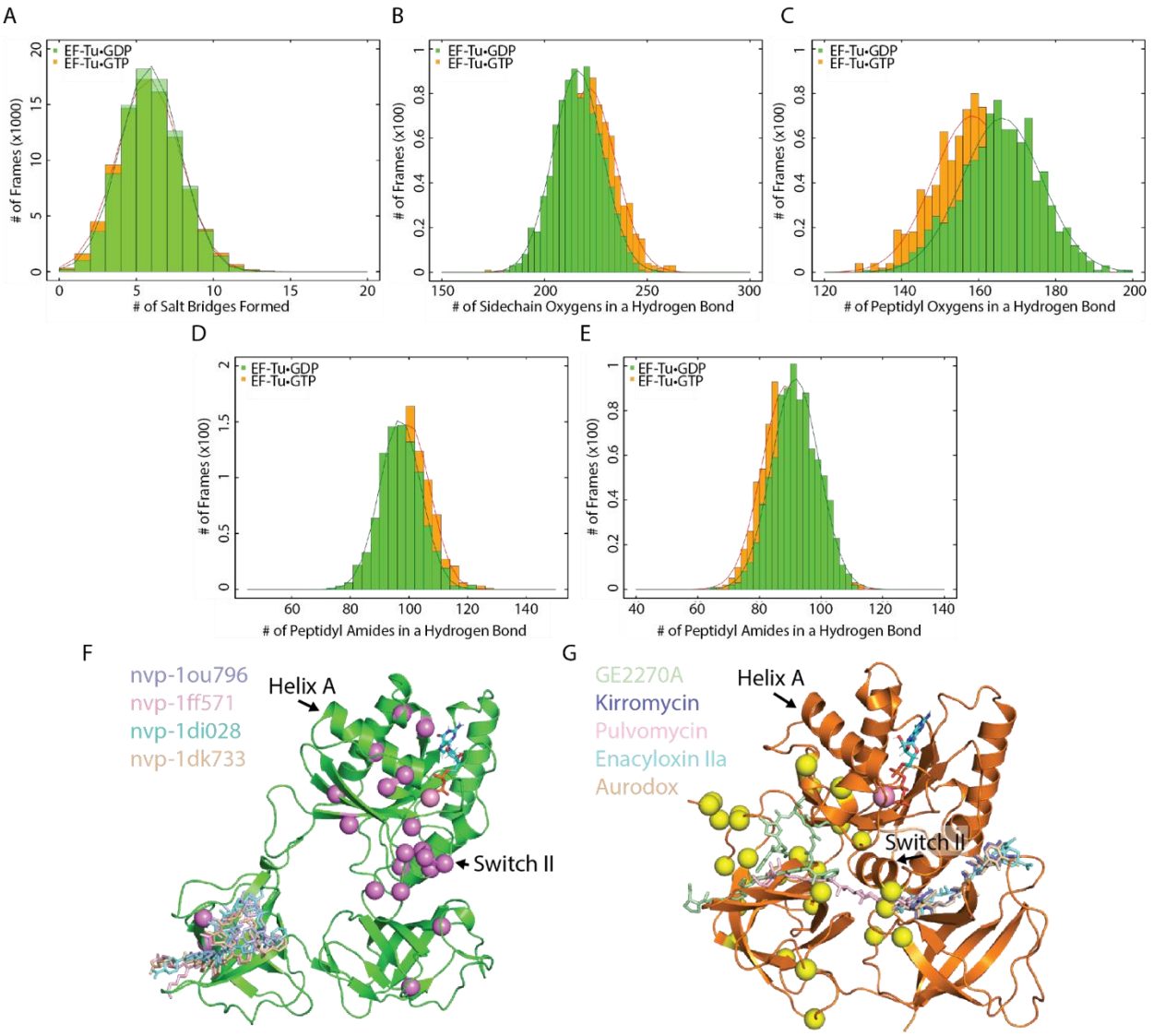

Figure 2.5 EF-Tu structural and dynamic contributions favoring the EF-Tu•GDP conformation. (A) Average number of salt bridges per frame in EF-Tu throughout 100 ns simulation. Average number of (B) sidechain and (C) backbone oxygens involved in hydrogen bonds that are within 3.0 Å and a 30° angle in the 100 ns simulation of EF-Tu•GTP and EF-Tu•GDP . Average number of (D) sidechain and (E) backbone nitrogen involved in hydrogen bonds that are within 3.0 Å and a 30° angle in the 100 ns simulation of EF-Tu•GTP and EF-Tu•GDP. Antibiotics and amino acids that stabilize (F) GDP and (G) GTP state. Residues that form hydrogen bonds for 30% more of the frames are shown in the structures of EF-Tu and are represented as pink (GDP) or yellow (GTP) spheres.

Water coordination entropically stabilizes EF-Tu•GTP

Comparing the EF-Tu•GTP and EF-Tu•GDP landscapes in Figure 2.4, the EF-Tu•GTP conformation adopts a lower $-T\Delta\Delta S°$ value, indicating that it is entropically stabilized. Johansen *et al.* and Kavaliauskas *et al*. have shown that EF-Tu•GTP can exhibit large scale conformational (domain) flexibility, likely contributing to the entropic stability of this state (Johansen et al., 2018; Kavaliauskas et al., 2018). To decipher if the more compact conformation available to EF-Tu•GTP is able to contribute to the entropic stability, we analyzed possible entropic contributions to this conformation such as overall flexibility or root mean squared fluctuation (RMSF) of the protein in our MD simulations (Fig 2.6A). An increase in RMSF indicates an entropically stabilized nucleotide bound state of EF-Tu because increased fluctuations indicate an increased number of available microstates. The RMSF values for the EF-Tu•GTP conformation are smaller than for the EF-Tu•GDP in every region of the protein except for residues 51-58 which are part of switch I, adjacent to helix A. This in turn means that switch I is less flexible when adopting the β-strands conformation in the GDP-bound state when compared to the α-helical conformation observed in the GTP-bound state. The β-strands conformation of switch I in EF-Tu•GDP is unusual amongst GTPases, as switch I is normally either unresolved or resolved as a loop in the available relevant structures (Al-Karadaghi, AEvarsson, Garber, Zheltonosova, & Liljas, 1996; Czworkowskil et al., 1994; Kihira et al., 2012; Simonetti et al., 2013). This may contribute to why the GDP states of SelB and IF2 are entropically favored compared to their GTP states (Table 2.1). However, it is unlikely that the change in switch I dynamics alone leads to the entropically favored GTP state.

Since protein dynamics alone do not define the entropic stability of EF-Tu•GTP, we also considered the microstates involving the surrounding water molecules. Therefore,

we calculated the solvent accessible surface area (SASA) of EF-Tu for both EF-Tu•GTP and EF-Tu•GDP, as well as the respective hydration shells over the course of our simulations. EF-Tu•GDP has, on average, a larger SASA (1041 $Å^2$ larger) when compared to the EF-Tu•GTP structure, which in turn will result in a larger hydration shell (Fig 2.6B, Table A1.3). To investigate if this increased surface area correlated directly to the actual number of water molecules coordinated by the protein, we calculated the hydration shell (the number of water molecules that surround the protein within 2.5 Å). EF-Tu•GTP coordinates, on average, 318 water molecules throughout the simulation, which is, on average, 16 water molecules fewer per frame when compared to the mean of 334 water molecules coordinated by EF-Tu•GDP (Fig 2.6C). This overall decrease in surface accessible surface area and water coordination allows us to explain the EF-Tu•GTP entropic stability relative to EF-Tu•GDP. Lim *et al*. estimate that the entropy contribution of water dimer release from protein coordination is 6 kJ/mol (Lim, Curran, & Garber, 2012). As such the coordination of 16 fewer water molecules by EF-Tu•GTP is comparable to the release of 8 water dimers from protein, which corresponds to 48 kJ/mol. Since the *in vitro* measured $T\Delta S^{\circ\ddagger}_{B}$ difference between EF-Tu•GTP and EF-Tu•GDP is ~18 kJ/mol (Table 2.1) we can estimate that the increased flexibility of EF-Tu•GDP (Fig 2.6A) contributes ~30 kJ/mol.

Forward engineering of EF-Tu`s free energy landscape

To verify our MD findings and to show that we can indeed modulate the free energy landscape of EF-Tu, we analyzed single amino acid substitution variants both in (H22G) and distal to (M112L) the nucleotide-binding pocket. We inspected the activation barriers for dissociation of GTP (reported in Mercier e*t al.*) and GDP (this work), as it defines EF-

Tu's nucleotide binding preference (above) (Mercier, Girodat, & Wieden, 2015). Consistent with our expectation, the H22G substitution, located at the N-terminus of helix A, significantly increases the entropic barrier for GTP dissociation; interestingly, this is compensated enthalpically to a similar extent (Table A1.4). The barrier for GDP dissociation, however, is only significantly affected enthalpically, consistent with a role of helix A as a nucleotide-sensing element. Our MD simulations confirm helix A as an entropic module because H22G leads to an increased SASA and a global reduction in RMSF from 0.95 to 0.90 Å per amino acid on average for the GTP conformation (Fig A1.8 D, F). Additionally, H22G increases the number of side chain hydrogen bonds per residue in the GTP conformation from 0.67 ± 0.05 to 0.80 ± 0.06 hydrogen bonds per residue for the GTP conformation, consistent with Mercier *et al*, while reducing backbone hydrogen bonds for the GDP conformation (Fig A1.8 B, C) (Mercier et al., 2015). The M112L substitution, which is distal to the binding site, does not lead to a significant change in the enthalpic barriers for dissociation, and only increases the entropic barrier for GTP and GDP dissociation to the same extent (Table A1.4). This is consistent with our MD simulations where M112L causes EF-Tu to coordinate 18 and 7 fewer water molecules for the GTP and GDP conformation, respectively, during the simulations (Fig A1.8 E). Importantly, these variants demonstrate that the thermodynamic landscape can be selectively manipulated to change only the kinetic barriers for nucleotide binding (M112L), or alter it for a particular of the two respective nucleotides (H22G) and drive the respective nucleotide binding preference into a specific direction.

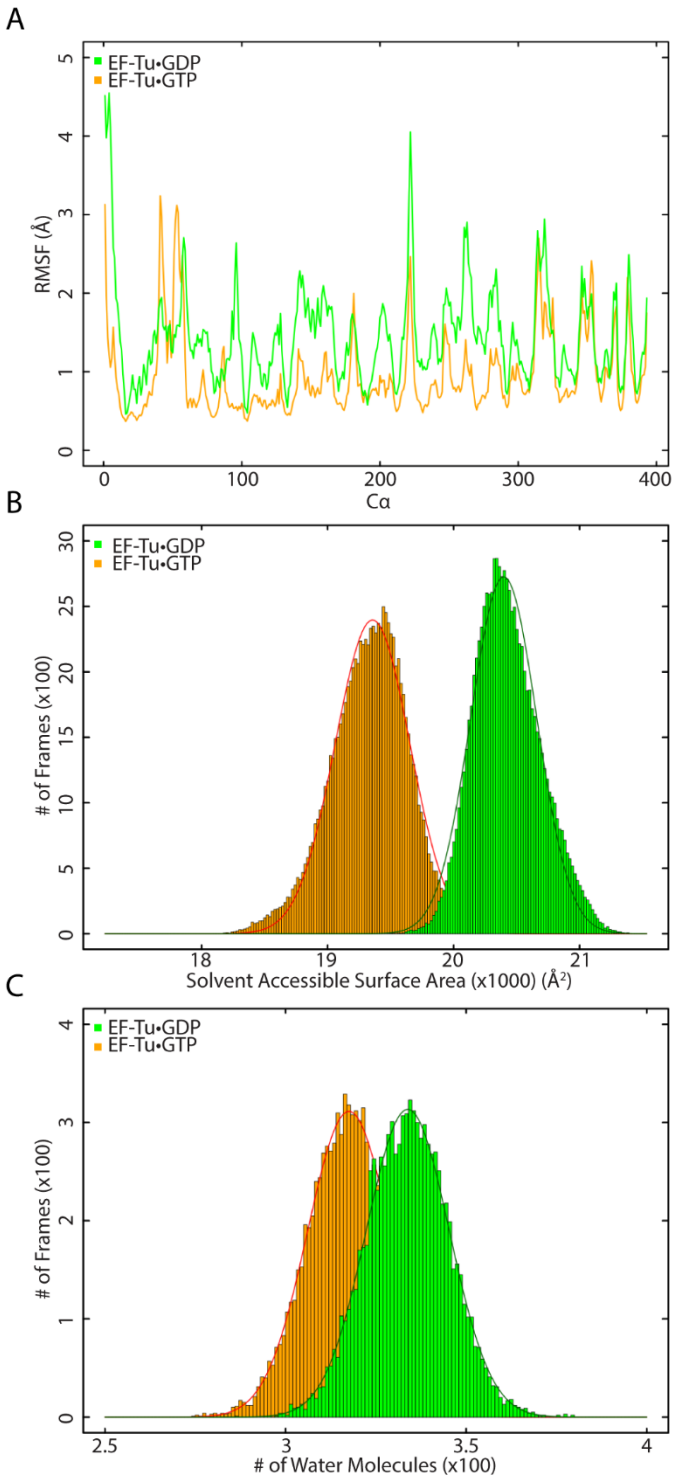

Figure 2.6 The entropic contributions of water coordination and protein flexibility. (A) RMSF of EF-Tu•GTP and EF-Tu•GDP MD simulations. (B) Solvent accessible surface area of EF-Tu•GTP and EF-Tu•GDP. (C) Water molecules within 2.5 Å of either EF-Tu•GTP or EF-Tu•GDP during the 100ns MD simulation.

2.6 Discussion

EF-Tu as a model system for biomolecular switches

Current strategies for the rational design of proteins lack the ability to develop biomolecular switches. As such, we used EF-Tu as a model protein to study and outline the thermodynamic and structural dynamics features that define protein switches. The ability to discriminate between nucleotides with a 60-fold difference in K_D along with the large conformational changes between nucleotide bound states made EF-Tu an ideal model to identify design principles that contribute to these distinct behaviors. The thermodynamic parameters of GTP and GDP binding were outlined in Talevera *et al*., but no information providing insight into the transition states, activation energies, or the structural features that lead to these parameters was reported, preventing exploitation of these features for use in protein engineering and investigation into their contribution to the evolution of this important class of regulators of fundamental biological processes (Talavera et al., 2018). We therefore determined these properties of EF-Tu to define its fundamental design features.

The thermodynamic landscape of EF-Tu has evolved via specific structural elements

When comparing the thermodynamic parameters that govern nucleotide binding in EF-Tu to other translational GTPases, EF-Tu's nucleotide binding is most closely related to EF-G (Table 2.1). The thermodynamic landscape of GTP binding for EF-Tu and EF-G are similar as both are driven by $T\Delta S°_B$. However, the $T\Delta S°_B$ of GTP for EF-Tu is 2-fold larger compared to EF-G, which ultimately results in the increased affinity that EF-Tu has for GTP relative to EF-G (Table 2.1, A1.2). Surprisingly, entropically favored binding of

GTP is not conserved amongst the translation factors, as IF2 and SelB bind GTP in an enthalpically favored process. Enthalpically favored GTP binding is more intuitive, as GTP makes three additional interactions with EF-Tu when it is bound than GDP, which should lead to a decrease in ΔH°B (Fig A1.1).

The largest differences between EF-Tu and the other translational GTPases are in the thermodynamic parameters that govern GDP binding. All of the translational GTPases are enthalpically favored in terms of GDP binding; in fact, they are all stabilized by about -25 kJ/mol except for IF2 ($\Delta H°_B$ = -40 kJ/mol, Table 2.1). In the translational GTPase family, EF-Tu is the only member that has a favorable $T\Delta S°_B$ for GDP binding (Table 2.1). The unique contribution of both $\Delta H°_B$ and $T\Delta S°_B$ for GDP enable the remarkable high affinity that EF-Tu has evolved for GDP, in comparison to the other translational GTPases. The evolution of the higher affinity EF-Tu has for GDP over GTP can be explained by two structural features of the protein: (1) switch I and (2) domain movement. EF-Tu is the only translational GTPase in which the switch I has been resolved in the GDP conformation. The other translational GTPases, EF-G, IF2, and RF3, all have disordered switch I elements (Kihira et al., 2012; Simonetti et al., 2013; Zhou et al., 2013). This allows EF-Tu to maintain hydrogen bonding in this structural element, whereas it is lost in the other translational GTPases. A similar enthalpic preference for binding GDP over GTP is observed for EF-G (Hauryliuk et al., 2008). It would be interesting to investigate if EF-G also employs the strategy of increasing backbone hydrogen bonding potential to drive this preference. Secondly, the large domain rearrangement of EF-Tu between EF-Tu•GDP and EF-Tu•GTP facilitates differences in the SASA and in turn the hydration sphere. The ability of EF-Tu•GTP to occupy the open (GDP-like conformation), recently shown by Johansen

et al and Kavliauskas *et al* (Johansen et al., 2018; Kavaliauskas et al., 2018), might also contribute to the measured entropic preference for GTP binding. Although, the timescale of the open to closed transition is too slow (ms timescale) to be captured in all-atoms MD simulations, the higher flexibility in helix A reported here for EF-Tu•GTP (compared to EF-Tu•GDP) is likely an indication of how this conformational change is triggered (Talavera et al., 2018). Helix A is adjacent to switch I which is one of the first structural elements predicted to undergo conformational change (Lai, Ghaemi, & Luthey-Schulten, 2017). Since helix A contacts switch I in the GTP-bound conformation, the increased flexibility of helix A observed here in short MD simulations is likely related to the large-scale conformational flexibility reported (Johansen et al., 2018; Kavaliauskas et al., 2018). Therefore, the favorable $T\Delta S°_B$ for GTP binding is further amplified by the domain rotation and separation.

The evolutionary advantage of increasing backbone hydrogen bonding rather than sidechain hydrogen bonds to stabilize the GDP conformation of EF-Tu is the increased sequence space that the EF-Tu can sample, creating a mechanistic feature that is robust with respect to mutations and sequence variations, consistent with EF-Tu as an essential protein. Since the backbone of the protein is what stabilizes the GDP conformation, the sidechains will have more freedom in their ability to vary without altering the stability of the GDP conformation. This is particularly important for an enzyme like EF-Tu whose sequence space is already limited due to the number of conserved interfaces EF-Tu has because of the variety of ligands it interacts with during its functional cycle. This includes interfaces with aa-tRNA, EF-Ts, nucleotides, and the ribosome.

Antibiotics target the structural features that stabilize the EF-Tu conformations

We aligned EF-Tu with the structures of EF-Tu bound to the following antibiotics: GE2270A, kirromycin, pulvomycin, enacyloxin IIa, aurodox, nvp-1ou796, nvp-1ff571, nvp-1di028, or nvp-1dk733 (PDB ID: 2C77, 1OB2, 2C78, 1OB5, 1HA3, 4G5G, 3U2Q, 3U6B, and 3U6K respectively) (Fig 2.5F, G) (LaMarche, Leeds, Amaral, et al., 2012; LaMarche et al., 2011; LaMarche, Leeds, Dzink-Fox, et al., 2012; Parmeggiani, Krab, Okamura, et al., 2006; Parmeggiani, Krab, Watanabe, et al., 2006; Vogeley, Palm, Mesters, & Hilgenfeld, 2001). These antibiotics induce either the GTP or GDP state of EF-Tu and are shown on the structures which they favor. Interestingly, antibiotics that favor the GDP-bound conformation bind in regions where hydrogen bonds stabilize the GTP-bound conformation and vice-versa. The antibiotics kirromycin, pulvomycin, enacyloxin IIa, and aurodox bind between domain I and III where switch II is located (Fig 2.5G). In this region of EF-Tu, nine hydrogen bonds that favor the GDP state are located, suggesting that these antibiotics may destabilize these hydrogen bonds leading to the 9.8- and 8-fold decrease in affinity to GDP in the case of pulvomycin and enacyloxin IIa, respectively (Table A1.6) (Anborgh, Okamura, & Parmeggiani, 2004; Cetin et al., 1996). The antibiotics may also add to the bonding potential of this region for the GTP state, as the off rate of GTP is decreased by 100-fold for kirromycin, GE2270A, pulvomycin, and enacyloxin IIa (Table A1.6) (Anborgh et al., 2004; Cetin et al., 1996; Fasano, Bruns, Crechet, Sander, & Parmeggiani, 1978). Likewise, the antibiotics that stabilize the GDP conformation of EF-Tu bind to domain II where seven hydrogen bonds stabilize the GTP conformation of EF-Tu (Fig 2.5F). To our knowledge there is no kinetic data available reporting the effect these antibiotics have on the kinetics of EF-Tu nucleotide binding. In summary, we propose that these antibiotics function by modulating the enthalpic contributions of intramolecular backbone hydrogen bonds thus inhibiting EF-Tu's function. In turn, this subtle approach of

modifying EF-Tu's backbone hydrogen bonding can be utilized for the development of novel antimicrobials, as well as the rational design of inducible switch properties by modulation through small molecular ligands.

Furthermore, to test our hypothesis that the open to closed transition does contribute to the measured entropic preference of GTP binding, we measured the entropic contribution to nucleotide binding in the presence of the antibiotic kirromycin. Kirromycin binds at the interface of domains I and III, directly targeting several hydrogen bonds favoring the GDP conformation in switch II (Fig 2.5G), and stabilizes the closed (GTP-bound) conformation of EF-Tu. To probe the structural features that contribute to the thermodynamic landscape of EF-Tu, we then performed nucleotide binding experiments in the presence of 5μM kirromycin. We observed that kirromycin reduces the k_{off} of GTP 6-fold (at 37°C), which is consistent with our hypothesis that conformational change from the closed to open conformation contributes to the free energy barrier for GTP dissociation. For the GDP branch, kirromycin enhances the k_{off} of by 9-fold (at 37°C), consistent with the contribution of hydrogen bonding in switch II to the enthalpic barrier of GDP dissociation. Altogether, kirromycin reduces the free energy of GTP binding so that EF-Tu has similar affinity for both GTP and GDP, demonstrating that specific modules identified in MD simulations (Fig 2.7) can be targeted to modulate nucleotide binding properties in EF-Tu.

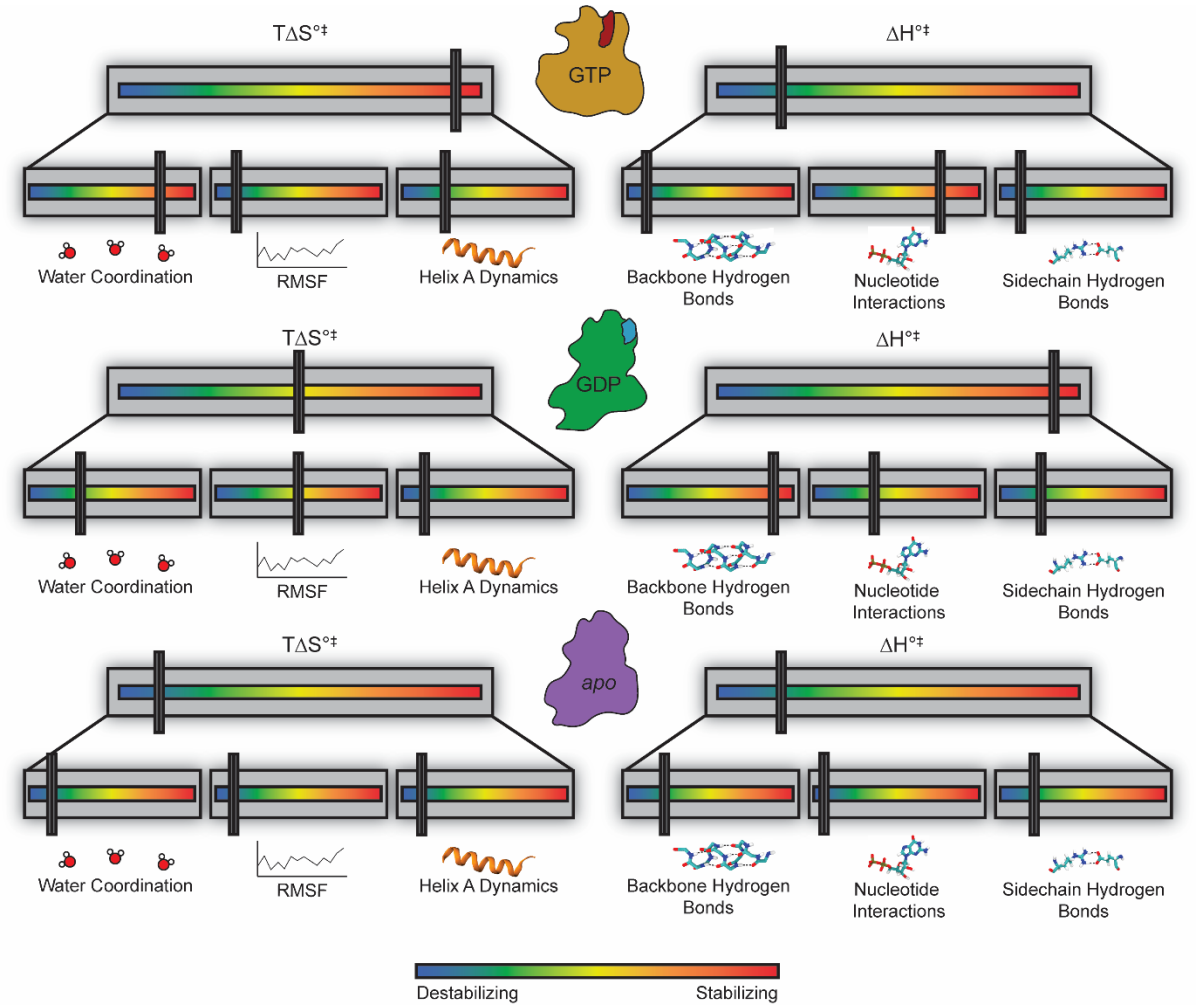

Figure 2.7 Features that enable the thermodynamic fine-tuning of the nucleotide-bound states of EF-Tu. EF-Tu•GTP is entropically stabilized through increased dynamics of regions like helix A and coordination of fewer water molecules than EF-Tu•GDP or *apo* EF-Tu. EF-Tu•GDP is entropically stabilized due to higher overall RMSF than EF-Tu•GTP or *apo* EF-Tu. EF-Tu•GDP is enthalpically stabilized from an increased number of backbone hydrogen bonds, where an increased number of sidechain hydrogen bonds has a minimal impact. *apo* EF-Tu is less stable than EF-Tu•GTP or EF-Tu•GDP and likely has little contribution from the highlighted features towards stabilizing the conformation.

Rational design of biomolecular switches

Here we demonstrate a workflow that can be applied to the rational design of molecular switches by forward engineering a quantifiable free energy difference in the 'on' and 'off' conformations. We show with EF-Tu that understanding the origins of the free energy change from the GTP- to the GDP- bound form guides analysis of MD simulations,

which can then be used as the focus for *in silico* screening of variants. Since this approach starts with thorough understanding of the thermodynamic landscape for ‘on’ to ‘off’ transition, the initial selection of a molecular switch is important for rational design. The workflow, however, is highly portable since it allows the manipulation of the free energy of switching by mutating amino acids distal from the nucleotide binding pocket and/or effector-binding sites.

2.7 Conclusion

Several structural and dynamic features play a role in contributing to the enthalpic stabilization of EF-Tu•GDP and the entropic stabilization of EF-Tu•GTP. For example, the entropic stabilization of EF-Tu is facilitated through coordinated water molecules, backbone flexibility, and helix A dynamics, whereas the features that contribute to EF-Tu enthalpic stabilization are backbone hydrogen bonds, nucleotide interactions, and sidechain hydrogen bonds (Fig 2.7). Evolution has fine-tuned the thermodynamic contribution of these different features in both conformations of EF-Tu, leading to the 60-fold higher affinity towards GDP.

Chapter 3

Protein Characterization for Personalized Medicine: Unveiling the Dynamics of D2 Dopamine Receptor Activation

3.1 Forward

Chapter 3 of this thesis focuses on the role of GPCRs in regulation of G-protein coupled signaling activity. This chapter is written for submission to *Proceedings of the National Academy of Sciences of the United States of America* (PNAS). The concept of the manuscript was developed by Hans-Joachim Wieden and I, and all experiments were performed by myself. Evan Mercier developed the Cα covariance analysis scripts and Darren Gemmill assisted in development of the D2R model for MD simulations. In this chapter MD simulations of 33 variants of the D2R receptor were performed based on biochemical data reported by Sung *et al.* to analyze the perturbations of D2R structural dynamics (Sung, Wilkins, Rodriguez, Wensel, & Lichtarge, 2016). Through a combinatorial approach of principal component analysis (PCA), Markov State Modelling (MSM), and clustering, 5 unique conformations of D2R prior to activation were revealed. By grouping variants that are high-, normal-, or low-activity into these clustered conformations I gain insight into how the D2R variants perturb the protein. Since low-activity variants are localized to cluster 2 I label this as a conformation of D2R that is less likely to lead to activation. Similarly, high-activity variants were localized to clusters 4 and 5. Using an in-house developed Cα covariance and shortest pathway analysis, an allosteric communication pathway for D2R was identified whereby allosteric communication via $G380^{6.42}$ inhibits D2R activation, and communication via $F382^{6.44}$ stimulates activity. The term allosteric communication refers to how distal regions of a protein are influenced, structurally or dynamically, by the perturbation at the proximal site. Allosteric communication pathway in this thesis refers to a sequence of amino acids whose dynamics

are correlated, indicating that perturbation of one of these amino acids would influence the dynamics of all others on the pathway.

Using the identified dynamic characteristics of the D2R variants I analyze the features of the V154I variant of D2R that leads to the rare disease Myoclonus Dystonia to unveil that this variant leads to dynamics that would classify it as a low-activity variant yet retains an allosteric communication pathway similar to high-activity variants. I provide for the first time information on the perturbation in D2R as a consequence of this variant since it retains wild-type-like GEF activity in the HEK293 cell line (Klein et al., 1999; Klein et al., 2000). Altogether, I provide an MD analysis of the D2R GPCR to revealing 5 different conformations that the G_i protein can populate, and which of these conformations is likely to lead to guanosine nucleotide exchange, explaining the transition problem of G_i binding which reflects an MWC model. Additionally, I show the allosteric communication pathway of D2R, providing for the first time a solution to the transmission problem of allostery for D2R.

3.2 Abstract

G-protein coupled receptors (GPCRs) are transmembrane proteins that activate signalling pathways upon binding to a receptor specific ligand. Previous studies have shown that GPCRs adopt multiple conformations prior to activation which can structurally resemble features of the active or inactive state (Casiraghi et al., 2019; Kobilka & Deupi, 2007; Lee et al., 2015; Nygaard et al., 2013; Weis & Kobilka, 2008). A detailed description of how GPCRs transition between these conformations is lacking and it is unclear how many of these conformations are sampled prior to activation. To gain a better understanding of the GPCR conformational ensemble and the transitions between them, I performed MD simulations of the D2 dopamine receptor (D2R). Using Markov State Modelling (MSM) I show five distinct conformations that the D2R can sample prior to activation. Of these conformations, one resembles the inactive crystal structure while two are more closely related to the activated conformation. To understand in greater detail the allosteric mechanism of D2R activation I processed the correlated dynamics of Cα atoms of D2R to describe allosteric pathways between the ligand-binding pocket of D2R to the G-protein interface. Two observed communication paths direct ligand binding information towards either $G380^{6.42}$ or $F382^{6.44}$, the pivot point for transmembrane helix (TM) 6 kinking, in low-activity and high-activity variants, respectively. This communication must proceed through $F202^{5.51}$ and $Y199^{5.48}$, residues predicted to be critical in GPCR activation, which partition communication between TM6 and TM3 (Drora et al., 2011). Finally, I demonstrate using our analysis pipeline that the D2R variant V154I (which is associated with the rare disease Myoclonus Dystonia) reveals dynamics similar to the low-activity variants, yet causes a disruption of Cα covariance similar to high-activity variants. Therefore, the V154I variants

has dynamics similar to low-activity variants, but lacks communication to TM6 that prevents its kinking, revealing for the first time insights into the molecular basis of the V154I D2R variant leading to Myoclonus Dystonia.

3.3 Introduction

Advancements in sequencing technologies are opening up avenues for administering patient-specific personalized medicine. Personalized medicine is a promising approach for treatment of diseases ranging from cancer to neurological disorders, and is proving essential for preventative care (Deng & Nakamura, 2017; Prendes-Alvarez & Nemeroff, 2018; Strafella et al., 2018). Implementation of personalized medicine is restricted due to the difficulties in connecting genotype to phenotype (Roden, 2011). Individual genomes can vary at up to five million sites, making it difficult to directly link subtle changes like a single nucleotide polymorphism (SNP) to a particular disease or disability, especially if they are patient specific (Consortium, 2015). Additionally, the impact that a large number of SNPs or other genetic variation have on protein function is uncharacterized.

To aid in this venture I propose a computational pipeline, Protein Characterization for Personalized Medicine (PCPM), capable of sorting protein genotypes into phenotypical categories based on their structural dynamics. Thereby, PCPM will provide critical information allowing for direct application of personalized medicine. To validate our PCPM technology, I employed it to study the structural dynamics of GPCRs. Mutations in GPCRs lead to a plethora of diseases and disorders from cancer to color blindness (Schönenberg et al., 2004). Additionally, GPCRs are the target of roughly a third of all pharmaceutical drugs making it critical to understand the impact of mutations for administration of the optimal therapy (Hauser et al., 2017; Rask-Andersen et al., 2014; Santos et al., 2017). GPCR-targeting drugs mimic the mechanism of agonists, partial agonists, or antagonists either activating or deactivating the protein receptor. The treatment

can be primary, targeting an impaired GPCR, or secondary, where the alteration of the GPCR activity impacts a downstream process. Regardless, treatments are often patient-specific where point mutations result in attenuation of the efficacy of the drug. Therefore, identification of how particular GPCR variants alter the protein's functionality is essential for proper treatment. Altogether, these features make GPCRs prime targets for personalized medicine.

The fundamental principle of PCPM is to study the resting state of a protein to understand how the conformational ensemble is altered *via* mutations. GPCRs can adopt several conformations prior to binding to ligand (agonist, antagonist, partial-agonist, reverse agonist, G-protein, or arrestin), some of which have a higher or lower probability of transitioning into the activated state (Casiraghi et al., 2019; Kobilka & Deupi, 2007; Manglik et al., 2015; Nygaard et al., 2013). When the equilibrium of the protein's conformational landscape is shifted (through mutations), the probability of transitioning into the active state and sensitivity to ligands is altered. Therefore, understanding how mutations modify the conformational landscape of a GPCR prior to activation will inform on a mutation's particular impact on receptor activity.

Here I investigate the GPCR D2R using PCPM to investigate how single or double mutations affect the dynamics of the receptor, ultimately leading to modulation of its activity. Our approach analyzes the overall dynamics of the protein by consolidating the protein's principal components (PC), the dominant conformational ensembles, and Cα covariance describing allosteric communication pathways in the presence of each substitution. By combining these factors, I categorize variants into a phenotypical category of high, normal, or low activity, indicating that they lead to a higher, normal, or lower

probability of being activated upon dopamine binding. D2R was used as a proof-of-concept system for our PCPM pipeline, because mutations to this receptor are linked to the rare disease Myoclonus Dystonia, and it is a prime target for Parkinson's disease, depression, and schizophrenia (Bonci & Hopf, 2005; Klein et al., 1999; Masri et al., 2008; McCall, Lookingland, Bédard, & Huff, 2005). Recently Sung *et al.* (2016) performed sequence alignments of the UniRef90 database to identify several amino acid variant pairs in the D2R receptor that co-evolve together (Suzek et al., 2015). The co-evolved D2R variant pairs are distal on the protein structure and lead to non-additive changes to the activity of the GPCR, as measured by changes in the receptor activity on the surface of HEK293 cell (Sung et al., 2016; Suzek et al., 2015). Interestingly, these variants do not have significantly different affinities to dopamine but are activated by the ligand to different extents (Table A3.1). Therefore, these amino acids must be allosterically coupled. These properties of the D2R variants characterized by Sung *et al.* provide an excellent data set to develop a standard for our PCPM pipeline, as the impact that these mutations have on the dynamic features of D2R can be analyzed and correlated to the respective activity of the receptor.

Here I report for the first time 5 distinct conformational states of D2R prior to ligand binding by employing MD simulations and Markov State Modelling (MSM). The low-, normal-, or high-activity variants identified by Sung *et al.* (2016) partition into specific conformational states allowing us to identify structural dynamic features of D2R that are required prior to activation. Additionally, I measured Cα covariance to predict the allosteric activation of D2R, revealing that low-activity variants block activation by rigidifying TM6, preventing helical rearrangement. This analysis also shows that $Y199^{5.48}$ (superscript refers to Ballesteros-Weinstein numbering, where the first X is the transmembrane helix in which

the residue resides and the second is the position relative to the most conserved residue) is a critical hub for partitioning information leading to activation (Balesteros & Weinstein, 1995). Combining the dynamic features of the D2R variants coupled with Cα covariance I provide an analysis that allows us to identify the V154I variant of D2R as a protein with dynamic features resembling a low-activity variant but with the allosteric communication network of high-activity variants. Therefore, this analysis provides an explanation for the confounding results that V154I is linked to Myoclonus Dystonia, yet, little to no observable changes in *in vivo* ligand binding or activity of the protein were identified (Klein et al., 1999; Klein et al., 2000).

3.4 Materials and methods

D2 Dopamine homology model construction

Construction of a D2R homology model was performed using a similar approach as described in Platania *et al.,* 2012 (Platania, Leggio, Drago, & Bucolo, 2012). In brief, the X-ray crystal structure of the human dopamine D3 receptor (D3R)-Lysozyme chimera was retrieved from the protein database (Protein Data Bank-code 3PBL) (Chien et al., 2010). The amino acid sequences of the human dopamine D2 and D3 receptors in the FASTA format were retrieved from the UniProt server (UniProt ID: P14416) (The UniProt Consortium, 2017). Clustal Omega was used to align these sequences which were then used to create a homology model of D2R in combination with the crystal structure of D3R using the SWISS-MODEL server (Arnold et al., 2006; Goujon et al., 2010; Lorenza Bordoli et al., 2008; McWilliam et al., 2013; Sievers et al., 2011). The N-terminus (amino acids 1-31) and ICL3 (amino acids 222 and 319) of D3R were not resolved in the crystal structure and therefore, the N-terminus (amino acids 1-37) and ICL3 (amino acids 222-363) of D2R were excluded from the homology model (Chien et al., 2010).

The resulting homology model of D2R was embedded into an 80x80 Å phosphatidylcholine (POPC) bilayer which was generated using the VMD-1.9.1 software package (Humphrey et al., 1996). Hydrogen atoms were added to the model using the psfgen package in VMD, where only the ε-nitrogen of histidine was protonated (Humphrey et al., 1996). The system was then solvated by adding water molecules extending 10Å from the surfaces of the POPC bilayer using the solvate package in VMD (Humphrey et al., 1996).

Molecular dynamics simulations

MD simulations were performed as previously described in Wieden *et al.* 2012 and Mercier *et al.*, 2015 using the NAMD 2.6 software with CHARMM27 force fields (Brooks et al., 2009; Mercier et al., 2015; Phillips et al., 2005; Wieden et al., 2010). In brief, the water, followed by the lipid bilayer, and finally the protein in the model of the D2R embedded in the POPC bilayer were minimized for 10 000 steps using two iterative rounds. This was then followed by a 100 000 step minimization of the entire system. Na^+ and Cl^- ions were added to the system corresponding to a concentration of 100 mM using the autoionize package in VMD (Humphrey et al., 1996). The system was then relaxed for another 100 000 steps until the energy was constant for 1000 steps. D2R variants were constructed by modifying the minimized D2R model with the mutator plugin V1.3 in VMD (Humphrey et al., 1996). The water, POPC bilayer, and then finally the protein were minimized for 10 000 steps for each D2R variant, before Na^+ and Cl^- ions were added to 100 mM. Each D2R variant was minimized for a final 100 000 steps until a constant energy was maintained for 1000 steps.

MD simulations were performed at 1 atm pressure using a Nosé-Hoover-Langevin piston in an NPT ensemble using periodic boundary conditions with a 12 Å cut-off distance for non-bonded interactions. The system was equilibrated and heated for 300 000 steps to 300 K or 350 K at 0.5 fs time steps. Simulations were performed at a time step of 2 fs using the velocities from the 300 K and coordinates from the 350 K equilibrations for 100 ns.

Principal component analysis

Principal components were measured using NMWiz in Prody 1.10.6 and visualized with VMD (Bakan et al., 2014; Bakan, Meireles, & Bahar, 2011; Humphrey et al., 1996). The number of populations in the PCA landscape (PC1 x PC2 2D heat map) was determined by peak selection of maximums in the Z-score of the heat map.

Cα covariance Analysis

C_α covariance was calculated using Carma software using equation 3.1 or through an in-house developed approach using equation 3.2 (Glykos, 2006).

$$c_{ij} = \frac{\langle (x_{i,t} - \bar{x}_i) \bullet (x_{j,t} - \bar{x}_j) \rangle}{\left(\langle (x_{i,t} - \bar{x}_i) \rangle^2 \langle (x_{j,t} - \bar{x}_j) \rangle^2 \right)^{1/2}} \tag{3.1}$$

$$\theta_{(t)} = \arccos\left(\frac{(x_{i,t} - x_{i,t-dt}) \bullet (x_{j,t} - x_{j,t-dt})}{|x_{i,t} - x_{i,t-dt}||x_{j,t} - x_{j,t-dt}|} \right) \tag{3.2}$$

Here c_{ij} is the normalized covariance between amino acids i and j, $x_{i,t}$ and $x_{j,t}$ are the Cartesian coordinates of the Cα of amino acids i and j at frame t, $\bar{x}_i$ and $\bar{x}_j$ are the time-averaged Cα Cartesian coordinates of amino acids i and j, and $\langle\ \rangle$ indicate the time-averaging of the quantities inside the brackets and magnitude respectively. In equation 3.2 $\theta_{(t)}$is the angle between the vectors produced from $x_{i,t} - x_{i,t-dt}$ and $x_{j,t} - x_{j,t-dt}$ and $|\ |$ denotes the magnitude of that vector. The normalized covariance calculated from each frame using equation 3.1 was used to plot a histogram where amino acids were defined to have significant covariance if they deviated more than 3 standard deviations from the mean of the histogram. Likewise, $\theta_{(t)}$ for each frame was used to create a histogram to determine which C_α pairs have significant covariance. The histogram was fit with equation 3.3 where $E(\theta)$ is the expected counts and C_{total} is the total number of θ counted. If the $\theta_{(t)}$ histogram deviates from a random distribution then the amino acid pair are considered as covariant.

$$E(\theta) = C_{total}\frac{1}{2}\sin(\theta)d\theta \quad (3.3)$$

A χ^2 analysis was used to determine which C_α pairs deviate from a random distribution.

Network construction

All protein networks were constructed in Gephi-0.9.1 were each node represents an amino acid and edges are drawn between amino acids if they have significant covariance (described above) and they maintain a distance of 4.5 Å between their Cα's for 75% of the simulation time. The size of each node is determined by the nodes, Betweenness Centrality ($Bx(n)$) value which was calculated with equation 3.4 where σ_{st} is the number of shortest paths from node s to t and $\sigma_{st}(n)$ is the number of shortest paths from node s to t that pass through node n.

$$Bx(n) = \sum_{s\neq n\neq t}\frac{\sigma_{st}(n)}{\sigma_{st}} \quad (3.4)$$

Shortest path analysis

Shortest paths (SPs) were determined as paths that cross the fewest number of nodes in order to connect amino acids involved in dopamine binding (D) with amino acids involved in G-protein interactions (G). SP(n) is the occurrence of an amino acid on a SP between amino acid groups G and D was calculated with equation 3.5, where $\sigma_{st}(n)$ is the number of shortest paths between amino acid s and t passing through node n. The SPs were then normalized by dividing SP(n) by the amino acid with the highest SP(n) value.

$$SP(n) = \sum_{s\in D}\sum_{t\in G}\sigma_{st}(n) \quad (3.5)$$

Markov state model

Each of the trajectories were projected into a reduced dimension space by measuring the Φ, Ψ, and χ dihedral angles. The time-independent components of the dihedral angles were calculated using the MSMBuilder (Beauchamp et al., 2011). A lag time of 1ns with 8 time independent component analysis (tICA) and 200 MSM microstates was used. The number of microstates was reduced to match the tICA plot. This was then used to determine the Markov State Model.

3.5 Results

Assessment of the D2R simulations

MD simulations on 33 variants of D2R identified by Sung *et al*. (2016) were performed for 100 ns each to assess the conformational equilibrium of the respective D2R. These D2R variants range from negligible activity (L379F) to variants with a 6-fold increased activity (Y199F) (Table A2.1). To infer the stability of our MD simulations, I measured the RMSD during the course of the 100 ns simulation, a simulation length often used to study D2R dynamics, altogether totalling 3.4 μs of simulation time for the 33 variants alongside wild type (wt) D2R (Kaczor et al., 2016; Podder, Pandey, & Latha, 2016; Salmas, Yurtsever, & Durdagi, 2017). All of the D2R variant simulations were stable after 10-30 ns of production time (Fig A2.1A). This is reflected in the RMSD that reaches values ~2-4 Å which then are maintained for the remainder of the simulations (Fig A2.1A).

Dynamic diversity of D2R and variants

To understand the diversity of the dynamics available to D2R before activation, I performed a principal component analysis for wt D2R (Fig 3.1A) and each variant (Fig A2.2). The PC1 of high-activity variants (>2-fold increase in activity as reported by Sung *et al*. – Y199F, V91S, T205M, L171P, I48T, F202L/Y213I, and F110W) involves opening of the ligand-binding pocket (Fig 3.1B). In contrast, PC1 of the low-activity variants (<2-fold activity as reported by Sung *et al.* (2016) – L379F, S193G/C385M, S193G, N124H/L379F) shows that the dominant motion is closing of ligand-binding pocket (Figure 3.1C). Remarkably, Sung *et al.* (2016) showed that these variants do not have an impact on the affinity of D2R towards dopamine or serotonin (at most a 1.25- or 1.28-fold increase or

decrease in K_i respectively) (Table A2.1). This suggests that these different motions do not contribute to the binding of the ligand, but indicate that the conformational sampling of D2R prior to ligand binding may influence the receptor's activity. For a more detailed investigation of these motions the distances of the TM helices on the extracellular and surface (Fig 3.1 D, E) were analysed. In comparison with wt D2R the high-activity variants exhibit a movement of TM3 away from the ligand binding pocket, opening the receptor (Fig 3.1 D). In contrast, the low-activity variants display a movement of TM6 and TM7 inwards to the ligand binding pocket consistent with the principal component identified for these variants (Fig 3.1 C, E).

The number of populations revealed by the PCA indicates that low-activity variants are more dynamic and can adopt more states (Fig 3.1F). This is also reflected in the average Root Mean Squared Fluctuation (RMSF) of the variants (Fig 3.1G). In particular, the low-activity variants have an increased flexibility in ECL1 and 2 (E99-F102 and G173-A185) (Fig 3.1G). Consistent with this, the high-activity variants adopt fewer states, identified by PCA, and have a lower average RMSF except for ICL3 and ECL3 (Fig 3.1 F, G).

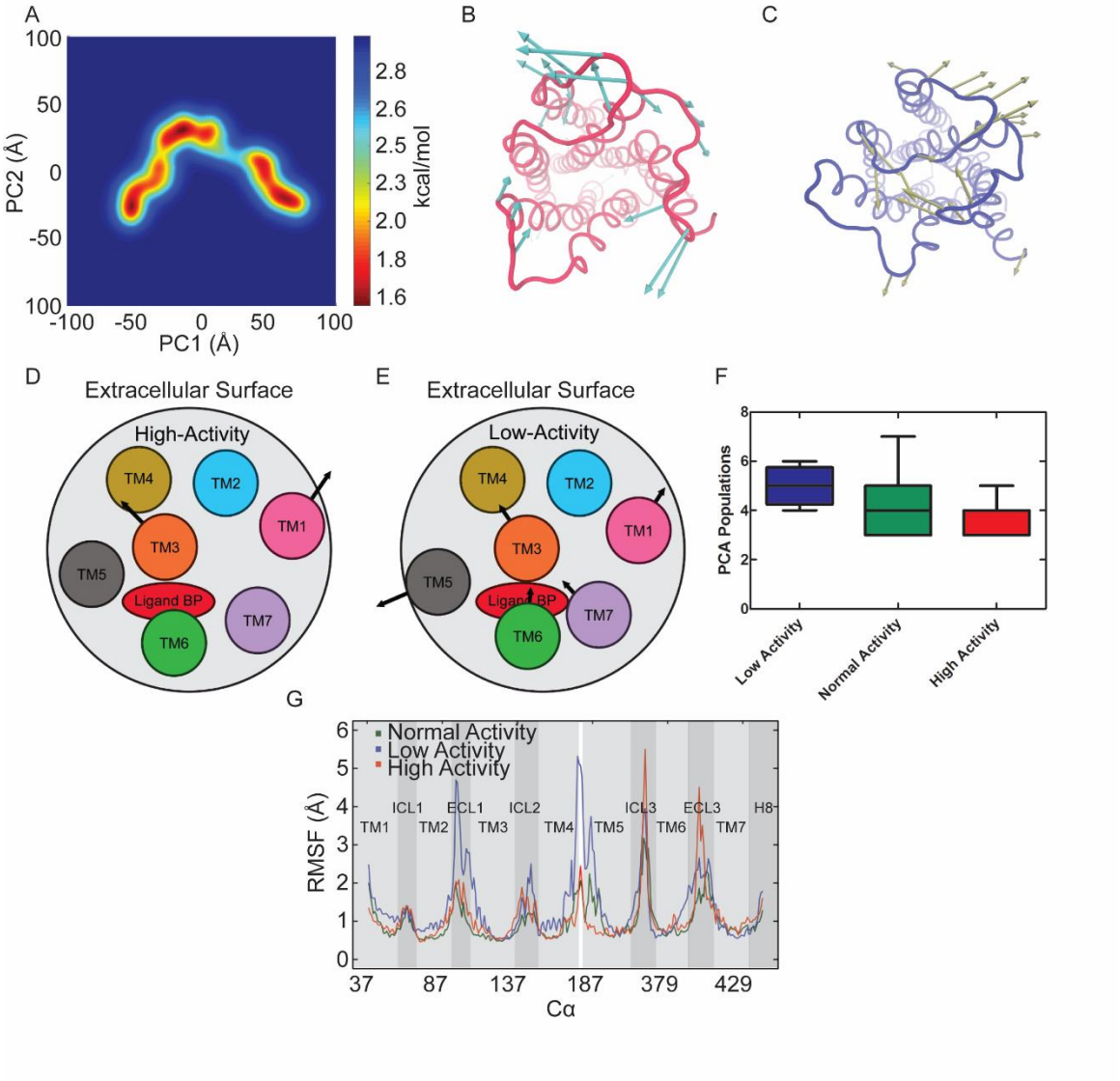

Figure 3.1 Dynamics of the wt and variants of D2R. (A) PCA of wt D2R. (B) PC1 of Y199F (high-activity) D2R, cyan arrows indicate the direction and magnitude of PC1. (C) PC1 of L379F (low-activity) D2R, tan arrows indicate the direction and magnitude of PC1. (D,E) Average distance of the high- and low-activity variants, extracellular TM helices compared to wt D2R, arrows indicate the magnitude of the distance. (F) Number of populations identified by PCA for the high-, normal-, and low-activity variants. (G) Average RMSF of low-, normal-, and high-activity variants of D2R

Conformations of the D2R correlate with receptor activity

The different states identified by PCA are based on the dynamic properties of the protein. To assess the stability of these states, and to identify different variants that sample the same states, I performed tICA and MSM. tICA was used to identify the number of stable conformations that the wt D2R and the variants could adopt (Fig A2.3). The number of conformations were equal to the number of k_{means} clusters that were present (Fig A2.3). Although there is no significant difference between low-, normal-, and high-activity variants for the number of conformations, the trend is the same as it was for the number of states identified for PCA. Consistent with the PCA analysis, the low- and high-activity variants have the most and fewest states or conformations respectively (Fig 3.2A).

To determine if the states identified by tICA are similar between the different variants, all of the tICA identified states were clustered with maxcluster (Ortiz, Strauss, & Olmea, 2002). Maxcluster revealed that within all of the variants of D2R five unique conformations of the GPCR are sampled (Fig 3.2B). Comparing these conformations indicates that conformation 2 is usually sampled by the low-activity variants, where conformation 3 is sampled by the normal-activity variants, and conformations 4 and 5 are predominately sampled by the high-activity variants (Fig 3.2C). Altogether, this suggests that the variants lead to a shift in the frequency by which the respective conformations are sampled by D2R prior to ligand activation.

Through summation of the transition probabilities between the different tICA states (Fig A2.4) a transition matrix was applied to the maxcluster conformations (Fig 3.2D-F). Low-activity variants have a higher probability of transitioning between conformations 1 and 2 and a low probability of sampling conformations 3, 4, and 5 (Fig 3.2D). Normal-

activity variants have a tendency to transition between conformations 2 and 3, with a lower probability of transitioning between conformations 1, 4, and 5 (Fig 3.2E). Lastly, high-activity variants transition between conformations 4 and 5 using a path that takes the variant through conformation 2. These variants rarely transition to conformations 1 or 3 (Fig 3.2F). It is interesting to note that all of the variants regardless of the activity transition through conformation 2, the conformation most occupied by the low-activity variants. This suggests that D2R may have to pass through conformation 2 on the path to activation and that the low-activity variants stall the protein in this state, preventing adequate activation of the receptor.

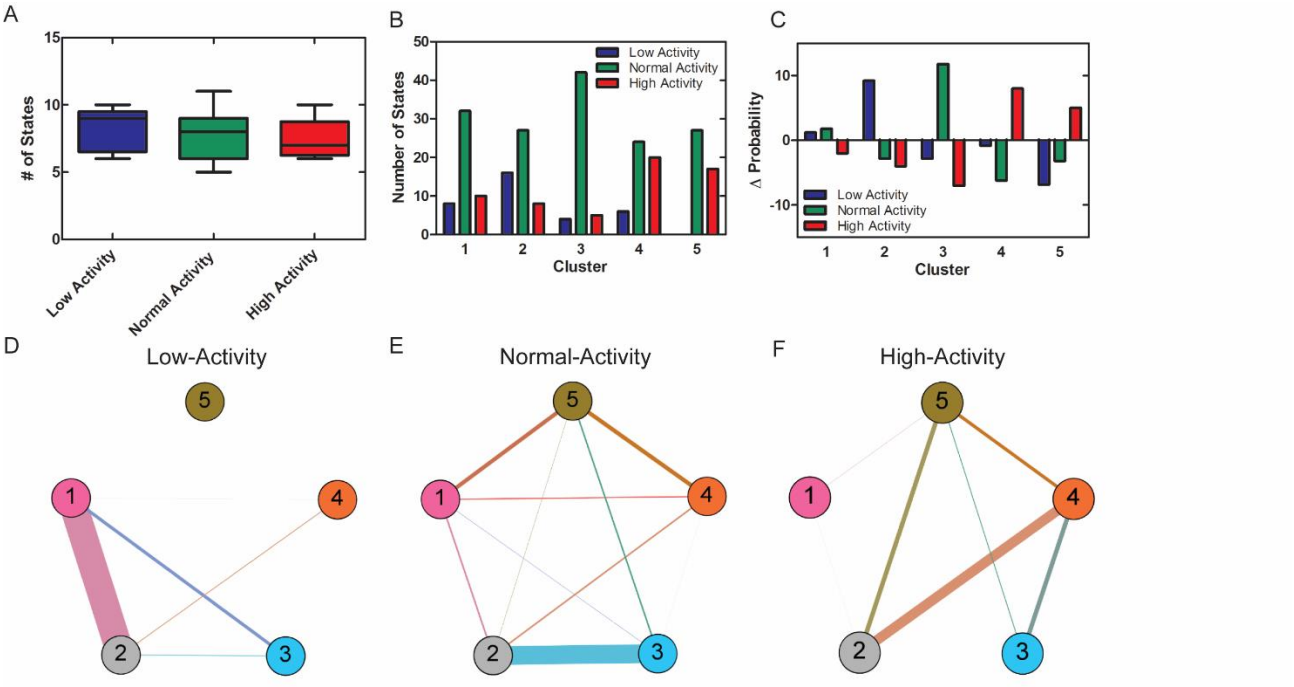

Figure 3.2 Markov state model (MSM) identified conformations of D2R and the probability of transitions between them. (A) Number of states for low-, normal-, and high-activity variants of D2R as identified by tICA. (B) The 5 Maxcluster conformations of D2R and the number of low-, normal-, and high-activity variant states that are assigned to each conformation. (C) The change in probability of low-, normal-, or high-activity variants being located in each of the Maxcluster conformations. (D-F) MSM transitions between each of the conformations identified by Maxcluster.

Features of the D2R conformations

Maxcluster separates structures into different clusters using 3D-Jury which produces a Max-sub score based on Cα's within 3.5 Å of each other in the structure after optimal alignment (Ginalski, Elofsson, Fischer, & Rychlewski, 2003; Siew, Elofsson, Rychlewski, & Fischer, 2000). This does not give a detailed description of the features that separate the 5 conformations. As such, I investigated the structural dynamic differences between these conformations. The first parameter I looked at was the Solvent Accessible Surface Area (SASA) of the protein (Fig 3.3A). Cluster 3 has the lowest SASA of all conformations with an average of 1.46×10^4 Å^2, where the rest have a similar average, within 240 Å^2 of each other. This indicates that cluster 3, which is populated by the normal-activity variants, is the most compact conformation of the protein. This is consistent with our findings where the dominant motion for the high-activity variants is an opening of the extracellular surface where low-activity variants open at the intracellular surface (Fig 3.1B, C, A2.10, A2.11). A more compact conformation of D2R may suggest that this conformation is not ideal for ligand binding, therefore, the protein has to transition into another state to open up for ligand docking.

To understand the enthalpy, which reflects the stability of each of the states, I measured the backbone and side chain hydrogen bonds and salt bridges of the protein (Fig 3.3B, A2.9). There was little to no difference in the number of side chain hydrogen bonds or salt bridges between the D2R conformational clusters (Fig A2.9). However, as has been shown previously, backbone hydrogen bonds are a major contributor to the enthalpic stability of a protein conformation (Girodat et al., 2019). Here I see that clusters 3 and 5 have ~0.08 fewer backbone hydrogen bonds per residue than the other clusters (Fig 3.3B).

With 263 residues in the simulation this would account for a mean change of ~21 hydrogen bonds. Since hydrogen bonds can have a dissociation energy of <16kJ/mol, these differences likely contribute significantly to the enthalpy of the different clusters (Steiner, 2002). Altogether this suggests that conformation 3 and 5 are enthalpically more stable than the other conformations of D2R. The enthalpic stability of conformation 3 is likely the reason why the normal-activity variants, which should have a similar conformational ensemble of wild-type D2R, predominately reside within this cluster. The variants leading to lower or higher activity of D2R perturb the protein enough to allow for escape from the enthalpic stability of conformation 3, whereas normal-activity variants do not.

Since activation of GPCRs requires a conformational change of TM6, I measured the RMSD of this helix, as well as of the whole protein (Fig 3.3 C, D) (Farrens et al., 1996; Rasmussen, DeVree, et al., 2011; Yao et al., 2006). The RMSD values are a comparison from the clustered states to the initial homology model of the wt D2R (Fig 3 C, D). Cluster 5 has the largest overall RMSD as well as in TM6; therefore, TM6 of cluster 5 is in the most different conformation compared to the inactive state of D2R (Fig 3.3C, D). As kinking of TM6 is required for activation, this suggests that TM6 is more dynamic in cluster 5 and has a higher probability of forming the respective bend. Interestingly, cluster 3 also has a high RMSD for TM6 (Fig 3.3 D). This suggests that normal activity requires flexibility of TM6. However, the RMSD over the whole protein suggests that cluster 3 is overall similar to clusters 1, 2, 4 with values ranging from 2.5 to 2.7 Å (Fig 3.3 C). Regardless, cluster 5 still deviates the most from the inactive conformation of the wt D2R prior to simulation, suggesting that it is likely the closest to the active conformation (Fig 3.3D).

The major differences in the overall conformation of the D2R receptor can be highlighted by the changes in the TM distances (Fig 3.3 E, F). With respect to the EC surface, clusters 1 and 2 are similar. However, clusters 3, 4, and 5 undergo a movement of TM6 inwards in the direction of TM3, where the movement is smallest in cluster 3 and largest in cluster 5 (Fig 3.3E). In addition, cluster 3 and 4 also. exhibit a movement of TM4 away from the core of D2R or helical bundle, which is not as prevalent in cluster 5 (Fig 3.3E). The approximately 3Å shorter distance between TM7 and TM5 in cluster 5 separates this conformation from cluster 3 and 4 (Fig A2.4). Intriguingly, a ~3Å movement of TM7 is observed on the IC surface of an intermediate state of the β2-adrenergic receptor (Nygaard et al., 2013). This may suggest that prior to adopting an intermediate conformation TM7 is required to pivot, where the EC surface closes and then opens, closing the IC surface and entering into the intermediate state. This suggests that cluster 5 is a conformation sampled immediately before an intermediate conformation of D2R during G-protein binding.

With respect to the IC surface, cluster 1 is the only cluster where TM5 is close to the helical bundle (Fig 3.3F). All other clusters exhibit a ~8Å movement of TM5 away from the helical core (Fig A2.5). The movement of TM5 is the only difference between cluster 1 and 2 in terms of helical rearrangement (Fig 3.3F). Cluster 3 contains a movement of TM4 towards TM5 and TM1 and 7 towards TM6 with respect to cluster 1 (Fig 3.3F). In addition, cluster 4 exhibits an outward movement of TM7 and an inward movement of TM2 and TM6 (Fig 3.3F). The most intriguing feature is that TM6 in cluster 5 undergoes a shift towards TM3 by ~4Å (Fig A2.5). Activation of GPCRs requires TM6 to bend, causing a ~14Å outward movement of TM6 relative to the helical bundle (Farrens et al., 1996; Gether

et al., 1997; Rasmussen, Choi, et al., 2011; Rasmussen, DeVree, et al., 2011). This indicates that cluster 5 requires a motion of TM6 inwards. This motion may be necessary prior to activation to allow TM6 to act like a loaded spring.

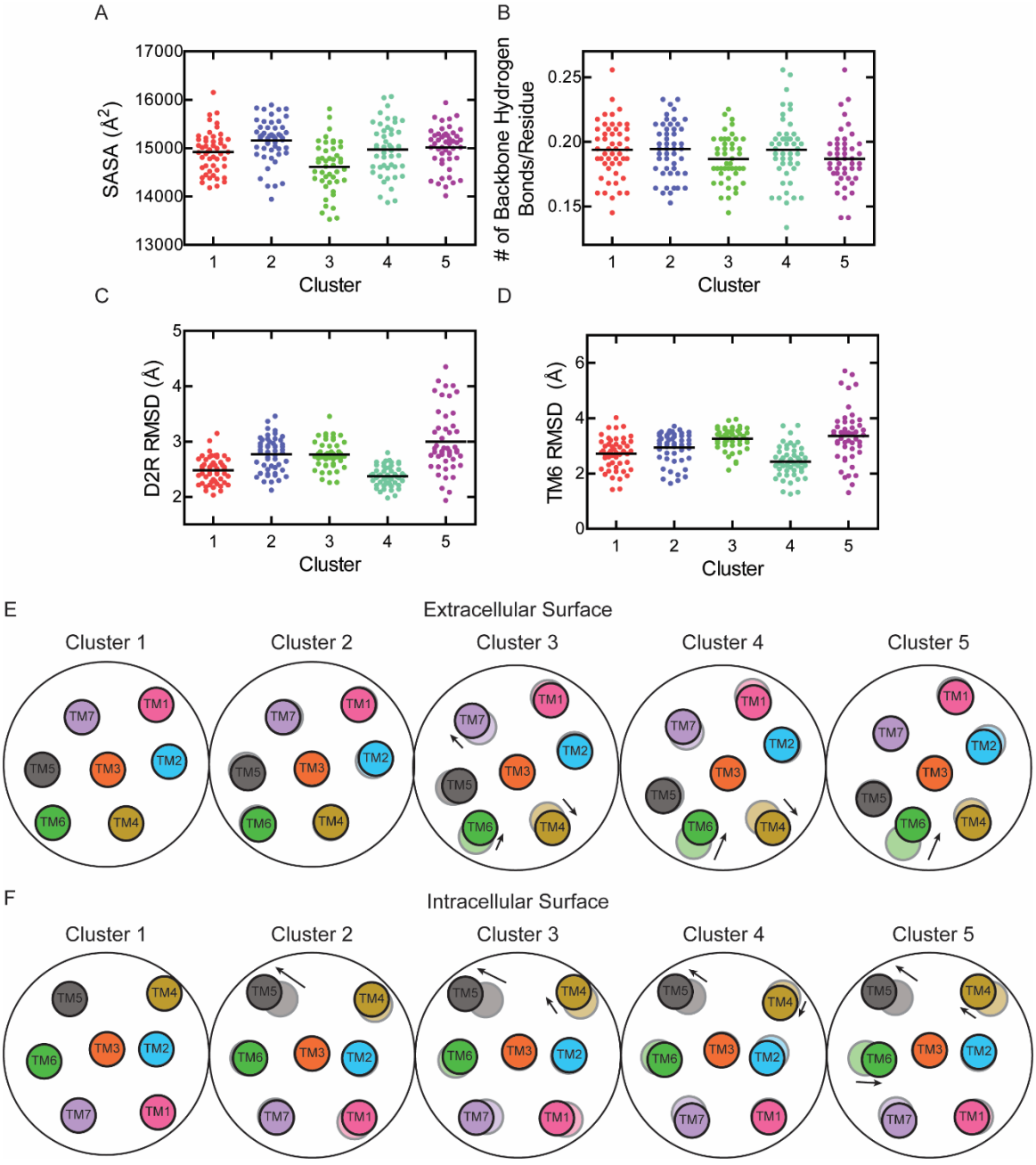

Figure 3.3 Structural features of the D2R clusters identified by Maxcluster. (A) Solvent Accessible Surface Area (SASA) measured by extending the radius of each non-hydrogen atom in the protein by 1.4Å and measuring the area that is not in direct contact with a non-water molecule. (B) Number of backbone hydrogen bonds measured as potential hydrogen bond donors and acceptors within 3Å and 150-210° of each other. (C-D) RMSD of TM6 and whole protein compared to the model of wt D2R before simulation. TM helix rearrangement from the extracellular (E) and intracellular (F) surfaces. Each helical arrangement is overlaid onto cluster 1 (transparent) to display relative TM movements. Arrows indicate largest changes of TM helices distances as compared to cluster 1.

D2R Cα covariance networks

To unveil the underlying dynamics that give rise to the activity of D2R, I constructed Cα covariance protein structure networks (ccPSN). Although our ccPSN is related to Cα covariance that has been used by Sethi *et al.* (Sethi et al., 2009), the main difference is that I calculate the angle (θ) between the vectors of the Cα's of amino acid i and j. These vectors are determined by subtracting the Cartesian coordinates of the Cα at frame t by the Cartesian coordinates at frame t-1 (eq 3.2). Using this approach, I incorporated a χ^2 test to identify the Cα pairs that deviate significantly from a random distribution (eq 3.3) (Figure A2.6). The ccPSN was constructed, where each node represents a Cα and edges are drawn between nodes if they have significant covariance (eq 3.3) and are within 4.5Å (75% of the time). Since a cutoff of 4.5Å was used for the network, the ccPSN often resembles the structure of the D2R. This is exemplified by the TM helices maintaining a cluster of connections (Fig A2.4). Interestingly, the L171P and L379F variant ccPSN deviate from the wild type ccPSN and are amongst the most active (L171P) and the least active (L379F) variants, indicating that disturbing the wild type ccPSN can dramatically alter the activity of D2R (Fig A2.4).

The generated ccPSNs were then used to create a 'shortest path' (SP) between the ligand binding site and the G-protein interface. An SP is defined as the shortest distance in the network between two distal nodes, taking into consideration edge length, and describes the most likely pathway for information propagation arising from ligand binding. Shortest paths were determined between all residues that are involved in dopamine and G-protein binding as proposed by Kling *et al.* (2013) (Kling, Lanig, Clark, & Gmeiner, 2013). I summed the total number of times that an amino acid is found on a SP and plotted them on

the D2R structure (Fig 3.4). This analysis is utilized to identify residues that are most likely to be involved in communicating the information of ligand binding to the G-protein interface. Interestingly, the variants that lead to the highest (Y199F) and the lowest activity (L379F) are both located on the SPs. In the low-activity variants L379$^{6.41}$ is more often traversed in a SP than in the normal- or high-activity variants. This indicates that communication from the ligand binding site to the G-protein interface mediated through L379$^{6.41}$ does not lead to activation of the protein. Low-activity variants also preferentially pass through G380$^{6.42}$ in the SP and which is the most observed node for the L379F variant, intriguingly G380$^{6.42}$ is adjacent to the transmission switch in D2R. In comparison, the normal- and high-activity variants have less communication through the SPs with TM6, most of the communication for high-activity variants is directed to F382$^{6.44}$. Our data demonstrates that the more often G380$^{6.42}$ appears on a SP, the lower the activity is, which is consistent with Bhattacharya *et al.* (2016) where they suggest that an allosteric communication pathway through TM6 stabilizes the helix in the inactive conformation (Bhattacharya et al., 2016). The communication to G380$^{6.42}$ preventing TM6 flexibility is also consistent with cluster 5 having the highest RMSD for TM6, suggesting that high-activity variants have a more dynamic TM6. The SPs in the highest activity variants are less likely to pass through TM6 and more likely to enter into TM3 via residue F202$^{5.51}$ (Fig 3.4). Communication is lost specifically to L379$^{6.41}$ and G380$^{6.42}$ in comparison to the low-activity variants and is directed to TM3 residues such as L123$^{3.41}$ and C126$^{3.44}$. As the Y199F variant of D2R leads to the largest increase in activity (~6-fold) it is likely that Y199$^{5.48}$ is a branch point in the communication between the ligand binding site and the G-protein interface. Therefore, it is likely that activation of the protein involves diversion of

the communication from TM6 and dissipates it elsewhere in the protein such as TM3 through $Y199^{5.48}$.

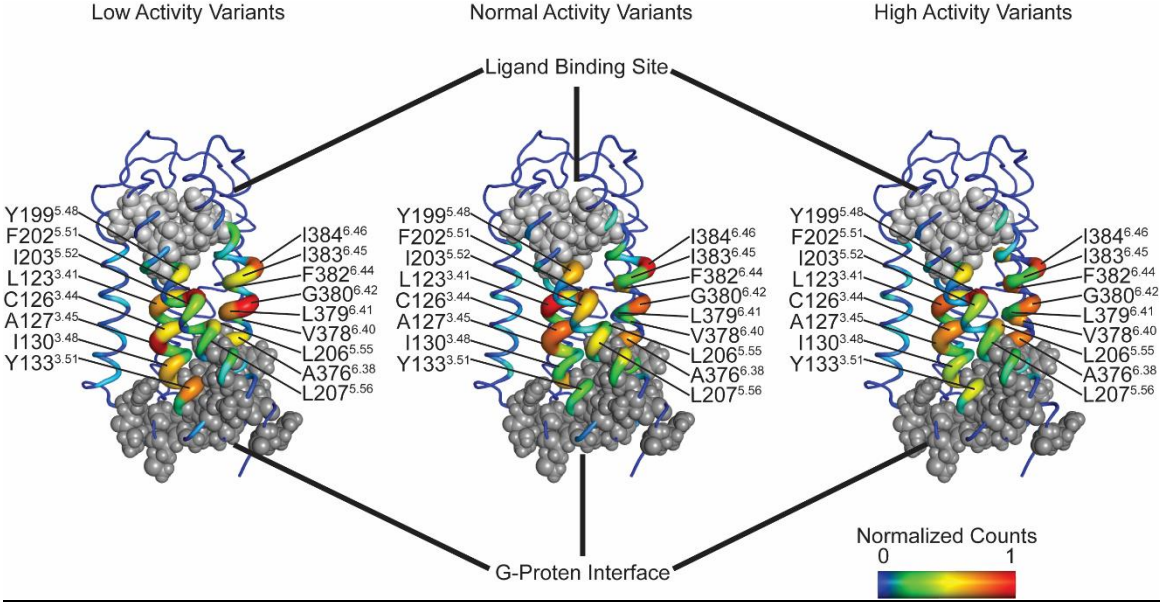

Figure 3.4 The shortest communication paths between the ligand binding pocket and G-protein interface. Summation of the residues in D2R that lie on the shortest communication paths, determined from ccPSN, from the ligand binding site to the G-protein interface. The residues are colored according to the number of times they occur on the path.

Features of the Myoclonus Dystonia-linked V154I variant of D2R

To use the analysis of the dynamics of D2R on a clinically relevant variant, I investigated the V154I variant linked to the rare disease Myoclonus Dystonia (Klein et al., 1999). Interestingly, this mutation does not alter D2R's affinity towards or activity upon binding dopamine in HEK293 cells; therefore, if there is a correlation of V154I and Myoclonus Dystonia, it may impact more relevant cell types such as those found in the central nervous system (Klein et al., 2000). The impact that the V154I substitutions has on the protein will likely be revealed through changes in the structural dynamics, as our

analysis has shown that single point mutations can shift the conformational landscape of the protein and alter correlated dynamics. As such, I aimed to sort the V154I variant into a low- or high-activity class of D2R. To this end, I measured the distances of the TM helices of the receptor. Consistent with a low-activity variant, the TM5 moves to occlude the ligand binding site (Fig 3.5A). Although the observed motion is different than the corresponding motion present in the low-activity variants where TM6 and 7 move to occlude the ligand binding site (Fig 3.1E), the consequence is similar.

Consistently with this, the overall dynamics of V154I are similar to those of the low-activity variants, where PC1 involves closing of the ligand binding pocket by movements of the ECL2 and 3 (Fig 3.5B). This correlates to the RMSF of ECL2 (amino acids 173-185) for V154I which is larger than wt (Fig 3.5C) and consistent with the higher RMSF observed in low-activity variants (Fig 3.1G).

For a more detailed investigation into the activation of the V154I variant of D2R I performed a SP analysis. This analysis reveals that between the ligand binding pocket and the G-protein interface communication primarily occurs through TM3 rather than to $G380^{6.42}$ of TM6 (Fig 3.5D). The amino acid involved in the largest number of shortest paths is $L123^{3.41}$, an amino acid often present in high-activity SP (Fig 3.4). The loss of communication to $G380^{6.42}$ indicates that TM6 of V154I is likely to be more dynamic and may be more likely to kink in the presence of a G-protein or ligand capable of inducing the conformational change in TM6. Altogether, this suggests that the V154I variant of D2R, which does not have altered binding affinity or activity towards dopamine, has a unique conformational landscape that has features of both low- and high-activity variants (Klein et al., 2000).

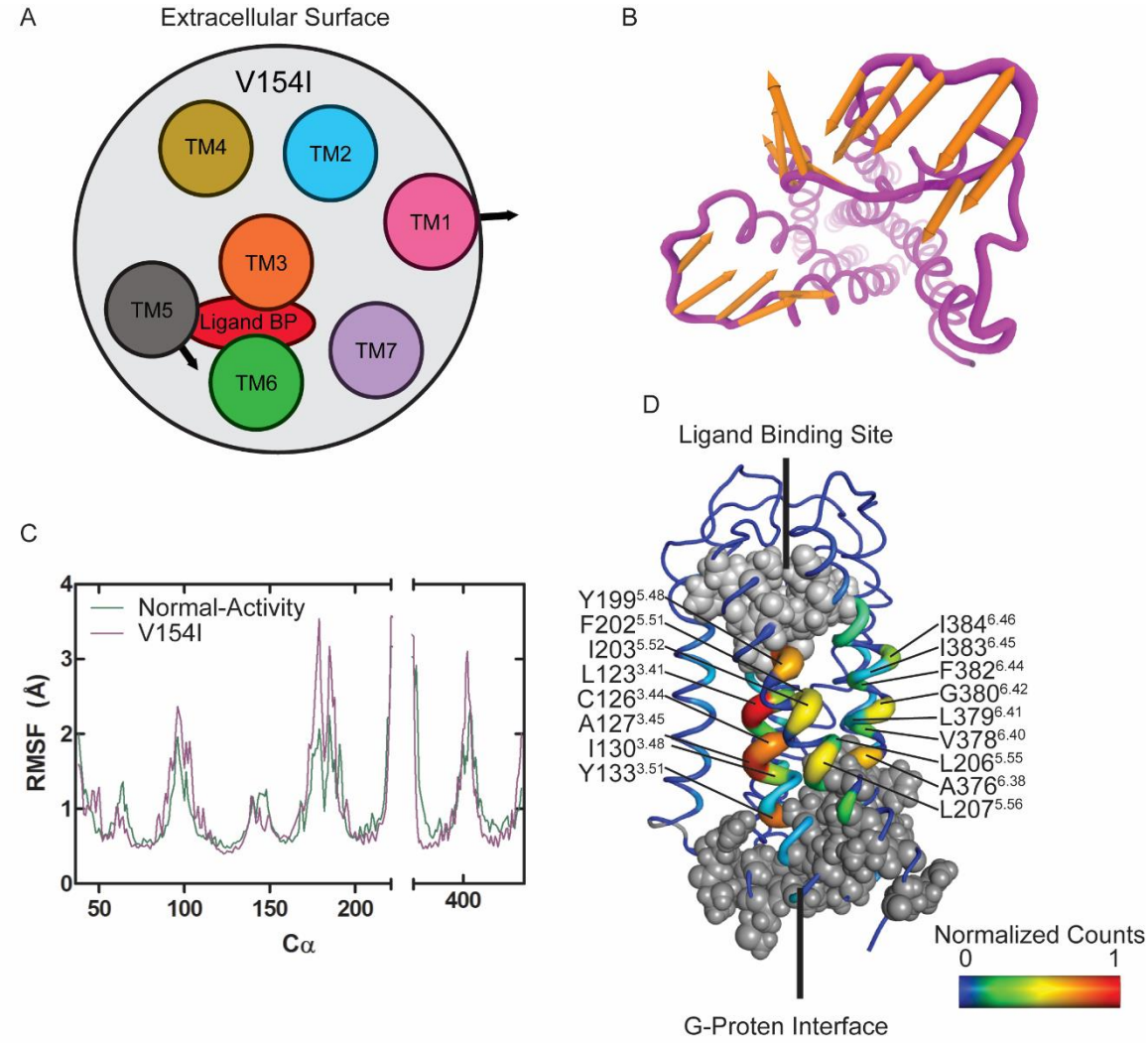

Figure 3.5 Dynamics of the V154I D2R variant which is linked to Myoclonus Dystonia. (A) Extracellular TM distances, black arrows indicate the magnitude of the TM movement compared to wt. (B) PC1 visualized on D2R where the orange arrows indicate the magnitude and direction of PC1. (C) RMSF of the normal-activity variants and of the V154I variant of D2R. (D) Shortest path analysis of V154I variant of D2R.

3.6 Discussion

The conformations of D2R prior to activation

Evidence for conformational ensembles of GPCRs prior to ligand activation has been shown with NMR experiments, and yet, atomistic descriptions of these conformations is lacking (Casiraghi et al., 2019; Kobilka & Deupi, 2007; Lee et al., 2015; Manglik et al., 2015; Nygaard et al., 2013; Weis & Kobilka, 2008). Here I identified 5 different conformational ensembles that D2R can adopt prior to activation (Fig 3.2B, C). The structural differences between these conformations can be described by the changes in the TM arrangement (Fig 3.3 E and F). The observed changes on the extracellular surface of the receptor primarily involve movements of TM4, 6, and 7. In particular TM4 and TM6 move outward and inward, respectively, towards the helical bundle in clusters 3, 4, and 5 compared to cluster 1 and 2. Inactive clusters have a TM5 that is closer to the helical bundle on the intracellular side where variants more likely to be activated have TM6 closer to the helical bundle. This is contradictory to structural studies of GPCRs in the active conformation where TM6 undergoes an 8-14Å movement away from the helical core to allow for G-protein binding (Choe et al., 2011; Rasmussen, DeVree, et al., 2011). This finding suggests that the variants more likely to lead to activation have a more closed off intracellular surface. Two possible explanations can describe these findings: 1 – the closing of the intracellular surface is required to provide the initial contact surface with the G-protein which induces the intracellular surface opening identified in the classical activated state of GPCRs, or 2 – the opening of the extracellular end, identified for high-activity variants, is required to facilitate proper coordination of dopamine. The recent crystal structure of D2R suggests that the dopamine binding pocket is deep within the GPCR

helical bundle, deeper than most GPCRs (Wang et al., 2018). This indicates that for proper positioning of dopamine the D2R must open wider at the extracellular surface than other GPCRs, therefore, the high-activity variants are able to better accommodate dopamine.

The conformations identified here can be separated into groups that are more or less likely to lead to G-protein activation, based on the clustering of low-, normal-, and high-activity variants (Fig 3.6). Here it can be observed that clusters 1 and 2 are less likely to lead to activation as low-activity variants cluster into these conformations. Additionally, these conformations are likely more flexible, with a closed ligand binding pocket, and transfer information to the G-protein interface of TM3, as well as to G380$^{6.42}$. Cluster 3 constitutes the most occupied cluster for the normal-activity variants. I assigned this group mid-ranged flexibility with a semi-open ligand binding pocket and G-protein interface (Fig 3.6). Lastly cluster 4 and 5 constitute the high-activity variants and as such these clusters are the least dynamic and have SPs from the ligand binding pocket to F382$^{6.44}$ as well as midway down TM3, activating G-protein signalling.

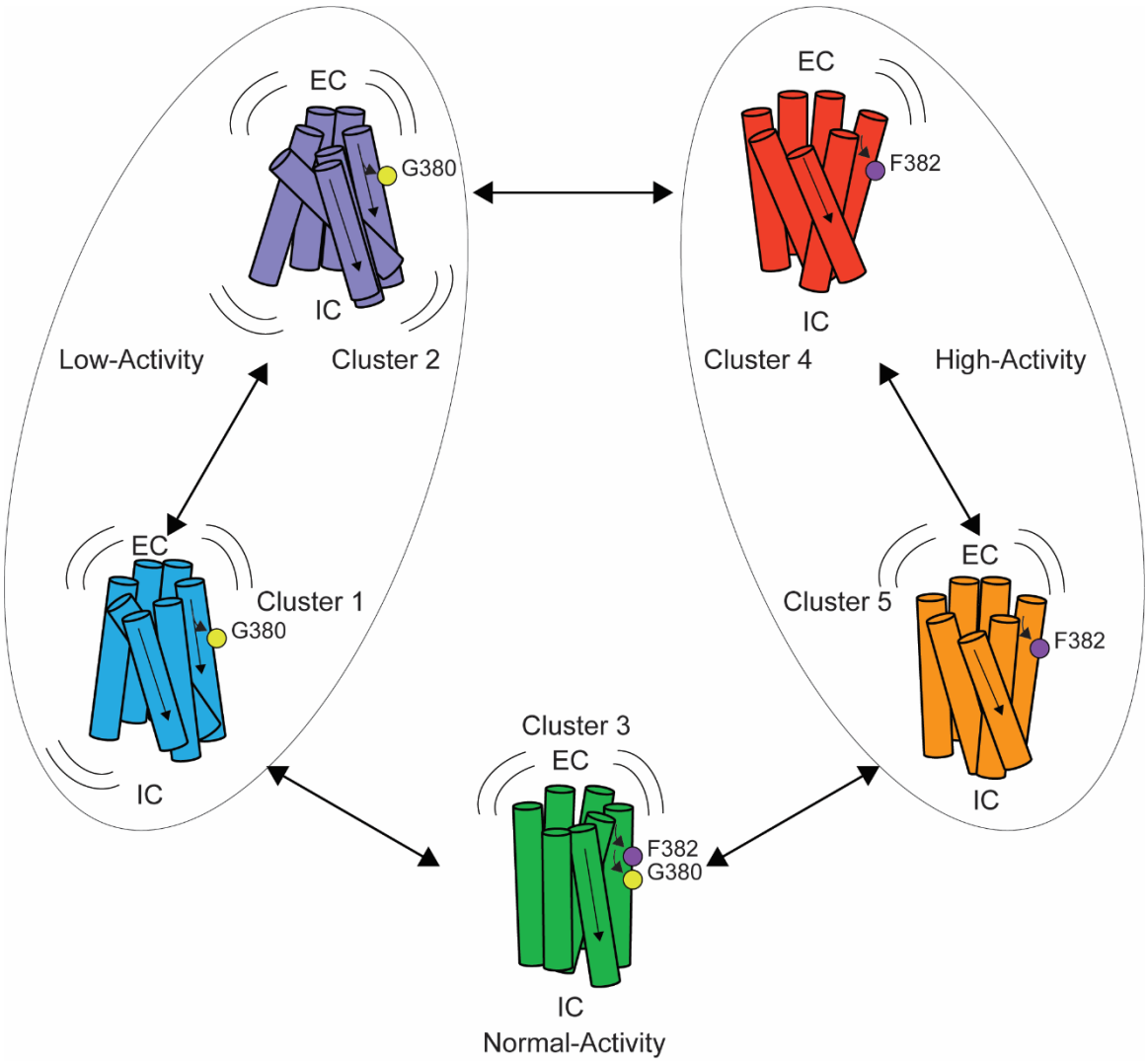

Figure 3.6 Conformational dynamics and signaling of D2R prior to activation, leading to differences in ligand binding-induced activation of guanosine nucleotide exchange in the coupled G-protein (EC- extracellular, IC – intracellular).

The multitude of conformations that GPCRs can visit before and during activation is a fundamental feature that allows for regulation of signalling pathways. If one considers a single conformation of a GPCR with high affinity for its ligand, then the presence of any ligand at sufficient concentrations would trigger the transduction pathway. However, different conformations of GPCRs with a diverse probability of being activated would

reduce the noise upon activation of signal transduction pathways. The reduced noise would arise from the ability of the different conformations to dampen the protein's activation upon the arrival of different concentrations of ligand. The conformational ensemble of GPCRs prior to ligand binding is a feature that can be exploited by small molecules or peptides as potential therapeutics. Molecules that promote a particular conformation of the GPCR would modulate the activity of that receptor, providing therapeutic control over GPCR activity.

An increase in global D2R dynamics reduces D2R activity

The presented data supports the hypothesis that the more dynamic and flexible the D2R receptor is, the lower the activity will be. This is supported by the larger RMSF values observed here for the low-activity variants, especially in ECL 1 and 2, as well as the increased number of states that they can adopt, identified by PCA (Fig 3.1F, G). The majority of the TM helices do not differ in flexibility, however. The increased dynamics ultimately leading to lower activity may be a feature of PC1 for the low-activity variants in which the ECL and ICL are undergoing a closing and opening motion, respectively (Fig 3.1C, A2.10, A2.11). Since the low-activity variants simulated here do not alter the binding affinity towards dopamine significantly (<1.3-fold change), there are two mechanisms by which the increased flexibility and the closing motion of the low-activity variants can diminish D2R activity (Sung et al., 2016). (1) The closing of the ECL decreases the association rate (k_{on}) of ligand to D2R; however, to maintain a similar affinity the dissociation rate (k_{off}) is decreased on a similar scale. Under *in vivo* conditions, where dopamine is not at equilibrium, the rapid arrival of the ligand will require more time for successful binding due to the lower k_{on}, resulting in a delay of D2R activity. (2) The

increased flexibility of the ECL can allow for dampening of the energy provided by ligand binding. Under normal conditions where ligand binding would stimulate the conformational change of TM6 leading to activation, this energy may be dissipated as heat through the increased dynamics of ECL 1 and 2 or ICL 2. This loss of energy could prevent the allosteric communication, identified by SP analysis, towards TM6 in particular towards $F382^{6.44}$, facilitating continued Cα covariance directed to $G380^{6.42}$ and subsequent rigidification of TM6. Regardless, the fact that the low-activity variants have increased flexibility is intriguing, as MD and NMR studies have shown that ligand binding induces more conformational heterogeneity, but G-protein binding reduces these dynamics (Bhattacharya & Vaidehi, 2014; Nygaard et al., 2013).

The reported simulations, which reflect the structural dynamics of D2R prior to ligand binding, suggest that a less dynamic receptor in a conformation similar to cluster 5 is more likely to lead to activation. This suggests that D2R is required to pass through a conformation similar to cluster 5 to lead to its activated state. Since ligand binding increases dynamics, I suggest that ligand binding allows the protein to search for a conformation similar to cluster 5, granting D2R a path to enter an activated state. Therefore, variants that skew the protein towards a conformation similar to cluster 5 are more likely to lead to an activated state of the protein describing the phenotypes characterized by Sung *et al*. (2016) (Table A2.1).

Since the low-activity variants sample primarily clusters 1 and 2 (Fig 3.2B), increased dynamics may be a feature of these conformational states. However, it cannot be ruled out that the increased flexibility of these variants provides the kinetic energy which allows them to adopt conformations within clusters 1 and 2. The former is more likely as

Fig 2D-F indicates that the normal- and high-activity variants can also transition through clusters 1 and 2, suggesting that increased kinetic energy is not required to enter into cluster 2.

The activation path of D2R: from the ligand binding pocket to the G-protein interface

To describe in better detail how the information of ligand binding to the dopamine binding site of D2R is transmitted to the G-protein interface, a Cα covariance pathway was constructed (Fig 3.7). This pathway involves residues that are most frequently located on the shortest path between the dopamine binding site to the G-protein interface to describe the most likely direction that Cα covariance would be propagated. Residues were included if they were located in the shortest path for >75% of the time.

For low-activity D2R variants, $G380^{6.42}$ occurs on the shortest path between the dopamine binding site and the G-protein interface for low-activity variants (Fig 3.7). This is intriguing since $G380^{6.42}$ is the pivot point of D2R TM6 bending. The high-activity variants partition the signal from $G380^{6.42}$ to $F382^{6.44}$ which undergoes a conformational change upon activation (Fig 3.4, 3.7). This implies that $G380^{6.42}$ acts primarily as an important residue for relaying Cα covariance traveling from the ligand-binding pocket to the G-protein interface, likely preventing TM6 movement as it is found in low-activity variants. High-activity variants divert the Cα covariance pathway from $G380^{6.42}$ and transfer this information to $F382^{6.44}$. This change in the pathway could be the signal to induce the conformational change of $F382^{6.44}$ that occurs upon receptor activation, and is involved in ligand-dependent activity (Granja-Galeano et al., 2017; Han, Feng, Chen, Gerard, & Boisvert, 2015; Masureel et al., 2018).

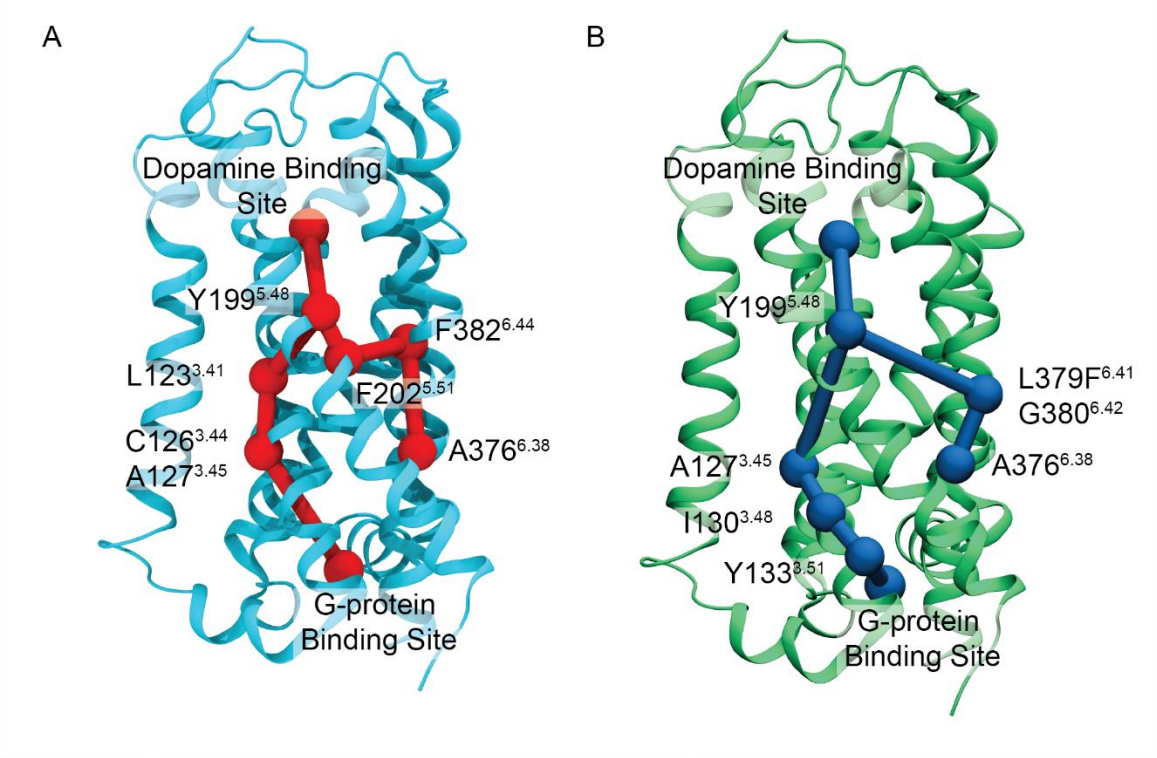

Figure 3.7 Cα covariance communication pathway displayed on the structure of D2R. (A) The Cα covariance communication pathway for high-activity variants, bifurcated by Y199$^{5.48}$ towards F382$^{6.44}$ or A127$^{3.45}$. (B) The Cα covariance communication pathway for low-activity variants, bifurcated by Y199$^{5.48}$ towards G380$^{6.42}$ or Y133$^{3.51}$.

The second pathway that the Cα covariance takes from the ligand-binding pocket to the G-protein interface proceeds through TM3. This communication passes through F202$^{5.51}$ to L123$^{3.41}$ to A127$^{3.45}$ for high-activity variants (Fig 3.7). For the low-activity variants, the communication continues towards I130$^{3.48}$ and Y133$^{3.51}$ (Fig 3.7). The role of these residues in the activation of D2R is unknown as the only biochemical data available is on the impact of amino acid substitutions at these positions have on ligand binding (Javitch, Fu, Chen, & Karlin, 1995). Further investigation into the role of these amino acids is required. However, one hypothesis is that they prevent the Cα pathway towards F382$^{6.44}$ or G380$^{6.42}$ of TM6, to modulate the Cα covariance directed towards these residues.

Therefore, I propose that TM3 of D2R acts as an allosteric signal quencher where dynamics are processed to the G-protein interface without passing through $F382^{6.44}$ or $G380^{6.42}$.

Using PCPM to identify the functionality of D2R variants

To demonstrate that our PCPM analysis pipeline can score the activity of other D2R variants, I analyzed the Myoclonus Dystonia linked V154I variant. Our analysis reveals that this variant of the D2R exhibits similar dynamics as the low-activity variants. However, the SP analysis describing signalling from the ligand binding pocket to the G-protein interface is rather similar to that of high-activity variants. This combinatorial effect likely leads to little to no change in activity of the receptor in the presence of dopamine observed in HEK293 cells, but the impact in other cell lines is unknown (Klein et al., 2000). For instance, any conditions where the dynamics of the receptor are reduced would lead this variant to mimick a high-activity variant due to the communication propagation. One such condition could be increased cholesterol, which can influence the dynamics of GPCRs (Patra et al., 2015). Although the activity of V154I is similar to wild-type under optimal conditions, the structural dynamics of the protein are altered significantly indicating that the exact phenotype has not yet been explored.

The analysis pipeline developed here is now available for the analysis of newly sequenced genomes that have a mutation in the *drd2* gene. Simulations of D2R variants can reach 100ns in roughly 3 days with commonly available computational resources, providing rapid phenotypical descriptions of the respective genotype. The obtained characterisation can then provide critical information for the decision to administer agonist, antagonist, partial agonist, or reverse agonist providing a new analysis tool for personalized medicine.

The PCPM pipeline is not limited to D2R or GPCRs as any protein will have a conformational ensemble prior to ligand binding or activation. Characterization of how mutations affect these ensembles can have a dramatic impact on the way that proteins function. Therefore, this pipeline is amenable to any protein with a variety of functionallycharacterized mutations, which can then be used as a standard for the structural dynamics of the protein against which a newly identified variant can be tested.

Chapter 4

Near-Cognate aminoacyl-tRNA Accommodation Proceeds through an Alternative Pathway

4.1 Forward

Chapter 4 is an investigation into the long outstanding question of how EF-Tu and the 70S ribosome recognize the presence of cognate aa-tRNA to selectively facilitate aa-tRNA accommodation. This chapter is written in the format for submission to Nature Communications. All experiments were performed, and the chapter was written by myself with aid from Hans-Joachim Wieden in collaboration with Karissa Sanbonmatsu at Los Alamos National Laboratory and Scott C. Blanchard at Weill Cornell Medical College. By employing Gō-like model simulations of tRNA from the A/T to A/A state, the accommodation pathway was sampled for both cognate and near-cognate tRNA. The results of the simulations show that near-cognate tRNA accommodates using an alternative pathway whereby the elbow of the tRNA attempts to accommodate before the tRNA base-pairs with the mRNA. The presence of aminoglycosides prevent tRNA from proceeding through the alternative near-cognate accommodation pathway, indicating that it is a likely selection criterion utilized by the ribosome. Additionally, the impact of the antibiotics evernimicin and hygromycin A on accommodation were investigated. Lastly, the Cα covariance was analyzed for EF-Tu bound to the ribosome in analogy to chapter 3. Instead of the Cα residue in protein, the C1’ atom was used for the respective RNAs to incorporate nucleic acid in the communication pathway analysis. Using this approach, the transmission problem of allostery was addressed with respect to how EF-Tu-dependent GTP hydrolysis is stimulated by the ribosome and cognate tRNA-mRNA base-pairing.

4.2 Abstract

Aminoacyl (aa)-tRNA incorporation requires additional factors that contribute to the fidelity of translation as the efficiency of cognate aa-tRNA incorporation into the ribosome is greater than what can be predicted by Watson-Crick base-pairs between the codon and anticodon. Here I investigate the differences between cognate and near-cognate tRNA accommodation by employing structure-based simulations of aa-tRNA accommodation. Surprisingly, the data reveal that near-cognate aa-tRNA accommodation can proceed through an alternative pathway. This alternative pathway for the tRNA is not observed in the presence of aminoglycosides gentamicin and neomycin, indicating that blocking of the alternative pathway may induce misreading. Additionally, I characterized the dynamics of accommodation in the presence of the less characterized antibiotics, evernimicin and hygromycin A, providing critical information on their mechanisms of stalling translation. I show that the antibiotic evernimicin stalls accommodation by inducing unconventional conformations of the tRNA, whereas hygromycin A prevents the proper coordination of the A-site acceptor stem. Taken together, these results elucidate selection criteria that the ribosome imposes on tRNA during proofreading, allowing it to discriminate against near-cognate tRNAs during accommodation.

4.3 Introduction

Currently, antimicrobial resistant (AMR) bacteria and multi-drug resistant fungi such as *Candida auris* are becoming a major health and economic concern (Jeffery-Smith et al., 2018; World Health Organization, 2017). This is a compounding effect from the increased rates of bacteria gaining AMR with the decreased rate at which novel antibiotics are developed. Due to the effectiveness of antibiotics there is minimal economic benefit for industrial companies to develop novel antibiotics (Ventola, 2015). Therefore, the public sector must focus on strategies for the identification and rational design of antibiotics. A detailed mechanistic description of how conventional antibiotics function will greatly aid in the rational design of novel antibiotics by providing insights into mechanistic strategies that lead to successful antibiotics.

A large number of antibiotics target the bacterial ribosome and impair the process of protein synthesis as their major mode of action (Wilson, 2014). All four phases of ribosome-dependent protein synthesis (initiation, elongation, termination, and recycling) are targeted by antibiotics that impede translation. Of these phases, the most frequently targeted is elongation (Wilson, 2009). Elongation can be subdivided into aa-tRNA selection, peptide bond formation, and translocation. Aa-tRNA selection is facilitated by EF-Tu and elongation is promoted by EF-G. During aa-tRNA selection, the aa-tRNA undergoes a dramatic conformational change from the A/T state to the A/A state in a process called accommodation. Accommodation is often targeted by antibiotics such as aminoglycosides, as disruption of the process can slow protein synthesis and decrease the fidelity of peptide chain synthesis (Wilson, 2009, 2014).

Aa-tRNA selection consists of several sequential steps involving the 70S ribosome bound to an mRNA and a ternary complex of EF-Tu, aa-tRNA, and GTP. The first step is defined by binding of the ternary complex to the 30S subunit of the ribosome. Codon-anticodon interactions are rapidly formed, followed by closure of the 30S subunit at the A-site (Loveland et al., 2017; Ogle et al., 2001). 30S subunit closure engages EF-Tu on the 50S subunit, forming interactions between EF-Tu and the Sarcin Ricin loop (SRL). These interactions have been proposed to stimulate GTP hydrolysis, defining this complex as the GTPase activated state of EF-Tu (Voorhees et al., 2010). GTP hydrolysis is followed by Pi release, inducing conformational changes in EF-Tu, and stimulating accommodation of the aa-tRNA into the A-site of the ribosome (Kothe & Rodnina, 2006; Rodnina & Wintermeyer, 2001). EF-Tu gates accommodation of cognate aa-tRNA by hydrolyzing GTP at a 10-fold faster rate in the presence of cognate codon-anticodon interactions, a process that is still poorly understood (Pape et al., 1998). Binding of the aa-tRNA to mRNA induces a conformational change or 'flipping out' of the conserved bases A1492, A1493, and G530 of the 16S rRNA (Ogle et al., 2001). Recently, it has been shown that near-cognate (containing a single mismatch between the codon and anticodon) aa-tRNA also induces the 'flipping-out' of A1492, A1493, and G530, suggesting that these bases cannot distinguish between cognate and near-cognate aa-tRNA, and changes their conformation merely based on interacting with the codon and anticodon mini-helix (Loveland et al., 2017). Altogether, these features contribute to, yet do not completely explain, the remarkable degree of fidelity of translation (Parker, 1989).

Aminoglycosides as well as orthosomycin are two classes of antibiotics that specifically impact accommodation of aa-tRNA. The aminoglycosides, such as gentamycin

(GEN) and neomycin (NEO), bind to h44 of the 30S ribosomal subunit and decrease the fidelity of decoding (Borovinskaya et al., 2007; Davies, Gorini, & Davis, 1965; Wasserman et al., 2015). Structural studies suggest that binding of aminoglycosides results in the 'flipping out' of A1492 and A1493 of the 16S rRNA in the absence of aa-tRNA. Since A1492 and A1493 are already in the 'flipped-out' position prior to aa-tRNA binding it was predicted that this would accelerate near-cognate aa-tRNA accommodation (Borovinskaya et al., 2007; Wasserman et al., 2015). However, since binding of near-cognate aa-tRNA can facilitate the 'flipping-out' of A1492 and A1493 it is not clear if this is indeed the mechanism by which aminoglycosides induce miscoding. Other aminoglycosides, such as hygromicin A (HGR), bind to the peptidyl transferase center (PTC) and prevent the A-site aa-tRNA from interacting with the P-site aa-tRNA(Guerrero & Modolell, 1980; Polacek, Swaney, Shinabarger, & Mankin, 2002; Polikanov et al., 2015). In doing so, HGR increases the oscillation of the aa-tRNA between the A/T and A/A state (Polikanov et al., 2015). When the A-site aa-tRNA does enter the A/A state, HGR induces a unique conformation of the A-site aa-tRNA where A76 stacks with the antibiotic and A2602 of the 23S rRNA (Polikanov et al., 2015). Although structural data is available for the A/A state aa-tRNA conformation in the presence of HGR, there is no structural description of how HGR induces oscillations between the A/A and A/T conformations.

The orthosomycin class antibiotic evernimicin (EVN) impacts translation earlier in the accommodation of aa-tRNA by binding to the minor grooves of H89 and H91 of the 50S (Arenz et al., 2016). Binding of EVN is predicted to prevent elbow accommodation of aa-tRNA, as the antibiotic overlaps with the elbow of the aa-tRNA in the A/A conformation (Arenz et al., 2016). In doing so EVN stabilizes an intermediate conformation of the aa-

tRNA as resolved by single molecule fluorescence resonance energy transfer (smFRET) experiments (Arenz et al., 2016). It is still unclear what the intermediate aa-tRNA conformation interacting with EVN is as no structural data of the aa-tRNA stalled in the accommodation corridor are available.

Despite the numerous structural and biochemical studies available, several questions on how the ribosome discriminates between cognate aa-tRNA and near-cognate still remain, including, are the accommodation pathways of cognate and near-cognate aa-tRNA the same? This then leads to questions about the antibiotics that affect the accommodation pathway such as: How do aminoglycosides induce mis-incorporation? Does the near-cognate accommodation mimic cognate accommodation in the presence of these antibiotics? How does the aa-tRNA enter into the unique conformation observed with HGR bound? What feature of HGR causes the oscillation of the aa-tRNA between the A/T and A/A states? What are the structures of the intermediates induced by EVN and how does the antibiotic interact with aa-tRNA?

To answer these questions, I simulated cognate and near-cognate tRNA accommodation into the ribosome using all-atom structure based Gō-like models of the 70S ribosome bound to mRNA and ternary complex. Our simulations reveal that near-cognate aa-tRNA accommodates using an alternative pathway, where base-pairing does not occur until after elbow accommodation has initiated. Additionally, near-cognate aa-tRNA has inherent flexibility in the A-site leading to an improperly positioned aa-tRNA, preventing suitable coordination for peptide bond formation. The obtained simulations reveal that the alternative pathway of near-cognate aa-tRNA accommodation is abolished in the presence of GEN or NEO. These antibiotics also increase the time required for codon-anticodon

interactions to form (codon searching), likely due to the reduced access the anticodon has to the codon from the induced 'flipped-out' conformation of A1492, and A1493. Additionally, I report unconventional conformations of the aa-tRNA formed in the presence of HGR, where peptide bond formation could not occur. Finally, I show that EVN induces a plethora of conformations of the aa-tRNA during accommodation by interacting with the major groove of the tRNA.

4.4 Materials and methods

70S•EF-Tu•nucleotide•tRNA•mRNA model building

Models of the 70S•EF-Tu•tRNA•mRNA with cognate or near-cognate codon-anticodon interactions were derived from the cryo-EM structures from Loveland *et al*. (PDB ID: 5UYK - C_I, 5UYL - C_{II}, 5UYM - C_{III}, 5UYN - NC_I, 5UYP - NC_{II}, and 5UYQ - NC_{III}) (Loveland et al., 2017). Either GTP or GDP along with Mg^{2+} was added to each system by aligning EF-Tu with crystal structures of EF-Tu containing bound nucleotide (PDB ID: 1EFT and 1EFC respectively) (Kjeldgaard et al., 1993; Song et al., 1999). All alignments were performed with VMD 1.9.2 (Humphrey et al., 1996). The GDPNP from 1EFT was manually converted to GTP by replacing the nitrogen separating the γ and β phosphates with an oxygen. The fully accommodated tRNA conformations (C_{IV} and NC_{IV}) were constructed by aligning C_{III} or NC_{III} with the cryo-EM structure of aa-tRNA in the post-accommodated state (PDB ID: 4V66). The coordinates of the accommodated tRNA were added to C_{III} or NC_{III} and the coordinates of the previous tRNA were removed. The A-site tRNA in NC_{IV} was manually altered to the sequence of $tRNA_{Lys}$ as it is in $NC_{I\text{-}III}$ with the swapna package in UCSF Chimera (Pettersen et al., 2004).

Models containing EF-Tu in the open or GDP conformation (OC_{IV} and ONC_{IV}) were constructed by aligning and replacing EF-Tu with the crystal structure of EF-Tu in the GDP conformation (PDB ID: 1EFC). Coordinates for GEN and NEO in models $GOC_{I\text{-}IV}$, $GONC_{I\text{-}IV}$, $NOC_{I\text{-}IV}$, and $NONC_{I\text{-}IV}$ were adapted from aligned structures of the 70S bound to the antibiotics (PDB ID: 4V53 and 4WOI, respectively) (Borovinskaya et al., 2007; Wasserman et al., 2015). Nucleotides A1492 and A1493 of the 16S rRNA along with A1912 of the 23S were also adapted from these structures after alignments. Similarly,

coordinates of EVN and HGR were derived by aligning the 70S with the structures of EVN and HGR bound (PDB ID: 5KCS and 5DOY, respectively) (Arenz et al., 2016; Polikanov et al., 2015).

The energy of each of the models was minimized using the steepest descent approach in GROMACS v4.5.4 with AMBERFF99S force fields (Hess, Kutzner, Van Der Spoel, & Lindahl, 2008; Hornak et al., 2006; Pronk et al., 2013; Van Der Spoel et al., 2005; Wang, Cieplak, & Kollman, 2000). Minimizations were performed in an explicit solvent system within TIP3P at a concentration of 100mM NaCl for 10 000 steps. The energy of the A-site tRNA for C_{IV} and $NC_{IV,}$ followed by water molecules and then the entire system, was minimized sequentially.

Structure based simulations

All atom structure based models were constructed using Smog-2.1.0 (Whitford et al., 2008). Simulations were performed as described in Whitford *et al.* at a temperature of 60ε with Langevin dynamics, where ε is the reduced energy unit (Whitford et al., 2010). The simulations were performed with a step size of 0.005 for a minimum of 3×10^6 steps. A single Gaussian energy basin approach was used where the contacts native to the C_{IV} conformation are set as an energy minima. Therefore, the simulation will start in the C_I conformation and proceed to the C_{IV} conformation.

Reaction coordinate calculations

The reaction coordinate R_{elbow} monitoring tRNA accommodation was used as previously described in Yang *et al.* (Yang, Noel, & Whitford, 2017). This reaction coordinate describes the distance between the O3' atoms of U8 in the P-site tRNA and U60

in the A-site tRNA. R_{codon} was measured between the N3 of the wobble position C in the mRNA and the N1 atom of G34 in the A-site tRNA for cognate codon-anticodon interactions. For near-cognate codon-anticodon interactions, R_{codon} was measured between the N1 atom of the G in the wobble position of the mRNA and the N3 atom of U34 in the A-site tRNA. R_3 is defined by the distance between the center of mass of A76 for both the A-site and P-site tRNA (Whitford et al., 2010). Free energy landscapes were calculated using the g_sham package in GROMACS v4.5.4 (Hess et al., 2008; Pronk et al., 2013; Van Der Spoel et al., 2005).

tRNA-mRNA angle calculations

The angle between the tRNA and mRNA ($\theta_{t\text{-}m}$) (Fig A3.2) was determined with equation 4.1, where v_m is the vector produced between the centers of mass of residues 6 and 8 of the mRNA (or positions 1 and 3 in the codon), v_t is the vector between the center of mass of the anticodon (residue 34 to 36) of the tRNA with the center of mass of U60, and |•| denotes magnitude.

$$\theta_{t-m} = \arccos\frac{(v_m \cdot v_t)}{|v_m||v_t|} \tag{4.1}$$

Convergence of simulations

Convergence of the simulations was determined as in Vaiana and Sanbonmatsu (2005) by analyzing the time dependence of the average deviations σ(t) (eq 4.2). $\Delta G(i,j)_t$ is the free energy landscape of R_{elbow} and R_{codon} at time t and $\Delta G(i,j)_{t0}$ is the free energy landscape of R_{elbow} and R_{codon} at time 0 (after 1000 frames of simulation), and N is the number of grid points on the free energy landscape. Simulations were considered to have converged when σ(t) reached a plateau.

$$\sigma(t) = \sqrt{\frac{\sum_{i,j}(\Delta G(i,j)_t - \Delta G(i,j)_{t0})^2}{N}} \quad (4.2)$$

Cα and C1' covariance protein structure network (ccPSN)

Covariance matrices were calculated using the same approach as in chapter 3 using an in-house developed approach outlined in equation 4.3.

$$\theta_{(t)} = \arccos\left(\frac{(x_{i,t} - x_{i,t-dt}) \bullet (x_{j,t} - x_{j,t-dt})}{|x_{i,t} - x_{i,t-dt}||x_{j,t} - x_{j,t-dt}|}\right) \quad (4.3)$$

where $x_{i,t}$ and $x_{j,t}$ are the Cartesian coordinates of the Cα or C1' of amino acid or nucleic acid i and j at frame t, $\theta_{(t)}$ is the angle between the vectors produced from $x_{i,t} - x_{i,t-dt}$ and $x_{j,t} - x_{j,t-dt}$ and $|\bullet|$ denotes the magnitude of that vector. To identify residues with significant covariance, $\theta_{(t)}$ values at each frame were plotted as a histogram which was fit with equation 4.4. In equation 4.4, $E(\theta)$ is the expected number of counts for a random distribution of $\theta_{(t)}$ values and C_{total} is the total number of θ counted,

$$E(\theta) = C_{total}\frac{1}{2}\sin(\theta)d\theta \quad (4.4)$$

A χ^2 analysis was subsequently used to determine which C_α, C1', and C_α-C1' pairs deviate from a random distribution.

Network construction

All networks were constructed in Gephi-0.9.1 where each node represents an amino acid and edges are drawn between amino acids if they have significant covariance and they are within a distance of 4.5 Å for C_α's or 10.5Å for C1' atoms for 75% of the simulation time. Betweenness Centrality ($Bx(n)$) values were calculated with equation 4.5 where σ_{st}

is the number of shortest paths from node s to t and $\sigma_{st}(n)$ is the number of shortest paths from node s to t that pass through node n, and this value determines the size of the node.

$$Bx(n) = \sum_{s \neq n \neq t} \frac{\sigma_{st}(n)}{\sigma_{st}} \tag{4.5}$$

4.5 Results

Accommodation of near-cognate tRNA proceeds through an alternative pathway

Recently, the structure of the ternary complex bound to the 70S ribosome in three different conformations prior to accommodation was resolved using cryo-EM (Fislage et al., 2018; Loveland et al., 2017). Loveland *et al.* labelled these different conformations as C_I, C_{II}, and C_{III} or NC_I, NC_{II}, and NC_{III} for cognate or near-cognate aa-tRNA, respectively. I will use the same nomenclature here (Fig 4.1 A-C). The differences between the C and NC nomenclature is the presence of cognate or near-cognate tRNA, respectively. C_I and NC_I both contain EF-Tu bound to the 70S ribosome without interactions with the 50S subunit or base-pairing between the aa-tRNA and mRNA (Fig 4.1A). C_{II} and NC_{II} also lack EF-Tu interactions with the 50S but aa-tRNA–mRNA base-pairing has occurred (Fig 4.1B). EF-Tu engages with the SRL of the 50S in C_{III} and NC_{III} while the aa-tRNA is in the A/T state (Fig 4.1C). Lastly, I have modelled the C_{IV} and NC_{IV} conformations where aa-tRNA has accommodated into the A/A state and EF-Tu has undergone a conformational change (Fig 4.1D).

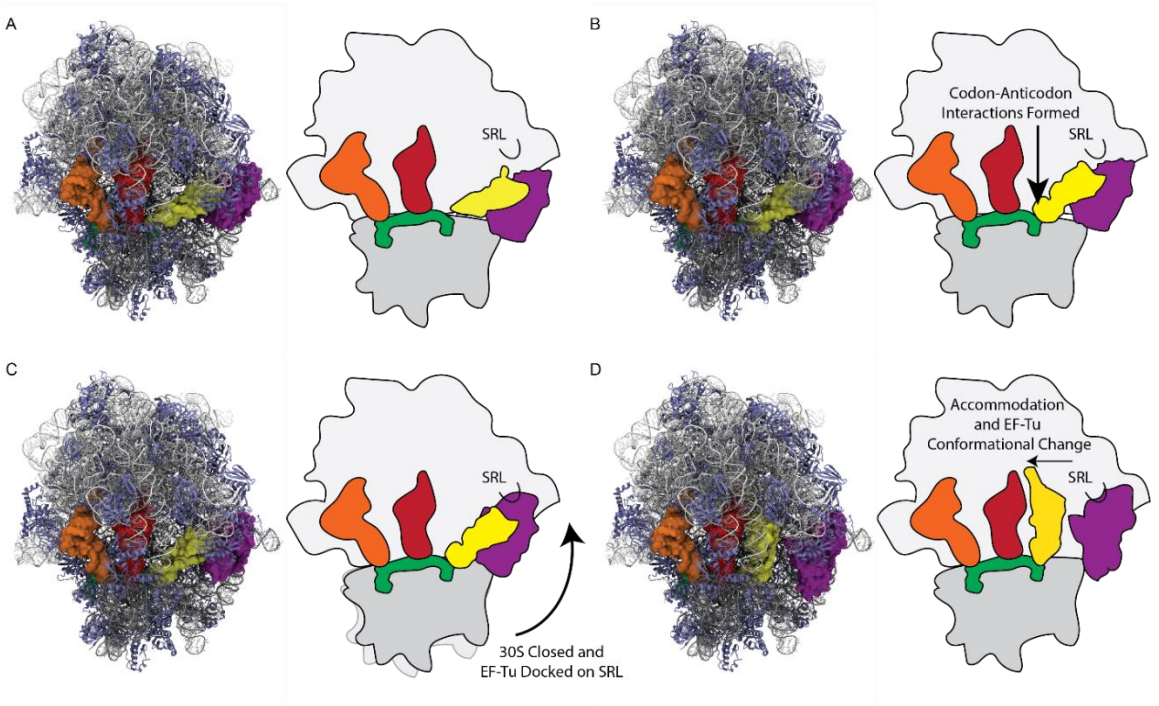

Figure 4.1 The conformations of 70S•EF-Tu•aa-tRNA complex. (Left) Structure of the 70S with rRNA in grey, ribosomal proteins in light blue, A-site tRNA in yellow, P-site tRNA in red, E-site tRNA in orange, and mRNA in green. (Right) Cartoon representation of the structure. (A) The C_I or NC_I conformation: codon-anticodon interactions not formed, and EF-Tu not engaged with SRL. (B) C_{II} or NC_{II} conformation: codon-anticodon interactions formed and EF-Tu not engaged with SRL. (C) C_{III} or NC_{III} conformation: codon-anticodon interactions formed and EF-Tu engaged with SRL. (D) C_{IV} or NC_{IV} conformation: tRNA accommodated into the A/A state and EF-Tu has undergone a conformational change.

Accommodation of aa-tRNA from the A/T to the A/A state was observed by simulating from the C_I to the C_{IV} conformation using a single basin approach (Fig 4.2A) (Noel & Onuchic, 2012). During these simulations, the aa-tRNA passes through conformations C_{II} and C_{III} (Fig 4.1 B-C), verifying that I am sampling the same accommodation pathway resolved by cryo-EM in Loveland *et al.* (Loveland et al., 2017). To assess the completeness of the simulations, I measured the convergence of the time-dependent deviations of the system $\sigma(t)$ (Fig A3.1). All simulations converged at < 10

million time steps. Convergence is considered when $\sigma(t)$ approaches a plateau as per Vaiana *et al.* (2005).

Previously, it has been shown that accommodation of the elbow region of the tRNA can occur through three different pathways and multiple excursions (Whitford et al., 2010). The three pathways are defined by the path the acceptor stem of the accommodating tRNA takes, which can be: (1) progressing through the major groove of H89, (2) passing over the A-loop, or (3) moving between H89 and the A-loop. To investigate the accommodation pathways for cognate and near-cognate tRNA, the reaction coordinates R_{elbow} and R_{codon} were used (Fig 4.2A, B, C). R_{elbow} describes the distance between the A-site and P-site tRNA elbow, measuring the position of the tRNA in the accommodation corridor and R_{codon} describes the distance between the codon of the mRNA and the anticodon of the tRNA. I observe that cognate tRNA proceeds to a fully accommodated state, passing through C_{II} and C_{III} to reach C_{IV} in sequential order (Fig 4.2A, S6, 7). Surprisingly, I identify an alternative path that near-cognate tRNA can take to accommodate into the A/A state (Fig 4.2B, C). Near-cognate tRNA can proceed through the same pathway as cognate tRNA (16/20 simulations) (Fig 4.2B). However, it was also observed that near-cognate tRNA attempts an elbow first movement, before the codon-anticodon interactions have formed (4/20 simulations) ($Path_{NC}$) (Fig 4.2C). This allows near-cognate tRNA to reach C_{III} without passing through the C_{II} conformation (Fig 4.2B). Due to the single basin approach used in these simulations the near-cognate system will reach the fully accommodated state NC_{IV}, so I cannot interpret if this pathway leads to rejection of the near-cognate aa-tRNA.

Since the final step in accommodation is movement of the CCA-end towards the PTC, an R_3 value of <10Å is a good indication of a fully accommodated tRNA (Fig 4.2D).

The average time for both cognate and near-cognate to reach the A/A state is 4.7 ± 2.1 x 10^6 or 4.6 ± 2.5 x10^6 time steps respectively (Table A3.1). Interestingly, the R_3 distances of cognate and near-cognate aa-tRNA after accommodation are 6.3 ± 0.3 and 9.6 ± 0.4 Å, respectively (Fig 4.2D, Table A1.1). This suggests that although the CCA end of the near-cognate complex is approaching the PTC, it is in an unconventional conformation. This conformation likely will have an impact on peptide bond formation as the tRNA conjugated amino acids are too far apart for the condensation reaction to occur.

To explain how the near-cognate aa-tRNA accommodation path leads to a large R_3 value, I measured possible distortions of the aa-tRNA. The angle between the vector derived from the mRNA codon nucleotides 1 and 3 and the vector derived from the aa-tRNA elbow to anticodon ($\theta_{t\text{-}m}$) describes the position of the tRNA in the mRNA channel. While the cognate aa-tRNA forms an average angle of 132°, near-cognate adopts three different populations with average angles of 121, 127, and 131° (Fig 4.2E). This suggests that near-cognate codon-anticodon interactions can lead to an inherently flexible tRNA positioned in the A-site. The dynamic nature of near-cognate tRNA in the A-site, in conjunction with the more distant R_3, likely hinders peptide bond formation.

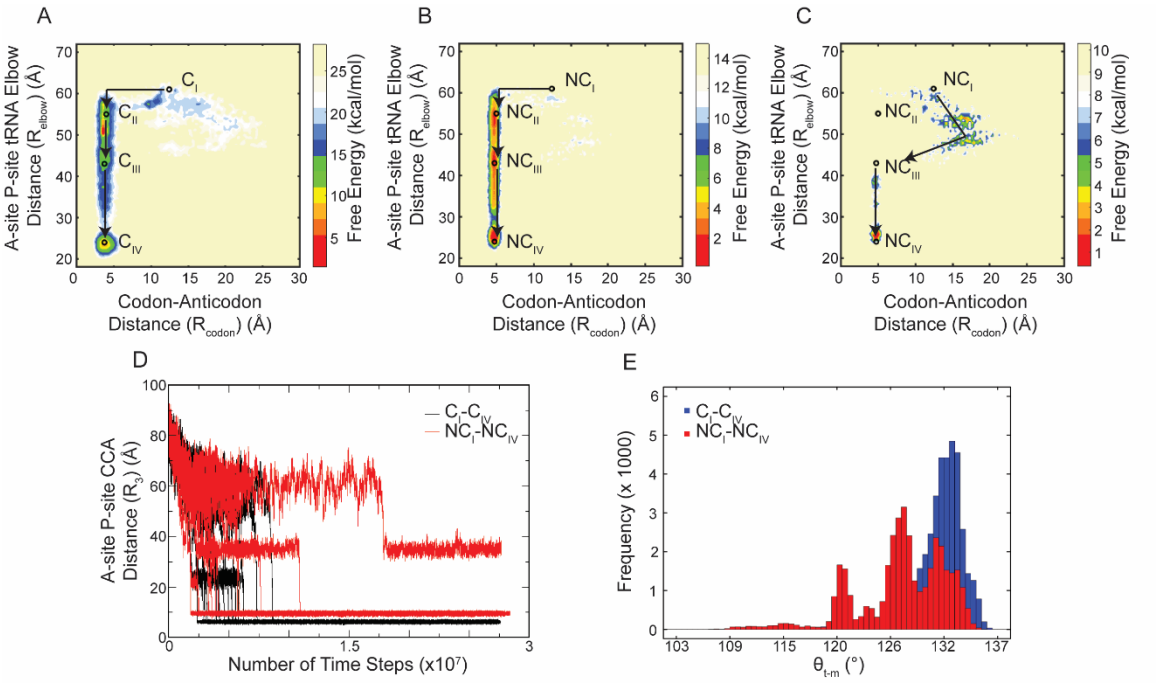

Figure 4.2. The Accommodation pathway of cognate and near-cognate tRNA-mRNA interactions. (A) Cognate and (B) near-cognate tRNA accommodation starts from the C_I conformation and follows a path to $C_{II} - C_{III} - C_{IV}$ as measured by the reaction coordinates R_{elbow} and R_{codon}. (C) Near-cognate aa-tRNA accommodation following $Path_{NC}$ proceeding through states $NC_I - NC_{III} - NC_{IV}$. (D) The reaction coordinate R_3 over the course of the simulations. (E) mRNA – tRNA angles once the simulation has reached the A/A state.

Aminoglycosides prevent $Path_{NC}$ and induce pre-codon recognition fluctuations

NEO and GEN induce incorporation of incorrect amino acids into the growing peptide chain by allowing for accommodation of near-cognate aa-tRNA. If the role of $Path_{NC}$ is to intervene with the accommodation of near-cognate aa-tRNA then GEN and NEO should prevent $Path_{NC}$ (Benveniste & Davies, 1973; Davies & Davis, 1968; Davies et al., 1965). To test this hypothesis, I simulated both cognate and near-cognate accommodation in the presence of GEN and NEO. Since structural studies show that

binding of GEN and NEO induce the `flipped-out` conformation of residues A1492 and A1493 of h44 of the 16S rRNA, they were modelled into this conformation (Fig 4.3 A, D).

In these simulations there is no evidence for $Path_{NC}$ in the cognate or near-cognate systems with GEN or NEO bound (Fig 4.3 B-C, E-F, Fig A3.4 A-D). Interestingly, I observe fluctuations in the tRNA at the anticodon stem loop before codon-anticodon interactions are formed for accommodation with GEN bound as well as cognate accommodation with NEO bound (Fig 4.4 B-C, E). This behaviour is not observed in the simulations without antibiotic or in the near-cognate simulation in the presence of neomycin (Fig 4.2 A, B, C, Fig 4.3F). The fluctuations of the anticodon stem loop when GEN is bound are supported by the findings of Tsai *et al.* where they show that the antibiotic induces short lived states of aa-tRNA bound to the 70S states, which ultimately leads to a loss of A-site aa-tRNA (Tsai et al., 2013). Again, the simulations utilize a single basin approach. Therefore, I do not observe the dissociation of A-site aa-tRNA. Regardless, the dynamics of the anticodon in the A-site are indicative of a stalled complex during accommodation, likely reflecting the short-lived states resolved by smFRET by Tsai *et al.* (2013). Furthermore, the behaviour observed here likely would lead to a higher probability of aa-tRNA rejection. These fluctuations reflect the anticodon of the tRNA searching for the codon of the mRNA, so I denote this behaviour as codon searching. Although cognate accommodation in the presence of NEO also exhibits codon searching it is less than in the GEN containing simulations (Fig 4.3 E). Wang *et al.*, show that NEO at high concentrations (20 μM) prevents accommodation of both cognate and near-cognate aa-tRNA (LaMarche, Leeds, Amaral, et al., 2012; Wang et al., 2012). The concentration of NEO in our simulations is 26.4μM, therefore, it is likely that the observed fluctuations before codon-

anticodon interactions are formed contribute to the lack of accommodation observed in Wang *et al* (Fig 4.4E) (Wang et al., 2012). The fluctuations of the anticodon stem loop are not observed for near-cognate accommodation in the presence of NEO, suggesting near-cognate accommodation is not as affected by this mechanism (Fig 4.3F). As such, NEO should induce more miscoding, favoring near-cognate tRNA due to the loss of these fluctuations. This is supported by Zhang *et al.* where they show that NEO induces more miscoding than GEN (Zhang, Pavlov, & Ehrenberg, 2018). The likely cause of the codonsearching is the fact that A1492 and A1493 are 'flipped out' prior to forming the codon-anticodon interactions (Fig 4.3 A, D). As a result, these nucleic acids provide a steric barrier making it less likely that the anticodon of the tRNA will sample the codon.

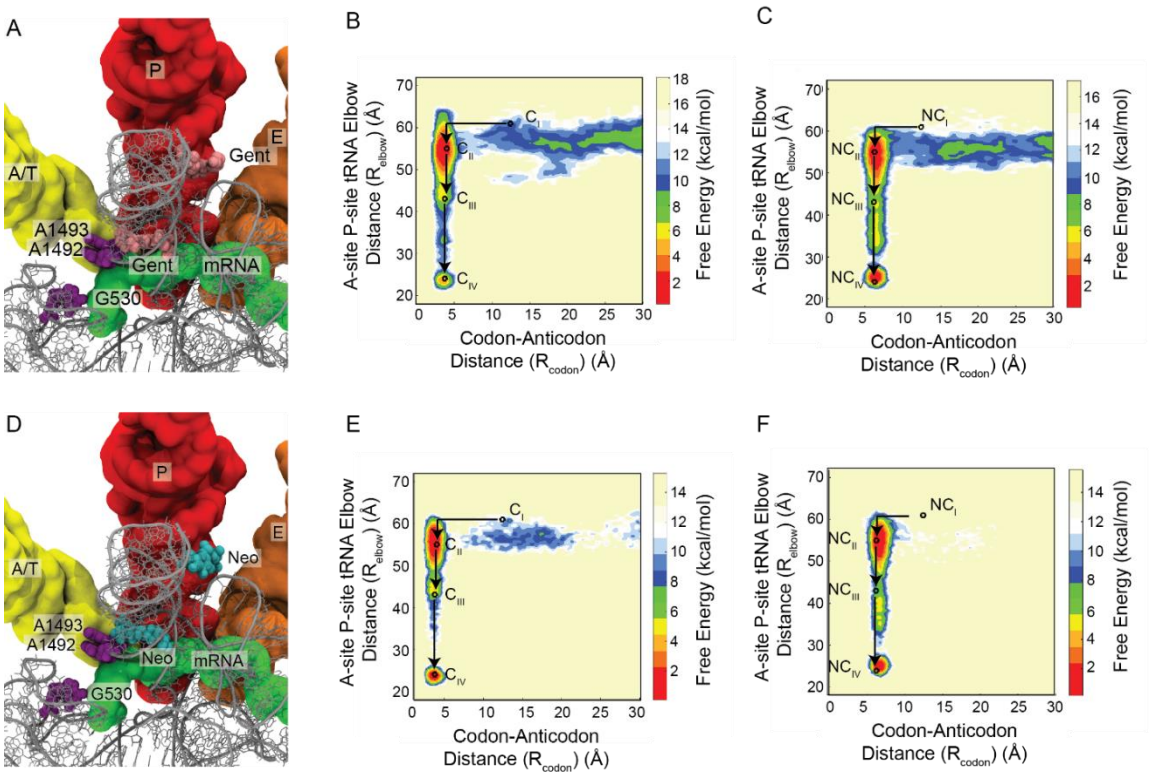

Figure 4.3 Aminoglycosides preventing the alternative pathway of near-cognate aa-tRNA accommodation. Visualization of (A) GEN and (D) NEO binding sites in h44 on the 16S rRNA and the 'flipped-out' positions of A1492 and A1493 at the start of the simulation. Free energy landscapes of accommodation defined by R_{elbow} and R_{codon} for cognate (B-GEN, E-NEO) and near-cognate (C-GEN, F-NEO) tRNA-mRNA interactions.

EVN induces intermediate conformations of tRNA that delay accommodation

Unlike GEN and NEO the direct role of EVN in accommodation of tRNA is unclear. The previously proposed mechanism of action for EVN, based on the available structural data, is to prevent accommodation of the A-site tRNA by providing a steric barrier in the accommodation corridor (Arenz et al., 2016; Mikolajka et al., 2011). To gain a better appreciation for the impact that EVN has on accommodation, I performed simulations with EVN bound to H89 (Fig 4.4A, D). The reaction coordinates of R_{elbow} and R_{codon}, describing the accommodation pathway reveal that EVN had no observable impact on cognate or near-

cognate accommodation from C_I to C_{III} or NC_I to NC_{III} (Fig 4.4B, C). However, both simulations indicate that the aa-tRNA has a high residency at the C_{II} or NC_{II} state (Fig 4.4B, C). Likely, the tRNA is stalled in a conformation that delays the movement towards C_{III} or NC_{III}. Additionally, between C_{III} and C_{IV} and likewise between NC_{III} and NC_{IV} an intermediate population is observed (Fig 4.4B, C).

To get a better understanding of the intermediate conformation induced by EVN, I measured the $\theta_{t\text{-}m}$. For both cognate and near cognate simulations, EVN inhibits tRNA accommodation at specific positions in the accommodation corridor (Fig 4.4D). None of the observed angles are comparable to the $\theta_{t\text{-}m}$ value for cognate tRNA in the absence of antibiotics (Fig 4.4D). Interestingly, one of the $\theta_{t\text{-}m}$ values that the near-cognate tRNA adopts in the presence of EVN is the same as near-cognate in the absence of antibiotic (127°), suggesting that in the presence of EVN the tRNA can only adopt a conformation similar to the near-cognate tRNA and not the cognate.

Since the tRNA reaches C_{IV} or NC_{IV} and multiple angles of the tRNA are observed in the presence of EVN, it is unlikely that the antibiotic simply acts as a steric inhibitor for accommodation. Visualization of the simulations revealed that EVN prevents the accommodation of the tRNA into the A-site by directly interacting with the major groove of the tRNA (Fig 4.5E). Our data supports that tRNA can move past the antibiotic by compressing at the elbow region (Fig 4.5E). Regardless, these interactions delay the accommodation and result in the states with unique defined mRNA-tRNA angles (Fig 4.5D)

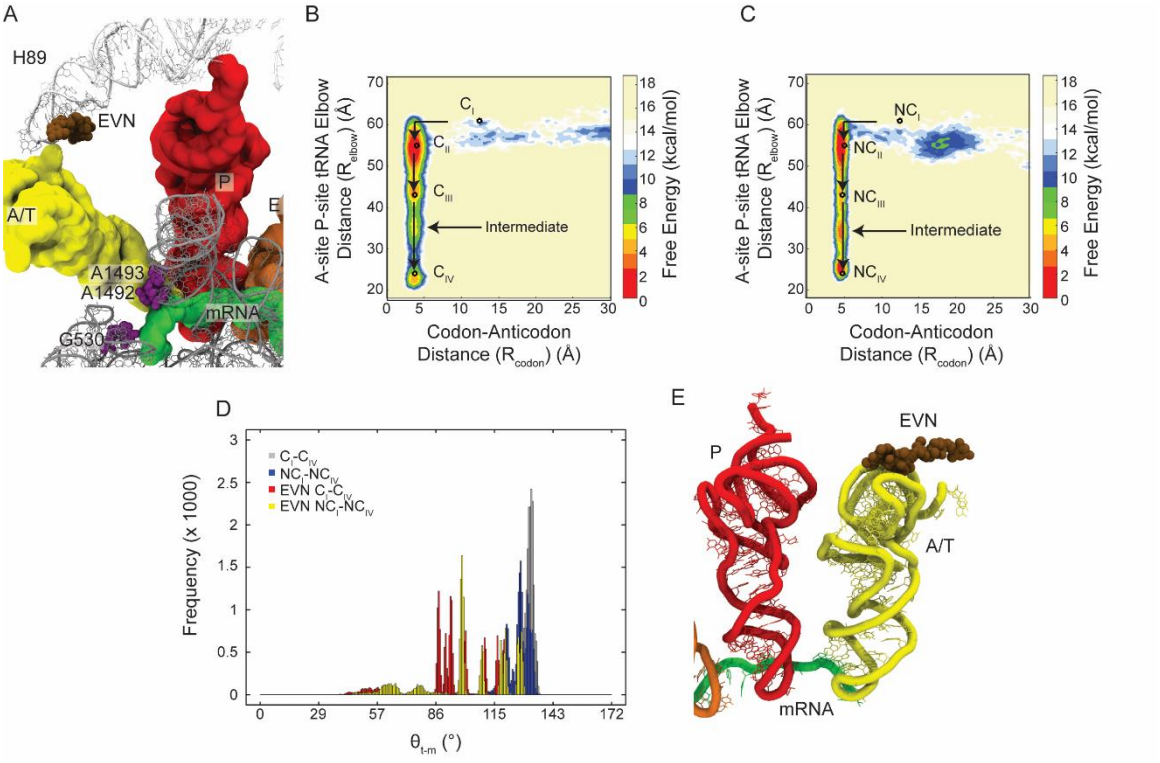

Figure 4.4 EVN prevents proper accommodation of cognate aa-tRNA. (A) Structural representation of EVN bound to the H89 of the 50S ribosomal subunit. Free energy landscapes of the accommodation pathway of cognate (B) and near-cognate (C) tRNA into the ribosomal A-site. (D) $\theta_{t\text{-}m}$ of tRNA incorporation for cognate and near-cognate aa-tRNA in the presence and absence of EVN. (E) EVN interacting with the major groove of tRNA during the accommodation pathway, inducing compression of the tRNA.

HGR prevents coordination of A-site tRNA CCA end

HGR binds adjacent to the P-site tRNA in the PTC and inhibits peptide bond formation in addition to stalling the accommodation of A-site aa-tRNA from the A/T to the A/A state (Fig 4.5A) (Guerrero & Modolell, 1980; Polacek et al., 2002; Polikanov et al., 2015). However, when the aa-tRNA does accommodate into the A/A state it adopts a unique conformation where A76 of the tRNA stacks with HGR. To investigate how HGR induces this unique conformation of tRNA in the A-site, identified by X-ray crystallography, I performed accommodation simulations in the presence of HGR. Our

simulations reveal several unique conformations of the aa-tRNA during accommodation which can be observed in both the cognate and the near-cognate simulations (Fig 4.5A-E). Among these conformations the canonical conformation where A76 stacks with HGR can be observed (Fig 4.5A). Additional conformations of the tRNA induced by HGR include conformations in which the CCA end of the A-site tRNA folds back on itself (Fig 4.5B), or where the CCA end of the aa-tRNA is positioned downwards towards the decoding center where the P-site tRNA and the mRNA interact (Fig 4.5C). It is likely that given a longer timescale the tRNA would transition between these conformations, exhibiting the back and forth oscillation of the tRNA observed by smFRET.

As a result of these unique conformations, the CCA end of the tRNA does not efficiently accommodate. In the presence of HGR, the CCA end of the tRNA accommodates after $5.6 \pm 3.1 \times 10^6$ time steps compared to cognate in the absence of antibiotic which accommodates after $4.7 \pm 1.1 \times 10^6$ time steps (Figure 4.5D, Table A3.1). Surprisingly, near-cognate aa-tRNA accommodates faster ($2.7 \pm 1.1 \times 10^6$ time steps) in the presence of HGR than without antibiotic ($4.6 \pm 2.5 \times 10^6$ time steps) (Figure 4.5E, Table A3.1). Therefore, HGR enhances the rate of near-cognate accommodation. Additionally, the distance of the CCA ends between the bound tRNAs (R_3) is on average of 0.8 Å longer for cognate in the presence of HGR (7.1 ± 0.3 Å) than in the absence (Table A3.1). This again verifies structural findings that the CCA end of the A-site tRNA cannot approach the PTC for efficient peptide bond formation.

.

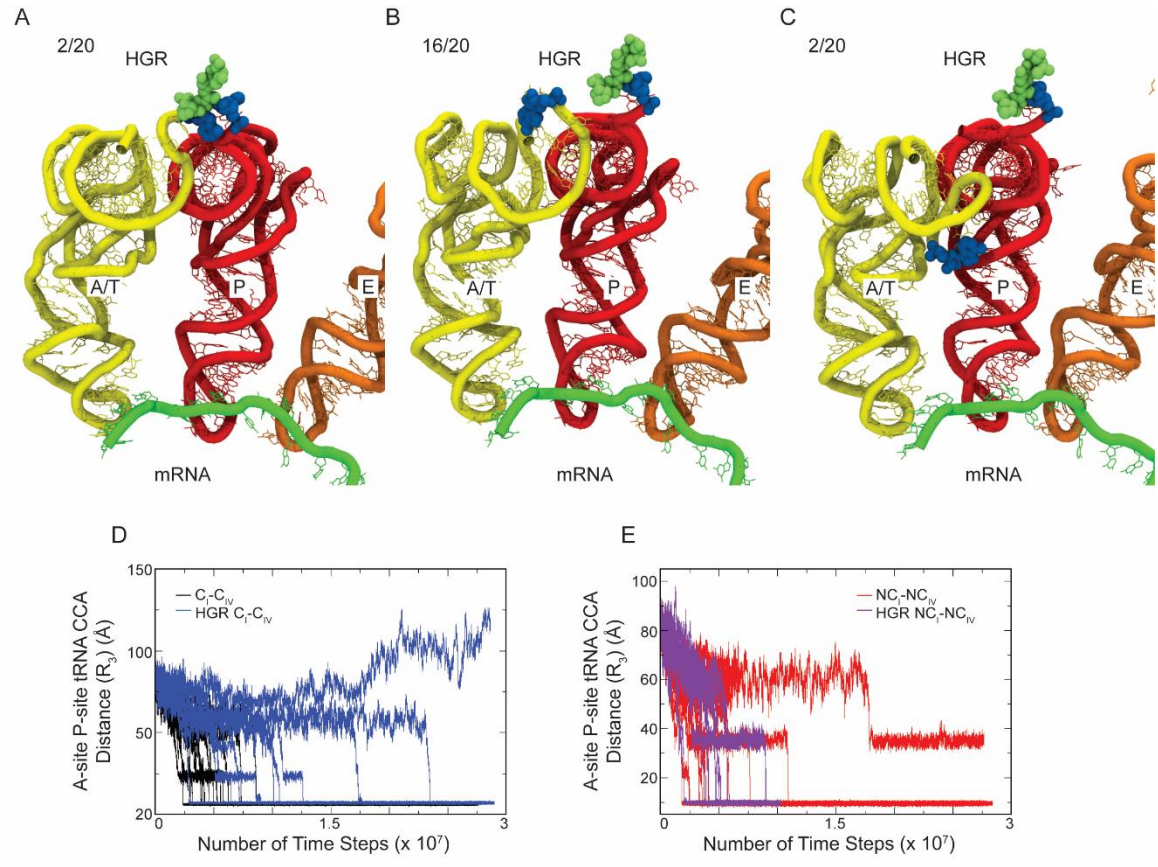

Figure 4.5 Impact of HGR on the accommodation of cognate and near-cognate aa-tRNA. (A) Conformations of cognate tRNA during accommodation in the presence of HGR (green) (A76 highlighted in blue). Distance of A-site – P-site CCA (R_3) for cognate (B) and near-cognate (C) aa-tRNA in the presence and absence of HGR.

EF-Tu correlated amino acid and nucleic acid dynamics

To investigate the transmission problem of allostery responsible for the 10^5-fold stimulation of GTP hydrolysis for EF-Tu during its interaction with the ribosome and cognate tRNA, the correlated dynamics of each amino acid and nucleic acid at the A-site were analyzed (Fig 4.6). This approach has previously been used to investigate the mechanism by which aa-tRNA synthetases bind to and catalyze the aminoacylation of

specific tRNA (Sethi et al., 2009). Sethi *et al.* utilized correlated Cα dynamics to investigate how the protein can respond to perturbation of tRNA binding, leading to activation of the enzyme. Using an approach similar to the one used in chapter 3, perturbations induced by ribosome binding in the EF-Tu•aa-tRNA•GTP ternary complex were investigated. To include nucleic acids into the analysis, the C1' atom of the ribose sugar was used to monitor the dynamics of the nucleic acids. To convert the covariance of Cα and C1' dynamics into a network, a cutoff distance of 10.5Å was used to draw edges between nucleic acids and between nucleic and amino acids (Fig 4.6 A,B). This distance was selected as it is slightly larger than the distance between C1' atoms involved in base-pairing in RNA helices present in the ribosome (~10.2Å), therefore, base-pairing correlated dynamics will be resolved within the network.

Using the parameters given above a Cα/C1' covariance Protein Structure Network (ccPSN) was constructed where each node represents an amino or nucleic acid and edges are drawn between them if they meet the requirement of having significant covariance and are within the cut-off distances for >75% of simulation time. The resulting network of the A-site is rather dispersed, where ribosomal proteins generally only interact with the rRNA or tRNA and there are only a few inter-protein connections (Fig 4.6A). Two RNA species are observed to connect to EF-Tu, both the 16S rRNA and the A-site tRNA (Fig 4.6A). Interestingly, L11 and L10, which together with L7/L12 make the L7/L12 stalk that directly interacts with EF-Tu, is distal from the protein (Fig 4.6A). Because L7/L12 is not resolved in contact with EF-Tu, it was left out of the simulation; however, it likely provides an additional interaction surface for which communication can be relayed to EF-Tu. Regardless, the two pathways observed here represent known interaction surfaces with EF-

Tu that are required for GTP hydrolysis activation. In domain II of EF-Tu, the residue that connects EF-Tu with the 16S rRNA (residues G360 and G361) is G222 (Fig 4.6B). Mutation of this residue has previously been shown to diminish EF-Tu GTP hydrolysis at 10 mM Mg^{2+} indicating the importance of this connection during allosteric activation of EF-Tu (Vorstenbosch et al., 1996). There are two main connections between EF-Tu and the tRNA in the network, between C74 of the tRNA to P54 of EF-Tu and between C3 of the tRNA and D86 and Y87 of EF-Tu (Fig 4.6B). Both of the latter residues are part of switch II (residues 84-97) containing H84 which has been proposed to be involved in coordination of a catalytic water leading to GTP hydrolysis (Daviter et al., 2003). Additionally, the tRNA interacts with domain III of EF-Tu and if these interactions are critical for activation, then the correlated dynamics must pass through the residues connecting domain I and III, creating a bottleneck for signal transmission. The residues involved are T382 and A376 of domain III to Q124 and L120 of domain I, respectively (Fig 4.6B). If correlated dynamics from the 16S rRNA or the tRNA are relayed through domain II to domain I of EF-Tu, then they must proceed through the bottleneck residues pairs of R205/P200, E215/T93, and R230/Q97 (Fig 4.6B). This again identifies switch II residues T93 and Q97 along with D86 and Y87 as residues that appear to be important in the allosteric communication pathway for EF-Tu on the ribosome, suggesting that they are critical for the allosteric mechanism of stimulated GTP hydrolysis on the ribosome. Taken together, these data support a four-fold signal relay from the ribosome to switch II of EF-Tu, pointing at the importance of this element for GTP hydrolysis activation and suggesting redundancy of the covariance network.

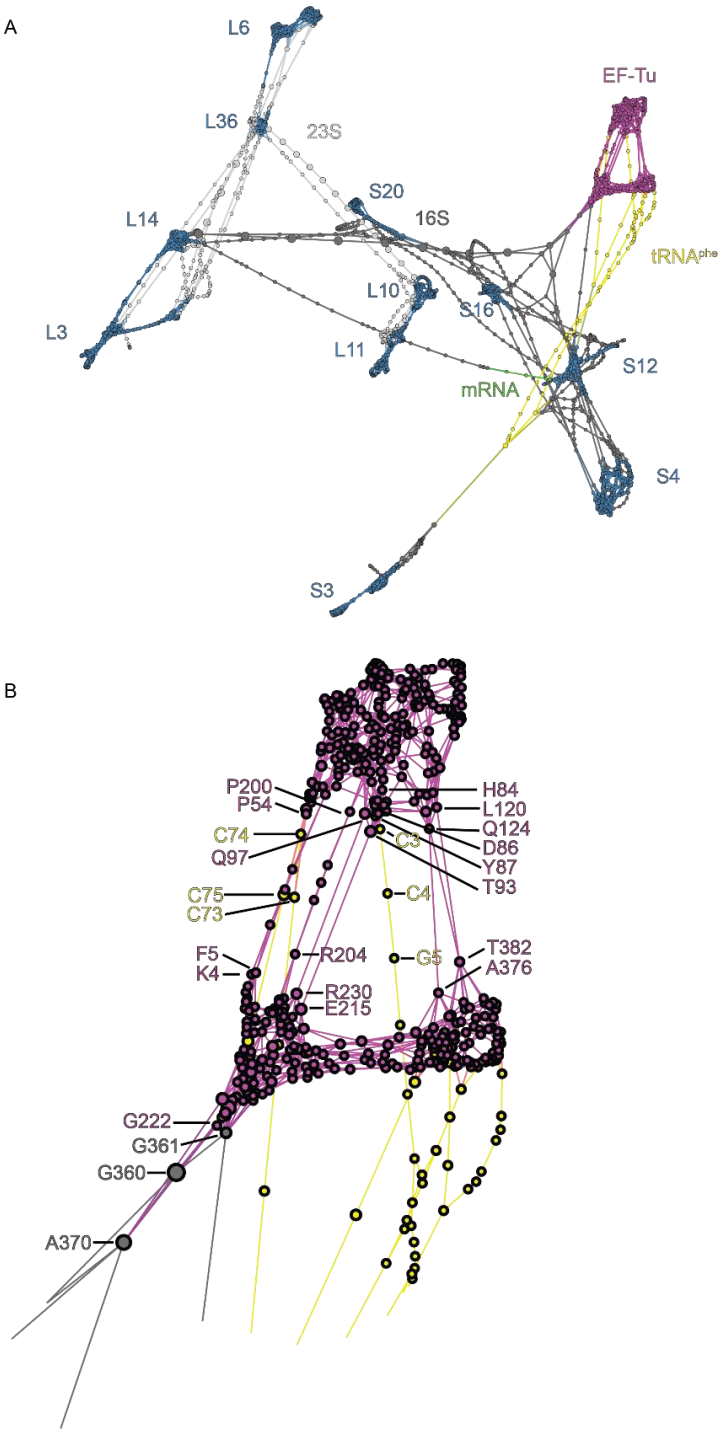

Figure 4.6 Correlated amino acid and nucleic acid dynamics of EF-Tu bound to the ribosome. (A) Correlated dynamics of A-site residues as defined by a 20Å radius around EF-Tu. Ribosomal proteins (blue), A-site tRNA (yellow), rRNA(gray), and EF-Tu (pink) are highlighted. (B) Correlated dynamics of EF-Tu (pink) and the main contact points with 16S rRNA (gray) and $tRNA^{phe}$ (yellow). Residues at the bottleneck of possible allosteric communication pathways are highlighted by labelling.

4.6 Discussion

Effects of the alternative accommodation pathway for near-cognate aa-tRNA

Our data supports an alternative accommodation pathway ($Path_{NC}$) for near-cognate tRNA (Fig 4.2 A, B). The implications of $Path_{NC}$ are that the near-cognate tRNA will enter into the A-site with a lower enthalpic contribution to binding as codon-anticodon interactions are not formed. Thermodynamically speaking, it is likely that this pathway could lead to rejection of the incoming aa-tRNA, as a major energy contributor for incorporation of tRNA is missing. Since our simulations utilize a single basin approach, tRNA rejection during $Path_{NC}$ is not observed.

In the case where the tRNA does accommodate, whether it takes $Path_{NC}$ or not, the resulting tRNA adopts different angles for near-cognate when compared to cognate tRNAs resulting in a 2.3 Å longer final R_3 (Table A1.1). As a consequence of this, the missing codon-anticodon interactions allow the tRNA to be misaligned in the A-site. Misaligned near-cognate tRNA has been proposed earlier as a mechanism by which near-cognate aa-tRNA fail to stimulate EF-Tu dependent GTP hydrolysis (Sanbonmatsu, 2006). The obtained data suggests that the misaligned near-cognate tRNA can also contribute to the fidelity of protein synthesis by preventing incorporation of incorrect amino acids. By inducing an increased R_3 value, the misalignment of the tRNA will prevent the activated amino acid from being properly positioned in the PTC. The increased populations of near-cognate tRNA-mRNA angles indicates that the tRNA is inherently flexible in the A-site. This suggests that near-cognate tRNA is relatively unstable at this position, likely leading to a higher probability of fluctuating back to the A/T state for subsequent tRNA rejection.

GEN and NEO induce enhanced codon searching leading to tRNA rejection

The observed codon searching in the presence of GEN or cognate accommodation in the presence of NEO is indicative of tRNA rejection. Likely, it is a result of A1492 and A1493 adopting the 'flipped-out' position which is induced by the antibiotics. This nucleotide conformation occludes the codon of the mRNA, reducing by 2.4Å the size of cavity through which the anticodon has to proceed to reach the codon. However, this is not small enough to prevent codon-anticodon interactions. Nonetheless, it may be enough to reduce the rate or frequency at which base-pairing occurs. The enhanced codon searching is consistent with Wang *et al.* who show that in the presence of 20 μM NEO the aa-tRNA is not likely to accommodate (Wang et al., 2012). Based on the size of the simulated molecular system and the number of NEO molecules present, our simulations are at a concentration of 26.4 μM which should reflect the 20 μM used in the experimental studies. Therefore, I propose that codon-searching likely results in rejection of the tRNA, however, our simulations utilize a single basin approach, which biases the system to the accommodated state. Once the tRNA has surpassed the steric barrier imposed by A1492 and A1493, accommodation proceeds at a ~2-fold faster rate than without antibiotic (Table A1.1). This is consistent with Tsai *et al.* (2013) who observed rapid accommodation rates using smFRET for aa-tRNA in the presence GEN. Consistent with their findings, I propose that this is due to A1492 and A1493 adopting the flipped-out conformation and recognizing the near-cognate codon-anticodon interactions as cognate.

Additionally, GEN and NEO prevent $Path_{NC}$, indicating that these antibiotics influence this accommodation route. The increased codon searching in the presence of GEN and NEO should favor $Path_{NC}$ as it occurs in the absence of codon-anticodon interactions.

I suggest that the absence of $Path_{NC}$ is a result of the 2-fold faster accommodation rate in the presence of these antibiotics. In the absence of antibiotics elbow accommodation occurs on average after 2.7 ± 1.8 x 10^6 time steps, the same number of time steps required for full accommodation in the presence of GEN and NEO (Table A1.1). This results in a scenario where accommodation occurs in the presence of GEN and NEO before the elbow of the tRNA can fluctuate into the A-site in the absence of codon-anticodon interactions.

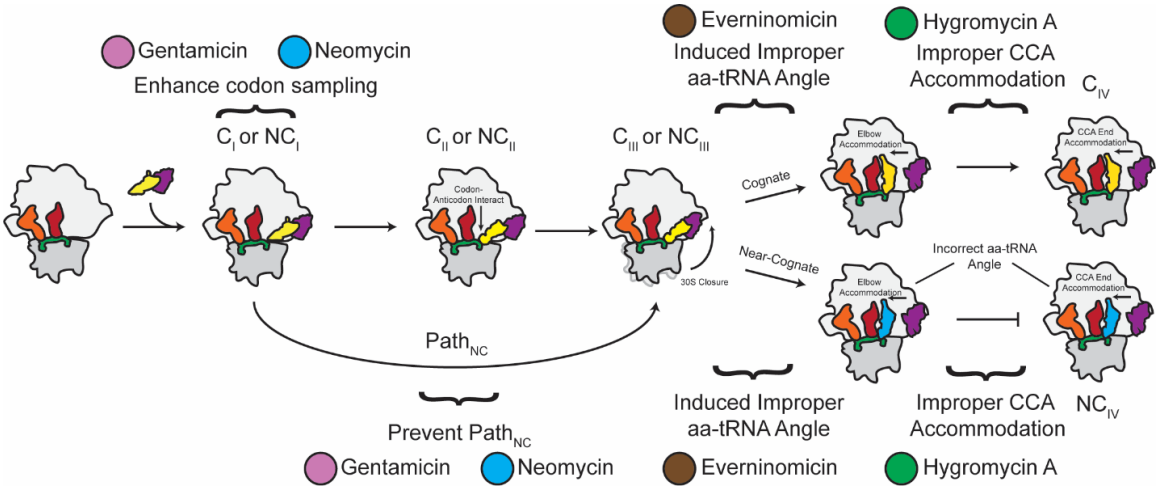

Figure 4.7 Model of cognate and near-cognate tRNA accommodation and the molecular mechanisms by which antibiotics disrupt accommodation.

EVN-induced stalled complexes indicates a novel mechanism for antibiotics

Previous reports on EVN predicted that the antibiotic prevents accommodation by blocking the aa-tRNA accommodation corridor (Arenz et al., 2016). If this is the mechanism of EVN action then it would be expected to have visualized a stalled aa-tRNA conformation unable to accommodate; however, I observed several stalled conformations alongside accommodation of the aa-tRNA (Fig 4.4D). The presented data show, for the first time, that the aa-tRNA stalls at different positions during accommodation as it tries to

surpass the EVN barrier. It stalls at first contact, during compression, and through direct interactions with the major groove of the tRNA (Fig 4.4). The binding of EVN to the major groove of the tRNA is similar to the interaction of H89 with the tRNA during accommodation (Noel & Whitford, 2016; Whitford et al., 2010). Our data supports a mechanism by which EVN is not only a steric barrier for accommodation, but also stalls accommodation of tRNA by interacting with the major groove of the tRNA. Alongside the major groove, the minor groove of the tRNA is an additional available interaction surface of the acceptor stem while the aa-tRNA is in the accommodation corridor. Development of an antibiotic to interact with the minor groove of the acceptor stem would likely inhibit or reduce the rate of aa-tRNA accommodation similar to EVN providing a target site for a novel antibiotic.

The ribosome treats cognate tRNA as near-cognate in the presence of HGR

The predicted mechanism of HGR is to prevent accommodation of the A-site aa-tRNA into the PTC. Our data supports this model, but also provides new insight into the mechanistic basis of how HGR is preventing accommodation. The main finding is that the positioning of the CCA end of the A-site aa-tRNA is disrupted, either being too far from the PTC, bent back on itself, or directed towards the mRNA channel (Fig 4.5A). Since the majority of simulations show that the CCA end is either folded back on itself or positioned away from the PTC, I suggest that the ribosome is treating the aa-tRNA as near-cognate. The average distance of the A-site and P-site A76 (R_3) is increased by 0.8Å in the presence of HGR for cognate tRNA (Table A1.1). Although this is not quite the same distance of 9.6 Å for near-cognate, the observed R_3 distance is too far from the PTC to allow for peptide bond formation. Interestingly, HGR has little to no effect on the accommodation of near-

cognate tRNA. The CCA ends adopt distances similar to that of near-cognate tRNAs without antibiotic at the end of the simulation (when convergence has occurred) (Fig 4.5C). It is likely that the inherent large R_3 already observed for the near-cognate does not allow HGR to disrupt near-cognate accommodation.

The importance of switch II in GTP-hydrolysis activation

The ccPSN indicates that the majority of ribosome binding information in the form of correlated amino or nucleic acid dynamics is relayed from the 16S rRNA or tRNA to switch II of EF-Tu. This information transfer has evolved into a split-trigger mechanism where four different pathways lead to communication between previously described elements important for GTP stimulation (h5 16S rRNA and cognate tRNA) and switch II (Fig 4.7). Consistent with such a role, the residues that make up the bottleneck in the ccPSN identified here are highly conserved as well, where E215, R204 and P200 are 100%, Q97, T93 are >99%, and R230 is 96% conserved (50 bacterial sequences aligned, 29 gram negative, and 21 gram positive) indicating that this structural dynamic feature of EF-Tu is deep-branching, since the average amino acid conservation in EF-Tu is ~74%. Several mutagenic studies have been performed on switch II to describe the importance of this element, most of which have led to a decrease in GTPase activity of EF-Tu. The H84A variant abolishes GTPase activity, while the C81A and C81S variants reduce the GTPase activity of EF-Tu by 4-fold (Daviter et al., 2003; Mercier, 2013). One natural variant, R230C, which is resistant to pulvomycin, has a 20% increased doubling time in *E. coli*, which can be explained by a reduced rate of EF-Tu GTP hydrolysis (Zeef et al., 1994). Additionally, the G83A variant of *E. coli* EF-Tu has no observable ribosome-stimulated GTP hydrolysis, demonstrating the essentiality of switch II sensing the cognate codon-

anticodon interactions (Knudsen, Wieden, & Rodnina, 2001). Further support for the observed 'bottleneck residues' identified by ccPSN as being essential for ribosome stimulated EF-Tu GTP hydrolysis is the dependency on intact tRNA. Piepenburg *et al.* have shown that two tRNA half fragments (separated at the TΨC loop) are incapable of inducing the ribosome-dependant stimulation of EF-Tu's GTP hydrolysis (Piepenburg et al., 2000). This would likely disrupt the communication from the tRNA to EF-Tu, including disrupting the communication from C3 of the tRNA to Y87 of switch II (Fig 4.7B).

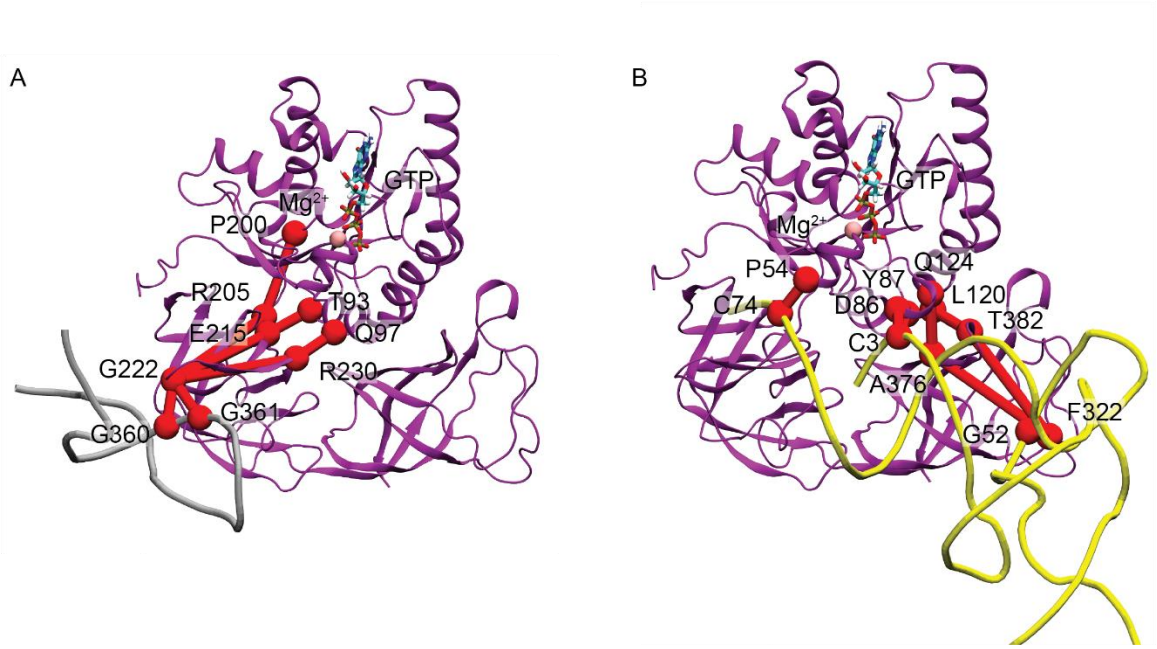

Figure 4.8 Most likely paths for Cα covariance to be propagated to EF-Tu GTP binding site. (A) Cα covariance originating from h5 of the 16S rRNA (gray) to the GTP binding site of EF-Tu (purple). (B) Cα covariance originating from aa-tRNA (yellow) to the GTP binding site of EF-Tu (purple). Residues that make up bottlenecks in the ccPSN are highlighted as spheres (red) and connections between them are drawn as lines (red) to describe probable pathways by which ribosome binding information can be propagated.

Interestingly, no Cα/C1' connections originate from the SRL of the 23S rRNA. Structural studies have predicted that the SRL coordinates H84 for proper coordination of an activated water molecule, indicating that it plays a major role in GTP hydrolysis

(Schmeing et al., 2009). The role of these pathways directed towards switch II are still unclear, however, it is likely that they are involved in the rearrangement of switch II required for positioning of H84 for coordination of the catalytic water. A hydrophobic gate consisting of V20 and I60 has been proposed to prevent H84 from spontaneously coordinating a water molecule leading to hydrolysis, therefore, to get past the hydrophobic gate it is likely that coordinated dynamics are required (Berchtold et al., 1993). In this context, dynamics coming from four directions may be required to properly position H84 for the attack, disruption of which should reduce that catalytic activity of EF-Tu.

4.7 Conclusion

Accommodation of tRNA into the ribosomal A-site is a complex process requiring multiple steps. Here, I provide the first molecular dynamics explanation for the differences between cognate and near-cognate transitions from the A/T to the A/A state. Near-cognate accommodation proceeds through an alternative pathway leading to improper tRNA/mRNA angles resulting in the CCA end of the tRNA being improperly positioned in the PTC. NEO and GEN block the alternative pathway and induce codon searching by occluding the codon, indicating that these antibiotics induce miscoding by preventing $Path_{NC}$. Lastly, EVN induces improper tRNA-mRNA angles through direct interactions with the tRNA, implying that the antibiotic slows the accommodation of both cognate and near-cognate aa-tRNA. HGR displaces the CCA end of the tRNA away from the PTC, indicating that the antibiotic stalls translation through prevention of peptide bond formation. The detailed structural dynamics description of how these antibiotics disrupt accommodation helps to lay the foundation for therapeutic development of accommodation blockers.

Chapter 5

Conclusion

5.1 Regulation of EF-Tu nucleotide binding

Of the three problems of allostery, only the transition problem has previously been investigated in-depth for nucleotide binding to EF-Tu, where EF-Tu solves this problem with the MWC model, leaving the equilibrium and transmission problems elusive (Johansen et al., 2018; Kavaliauskas et al., 2018). Evidence for the KNF model does exist in the case where Pi release limits EF-Tu conformational change when EF-Tu is in complex with the ribosome (Kothe & Rodnina, 2006). To address the equilibrium problem, the thermodynamic landscapes and activation energies of nucleotide binding were determined using a pre-steady state stopped-flow technique. Coupling the temperature dependence of these experiments with the Eyring-Polani equation revealed that the activation barriers for nucleotide association are the same for GTP and GDP, indicating that EF-Tu does not discriminate between the two nucleotides during this half-reaction. The major differences in the entropic, enthalpic, and free energy landscapes are the activation barriers of nucleotide dissociation. EF-Tu•GTP is entropically stabilized, whereas EF-Tu•GDP is enthalpically stabilized as the barriers for dissociation are greater for the respective conformation. As such, the presence or absence of the γ-phosphate defines the thermodynamics of EF-Tu's nucleotide-dependent conformation, consistent with Kothe and Rodnina showing that Pi release triggers the conformational change in EF-Tu (Kothe & Rodnina, 2006). The structural features that energetically stabilize the respective conformations of EF-Tu were investigated using 100 ns MD simulations. These simulations reveal that EF-Tu•GTP is entropically stabilized due to a decreased water coordination shell whereas EF-Tu•GDP is enthalpically stabilized due to an increased number of hydrogen bonds amongst the backbone atoms. To probe these structural dynamic elements, site-

directed mutagenesis performed to target the hydrogen bonds stabilizing EF-Tu•GDP and targeted the conformational dynamics of EF-Tu with kirromycin, locking it in the classical GTP conformation. The MD findings were validated as the H22G variant of EF-Tu reduces the enthalpic barrier of GDP dissociation by reducing the number of hydrogen bonds available to EF-Tu•GDP. Kirromycin binding to EF-Tu inverses the rates of GDP and GTP dissociation, where the rate of GTP dissociation was 6-fold slower than GDP at 37°C, verifying that the structural dynamics of EF-Tu define the nucleotide dissociation rates.

In chapter 2, the equilibrium problem of nucleotide binding to EF-Tu was investigated, specifically how nucleotide binding changes the thermodynamic landscape of EF-Tu. The results indicate that the *apo* form of EF-Tu recognizes both GTP and GDP similarly. Since the structural and dynamic properties of EF-Tu define nucleotide binding, it is likely that the *apo* form of EF-Tu is a unique conformation or ensemble of conformations compared to EF-Tu•GTP or EF-Tu•GDP. It cannot be ruled out that the *apo* conformation of EF-Tu is roughly a 50/50 split representation of both the GTP and GDP conformation, although this is unlikely. The entropically-stabilized EF-Tu•GTP conformation indicates that GTP binding utilizes a type III solution to the equilibrium problem, where there is no change in conformation but there is a change in protein dynamics. If we consider *apo* as a unique conformation, a type III mechanism is unlikely because EF-Tu•GTP is a unique conformation distinct from the apo conformation, therefore, GTP binding must undergo a type II solution to the equilibrium problem. GDP binding, which is both enthalpically and entropically stabilized compared to the *apo* conformation of EF-Tu, is a type II solution to the equilibrium problem. Therefore, both

nucleotides utilize the type II solution, changing both the conformation of the protein upon ligand binding as well as changing the protein's overall dynamics.

Understanding the design principles that EF-Tu utilizes to regulate nucleotide binding and how conformational rearrangements within the protein stabilize the bound state of the protein provides a platform with which synthetic molecular switches can be developed. This is of great interest to the protein engineering field as our current understanding of protein switches is lacking a structural dynamics interpretation, impeding their development. The detailed kinetic and structural dynamic description of EF-Tu provides evidence for how a universally conserved protein switch has evolved to bind to two separate ligands with differential affinity while adopting unique conformations. This research provides useful insights for the design of synthetic molecular switches. The properties critical to fine-tuning ligand binding affinity are the rate of dissociation alongside the dynamics of each conformation since they provide the thermodynamic stability of the nucleotide bound state of EF-Tu. Altering these properties provides a handle for which the switching behaviour of a developed molecular switch can be manipulated.

5.2 D2R conformational landscape and activation pathway

The conformational landscape of D2R prior to ligand binding and receptor activation has been elusive. This is likely due to the conditions as a result of the crystallisation of GPCRs, such as lattice formation inducing a single specific conformation of the GPCR or the common practice of conjugating lysozyme to the extracellular surface of the protein. Since NMR has shown that several conformations of GPCRs exist in the absence of ligand, an atomistic view of these conformations is required to fully understand the MWC model of GPCR activation (Casiraghi et al., 2019; Kobilka & Deupi, 2007; Lee et al., 2015; Manglik et al., 2015; Nygaard et al., 2013; Weis & Kobilka, 2008). If the MWC model holds true for GPCRs then there will be an ensemble of several activated-like and inactive-like structures of the receptor prior to ligand binding. To investigate the conformation landscape of the receptor prior to ligand binding, MD simulations were performed totalling 3.3 μs of simulation time. Using PCA, MSM, and Maxclustering, 5 different conformations of D2R were identified prior to ligand binding, where conformation 2 represents the inactive form and conformations 4 and 5 are closer to the activated conformation. Altogether, this provides evidence that D2R utilizes a MWC model where there is an ensemble of conformations available to the protein prior to ligand binding. However, the protein does not adopt the fully active conformation on the time-scale of our simulations. Therefore, ligand binding likely does induce rearrangements of the protein, which would indicate some form of a KNF model where ligand binding is required to reach the fully active conformation of the GPCR. This implies that D2R adopts a twofold allosteric solution to the transition problem. The model suggests that conformations of the D2R exist prior to ligand binding that display properties of the activated state. Once ligand

binding occurs it provides the energy for the system to enter into the activated conformation. Inducing the conformations of D2R identified here through small molecule binding or perturbation through mutations can provide a platform for fine-tuning of the D2R.

Additionally, the transmission problem of the D2R was investigated by investigating the Cα covariance of the amino acids of the receptor. Using graph theory, the shortest pathway between nodes involved in dopamine binding and G-protein binding a pathway was derived, providing a platform for which ligand binding information could be relayed to the G-protein interface. This pathway shows that low-activity variants of D2R primarily communicate to $G380^{6.42}$ of D2R where high-activity variants transmit their signals to $F382^{6.44}$. The communication to $G380^{6.42}$ likely prevents the helical rearrangement of TM6 required for receptor activation, where the signal to $F382^{6.44}$ promotes reorganization of the amino acid, facilitating TM6 bending. The residues critical to this allosteric pathway are $Y199^{5.48}$ and $F202^{5.51}$, residues at the extracellular surface of D2R. It appears that these residues bifurcate the pathway between TM3 and TM6 allowing for Cα covariance to proceed to $G380^{6.42}$ or $F382^{6.44}$ and highlights them as critical residues. This is validated as Sung *et al* (2016) show that Y199F leads to a 6-fold increase in D2R activity, whereas ligand binding is not affected. D2R has solved the transmission problem by dividing allosteric pathways between TM3 and TM6 ultimately requiring the loss of communication to $G380^{6.42}$ for activation of the receptor. The combination of the biochemical data provided by Sung *et al* (2016) with the structural dynamic analysis performed here provides a description of GPCR's solution to the transmission problem of allostery. To display the universality of the pathway described above, further investigation

into the Cα covariance pathways capable of relaying ligand binding information to the G-protein interface for additional GPCRs is required.

The analysis described in chapter 3 outlines the Protein Characterization for Personalized Medicine (PCPM) pipeline which can be used to characterize the impact of mutations on the structural dynamics of a protein. I show that the V154I variant of D2R linked to Myoclonus Dystonia displays structural dynamics of both the low- and high-activity variants likely leading to the inability of groups to identify phenotypes of the variant in HEK293 cell lines (Klein et al., 2000). Therefore, I provide evidence for how the variant impacts the overall structural dynamics of the protein, which is likely to cause subtle phenotypical changes which may be better displayed in more relevant cell lines.

5.3 Structural dynamics of cognate aa-tRNA accommodation

Near-cognate aa-tRNA accommodation is limited by the rate of GTP hydrolysis of EF-Tu, as this system has a 650-fold reduced GTPase activity compared to cognate aa-tRNA (Rodnina, Gromadski, Kothe, & Wieden, 2005). How EF-Tu distinguishes which tRNA is present at the A-site based on a single base pair difference is still unknown. To investigate how EF-Tu senses the presence of the cognate codon, Gō-like (structure-based) simulations were performed to analyze the differences in dynamics for the accommodation pathway of each tRNA. The cognate tRNA ($tRNA^{phe}$) proceeded through the accommodation corridor similarly to what has previously been reported (Whitford et al., 2010). However, near-cognate tRNA ($tRNA^{lys}$) proceeded using an alternative pathway whereby the elbow of the tRNA attempts to accommodate before the base-pairs are formed between the tRNA and the mRNA. The result of this is that the tRNA is improperly positioned in the A/A state where the CCA end of the tRNA is not situated properly for peptide bond formation. The presence of aminoglycosides neomycin and gentamicin, which induce miscoding of mRNA, blocks the near-cognate pathway. This suggests that the pathway observed is a feature that the ribosome utilizes to discriminate cognate from near-cognate tRNA. With the accommodation simulation pipeline developed, the impact that other antibiotics have on accommodation could be measured. In the presence of evernimicin, the tRNA stalls in the accommodation corridor. Hygromycin A prevents proper positioning of the CCA end of the tRNA, preventing peptide bond formation. Altogether, our results show three different mechanisms by which antibiotics can inhibit tRNA accommodation or induce miscoding of mRNA, providing a platform for the development of novel antibiotics.

To investigate how GTP hydrolysis is rate-limiting for near-cognate accommodation, the transmission problem of allostery was addressed by measuring the Cα and C1' covariance of protein and RNA, respectively. Using the analysis outlined in chapter 3, a network describing Cα/C1' covariance pathways within the system for which ribosome binding information could be relayed to the GTP binding site was derived. This network revealed that the majority of information arising from the ribosome is directed towards switch II of EF-Tu where H84, the amino acid responsible for coordination of a catalytic water molecule, is located. Several mutagenic studies confirm the importance of correlated dynamics directed towards switch II in EF-Tu's ribosome stimulated GTP hydrolysis activity. The 4-fold trigger-switch for relaying ribosome binding information to switch II of EF-Tu is likely an insurance policy preventing GTP hydrolysis activation of EF-Tu when near-cognate or a dysfunctional ternary complex binds to the A-site. If these complexes do not activate the trigger-switch, GTP hydrolysis and subsequent aa-tRNA accommodation would likely be delayed.

Altogether, this chapter provides a structural dynamic description of how the ribosome and EF-Tu facilitate the accommodation of cognate over near-cognate aa-tRNA. Additionally, it describes three different mechanistic descriptions of how four contemporary antibiotics function. The three strategies observed by antibiotics in this report is: blocking the alternative near-cognate path, stalling the tRNA during accommodation by interacting with the grooves of the tRNA, or inducing the improper positioning of the CCA end of the tRNA. These mechanisms of protein synthesis inhibition can now be used to screen small molecules using similar simulations performed in this study to identify potential antibiotics. These antibiotics can then be tested *in vitro* and *in vivo* to validate

their applicability. In particular, this screening step will streamline the search and focus on compounds which are more likely to directly target translation. Lastly, the chapter displays through Cα/C1’ covariance how EF-Tu’s GTP hydrolysis activity is stimulated by ribosome binding. The covariance is directed towards switch II of EF-Tu which houses H84, predicted to be involved in coordination of the catalytic water molecule. This provides, for the first time, a description of how trGTPases address the transmission problem upon binding to the ribosome.

References

Abel, K., Yoder, M. D., Hilgenfeld, R., & Jurnak, F. (1996). An α to β conformational switch in EF-Tu. *Structure, 4*(10), 1153-1159.

Al-Karadaghi, S., AEvarsson, A., Garber, M., Zheltonosova, J., & Liljas, A. (1996). The structure of elongation factor G in complex with GDP: Conformational flexibility and nucleotide exchange. *Structure, 4*(5), 555-565.

Anborgh, P. H., Okamura, S., & Parmeggiani, A. (2004). Effects of the Antibiotic Pulvomycin on the Elongation Factor Tu-Dependent Reactions. Comparison with Other Antibiotics. *Biochemistry, 43*, 15550-15556.

Anborgh, P. H., & Parmeggiani, A. (1993). Probing the reactivity of the GTP- and GDP-bound conformations of Elongation Factor Tu in complex with the antibiotic GE2270 A. *J. Biol. Chem., 268*(33), 24622-24628.

Anderson, J. S., Bretscher, M. S., Clark, B. F., & Marcker, K. A. (1967). A GTP requirement for binding initiator tRNA to ribosomes. *Nature, 215*(5100), 490-492.

Antoun, A., Pavlov, M. Y., Andersson, K., Tenson, T., & Ehrenberg, M. (2003). The roles of initiation factor 2 and guanosine triphosphate in initiation of protein synthesis. *The EMBO Journal, 22*(20), 5593-5601.

Arenz, S., Juette, M. F., Graf, M., Nguyen, F., Huter, P., Polikanov, Y. S., Blanchard, S. C., & Wilson, D. N. (2016). Structures of the orthosomycin antibiotics avilamycin and evernimicin in complex with the bacterial 70S ribosome. *Proceedings of the National Academy of Sciences of the United States of America, 113*(27), 7527-7532.

Arnold, K., Bordoli, L., Kopp, J., & Schwede, T. (2006). The SWISS-MODEL workspace: a web-based environment for protein structure homology modelling. *Bioinformatics, 22*(2), 195-201.

Atilgan, A. R., Akan, P., & Baysal, C. (2004). Small-world communication of residues and significance for protein dynamics. *Biophysical Journal, 86*(1 Pt 1), 85-91.

Bakan, A., Dutta, A., Mao, W., Liu, Y., Chennubhotla, C., Lezon, T. R., & Bahar, I. (2014). Evol and ProDy for bridging protein sequence evolution and structural dynamics. *Bioinformatics, 30*(18), 2681-2683.

Bakan, A., Meireles, L. M., & Bahar, I. (2011). ProDy: protein dynamics inferred from theory and experiments. *Bioinformatics, 27*(11), 1575-1577.

Baldwin, J. M. (1993). The probable arrangement of the helices in G protein-coupled receptors. *The EMBO Journal, 12*(4), 1693-1703.

Balesteros, J. A., & Weinstein, H. (1995). Integrated methods for the construction of three-dimensional models and computational probing of structure-function relations in G protein-coupled receptors. *Methods in Neurosciences, 25*, 366-428.

Beauchamp, K. A., Bowman, G. R., Lane, T. J., Maibaum, L., Haque, I. S., & Pande, V. S. (2011). MSMBuilder2: Modeling Conformational Dynamics on the Picosecond to Millisecond Scale. *Journal of Chemical Theory and Computation, 7*(10), 3412-3419.

Becker, B., & Cooper, M. A. (2013). Aminoglycoside antibiotics in the 21st century. *ACS Chemical Biology, 8*(1), 105-115.

Benveniste, R., & Davies, J. (1973). Structure-Activity Relationships Among the Aminoglycoside Antibiotics: Role of Hydroxyl and Amino Groups. *Antimicrobial Agents and Chemotherapy, 4*(4), 402-409.

Berchtold, H., Reshetnikova, L., Reiser, C. O., Schirmer, N. K., Sprinzl, M., & Hilgenfeld, R. (1993). Crystal structure of active elongation factor Tu reveals major domain rearrangements. *Nature, 365*(6442), 126-132.

Bhattacharya, S., Salomon-Ferrer, R., Lee, A., & Vaidehi, N. (2016). Conserved Mechanism of Conforamtional Stability and Dynamics in G-Protein-Coupled Receptors. *Journal of Chemical Theory and Computation, 12*, 5575-5584.

Bhattacharya, S., & Vaidehi, N. (2014). Differences in allosteric communication pipelines in the inactive and active states of a GPCR. *Biophysical Journal, 107*(2), 422-434.

Biasini, M., Bienert, S., Waterhouse, A., Arnold, K., Studer, G., Schmidt, T., Kiefer, F., Gallo Cassarino, T., Bertoni, M., Bordoli, L., & Schwede, T. (2014). SWISS-MODEL: modelling protein tertiary and quaternary structure using evolutionary information. *Nucleic Acids Research, 42*(Web Server issue), W252-258.

Bjarnadottir, T. K., Gloriam, D. E., Hellstrand, S. H., Kristiansson, H., Fredriksson, R., & Schioth, H. B. (2006). Comprehensive repertoire and phylogenetic analysis of the G protein-coupled receptors in human and mouse. *Genomics, 88*(3), 263-273.

Blanchard, S. C., Gonzalez, R. L., Kim, H. D., Chu, S., & Puglisi, J. D. (2004). tRNA selection and kinetic proofreading in translation. *Nature Structural & Molecular Biology, 11*(10), 1008-1014.

Bochner, B. R., & Ames, B. N. (1982). Complete analysis of cellular nucleotides by two-dimensional thin layer chromatography. *Journal of Biological Chemistry, 257*(16), 9759-9769.

Bock, L. V., Blau, C., Schröder, G. F., Davydov, I. I., Fischer, N., Stark, H., Rodnina, M. V., Vaiana, A. C., & Grubmüller, H. (2013). Energy barriers and driving forces in tRNA translocation though the ribosome. *Nature Structural & Molecular Biology, 12*, 1390-1396.

Bockaert, J., & Pin, J. P. (1999). Molecular tinkering of G protein-coupled receptors: an evolutionary success. *The EMBO Journal, 18*(7), 1723-1729.

Bonci, A., & Hopf, F. W. (2005). The dopamine D2 receptor: New surprises from an old friend. *Neuron, 47*, 335-338.

Borovinskaya, M. A., Pai, R. D., Zhang, W., Schuwirth, B. S., Holton, J. M., Hirokawa, G., Kaji, H., Kaji, A., & Cate, J. H. D. (2007). Structural basis for aminoglycoside inhibition of bacterial ribosome recycling. *Nature Structural & Molecular Biology, 14*(8), 727-732.

Bos, J. L. (1989). *ras* oncogenes in human cancer: a review. *Cancer Research, 49*(17), 4682-4689.

Bourne, H. R., Sanders, D. A., & McCormick, F. (1991). The GTPase superfamily: conserved structure and molecular mechanism. *Nature, 349*(6305), 117-127.

Brodersen, D. E., Clemons, W. M., Jr., Carter, A. P., Morgan-Warren, R. J., Wimberly, B. T., & Ramakrishnan, V. (2000). The structural basis for the action of the antibiotics tetracycline, pactamycin, and hygromycin B on the 30S ribosomal subunit. *Cell, 103*(7), 1143-1154.

Brooks, B. R., Brooks, C. L., 3rd, Mackerell, A. D., Jr., Nilsson, L., Petrella, R. J., Roux, B., Won, Y., Archontis, G., Bartels, C., Boresch, S., Caflisch, A., Caves, L., Cui, Q., Dinner, A. R., Feig, M., Fischer, S., Gao, J., Hodoscek, M., Im, W., Kuczera, K., Lazaridis, T., Ma, J., Ovchinnikov, V., Paci, E., Pastor, R. W., Post, C. B., Pu, J. Z., Schaefer, M., Tidor, B., Venable, R. M., Woodcock, H. L., Wu, X., Yang, W., York, D. M., & Karplus, M. (2009). CHARMM: the biomolecular simulation program. *Journal of Computational Chemistry, 30*(10), 1545-1614.

Buckstein, M. H., He, J., & Rubin, H. (2008). Characterization of nucleotide pools as a function of physiological state in *Escherichia coli*. *Journal of Bacteriology, 190*(2), 718-726.

Burdett, V. (1986). Streptococcal Tetracycline Resistance Mediated at the Level of Protein-Synthesis. *Journal of Bacteriology, 165*(2), 564-569.

Burdett, V. (1996). Tet(M)-promoted release of tetracycline from ribosomes is GTP dependent. *Journal of Bacteriology, 178*(11), 3246-3251.

Butterfield, G. L., Lajoie, M. J., Gustafson, H. H., Sellers, D. L., Nattermann, U., Ellis, D., Bale, J. B., Ke, S., Lenz, G. H., Yehdego, A., Ravichandran, R., Pun, S. H., King, N. P., & Baker, D. (2017).

Evolution of a designed protein assembly encapsulating its own RNA genome. *Nature, 552*(7685), 415-420.

Capecchi, M. R. (1967). Polypeptide chain termination *in vitro*: isolation of a release factor. *Proceedings of the National Academy of Sciences of the United States of America, 58*(3), 1144-1151.

Carter, A. P., Clemons, W. M., Brodersen, D. E., Morgan-Warren, R. J., Wimberly, B. T., & Ramakrishnan, V. (2000). Functional insights from the structure of the 30S ribosomal subunit and its interactinos with antibiotics. *Nature, 407*, 340-348.

Casiraghi, M., Point, E., Pozza, A., Moncoq, K., Baneres, J. L., & Catoire, L. J. (2019). NMR analysis of GPCR conformational landscapes and dynamics. *Molecular and Cellular Endocrinology, 484*, 69-77.

Cetin, R., Krab, I. M., Anborgh, P. H., Cool, R. H., Watanabe, T., Sugyama, T., Izaki, K., & Parmeggiani, A. (1996). Enacyloxin Ila, an inhibitor of protein biosynthesis that acts on elongation factor Tu and the ribosome. *The EMBO Journal, 15*(10), 2604-2611.

Chien, E. Y. T., Liu, W., Zhao, Q. A., Katritch, V., Han, G. W., Hanson, M. A., Shi, L., Newman, A. H., Javitch, J. A., Cherezov, V., & Stevens, R. C. (2010). Structure of the Human Dopamine D3 Receptor in Complex with a D2/D3 Selective Antagonist. *Science, 330*(6007), 1091-1095.

Choe, H. W., Kim, Y. J., Park, J. H., Morizumi, T., Pai, E. F., Krauß, N., Hofmann, K. P., Scheerer, P., & Ernst, O. P. (2011). Crystal structure of metarhodopsin II. *Nature, 471*, 651-655.

Choudhury, P., & Flower, A. M. (2015). Efficient assembly of ribosomes is inhibted y deletion of *bipA* in *Escherichia coli*. *Journal of Bacteriology, 197*(10), 1819-1827.

Connell, S. R., Trieber, C. A., Dinos, G. P., Einfeldt, E., Taylor, D. E., & Nierhaus, K. H. (2003). Mechanism of Tet(O)-mediated tetracycline resistance. *The EMBO Journal, 22*(4), 945-953.

Consortium, T. G. P. (2015). A global reference for human genetic variantion. *Nature, 526*, 68-74.

Cooper, A., & Dryden, D. T. F. (1984). Allostery without Conformational Change - a Plausible Model. *European Biophysics Journal with Biophysics Letters, 11*(2), 103-109.

Czworkowskil, J., Wang, J., Steitz, T. A., & Moore, P. B. (1994). The crystal structure of elongation factor G complexed with GDP, at 2.7 Å resolution. *The EMBO Journal, 13*(16), 3661-3668.

Davies, J., & Davis, B. D. (1968). Misreading of ribonucleic acid code words induced by aminoglycoside antibiotics. The effect of drug concentration. *Journal of Biological Chemistry, 243*(12), 3312-3316.

Davies, J., Gorini, L., & Davis, B. D. (1965). Misreading of RNA Codewords Induced by Aminoglycoside Antibiotics. *Molecular Pharmacology, 1*, 93-106.

Daviter, T., Wieden, H. J., & Rodnina, M. V. (2003). Essentail role of histidine 84 in Elongation Factor Tu for the chemical step of GTP hydrolysis on the ribosome. *Journal of Molecular Biology, 332*, 689-699.

De Laurentiis, E. I. (2009). *Two partners of the ribosome, EF-Tu and LepA.* (M. Sc.), University of Lethbridge.

De Laurentiis, E. I., Mercier, E., & Wieden, H. J. (2016). The C-terminal Helix of Pseudomonas aeruginosa Elongation Factor Ts Tunes EF-Tu Dynamics to Modulate Nucleotide Exchange. *Journal of Biological Chemistry, 291*(44), 23136-23148.

De Laurentiis, E. I. M., F.; Wieden, H. J. (2011). Construction of a fully active Cys-less elongation factor Tu: Functional role of conserved cysteine 81. *Biochim. Biophys. Acta, 1814*(5), 684-692.

Demeshkina, N., Jenner, L., Westhof, E., Yusupov, M., & Yusupova, G. (2012). A new understanding of the decoding principle on the ribosome. *Nature, 484*(7393), 256-259.

Deng, X., & Nakamura, Y. (2017). Cancer precision medicine: from cancer screening to drug selection and personalized immunotherapy. *Trends Pharm. Sci., 38*(1), 15-24.

Doshi, U., Holliday, M. J., Eisenmesser, E. Z., & Hamelberg, D. (2016). Dynamical network ofresidue-residue contacts reveals copuled allosteric effects in recognition, catalysis, and mutation. *Proceedings of the National Academy of Sciences of the United States of America, 113*(17), 4735-4740.

Drora, R. O., Arlowa, D. H., Maragakisa, P., Mildorfa, T. J., Pana, A. C., Xua, H., Borhania, D. W., & Shaw, D. E. (2011). Activation mechanism of the β2-adrenergic receptor. *Proceedings of the National Academy of Sciences of the United States of America, 108*(46), 18684-18689.

Farrens, D. L., Altenbach, C., Yang, K., Hubbell, W. L., & Khorana, H. G. (1996). Requirement of rigid-body motion of transmembrane helices for light activation of rhodopsin. *Science, 274*(5288), 768-770.

Fasano, O., Bruns, W., Crechet, J. B., Sander, G., & Parmeggiani, A. (1978). Modification of Elongation-Factor-Tu Guanine Nucleotide Interaction by Kirromycin. *Eur. J. Biochem., 89*, 557-565.

Feuerstein, J., Goody, R. S., & Webb, M. R. (1989). The mechanims of guanosine nucleotide hydrolysis by p21 c-Ha-ras. *Journal of Biological Chemistry, 264*(11), 6185-6190.

Fischer, N., Neumann, P., Konevega, A. L., Bock, L. V., Ficner, R., Rodnina, M. V., & Stark, H. (2015). Structure of the *E. coli* ribosome-EF-Tu complex at <3Å resolution by C_s-corrected cyro-EM. *Nature, 520*, 567-570.

Fislage, M., Zhang, J., Brown, Z. P., Mandava, C. S., Sanyal, S., Ehrenberg, M., & Frank, J. (2018). Cryo-EM shows stages of intial codon selction on the ribosome by aa-tRNA in ternary complex with GTP and the GTPase-deficient EF-Tu^{H84A}. *Nucleic Acids Research, 46*(11), 5861-5874.

Flock, T., Ravarani, C. N. J., Sun, D., Venkatakrishnan, A. J., Kayikci, M., Tate, C. G., Veprintsev, D. B., & Babu, M. M. (2015). Universal allosteric mechanism for Gα activation by GPCRs. *Nature, 524*, 173-179.

Forchhammer, K., Leinfelder, W., & Bock, A. (1989). Identification of a Novel Translation Factor Necessary for the Incorporation of Selenocysteine into Protein. *Nature, 342*(6248), 453-456.

Frank, J., Gao, H., Sengupta, J., Gao, N., & Taylor, D. J. (2007). The process of mRNA-tRNA translocation. *Proceedings of the National Academy of Sciences of the United States of America, 104*(50), 19671-19678.

Fraser, C. M. (1989). Site-driected mutagenesis of β-adrenergic receptor. *Journal of Biological Chemistry, 264*, 9266-9270.

Fredriksson, R., Lagerstrom, M. C., Lundin, L. G., & Schioth, H. B. (2003). The G-protein-coupled receptors in the human genome form five main families. Phylogenetic analysis, paralogon groups, and fingerprints. *Molecular Pharmacology, 63*(6), 1256-1272.

Gether, U., Lin, S., Ghanouni, P., Ballesteros, J. A., Weinstein, H., & Kobilka, B. K. (1997). Agonists induce conformational changes in transmembrane domains III and VI of the β2 adrenoceptor. *The EMBO Journal, 16*(22), 6737-6747.

Ginalski, K., Elofsson, A., Fischer, D., & Rychlewski, L. (2003). 3D-Jury: a simple approach to improve protein structure predictions. *Bioinformatics, 19*(8), 1015-1018.

Girodat, D., Mercier, E., Gzyl, K. E., & Wieden, H. J. (2019). Elongation Factor Tu's Nucleotide Binding is Governed by a Thermodynamic Landscape Unique Among Bacterial Translation Factors. *Journal of the American Chemical Society*.

Girvan, M., & Newman, M. E. (2002). Community structure in social and biological networks. *Proceedings of the National Academy of Sciences of the United States of America, 99*(12), 7821-7826.

Glykos, N. M. (2006). Carma: a molecular dynamics analysis program. *Journal of Computational Chemistry, 27*(14), 1765-1768.

Goodsell, D. S. (1999). The molecular perspective: The *ras* oncogene. *Stem Cells, 17*(4), 235-236.

Goujon, M., McWilliam, H., Li, W. Z., Valentin, F., Squizzato, S., Paern, J., & Lopez, R. (2010). A new bioinformatics analysis tools framework at EMBL-EBI. *Nucleic Acids Research, 38*, W695-W699.

Granja-Galeano, G., Zappia, C. D., Fabián, L., Davio, C., Shayo, C., Fernández, N., & Monczor, F. (2017). Effect of mutation of Phe $243^{6.44}$ of the histamine H_2 receptor on cimetidine and ranitidine mechanism of action. *Biochem. Pharmacol., 146*, 117-126.

Grigorenko, B. L., Shadrina, M. S., Topol, I. A., Collins, J. R., & Nemukhin, A. V. (2008). Mechanism of the chemical step for the guanosine triphosphate (GTP) hydrolysis catalyzed by elongation factor Tu. *Biochimica et Biophyisca Acta, 1784*(12), 1908-1917.

Gromadski, K. B., Wieden, H. J., & Rodnina, M. V. (2002). Kinetic mechanism of elongation factor Ts-catalyzed nucleotide exchange in elongation factor Tu. *Biochemistry, 41*(1), 162-169.

Grutsch, S., Brüschweiler, S., & Tollinger, M. (2016). NMR methods to study dynamic alloster. *PLOS Computational Biology, 12*(3).

Gualerzi, C. O., & Pon, C. L. (2015). Initiation of mRNA translation in bacteria: structural and dynamic aspects. *Cellular and Molecular Life Sciences, 72*(22), 4341-4367.

Guerrero, M. C., & Modolell, J. (1980). Hygromycin A, a novel inhibitor of ribosomal peptidyltransferase *European Journal of Biochemistry, 107*, 409-414.

Guex, N., Peitsch, M. C., & Schwede, T. (2009). Automated comparative protein structure modeling with SWISS-MODEL adn Swiss-PdbViewer: A historical perspective. *Electrophoresis, 30*, 162-173.

Guo, C., & Zhou, H. X. (2016). Unidirectional allostery in the regulatory subunit Rlα facilitates efficient deactivation of protein kinase A. *Proceedings of the National Academy of Sciences of the United States of America, 113*(44), 6776-6785.

Guo, J., & Zhou, H. X. (2016). Protein Allostery and Conformational Dynamics. *Chemical Reviews, 116*(11), 6503-6515.

Han, X., Feng, Y., Chen, X., Gerard, C., & Boisvert, W. A. (2015). Characterization of G protein coupling mediated by the conserved $D134^{3.49}$ of DRY motif, $M241^{6.34}$, and $F251^{6.44}$ residues on human CXCR1. *FEBS Open Bio, 5*, 182-190.

Hanlon, C. D., & Andrew, D. J. (2015). Outside-in signaling--a brief review of GPCR signaling with a focus on the Drosophila GPCR family. *Journal of Cell Science, 128*(19), 3533-3542.

Harmar, A. J. (2001). Family-B G-protein-coupled receptors. *Genome Biol., 2*(12), 1-10.

Hauryliuk, V., Mitkevich, V. A., Draycheva, A., Tankov, S., Shyp, V., Ermakov, A., Kulikova, A. A., Makarov, A. A., & Ehrenberg, M. (2009). Thermodynamics of GTP and GDP binding to bacterial initiation factor 2 suggests two types of structural transitions. *J Mol Biol, 394*(4), 621-626.

Hauryliuk, V., Mitkevich, V. A., Eliseeva, N. A., Petrushanko, I. Y., Ehrenberg, M., & Makarov, A. A. (2008). The pretranslocation ribosome is targeted by GTP-bound EF-G in partially activated form. *Proceedings of the National Academy of Sciences of the United States of America, 105*(41), 15678-15683.

Hauser, A. S., Attwood, M. M., Rask-Andersen, M., Schioth, H. B., & Gloriam, D. E. (2017). Trends in GPCR drug discovery: new agents, targets and indications. *Nature Reviews Drug Discovery, 16*(12), 829-842.

Hauser, A. S., Chavali, S., Masuho, I., Jahn, L. J., Martemyanov, K. A., Gloriam, D. E., & Babu, M. M. (2018). Pharmacogenomics of GPCR Drug Targets. *Cell, 172*(1-2), 41-54 e19.

Heller, J. L. E., Kamalampeta, R., & Wieden, H. J. (2017). Takin a step back from back-translocation: an integrative view of LepA/EF4's cellular function. *Molecular and Cellular Biology, 37*(12), 1-14.

Hess, B., Kutzner, C., Van Der Spoel, D., & Lindahl, E. (2008). GROMACS 4: algorithms for highly efficient, load-balanced, and scalable molecular simulations. *Journal of Chemical Theory and Computation, 4*, 435-447.

Hirashima, A., & Kaji, A. (1970). Factor dependent breakdown of polysomes. *Biochemical and Biophysical Research Communications, 41*(4), 877-883.

Hirashima, A., & Kaji, A. (1973). Role of elongation factor G and a protein factor on the release of ribosomes from messenger ribonucleic acid. *Journal of Biological Chemistry, 248*(21), 7580-7587.

Hogg, T., Mesters, J. R., & Hilgenfeld, R. (2002). Inhibitory mechanisms of antibiotics targetting elongation factor Tu. *Current Protein & Peptide Science, 3*, 121-131.

Holliday, M. J., Camilloni, C., Armstrong, G. S., Vendruscolo, M., & Eisenmesser, E. Z. (2017). Networks of Dynamic Allostery Regulate Enzyme Function. *Structure, 25*(2), 276-286.

Hornak, V., Abel, R., Okur, A., Strockbine, B., Roitberg, A., & Simmerling, C. (2006). Comparison of multiple Amber force fields and development of improved protein backbone parameters. *Proteins, 65*, 712-725.

Hosseinzadeh, P., Bhardwaj, G., Mulligan, V. K., Shortridge, M. D., Craven, T. W., Pardo-Avila, F., Rettie, S. A., Kim, D. E., Silva, D. A., Ibrahim, Y. M., Webb, I. K., Cort, J. R., Adkins, J. N., Varani, G., & Baker, D. (2017). Comprehensive computational design of ordered peptide macrocycles. *Science, 358*(6369), 1461-1466.

Huang, H. C., & Klein, P. S. (2004). The Frizzled family: receptors for multiple signal transduction pathways. *Genome Biology, 5*(7), 234.

Humphrey, W., Dalke, A., & Schulten, K. (1996). VMD: visual molecular dynamics. *Journal of Molecular Graphics, 14*(1), 33-38.

Ishihama, Y., Schmidt, T., Rappsilber, J., Mann, M., Hartl, F. U., Kerner, M. J., & Frishman, D. (2008). Protein abundance profiling of the *Escherichia coli* cytosol. *BMC Genomics, 9*(102), 102.

Javitch, J. A., Fu, D., Chen, J., & Karlin, A. (1995). Mapping the binding-site crevice of the Dopmaine D2 receptor by the substituted-cysteine accessibility method. *Neuron, 14*, 825-831.

Jeffery-Smith, A., Taori, S. K., Schelenz, S., Jeffery, K., Johnson, E. M., Borman, A., Candida auris Incident Management, T., Manuel, R., & Brown, C. S. (2018). Candida auris: a Review of the Literature. *Clinical Microbiology Reviews, 31*(1).

Johansen, J. S., Kavaliauskas, D., Pfeil, S. H., Blaise, M., Cooperman, B. S., Goldman, Y. E., Thirup, S. S., & Knudsen, C. R. (2018). *E. coli* elongation factor Tu bound to a GTP analogue displays an open conformation equivalent to the GDP-bound form. *Nucleic Acids Res, 46*(16), 8641-8650.

Johansen, J. S., Kavaliauskas, D., Pfeil, S. H., Blaise, M., Cooperman, B. S., Goldman, Y. E., Thirup, S. S., & Knudsen, C. R. (2018). *E. coli* elongation factor Tu bound to a GTP analogue displays an open conformation equivalent to the GDP-bound form. *Nucleic Acids Research, 46*(16), 8641-8650.

Jonák, J., Anborgh, P. H., & Parmeggiani, A. (1998). Interaction of EF-Tu with EF-Ts: substitution of His-118 in EF-Tu destabilizes the EF-Tu•EF-Ts complex but does not prevent EF-Ts from stimulating the release of EF-Tu-bound GDP. *The FEBS Journal, 422*, 189-192.

Jones Jr., S. K., & Bennett, R. J. (2011). Fungal mating pheromones: choreographing the dating games. *Fungal Genetics and Biology, 38*(7), 668-676.

Joost, P., & Methner, A. (2002). Phylogenetic analysis of 277 human G-protein-coupled receptors as a tool for the prediction of orphan receptor ligands. *Genome Biology, 3*(11), 1-16.

Kaczor, A. A., Targowska-Duda, K. M., Budzynska, B., Biala, G., Silva, A. G., & Castro, M. (2016). In vitro, molecular modeling and behavioral studies of 3-{[4-(5-methoxy-1H-indol-3-yl)-1,2,3,6-tetrahydropyridin-1-yl]methyl}-1,2-dihydroquinolin-2-one (D2AAK1) as a potential antipsychotic. *Neurochemistry International, 96*, 84-99.

Karimi, R., & Ehrenberg, M. (1994). Dissociation rate of cognate peptidyl-tRNA from the A-site of hyper-accurate and error-prone ribosomes. *European Journal of Biochemistry, 226*(2), 355-360.

Karnoub, A. E., & Weinberg, R. A. (2008). Ras oncogenes: split personalities. *Nature Review Molecular Cell Biology, 9*(7), 517-531.

Kavaliauskas, D., Chen, C., Liu, W., Cooperman, B. S., Goldman, Y. E., & Knudsen, C. R. (2018). Structural dynamics of translation elongation factor Tu during aa-tRNA delivery to the ribosome. *Nucleic Acids Research, 46*(16), 8651-8661.

Kavaliauskas, D., Chen, C., Liu, W., Cooperman, B. S., Goldman, Y. E., & Knudsen, C. R. (2018). Structural dynamics of translation elongation factor Tu during aa-tRNA delivery to the ribosome. *Nucleic Acids Res, 46*(16), 8651-8661.

Kawashima, T., Berthet-Colominas, C., Wulff, M., Cusack, S., & Leberman, R. (1996). The structures of the *Escherichia coli* EF-Tu EF-Ts complex at 2.5 Å resolution. *Nature, 379*(8), 511-518.

Kiefer, F., Arnold, K., Kunzli, M., Bordoli, L., & Schwede, T. (2009). The SWISS-MODEL Repository and associated resources. *Nucleic Acids Research, 37*(Database issue), D387-392.

Kihira, K., Shimizu, Y., Shomura, Y., Shibata, N., Kitamura, M., Nakagawa, A., Ueda, T., Ochi, K., & Higuchi, Y. (2012). Crystal structure analysis of the translation factor RF3 (release factor 3). *FEBS Letters, 586*(20), 3705-3709.

Kjeldgaard, M., Nissen, P., Thirup, S., & Nyborg, J. (1993). The crystal structure of elongation factor EF-Tu from *Thermus aquaticus* in the GTP conformation. *Structure, 1*(1), 35-50.

Klein, C., Brin, M. F., Kramer, P., Sena-Esteves, M., De Leon, D., Doheny, D., Bressman, S., Fahn, S., Breakefield, X. O., & Ozelius, L. J. (1999). Association of a missense change in the D2 dopamine receptor with mycolonus dystonia. *Proceedings of the National Academy of Sciences of the United States of America, 96*, 5173-5176.

Klein, C., Gurvich, N., Sena-Esteves, M., Bressman, S., Brin, M. F., Ebersole, B. J., Fink, S., Forgren, L., Friedman, J., Grimes, D., Holmgren, G., Kyllerman, M., Lang, A. E., de Leon, D., Leung, J., Prioleau, C., Raymond, D., Sanner, G., Saunders-Pullman, R., Vieregge, P., Wahlström, J., Breakfield, X. O., Kramer, P. L., Ozelius, L. J., & Sealfon, S. C. (2000). Evaluation of the role of the D2 dopamine receptor in mycolonus dystonia. *Annals of Neurology, 47*, 369-373.

Kling, R. C., Lanig, H., Clark, T., & Gmeiner, P. (2013). Active-State Models of Ternary GPCR Complexes: Determinants of Selective Receptor-G-Protein Coupling. *PLOS ONE, 8*(6), 1-13.

Knudsen, C., Wieden, H. J., & Rodnina, M. V. (2001). The importance of structural transitions of the switch II region for the functions of elongation factor Tu on the ribosome. *Journal of Biological Chemistry, 276*(25), 22183-22190.

Kobilka, B. K., & Deupi, X. (2007). Conformational complexity of G-protein-coupled receptors. *Trends in Pharmacological Sciences, 28*(8), 397-406.

Koshland, D. E., Jr., Nemethy, G., & Filmer, D. (1966). Comparison of experimental binding data and theoretical models in proteins containing subunits. *Biochemistry, 5*(1), 365-385.

Kothe, U., & Rodnina, M. V. (2006). Delayed release of inorganic phosphate from elongation factor Tu following GTP hydrolysis on the ribosome. *Biochemistry, 45*(42), 12767-12774.

Lai, J., Ghaemi, Z., & Luthey-Schulten, Z. (2017). The conformational change in Elongation Factor Tu involves seperation of its domains. *Biochemistry, 56*, 5672-5979.

LaMarche, M. J., Leeds, J. A., Amaral, A., Brewer, J. T., Bushell, S. M., Deng, G., Dewhurst, J. M., Ding, J., Dzink-Fox, J., Gamber, G., Jain, A., Lee, K., Lee, L., Lister, T., McKenney, D., Mullin, S., Osborne, C., Palestrant, D., Patane, M. A., Rann, E. M., Sachdeva, M., Shao, J., Tiamfook, S., Trzasko, A., Whitehead, L., Yifru, A., Yu, D., Yan, W., & Zhu, Q. (2012). Discovery of LFF571: An Investigational Agen for Clostridium difficile Infection. *Journal of Medicinal Chemistry, 55*, 2376-2387.

LaMarche, M. J., Leeds, J. A., Amaral, K., Brewer, J. T., Bushell, S. M., Dewhurst, J. M., Dzink-Fox, J., Gangl, E., Goldovitz, J., Jain, A., Mullin, S., Neckermann, G., Osborne, C., Palestrant, D., Patane, M. A., Rann, E. M., Sachdeva, M., Shao, J., Tiamfook, S., Whitehead, L., & Yu, D. (2011). Antibacterial optimization of 4-aminothiazolyl analogues of the natural product GE2270 A:

identification of the cycloalkylcarboxylic acids. *Journal of Medicinal Chemistry, 54*(23), 8099-8109.

LaMarche, M. J., Leeds, J. A., Dzink-Fox, J., Gangl, E., Krastel, P., Neckermann, G., Palestrant, D., Patane, M. A., Rann, E. M., Tiamfook, S., & Yu, D. (2012). Antibiotic Optimization and Chemical Structure Sabilization of Thiomuracin A. *Journal of Medicinal Chemistry, 55*, 6934-6941.

Lee, Y., Choi, S., & Hyeon, C. (2015). Communication over the network of binary switches regulates the activation of A_{2A} adenosine receptor. *PLOS Computational Biology, 11*(2).

Lim, V. I., Curran, J. F., & Garber, M. B. (2012). Hydration shells of molecules in molecular association: A mechanism for biomolecular recognition. *Journal of Theoretical Biology, 301*, 42-48.

Lin, Y., Koga, N., Vorobiev, S. M., & Baker, D. (2017). Cyclic oligomer design with de novo αβ-proteins. *Protein Science, 26*, 2187-2194.

Liu, J., & Nussinov, R. (2017). Energetic redistribution in allostery to execute protein function. *Proceedings of the National Academy of Sciences of the United States of America, 114*(29), 7480-7482.

Lorenza Bordoli, L., Kiefer, F., Arnold, K., Benkert, P., Battey, J., & Schwede, T. (2008). Protein structure homology modeling using SWISS-MODEL workspace. *Nature Protocols, 4*(1), 1-13.

Louie, A., Ribeiro, N. S., Reid, B. R., & Jurnak, F. (1984). Relative affinities of all *Escherichia coli* aminoacyl-tRNAs for elongation factor Tu-GTP. *Journal of Biological Chemistry, 259*(8), 5010-5016.

Loveland, A. B., Demo, G., Grigorieff, N., & Korostelev, A. A. (2017). Ensemble cryo-EM elucidates the mechanism of translation fidelity. *Nature, 546*(7656), 113-117.

Manavathu, E. K., Fernandez, C. L., Cooperman, B. S., & Taylor, D. E. (1990). Molecular studies on the mechanism of tetracycline resistance mediated by Tet(O). *Antimicrobial Agents and Chemotherapy, 34*(1), 71-77.

Manglik, A., Kim, T. H., Masureel, M., Altenbach, C., Yang, Z., Hilger, D., Lerch, M. T., Kobilka, T. S., Thian, F. S., Hubbell, W. L., Prosser, R. S., & Kobilka, B. K. (2015). Structure insights into the dynamic process of β2-Adrenergic receptor signaling. *Cell, 161*, 1101-1111.

Maracci, C., Peske, F., Dannies, E., Pohl, C., & Rodnina, M. V. (2014). Ribosome-induced tuning of GTP hydrolysis by a translational GTPase. *Proceedings of the National Academy of Sciences of the United States of America, 111*(40), 14418-14423.

Maracci, C., & Rodnina, M. V. (2016). Review Translational GTPases. *Biopolymers, 105*(8), 463-475.

Masri, B., Salahpour, A., Didriksen, M., Ghisi, V., Beaulieu, J. M., Gainetdinov, R. R., & Caron, M. G. (2008). Antagonism of dopamine D2 receptor/β-arrestin 2 interactino is acommon property of clinically effective antipsychotics. *Proceedings of the National Academy of Sciences of the United States of America, 105*(36), 13565-13661.

Masureel, M., Zou, Y., Picard, L. P., van der Westhuizen, E., Mahoney, J. P., Rodrigues, J. P. G. L. M., Mildorf, T. J., Dror, R. O., Shaw, D. E., Bouvier, M., Pardon, E., Steyaert, J., Sunahara, R. K., Weis, W. I., Zhang, C., & Kobilka, B. K. (2018). Structural insights into binding specificity, efficacy and bias of a β2AR partial agonist. *Nature Chemical Biology, 14*, 1059-1066.

McCall, R. B., Lookingland, K. J., Bédard, P. J., & Huff, R. M. (2005). Sumanirole, a highly dopamine D_2 selective receptor agonist: in vitro and in vivo pharmacological characterization and efficacy in animal models of parkinson's disease. *J. Pharmacol. Exp. Ther., 314*(3), 1248-1256.

McWilliam, H., Li, W. Z., Uludag, M., Squizzato, S., Park, Y. M., Buso, N., Cowley, A. P., & Lopez, R. (2013). Analysis Tool Web Services from the EMBL-EBI. *Nucleic Acids Research, 41*(W1), W597-W600.

Mercier, E. (2013). *Structural dynamics of elongation factor Tu.* (Doctor of Philosophy), University of Lethbridge, Lethbridge Alberta, Canada.

Mercier, E., Girodat, D., & Wieden, H. J. (2015). A conserved P-loop anchor limits the structural dynamics that mediate nucleotide dissociation in EF-Tu. *Scientific Reports, 5*, 7677.

Mikolajka, A., Liu, H., Chen, Y., Starosta, A. L., Márquez, V., Ivanova, M., Cooperman, B. S., & Wilson, D. N. (2011). Differential effects of thiopeptide and orthosomycin antibiotics on translational GTPases. *Chemistry and Biology, 18*, 589-600.

Milon, P., Konevega, A. L., Gualerzi, C. O., & Rodnina, M. V. (2008). Kinetic checkpoint at a late step in translation initiation. *Molecular Cell, 30*(6), 712-720.

Milon, P., Maracci, C., Filonava, L., Gualerzi, C. O., & Rodnina, M. V. (2012). Real-time assembly landscape of bacterial 30S translation initiation complex. *Nature Structural & Molecular Biology, 19*(6), 609-615.

Moazed, D., & Noller, H. F. (1989). Intermediate states in the movement of transfer RNA in the ribosome. *Nature, 342*(6246), 142-148.

Mohr, D., Wintermeyer, W., & Rodnina, M. V. (2002). GTPase activation of elongation factors Tu and G on the ribosome. *Biochemistry, 41*(41), 12520-12528.

Monod, J., & Jacob, F. (1961). Teleonomic mechnisms in cellular metabolism, growth, and differentiation. *Cold Spring Harbor Symposia on Quantitative Biology, 26*, 389-401.

Monod, J., Wyman, J., & Changeux, J. P. (1965). On the Nature of Allosteric Transitions: A Plausible Model. *Journal of Molecular Biology, 12*, 88-118.

Neal, S. E., Eccleston, J. F., Hall, A., & Webb, M. R. (1998). Kinetic analysis of the hydrolysis of GTP by $p21^{N\text{-}ras}$. *Journal of Biological Chemistry, 263*(36), 19718-19722.

Nissen, P., Kjeldgaard, M., Thirup, S., Polekhina, G., Reshetnikova, L., Clark, B. F., & Nyborg, J. (1995). Crystal structure of the ternary complex of Phe-tRNAPhe, EF-Tu, and a GTP analog. *Science, 270*(5241), 1464-1472.

Noel, J. K., & Onuchic, J. N. (2012). The many faces of structure-based potentials: from protein folding landscapes to structural characterization of complex biomolecules. In D. N. (Ed.), *Computational Modeling of Biological Systems: From Molecules to Pathways* (pp. 31-54). Boston, MA: Springer

Noel, J. K., & Whitford, P. C. (2016). How EF-Tu can contribute to efficient proofreading of aa-tRNA by the ribosome. *Nature Communications, 7*, 13314.

Nussinov, R., & Tsai, C. J. (2015). Allostery without a conformational change? Revisiting the paradigm. *Current Opinion in Structural Biology, 30*, 17-24.

Nygaard, R., Zou, Y., Dror, R. O., Mildorf, T. J., Arlow, D. H., Manglik, A., Pan, A. C., Liu, C. W., Fung, J. J., Bokoch, M. P., Thian, F. S., Kobilka, T. S., Shaw, D. E., Mueller, L., Prosser, R. S., & Kobilka, B. K. (2013). The Dynamic Process of β2-Adrenergic Receptor Activation. *Cell, 152*, 532-542.

Ogle, J. M., Brodersen, D. E., Clemons, W. M., Jr., Tarry, M. J., Carter, A. P., & Ramakrishnan, V. (2001). Recognition of cognate transfer RNA by the 30S ribosomal subunit. *Science, 292*(5518), 897-902.

Ogle, J. M., Murphy, F. V., Tarry, M. J., & Ramakrishnan, V. (2002). Selection of tRNA by the ribosome requires a transition from an open to a closed form. *Cell, 111*(5), 721-732.

Ortiz, A. R., Strauss, C. E. M., & Olmea, O. (2002). MAMMOT (Matching molecular models obtained from theory): An automated method for model comparison. *Protein Science, 11*, 2606-2621.

Paleskava, A., Konevega, A. L., & Rodnina, M. V. (2012). Thermodynamics of the GTP-GDP-operated conformational switch of selenocysteine-specific translation factor SelB. *J Biol Chem, 287*(33), 27906-27912.

Pape, T., Wintermeyer, W., & Rodnina, M. V. (1998). Complete kinetic mechanism of elongation factor Tu-dependent binding of aminoacyl-tRNA to the A site of the *E. coli* ribosome. *The EMBO Journal, 17*(24), 7490-7497.

Pape, T., Wintermeyer, W., & Rodnina, M. V. (2000). Conformational switch in the decoding region of 16S rRNA during aminoacyl-tRNA selection on the ribosome. *Nature Structural & Molecular Biology, 7*(2), 104-107.

Parker, J. (1989). Errors and alternatives in reading the universal genetic code. *Microbiological Reviews, 53*, 273-298.

Parmeggiani, A., Krab, I. M., Okamura, S., Nielsen, R. C., Nyborg, J., & Nissen, P. (2006). Structural Basis of the Action of Pulvomycin and GE2770 A on Elongation Factor Tu. *Biochemisty, 45*, 6846-6857.

Parmeggiani, A., Krab, I. M., Watanabe, T., Nielsen, R. C., Dahlberg, C., Nyborg, J., & Nissen, P. (2006). Enacyloxin IIa pinpoints a binding pocket of elongation factor Tu for development of novel antibiotics. *Journal of Biological Chemistry, 281*(5), 2893-2900.

Parmeggiani, A., & Nissen, P. (2006). Elongation factor Tu-targeted antibiotics: four different structures, two mechanisms of action. *FEBS Letters, 580*(19), 4576-4581.

Parmeggiani, A., Swart, G. W. M., Mortensen, K. K., Jensen, M., Clark, B. F. C., Dente, L., & Cortese, R. (1987). Properties of a genetically engineerd G domain of elongation factor Tu. *Proceedings of the National Academy of Sciences of the United States of America, 84*, 3141-3145.

Patra, S. M., Chakraborty, S., Shahane, G., Prasanna, X., Sengupta, D., Maiti, P. K., & A., C. (2015). Differential dynamics of the serotonin$_{1A}$ receptor in membrane bilayers of varying cholesterol content revealed by all atom molecular dynamics simulation. *Molecular Membrane Biology, 32*(4), 127-137.

Perutz, M. F. (1970). Stereochemistry of cooperative effects in haemoglobin. *Nature, 228*(5273), 726-739.

Peske, F., Kuhlenkoetter, S., Rodnina, M. V., & Wintermeyer, W. (2013). Timing of GTP binding and hydrolysis by translation termination factor RF3. *Nucleic Acids Res.*, 1-9.

Petit, C. M., Zhang, J., Sapienza, P. J., Fuentes, E. J., & Lee, A. L. (2009). Hidden dynamic allostery in a PDZ domain. *Proceedings of the National Academy of Sciences of the United States of America, 106*(43), 18249-18254.

Pettersen, E. F., Goddard, T. D., Huang, C. C., Couch, G. S., Greenblatt, D. M., Meng, E. C., & Ferrin, T. E. (2004). UCSF Chimera—A visualization system for exploratory research and analysis. *Journal of Computational Chemistry, 25*, 1605-1612.

Phillips, J. C., Braun, R., Wang, W., Gumbart, J., Tajkhorshid, E., Villa, E., Chipot, C., Skeel, R. D., Kale, L., & Schulten, K. (2005). Scalable molecular dynamics with NAMD. *Journal of Computational Chemistry, 26*(16), 1781-1802.

Piepenburg, O., Pape, T., Pleiss, J. A., Wintermeyer, W., Uhlenbeck, O. C., & Rodnina, M. V. (2000). Intact aminoacyl-tRNA is required to trigger GTP hydrolysis by elongation factor Tu on the ribosome. *Biochemistry, 39*, 1734-1738.

Pingoud, A., Gast, F. U., Block, W., & Peters, F. (1983). The elongation factur Tu from *Escherichia coli*, aminoacyl-tRNA and guanosine tetraphophate form a ternary complex which is bound by programmed ribosomes. *Journal of Biological Chemistry, 258*(23), 14200-14205.

Platania, C. B. M. S., S., Leggio, G. M., Drago, F., & Bucolo, C. (2012). Homology modeling of dopamine D_2 and D_3 receptors: molecular dynamics refinement and docking evaluation. *PLOS ONE, 7*(9), 1-12.

Podder, A., Pandey, D., & Latha, N. (2016). Investigating the structural impact of S311C mutation in DRD2 receptor by molecular dynamics & docking studies. *Biochimie, 123*, 52-64.

Polacek, N., Swaney, S., Shinabarger, D., & Mankin, A. S. (2002). SPARK - A novel method to monitor ribosomal peptidyl transferase activity. *Biochemistry, 41*, 11602-11610.

Polikanov, Y. S., Starosta, A. L., Juette, M. F., Altman, R. B., Terry, D. S., Lu, W., Burnett, B. J., Dinos, G., Reynolds, K. A., Blanchard, S. C., Steitz, T. A., & Wilson, D. N. (2015). Distinct tRNA

Accommodation Intermediates Observed on the Ribosome with the Antibiotics Hygromycin A and A201A. *Molecular Cell, 58*, 832-844.

Popovych, N., Sun, S., Ebright, R. H., & Kalodimos, C. G. (2006). Dynamically driven protein allostery. *Nature Structural & Molecular Biology, 13*(9), 831-838.

Prendes-Alvarez, S., & Nemeroff, C. B. (2018). Personalized medicine: prediction of disease vulnerability in mood disorders. *Nuerscience Letters, 669*, 10-13.

Pronk, S., Páll, S., Schulz, R., Larsson, P., Bjelkmar, P., Apostolov, R., Shirts, M. R., Smith, J. C., Kasson, P. M., Van Der Spoel, D., Hess, B., & Lindahl, E. (2013). GROMACS 4.5: a high-throughput and highly parallel open source molecular simulaton toolkit. *Bioinformatics, 29*(7), 845-854.

Rask-Andersen, M., Masuram, S., & Schioth, H. B. (2014). The druggable genome: Evaluation of drug targets in clinical trials suggests major shifts in molecular class and indication. *Annual Review of Pharmacology and Toxicology, 54*, 9-26.

Rasmussen, S. G. F., Choi, H. J., Fung, J. J., Pardon, E., Casarosa, P., Chae, P. S., Devree, B. T., Rosenbaum, D. M., Thian, F. S., Kobilka, T. S., Schnapp, A., Konetzki, I., Sunahara, R. K., Gellman, S. H., Pautsch, A., Steyaert, J., Weis, W. I., & Kobilka, B. K. (2011). Structure of a nanobody-stabilized active state of the beta(2) adrenoceptor. *Nature, 469*(7329), 175-180.

Rasmussen, S. G. F., DeVree, B. T., Zou, Y., Kruse, A. C., Chung, K. Y., Kobilka, T. S., Thian, F. S., Chae, P. S., Pardon, E., Calinski, D., Mathiesen, J. M., Shah, S. T. A., Lyons, J. A., Caffrey, M., Gellman, S. H., Steyaert, J., Skiniotis, G., Weis, W. I., Sunahara, R. K., & Kobilka, B. K. (2011). Crystal structure of the β2 adrenergic receptor–Gs protein complex. *Nature, 477*, 549-555.

Rivalta, I., Sultan, M. M., Lee, N. S., Manley, G. A., Loria, J. P., & Batista, V. S. (2012). Allosteric pathways in imidazole glycerol phosphate synthase. *Proceedings of the National Academy of Sciences of the United States of America, 109*(22), 1428-1436.

Roden, D. M. (2011). Personalized medicine and the genotype-phenotype dilemma. *J. Interv. Card. Electrophysiol., 31*, 17-23.

Rodnina, M. V. (2018). Translation in Prokaryotes. *Cold Spring Harbor Perspectives in Biology, 10*(9).

Rodnina, M. V., Gromadski, K. B., Kothe, U., & Wieden, H. J. (2005). Recognition and selection of tRNA in translation. *FEBS Letters, 579*(4), 938-942.

Rodnina, M. V., Pape, T., Fricke, R., Kuhn, L., & Wintermeyer, W. (1996). Initial binding of the Elongation Factor Tu-GTP-aminoacyl-tRNA complex preceeding codon recognition on the ribosome. *Journal of Biological Chemistry, 271*(2), 646-652.

Rodnina, M. V., & Wintermeyer, W. (2001). Fidelity of aminoacyl-tRNA selection on the ribosome: kinetic and structural mechanisms. *Annual Review of Biochemistry, 70*, 415-435.

Salmas, R. E., Yurtsever, M., & Durdagi, S. (2017). Atomistic molecular dynamics simulations of typical and atypical antipsychotic drugs at the dopamine D2 receptor (D2R) elucidates their inhibition mechanism. *Journal of Biomolecular Structure & Dynamics, 35*(4), 738-754.

Sanbonmatsu, K. Y. (2006). Alignment/misalignment hypothesis for tRNA selection by the ribosome. *Biochimie, 88*(8), 1075-1089.

Sanbonmatsu, K. Y., Joseph, S., & Tung, C. S. (2005). Simulating movement of tRNA into the ribosome during decoding. *Proceedings of the National Academy of Sciences of the United States of America, 102*(44), 15854-15859.

Santos, R., Ursu, O., Gaulton, A., Bento, A. P., Donadi, R. S., Bologa, C. G., Karlsson, A., Al-Lazikani, B., Hersey, A., Oprea, T. I., & Overington, J. P. (2017). A comprehensive map of molecular drug targets. *Nature Reviews Drug Discovery, 16*(1), 19-34.

Sassone-Corsi, P. (2012). The cyclic AMP pathway. *Cold Spring Harbor Perspectives in Biology, 4*(12), 1-3.

Savelsbergh, A., Rodnina, M. V., & Wintermeyer, W. (2009). Distinct functions of elongation factor G in ribosome recycling and translocation. *RNA, 15*, 7772-7780.

Schlunzen, F., Zarivach, R., Harms, J., Bashan, A., Tocilj, A., Albrecht, R., Yonath, A., & Franceschi, F. (2001). Structural basis for the interaction of antibiotics with the peptidyl transferase centre in eubacteria. *Nature, 413*(6858), 814-821.

Schmeing, T. M., Voorhees, R. M., Kelley, A. C., Gao, Y. G., Murphy, F. V. t., Weir, J. R., & Ramakrishnan, V. (2009). The crystal structure of the ribosome bound to EF-Tu and aminoacyl-tRNA. *Science, 326*(5953), 688-694.

Schönenberg, T., Schulz, A., Biebermann, H., Hermsdorf, T., Römpler, H., & Sangkuhl, K. (2004). Mutant G-protein coupled receptors as a cause of human diseases. *Pharmacology & Therapeutics, 104*, 173-206.

Schummer, T., Gromadski, K. B., & Rodnina, M. V. (2007). Mechanism of EF-Ts-catalyzed guanine nucleotide exchange in EF-Tu: contribution of interactions mediated by helix B of EF-Tu. *Biochemistry, 46*(17), 4977-4984.

Scolnick, E., Tompkins, R., Caskey, T., & Nirenberg, M. (1968). Release factors differin in specificity for teminator codons. *Proceedings of the National Academy of Sciences of the United States of America, 61*, 768-774.

Scott, K., Diggle, M. A., & Clarke, S. C. (2003). TypA is a virulence regulator and is present in many pathogenic bacteria. *British Journal of Biomedical Science, 60*(3), 168-170.

Sethi, A., Eargle, J., Black, A. A., & Luthey-Schulten, Z. (2009). Dynamical networks in tRNA:protein complexes. *Proceedings of the National Academy of Sciences of the United States of America, 106*(16), 6620-6625.

Sharma, P. K., Xiang, Y., Kato, M., & Warshel, A. (2005). What are the roles of substrate-assisted catalysis and proximity effects in peptide bond formation by the ribosome? *Biochemisty, 44*(34), 11307-11314.

Shi, X., Khade, P. K., Sanbonmatsu, K. Y., & Joseph, S. (2012). Functional role of the sarcin-ricin loop of the 23S rRNA in the elongation cycle of protein synthesis. *Journal of Molecular Biology, 419*(3-4), 125-138.

Shukla, D., Meng, Y., Roux, B., & Pande, V. S. (2014). Activation pathway of Src kinase reveals intermeidate states as targets for drug design. *Nature Communications, 5*.

Sievers, F., Wilm, A., Dineen, D., Gibson, T. J., Karplus, K., Li, W. Z., Lopez, R., McWilliam, H., Remmert, M., Soding, J., Thompson, J. D., & Higgins, D. G. (2011). Fast, scalable generation of high-quality protein multiple sequence alignments using Clustal Omega. *Molecular Systems Biology, 7*(539), 1-6.

Siew, N., Elofsson, A., Rychlewski, L., & Fischer, D. (2000). MaxSub: an automated measure for the assessment of protein structure prediction quality. *Bioinformatics, 16*(9), 776-785.

Simonetti, A., Marzi, S., Fabbretti, A., Hazemann, I., Jenner, L., Urzhumtsev, A., Gualerzi, C. O., & Klaholz, B. P. (2013). Structure of the protein core of translation initiation factor 2 in apo, GTP-bound and GDP-bound forms. *Acta Crystallogr D Biol Crystallogr, 69*(Pt 6), 925-933.

Simonetti, A., Marzi, S., Fabbretti, A., Hazemann, I., Jenner, L., Urzhumtsev, A., Gualerzi, C. O., & Klaholz, B. P. (2013). Structure of the protein core of translation initiation factor 2 in apo, GTP-bound and GDP-bound forms. *Acta Crystallographics Section D, 69*(Pt 6), 925-933.

Song, H., Parsons, M. R., Rowsell, S., Leonard, G., & Phillips, S. E. V. (1999). Crystal structure of intact elongation factor EF-Tu from *Escherichia coli* in GDP conformation at 2.05Å Resolution. *Journal of Molecular Biology, 285*(3), 1245-1256.

Steiner, T. (2002). The hydrogen bond in the solid state. *Angewandte Chemie International Edition, 41*(1), 49-76.

Strafella, C., Caputo, V., Galota, M. R., Zampatti, S., Marella, G., Mauriello, S., Cascella, R., & Giardina, E. (2018). Applicaiton of precision medicine in neurodegenerative diseases. *Frontiers in Neurology, 9*.

Strauch, E. M., Bernard, S. M., La, D., Bohn, A. J., Lee, P. S., Anderson, C. E., Nieusma, T., Holstein, C. A., Garcia, N. K., Hooper, K. A., Ravichandran, R., Nelson, J. W., Sheffler, W., Bloom, J. D., Lee, K. K., Ward, A. B., Yager, P., Fuller, D. H., Wilson, I. A., & Baker, D. (2017). Computational design of trimeric influnza-neutralizing proteins targeting the hemagglutinin receptor binding site. *Nature Biotechnology*, 1-5.

Sung, Y. M., Wilkins, A. D., Rodriguez, G. J., Wensel, T. G., & Lichtarge, O. (2016). Intramolecular allosteric communication in dopamine D2 receptor revealed by evolutionary amino acid covariation. *Proceedings of the National Academy of Sciences of the United States of America, 113*(13), 3539-3544.

Suzek, B. E., Wang, Y., Huang, H., McGarvey, P. B., Wu, C. H., & UniProt, C. (2015). UniRef clusters: a comprehensive and scalable alternative for improving sequence similarity searches. *Bioinformatics, 31*(6), 926-932.

Talavera, A., Hendrix, J., Versees, W., Jurenas, D., Van Nerom, K., Vandenberk, N., Singh, R. K., Konijnenberg, A., De Gieter, S., Castro-Roa, D., Barth, A., De Greve, H., Sobott, F., Hofkens, J., Zenkin, N., Loris, R., & Garcia-Pino, A. (2018). Phosphorylation decelerates conformational dynamics in bacterial translation elongation factors. *Science Advances, 4*(3), eaap9714.

Thanbichler, M., Bock, A., & Goody, R. S. (2000). Kinetics of the interaction of translation factor SelB from Escherichia coli with guanosine nucleotides and selenocysteine insertion sequence RNA. *Journal of Biological Chemistry, 275*(27), 20458-20466.

The UniProt Consortium. (2017). UniProt: the universal protein knowledgebase. *Nucleic Acids Research, 45*, 158-169.

Thirup, S. S., Van, L. B., Nielsen, T. K., & Knudsen, C. R. (2015). Structural outline of the detailed mechanism for elongation factor Ts-mediated guanine nucleotide exchange on elongation factor Tu. *Journal of Structural Biology, 191*, 10-21.

Trzaskowski, B., Latek, D., Yuan, S., Ghoshdastider, U., Debinski, A., & Filipek, S. (2012). Action of molecular switches in GPCRs--theoretical and experimental studies. *Current Medicinal Chemistry, 19*(8), 1090-1109.

Tsai, A., Uemura, S., Johansson, M., Puglisi, E. V., Marshall, R. A., Aitken, C. E., Korlach, J., Ehrenberg, M., & Puglisi, J. D. (2013). The impact of aminoglycosides on the dynamics of translation elongation. *Cell Reports, 3*, 497-508.

Tsai, C. J., del Sol, A., & Nussinov, R. (2008). Allostery: Absence of a change in shape does not imply that allostery is not at play. *Journal of Molecular Biology, 378*, 1-11.

Tsai, C. J., & Nussinov, R. (2014). A Unified View of "How Allostery Works". *PLOS Computational Biology, 10*(2).

Valle, M., Sengupta, J., Swami, N. K., Grassucci, R. A., Burkhardt, N., Nierhaus, K. H., Agrawal, R. K., & Frank, J. (2002). Cryo-EM reveals an acive role for aminoacyl-tRNA in the accommodation process. *The EMBO Journal, 21*(133), 3557-3567.

Van Der Spoel, D., Lindahl, E., Hess, B., Groenhof, G., Mark, A. E., & Berendsen, H. J. C. (2005). GROMACS: fast, flexible, and free. *Journal of Computational Chemistry, 26*, 1701-1718.

Ventola, C. L. (2015). The antibiotic resistance crisis. *Pharmacology & Therapeutics, 40*(4), 277-283.

Verstraeten, N., Fauvart, M., Versees, W., & Michiels, J. (2011). The universally conserved prokaryotic GTPases. *Microbiology and Molecular Biology Reviews, 75*(3), 507-542, second and third pages of table of contents.

Voet, D., & Voet, J. G. (2010). *Biochemistry 4e*. Hoboken: John Wiley and Sons Inc.

Vogel, R., Mahalingam, M., Luedke, S., Huber, T., Siebert, F., & Sakmar, T. P. (2008). Functional role of the "Ionic Lock" - An interhelical hydrogen-bond network in family a heptahelical receptors. *Journal of Molecular Biology, 380*(4), 648-655.

Vogeley, L., Palm, G. J., Mesters, J. R., & Hilgenfeld, R. (2001). Conformational change of elongation factor Tu (EF-Tu) induced by antibiotic binding. Crystal structure of the complex between EF-Tu.GDP and aurodox. *Journal of Biological Chemistry, 276*(20), 17149-17155.

Voorhees, R. M., Schmeing, T. M., Kelley, A. C., & Ramakrishnan, V. (2010). The mechanism for activation of GTP hydrolysis on the ribosome. *Science, 330*(6005), 835-838.

Vorstenbosch, E., Pape, T., Rodnina, M. V., Kraal, B., & Wintermeyer, W. (1996). The G222D mutation in elongation factor Tu inhibits the codon-induced conformational changes leading to GTPase activation on the ribosome. *The EMBO Journal, 15*(23), 6766-6774.

Wagner, A., Simon, I., Sprinzl, M., & Goody, R. S. (1995). Interaction of Guanosine Nucleotides and Their Analogs with Elongation-Factor Tu from Thermus-Thermophilus. *Biochemistry, 34*(39), 12535-12542.

Wallace, A. C., Laskowski, R. A., & Thornton, J. M. (1995). LIGPLOT: a program to generate schematic diagrams of protein-ligand interactions. *Protein Eng., 8*(2), 127-134.

Wallin, G., & Aqvist, J. (2010). The transition state for peptide bond formation reveals the ribosome as a water trap. *Proceedings of the National Academy of Sciences of the United States of America, 107*(5), 1888-1893.

Wang, J., Cieplak, P., & Kollman, P. (2000). How well does a Restrained Eloectrostatic Potential (RESP) model perform in calculating conformational energies of organic and biological molecules? *Journal of Computational Chemistry, 21*(12), 1049-1074.

Wang, L., Pulk, A., Wasserman, M. R., Feldman, M. B., Altman, R. B., Cate, J. H. D., & Blanchard, S. C. (2012). Allosteric control of the ribosome by small-molecule antibiotics. *Nature Structural & Molecular Biology, 19*, 957-963.

Wang, S., Che, T., Levit, A., Shoichet, B. K., Wacker, D., & Roth, B. L. (2018). Structure of the D2 dopamine receptor bound to the atypical antipsychotic drug risperidone. *Nature, 555*, 269-273.

Wasserman, M. R., Pulk, A., Zhou, Z., Altman, R. B., Zinder, J. C., Green, K. D., Garneau-Tsodikova, S., Cate, J. H. D., & Blanchard, S. C. (2015). Chemically related 4,5-linked aminoglycoside antibiotics drive subunit rotation in opposite directions. *Nature Communications*, 1-12.

Weis, W. I., & Kobilka, B. K. (2008). Structural insights into G-protein-coupled receptor activation. *Current Opinion in Structural Biology, 18*(6), 734-740.

Weis, W. I., & Kobilka, B. K. (2018). The molecular basis of GPCR activation. *Annual Review of Biochemistry, 87*, 897-919.

Weissbach, H., Miller, D. L., & Hachmann, J. (1970). Studies on the role of factor Ts in polypeptide synthesis. *Archives of Biochemistry and Biophysics, 137*(1), 262-269.

Wheatley, M., Wootten, D., Conner, M. T., Simms, J., Kendrick, R., Logan, R. T., Poyner, D. R., & Barwell, J. (2012). Lifting the lid on GPCRs: the role of extracellular loops. *British Journal of Pharmacology, 165*(6), 1688-1703.

Whitford, P. C., Geggier, P., Altman, R. B., Blanchard, S. C., Onuchic, J. N., & Sanbonmatsu, K. Y. (2010). Accommodation of aminoacyl-tRNA into the ribosome involves reversible excursions along multiple pathways. *RNA, 16*, 1196-1204.

Whitford, P. C., Noel, J. K., Gosavi, S., Schug, A., Sanbonmatsu, K. Y., & Onuchic, J. N. (2008). An all-atom structure-based potential for proteins: Bridging minimal models with all-atom empirical forcefields. *Proteins, 75*, 430-441.

Wieden, H. J., Gromadski, K., Rodnin, D., & Rodnina, M. V. (2002). Mechanism of elongation factor (EF)-Ts-catalyzed nucleotide exchange in EF-Tu. Contribution of contacts at the guanine base. *Journal of Biological Chemistry, 277*(8), 6032-6036.

Wieden, H. J., Mercier, E., Gray, J., Steed, B., & Yawney, D. (2010). A combined molecular dynamics and rapid kinetics approach to identify conserved three-dimensional communication networks in elongation factor Tu. *Biophysical Journal, 99*(11), 3735-3743.

Wilden, B., Savelsbergh, A., Rodnina, M. V., & Wintermeyer, W. (2006). Role and timing of GTP binding and hydrolysis during EF-G-dependent tRNA translocation on the ribosome. *Proceedings of the National Academy of Sciences of the United States of America, 103*(37), 13670-13675.

Willard, S. S., & Koochekpour, S. (2013). Glutamate, glutamate receptors, and downstream signaling pathways. *International Journal of Biological Sciences, 9*(9), 948-959.

Wilson, D. N. (2009). The A-Z of bacterial translation inhibitors. *Critical Reviews in Biochemistry and Molecular Biology, 44*(6), 393-433.

Wilson, D. N. (2014). Ribosome-targeting antibiotics and mechanisms of bacterial resistance. *Nature Reviews Microbiology, 12*(1), 35-48.

Wittinghofer, A., & Vetter, I. R. (2011). Structure-function relationships of the G domain, a canonical switch motif. *Annual Review of Biochemistry, 80*, 943-971.

Wolf, H., Chinali, G., & Parmeggiani, A. (1977). Mechanism of the Inhibition of Protein Synthesis by Kirromycin. *Eur. J. Biochem., 75*, 67-75.

World Health Organization. (2017). *Prioritization of pathogens, to guide discovery, research and development of new antibiotics for drug-resistant bacterial infections, incuding tuberculosis*.

Yang, H., Noel, J. K., & Whitford, P. C. (2017). Anisotropic Fluctuations in the Ribosome Determine tRNA Kinetics. *Journal of Physical Chemistry B, 121*, 10593-10601.

Yao, X., Parnot, C., Deupi, X., Ratnala, V. R. P., Swaminath, G., Farrens, D., & Kobilka, B. K. (2006). Coupling ligand structure to specific conformational switches in the β2-adrenoceptor. *Nature Chemical Biology, 2*, 417-422.

Zeef, L. A. H., Bosch, L., Anborgh, P. H., Cetin, R., Parmeggiani, A., & Hilgenfeld, R. (1994). Pulvomycin-resistant mutants of *E. coli* elongation factor Tu. *The EMBO Journal, 13*(21), 5113-5120.

Zhang, J., Pavlov, M. Y., & Ehrenberg, M. (2018). Accuracy of genetic code translation and its orthogonal corruption by aminoglycosides and Mg^{2+} ions. *Nucleic Acids Research, 46*(3), 1362-1374.

Zhang, W., Dunkle, J. A., & Cate, J. H. (2009). Structures of the ribosome in intermediate states of ratcheting. *Science, 325*(5943), 1014-1017.

Zhang, Y., Li, X., & Spremulli, L. L. (1996). Role of the conserved aspartate and phenylalanine residues in prokaryotic and mitochondrial elongation factor Ts in guanine nucleotide exchange. *FEBS Letters, 391*(3), 330-332.

Zhou, J., Lancaster, L., Donohue, J. P., & Noller, H. F. (2013). Crystal Structures of EF-G-Ribosome Complexes Trapped in Intermediate States of Translocation. *Science, 340*(6140), 1543-1552.

Appendix 1

Supplemental Material for: Elongation Factor Tu's Nucleotide Binding is Governed by a Thermodynamic Landscape Unique Amongst Bacterial Translation Factors

Supplemental Discussion

Insights into the *apo* conformation of EF-Tu

The first structural insight into the *apo* conformation of EF-Tu was gleaned from the crystal structure of the EF-Tu•EF-Ts complex (Kawashima, Berthet-Colominas, Wulff, Cusack, & Leberman, 1996). In this structure, switch I of EF-Tu is disordered and the domain arrangement is similar to the GDP conformation. Subsequently, Thirup and co-workers were able to crystalize an EF-Tu•EF-Ts complex with EF-Tu in the closed GTP conformation, indicating that the EF-Tu•EF-Ts complex exhibits conformational flexibility (Thirup, Van, Nielsen, & Knudsen, 2015). The kinetic data reported here provides additional insight into the *apo* state of EF-Tu and suggests that the free *apo* state of EF-Tu adopts a unique conformation that is able to recognize GTP and GDP similarly. Similar association and different dissociation activation barriers support that nucleotide binding to this non-discriminatory conformation of EF-Tu is followed by conformational changes of EF-Tu that depend on the presence and absence of the gamma-phosphate in GTP. Therefore, the nucleotide release mechanism is likely the inverse in which a conformational change has to occur prior to nucleotide dissociation. This process would require a unique conformation for *apo* EF-Tu and is consistent with the reported conformational flexibility observed by Johansen *et al.* (2018) and Kavaliauskas *et al.* (2018).

Considering the entropic landscape of EF-Tu, the *apo* EF-Tu conformation is less stable than both EF-Tu•GTP and EF-Tu•GDP (Fig 2.4). Since EF-Tu employs water coordination to entropically stabilize the GTP conformation, it is likely that water coordination stabilizes EF-Tu•GTP and EF-Tu•GDP compared to *apo* EF-Tu. If GDP is removed from the structure of EF-Tu•GDP, the SASA increases by 109 $Å^2$. The difference

in SASA between EF-Tu•GTP and EF-Tu•GDP is 1041 $Å^2$ (Fig A1.6B) and since the entropy gap between EF-Tu•GDP and EF-Tu•GTP is similar to the entropy gap between *apo* EF-Tu and EF-Tu•GDP (Fig 2.4C) it is likely that SASA alone does not explain the entropy of the *apo* EF-Tu conformation. Therefore, *apo* EF-Tu cannot merely be a similar conformation to EF-Tu•GDP without nucleotide, but has to be a unique conformation. Another possible explanation for the entropy of *apo* EF-Tu is that this state is less flexible. This is unlikely as switch I is disordered in the EF-Tu•EF-Ts crystalized complex from Kawashima *et al.* (1996). If this is the conformation that switch I adopts in the *apo* state then it is likely going to be more flexible. However, this does agree with the observation that *apo* EF-Tu coordinates more water molecules, as a disordered switch I would have a larger SASA. Since *apo* EF-Tu has a higher $T\Delta S$ compared to EF-Tu•GTP or EF-Tu•GDP, which cannot be explained simply by the loss of nucleotide or *apo* EF-Tu being less flexible, then *apo* EF-Tu must adopt a unique conformation.

To directly compare the thermodynamic contributions of each nucleotide bound state relative to each other, we can use the law of mass-action. However, since GTP contains an additional phosphate compared to GDP mass is not conserved in the kinetic mechanism of EF-Tu nucleotide binding, preventing the implementation of mass action (Fig 2.1). The fact that there is no difference in the $\Delta H^{\ddagger}_{a}$ or $T\Delta S^{\ddagger}_{a}$ and that the mass is conserved in the respective halves of the nucleotide dissociation mechanism (k_{-1} and k_{-2}), which defines the thermodynamic landscape of nucleotide binding, indicates that the mass of P_i has little to no influence

The enthalpic stability of EF-Tu•GDP is targeted by EF-Ts for nucleotide dissociation

Since EF-Tu and EF-Ts have co-evolved, the residues involved in stabilizing the GDP conformation of EF-Tu are likely the same residues targeted by EF-Ts to help mediate GDP release. The current understanding is that EF-Ts stimulates GDP dissociation from EF-Tu through three factors: (1) destabilization of the Mg^{2+} coordination, (2) flipping of the P-loop and (3) destabilizing the nucleotide-ribose binding site (Kawashima et al., 1996; Schummer, Gromadski, & Rodnina, 2007; Wieden et al., 2002). Previously, the interactions between EF-Ts and helix B (switch II – amino acids 84-92), as well as helix D (amino acids 139-144) have been studied as EF-Ts makes direct interactions with these regions of EF-Tu (Jonák, Anborgh, & Parmeggiani, 1998; Schummer et al., 2007; Wieden et al., 2002; Wieden et al., 2010; Zhang, Li, & Spremulli, 1996). Crystal structures of the EF-Tu•EF-Ts complex show that residues in helix A of EF-Tu contact the C-terminal end of EF-Ts (Kawashima et al., 1996). Additionally, our group has previously shown that these interactions destabilize helices A and F and increase the rate of nucleotide release 10-fold (De Laurentiis et al., 2016). Since helix A is located in proximity to a number of interactions that stabilize the GDP conformation, it is likely that EF-Ts specifically disrupts these hydrogen bonds. Two possible mechanisms may explain how the C-terminus of EF-Ts helps to stimulate GDP dissociation: (1) it helps position EF-Ts properly onto EF-Tu in order for F81 to insert between H118 and H84 or (2) EF-Ts destabilizes the hydrogen bonding potential of helix A and as a consequence lowers the $\Delta H^{\ddagger}_{d}$ barrier favoring dissociation. Our data supports the latter hypothesis and is consistent with the crystal structure of the EF-Tu•GDPNP•EF-Ts complex where EF-Ts engages with EF-Tu in a conformation where the C-terminus does not pack against helix A (Thirup et al., 2015).

This structural model suggests that these interactions are not required for EF-Ts binding but are, instead, involved in promoting efficient nucleotide dissociation (Thirup et al., 2015)

Table A1.1. Temperature specific rate constants of nucleotide association and dissociation to EF-Tu. Previously reported rates for EF-Tu mant-nucleotide association and dissociation rates at 20°C are from Gromadski *et al*., 2002 (Gromadski et al., 2002). K indicates in the presence of 5μM Kirromycin.

	Temperature (°C)								
	4	6	12	15	20°C	22	25	29	37
mant•GDP k_{on} ($x10^6\ M^{-1}\ s^{-1}$)	0.3 ± 0.1	-	1.1 ± 0.1	-	2 ± 0.5	1.7 ± 0.1	-	2.1 ± 0.2	5.1 ± 0.3
mant•GDP k_{off} ($x10^{-3}\ s^{-1}$)	0.4 ± 0.1	-	0.8 ± 0.1	-	2 ± 1	1.4 ± 0.1	-	3.1 ± 0.1	7.1 ± 0.3
mant•GTP k_{on} ($x10^5\ M^{-1}\ s^{-1}$)	1.6 ± 0.1	-	2.6 ± 0.1	-	5 ± 1	4.0 ± 0.1	-	5.5 ± 0.1	9.1 ± 0.1
mant•GTP k_{off} ($x10^{-3}\ s^{-1}$)	-	11 ± 1	-	16 ± 1	30 ± 10	-	28 ± 4	-	60 ± 2
K mant•GDP k_{on} ($x10^6\ M^{-1}\ s^{-1}$)									3.5 ± 0.5
K mant•GDP k_{off} ($x10^{-3}\ s^{-1}$)									61 ± 6
K mant•GTP k_{on} ($x10^5\ M^{-1}\ s^{-1}$)									4.3 ± 0.3
K mant•GTP k_{off} ($x10^{-3}\ s^{-1}$)									9 ± 1

Table A1.2. Transition state thermodynamic properties governing nucleotide binding in EF-Tu compared to equilibrium determine thermodynamic properties. * Equilibrium values determined at 20°C by Talavera *et al*. 2018 – GTP values are for GDPγS, and K indicates in the presence of 5μM Kirromycin (Talavera et al., 2018).

	$\Delta H^{\circ\ddagger}_a$ kJ/mol	$\Delta H^{\circ\ddagger}_d$ kJ/mol	ΔH°_B kJ/mol	$T\Delta S^{\circ\ddagger}_a$ kJ/mol	$T\Delta S^{\circ\ddagger}_d$ kJ/mol	$T\Delta S^{\circ}_B$ kJ/mol	$\Delta G^{\circ\ddagger}_a$ kJ/mol	$\Delta G^{\circ\ddagger}_d$ kJ/mol	ΔG°_B kJ/mol	ΔH°_B* kJ/mol	$T\Delta S^{\circ}_B$* kJ/mol	ΔG°_B* kJ/mol
GTP	36 ± 2	35 ± 1	-1 ± 3	-4 ± 2	-46 ± 1	42 ± 5	40 ± 4	81 ± 2	-41 ± 6	-5 ± 3	36 ± 1	-41 ± 1
GDP	34 ± 4	61 ± 1	-27 ± 5	3 ± 4	-27 ± 1	30 ± 5	37 ± 7	88 ± 3	-50 ± 10	-26 ± 2	21 ± 1	-46 ± 1
K GTP									-46 ± 1	-	-	-
K GDP									-47 ± 4	-	-	-

Table A1.3. Entropic contributions summary of the EF-Tu•GTP and EF-Tu•GDP conformations. Coordinated water molecules were determined as water within 2.5Å of EF-Tu.

EF-Tu Conformation	SASA ($Å^2$) mean	SASA ($Å^2$) Standard Deviation	# of Water Molecules mean	# of Water Molecules Standard Deviation
GTP	19357	297	318	11
GDP	20398	261	334	11

Table A1.4. Difference in transition state thermodynamic properties governing nucleotide dissociation for EF-Tu variants compared to wild type (TΔΔS measured at 20°C). *-values reported in Mercier *et al* (Mercier et al., 2015).

	$\Delta\Delta H^{\circ\ddagger}_{d}$ kJ/mol	$T\Delta\Delta S^{\circ\ddagger}_{d}$ kJ/mol	$\Delta\Delta G^{\circ\ddagger}_{d}$ kJ/mol
H22G•GTP*	19 ± 4	18 ± 4	2 ± 8
H22G•GDP	-5 ± 3	2 ± 3	-7 ± 6
M112L•GTP*	1 ± 2	6 ± 2	-5 ± 5
M112L•GDP	1 ± 4	6 ± 4	-4 ± 7

Table A1.5. Location of waters that are resident (within 4.0Å of EF-Tu) in a single location in the EF-Tu•GTP or EF-Tu•GDP simulations during more than 50% of frames.

EF-Tu•GTP			EF-Tu•GDP		
Water Molecule ID	% of Frames	Position	Water Molecule ID	% of Frames	Position
6337	100	Mg^{2+} Coordination	6130	100	Mg^{2+} Coordination
6334	100	Mg^{2+} Coordination	6127	100	P-Loop (H22/T115/V104)
6142	100	GTP Interaction (Near G83)	6121	100	Mg^{2+} Coordination
6130	100	P-Loop (H22/H19)	6103	100	Mg^{2+} Coordination
14632	94.7	Helix D (S183/W184)	6100	100	Mg^{2+} Coordination
11764	89.0	Domain II (E243/K294/I298/T297)	6088	100	Mg^{2+} Coordination
28942	64.1	Helix D (R74/I199)	6112	99.9	Helix D (S173/W184/K187)
6136	60.8	Domain II/Switch II (I214/Q290)	47376	99.6	GDP (K24/V20)
11377	57.0	Switch II (H118/H84/Q214)	55629	91.0	Helix D (Y176/V12/I199/R74)
44749	53.8	Switch II (T64/T93/G94)	34896	67.22	Domain II (G296/T297/K294)
41926	52.6	Domain I (T167/I130/Y198)	15375	52.4	Domain II/III(R333/R230/P213)
45604	50.3	Domain III/Switch II (R333/T334/T93)			

Table A1.6. Summary of hydrogen bonds formed by the peptidyl backbone carboxylic acid oxygen (O) to a peptidyl backbone amide (N-H) of EF-Tu

Residue	% of frames a hydrogen bond is formed between a backbone O to a backbone N-H		% Difference (GDP-GTP)	Residue	% of frames a hydrogen bond is formed by a backbone O to a backbone N-H		% Difference (GDP-GTP)
	GTP	GDP			GTP	GDP	
1	1.21	0.01	-1.20	197	0.00	0.00	0.00
2	0.01	0.00	-0.01	198	0.00	0.00	0.00
3	77.23	0.02	-77.21	199	0.00	0.00	0.00
4	0.19	0.07	-0.12	200	0.00	0.00	0.00
5	0.06	1.67	1.61	201	0.00	0.01	0.01
6	1.96	0.00	-1.96	202	0.00	0.00	0.00
7	0.01	0.00	-0.01	203	0.00	0.12	0.12
8	0.00	0.00	0.00	204	12.39	14.74	2.36
9	0.00	0.00	0.00	205	81.96	88.79	6.83
10	88.37	81.54	-6.82	206	12.87	0.03	-12.83
11	0.00	0.00	0.00	207	0.00	0.00	0.00
12	42.80	74.47	31.67	208	0.03	0.03	0.00
13	100.59	91.67	-8.92	209	0.00	0.00	0.00
14	80.81	20.14	-60.67	210	4.47	6.98	2.51
15	92.67	84.86	-7.81	211	70.82	57.13	-13.69
16	4.78	0.00	-4.78	212	92.34	94.06	1.71
17	75.90	51.44	-24.46	213	0.00	0.00	0.00
18	0.00	0.00	0.00	214	3.76	0.00	-3.76
19	1.12	0.00	-1.12	215	29.80	0.00	-29.80
20	0.23	0.02	-0.21	216	35.69	45.04	9.36
21	0.00	0.00	0.00	217	0.00	0.01	0.01
22	0.00	0.00	0.00	218	77.17	76.61	-0.56
23	69.17	75.57	6.40	219	0.00	0.03	0.03
24	53.71	55.81	2.10	220	62.67	4.92	-57.74
25	58.71	60.40	1.69	221	10.26	0.13	-10.12
26	56.61	78.68	22.07	222	0.00	0.70	0.70
27	90.84	95.14	4.30	223	0.00	14.30	14.30

28	20.06	3.98	-16.08	224	57.54	24.22	-33.32
29	17.53	25.87	8.33	225	60.78	53.61	-7.17
30	48.03	84.00	35.97	226	81.29	73.56	-7.73
31	31.99	39.21	7.22	227	79.58	88.17	8.59
32	32.83	43.52	10.69	228	91.43	79.98	-11.46
33	47.01	57.50	10.49	229	78.10	65.29	-12.81
34	48.90	60.77	11.87	230	0.01	0.27	0.26
35	70.67	93.54	22.88	231	91.80	84.21	-7.59
36	29.80	0.87	-28.93	232	0.00	0.00	0.00
37	0.21	0.00	-0.21	233	66.82	51.80	-15.02
38	0.18	0.00	-0.18	234	27.71	16.60	-11.11
39	0.00	0.00	0.00	235	0.09	0.02	-0.07
40	0.04	0.09	0.04	236	70.03	77.52	7.49
41	0.62	0.09	-0.53	237	0.32	0.66	0.33
42	7.73	0.12	-7.61	238	1.30	3.87	2.57
43	0.03	0.00	-0.03	239	0.00	0.00	0.00
44	0.97	0.01	-0.96	240	80.53	72.02	-8.51
45	16.81	3.20	-13.61	241	0.00	0.00	0.00
46	56.29	97.14	40.86	242	63.71	54.27	-9.44
47	0.26	47.90	47.64	243	70.54	88.99	18.44
48	0.00	0.07	0.07	244	0.06	7.43	7.38
49	0.02	0.01	-0.01	245	17.57	46.74	29.18
50	0.02	22.50	22.48	246	0.00	20.36	20.36
51	0.00	0.00	0.00	247	0.23	0.00	-0.23
52	28.76	0.00	-28.76	248	0.27	0.04	-0.22
53	30.53	7.03	-23.50	249	0.02	0.76	0.73
54	36.70	0.04	-36.66	250	0.73	0.00	-0.73
55	33.93	72.44	38.51	251	77.40	88.71	11.31
56	0.91	1.02	0.11	252	0.00	0.00	0.00
57	0.00	7.50	7.50	253	80.41	75.20	-5.21
58	9.06	19.29	10.23	254	11.38	41.43	30.06
59	0.00	0.00	0.00	255	69.37	71.23	1.87
60	0.01	37.36	37.34	256	0.00	0.00	0.00

61	0.00	0.00	0.00	257	82.76	80.90	-1.86
62	0.00	83.49	83.49	258	34.41	86.09	51.68
63	0.00	0.00	0.00	259	90.06	80.60	-9.46
64	0.01	0.24	0.23	260	8.39	0.96	-7.43
65	67.28	37.21	-30.07	261	0.00	0.00	0.00
66	0.00	0.00	0.00	262	0.00	0.00	0.00
67	92.04	82.22	-9.82	263	76.74	20.27	-56.48
68	0.00	0.00	0.00	264	75.58	0.00	-75.58
69	86.28	93.29	7.01	265	0.00	21.99	21.99
70	0.01	0.01	0.00	266	0.02	14.76	14.73
71	0.36	0.28	-0.08	267	0.62	0.04	-0.58
72	0.00	0.00	0.00	268	73.78	69.17	-4.61
73	0.00	0.00	0.00	269	12.13	9.58	-2.56
74	46.88	54.87	7.99	270	1.97	0.17	-1.80
75	38.80	81.66	42.86	271	0.00	0.04	0.04
76	20.79	38.18	17.39	272	38.79	60.31	21.52
77	88.12	70.77	-17.36	273	0.00	0.00	0.00
78	63.57	61.88	-1.69	274	15.10	22.40	7.30
79	18.14	22.24	4.10	275	66.58	84.68	18.10
80	27.26	76.31	49.06	276	59.89	82.69	22.80
81	0.00	0.03	0.03	277	76.62	86.39	9.77
82	0.00	0.00	0.00	278	13.88	16.57	2.69
83	14.34	13.07	-1.28	279	50.97	9.16	-41.81
84	5.37	46.41	41.04	280	0.01	0.00	-0.01
85	0.41	59.43	59.02	281	0.02	4.14	4.12
86	14.18	50.62	36.44	282	33.41	8.83	-24.58
87	5.66	69.76	64.10	283	2.52	9.43	6.91
88	68.42	49.17	-19.26	284	0.00	0.03	0.03
89	20.67	69.97	49.30	285	0.01	0.71	0.70
90	13.64	6.44	-7.20	286	0.00	0.00	0.00
91	100.00	0.00	-100.00	287	0.08	0.13	0.06
92	42.63	0.13	-42.50	288	1.01	0.00	-1.01
93	0.32	0.31	-0.01	289	0.00	0.00	0.00

94	29.59	2.67	-26.92	290	86.70	36.88	-49.82
95	13.29	0.02	-13.27	291	78.53	70.72	-7.81
96	0.00	0.03	0.03	292	67.92	86.02	18.10
97	0.00	0.02	0.02	293	89.27	84.69	-4.58
98	0.00	0.00	0.00	294	0.64	0.34	-0.30
99	1.34	1.13	-0.21	295	0.34	0.07	-0.28
100	1.93	0.68	-1.26	296	0.00	0.00	0.00
101	67.96	54.16	-13.80	297	0.01	0.00	-0.01
102	70.24	71.14	0.90	298	0.00	0.00	0.00
103	85.22	89.09	3.87	299	0.21	9.04	8.83
104	0.00	0.00	0.00	300	0.00	0.00	0.00
105	98.70	97.48	-1.22	301	56.88	50.76	-6.12
106	67.37	50.23	-17.13	302	63.14	70.27	7.12
107	0.00	0.00	0.00	303	59.50	56.06	-3.44
108	0.00	0.00	0.00	304	86.66	86.84	0.19
109	0.00	0.00	0.00	305	87.28	84.62	-2.66
110	3.21	1.32	-1.89	306	63.20	61.72	-1.48
111	0.00	0.00	0.00	307	38.57	42.24	3.68
112	49.71	41.34	-8.37	308	46.94	73.92	26.98
113	44.08	57.74	13.67	309	76.81	57.22	-19.59
114	66.96	60.49	-6.47	310	24.31	61.01	36.70
115	1.92	3.04	1.12	311	16.93	0.31	-16.62
116	20.09	39.31	19.22	312	83.04	93.72	10.68
117	95.74	86.03	-9.71	313	1.86	2.97	1.11
118	67.49	50.40	-17.09	314	0.01	0.01	0.00
119	37.71	40.49	2.78	315	0.09	0.00	-0.09
120	47.97	53.08	5.11	316	0.63	2.29	1.66
121	89.57	67.08	-22.49	317	0.02	0.00	-0.02
122	85.46	100.00	14.54	318	0.16	1.13	0.98
123	0.34	0.17	-0.18	319	0.00	0.00	0.00
124	0.00	0.00	0.00	320	0.00	0.00	0.00
125	0.00	0.00	0.00	321	0.21	0.00	-0.21
126	0.00	0.00	0.00	322	75.17	82.58	7.41

127	0.19	0.00	-0.19	323	3.18	5.54	2.37
128	0.61	5.64	5.03	324	1.27	6.37	5.10
129	61.30	41.51	-19.79	325	0.00	0.00	0.00
130	0.00	0.00	0.00	326	27.53	2.96	-24.58
131	93.10	91.78	-1.32	327	0.00	0.00	0.00
132	46.34	60.49	14.14	328	8.67	23.31	14.64
133	47.54	53.44	5.90	329	57.89	79.08	21.19
134	79.70	81.29	1.59	330	51.87	46.08	-5.79
135	87.61	88.71	1.10	331	49.81	42.76	-7.06
136	17.66	18.28	0.62	332	0.12	9.61	9.49
137	1.13	0.42	-0.71	333	0.00	0.01	0.01
138	0.00	0.00	0.00	334	0.00	0.00	0.00
139	0.13	0.24	0.11	335	10.31	25.51	15.20
140	0.00	0.00	0.00	336	0.00	0.06	0.06
141	0.03	0.02	-0.01	337	94.16	97.00	2.84
142	11.76	11.40	-0.36	338	35.83	2.02	-33.81
143	51.93	54.37	2.43	339	0.06	0.01	-0.04
144	35.02	31.78	-3.24	340	49.77	66.37	16.60
145	46.82	40.70	-6.12	341	30.50	0.06	-30.44
146	38.81	50.89	12.08	342	50.54	57.03	6.49
147	46.83	51.18	4.34	343	0.00	0.00	0.00
148	26.24	31.69	5.44	344	3.61	3.79	0.18
149	30.44	26.38	-4.07	345	5.08	4.16	-0.92
150	54.06	65.32	11.27	346	0.01	0.12	0.11
151	36.56	62.02	25.47	347	0.00	0.00	0.00
152	28.50	32.59	4.09	348	7.58	6.77	-0.81
153	56.58	62.39	5.81	349	1.09	0.24	-0.84
154	47.07	56.88	9.81	350	22.52	31.14	8.62
155	46.87	28.91	-17.96	351	1.82	0.59	-1.23
156	11.99	4.82	-7.17	352	3.96	0.84	-3.11
157	60.80	26.60	-34.20	353	0.00	0.00	0.00
158	10.04	1.01	-9.03	354	14.76	31.93	17.18
159	4.69	0.54	-4.14	355	0.00	0.00	0.00

160	3.79	8.74	4.96	356	75.98	66.42	-9.56
161	0.00	0.00	0.00	357	0.00	0.00	0.00
162	6.47	1.97	-4.50	358	84.24	79.26	-4.99
163	29.71	18.30	-11.41	359	80.16	76.91	-3.24
164	0.17	0.19	0.02	360	53.37	49.69	-3.68
165	0.93	1.18	0.24	361	72.23	46.26	-25.98
166	0.00	0.00	0.00	362	0.00	0.00	0.00
167	0.19	0.20	0.01	363	0.00	0.00	0.00
168	23.13	35.24	12.11	364	0.03	0.31	0.28
169	0.00	0.00	0.00	365	0.00	21.94	21.94
170	94.14	96.98	2.83	366	79.88	76.21	-3.67
171	0.00	0.00	0.00	367	0.01	0.00	-0.01
172	28.33	23.53	-4.80	368	0.19	7.13	6.94
173	1.72	1.99	0.27	369	0.20	0.29	0.09
174	23.10	53.31	30.21	370	3.62	1.96	-1.67
175	61.49	59.64	-1.84	371	0.01	0.04	0.03
176	41.96	99.08	57.12	372	54.11	60.94	6.83
177	0.03	0.23	0.20	373	0.00	0.00	0.00
178	1.04	0.00	-1.04	374	28.54	50.63	22.09
179	0.16	0.00	-0.16	375	89.18	90.46	1.28
180	2.29	0.01	-2.28	376	82.00	94.09	12.09
181	29.60	54.92	25.32	377	26.76	69.16	42.40
182	36.96	34.46	-2.50	378	15.82	1.82	-14.00
183	9.67	6.93	-2.73	379	0.46	0.88	0.42
184	6.08	6.24	0.17	380	0.00	0.00	0.00
185	57.09	41.60	-15.49	381	58.27	57.03	-1.23
186	70.92	65.61	-5.31	382	0.03	0.00	-0.03
187	49.54	49.24	-0.30	383	48.78	50.62	1.84
188	74.81	67.53	-7.28	384	90.50	89.48	-1.02
189	59.34	56.07	-3.28	385	87.06	91.74	4.69
190	53.47	46.24	-7.22	386	72.61	63.10	-9.51
191	85.66	72.19	-13.47	387	51.16	39.21	-11.94
192	32.72	23.12	-9.60	388	0.00	19.78	19.78

193	54.11	56.12	2.01	389	0.00	0.00	0.00
194	80.98	69.36	-11.62	390	86.87	84.22	-2.64
195	9.22	0.30	-8.92	391	0.00	0.00	0.00
196	0.02	0.00	-0.02	392	0.00	0.00	0.00

Table A1.7. The modulation of *E. coli* EF-Tu nucleotide binding kinetics by antibiotics. Values determined by * - Fasano *et al*. 1978 , †- Anborgh and Parmeggiani, 1993, £ - Anborgh *et al*. 2004, and ℓ Cetin *et al*. 1996 (Anborgh et al., 2004; Anborgh & Parmeggiani, 1993; Cetin et al., 1996; Fasano et al., 1978).

Antibiotic	GTP on rate (s^{-1} M^{-1})	GTP off rate (s^{-1})	GTP Affinity (nM)	GDP on rate (s^{-1} M^{-1})	GDP off rate (s^{-1})	GDP Affinity (nM)	Temp. (°C)
No antibiotic	$1.6 \pm 0.1 \times 10^5$	$1.1 \pm 0.1 \times 10^{-2}$	60	$0.3 \pm 0.1 \times 10^6$	$0.4 \pm 0.1 \times 10^{-3}$	1	4
No antibiotic*	1.0×10^4	5.9×10^{-3}	590	2.6×10^5	2.3×10^{-4}	0.9	0
Kirromycin*	1.2×10^5	1.7×10^{-4}	1.4	9.0×10^5	7.4×10^{-4}	0.8	0
GE2270 A †	1.3×10^4	0.15×10^{-4}	1.2	3.5×10^5	2.3×10^{-4}	0.7	0
Pulvomycin£	5.1×10^4	0.3×10^{-4}	0.6	6.0×10^5	5.9×10^{-5}	9.8	0
Enacyloxin IIaℓ	3.9×10^5	2.8×10^{-4}	0.7	7.8×10^4	6.2×10^{-4}	8	0

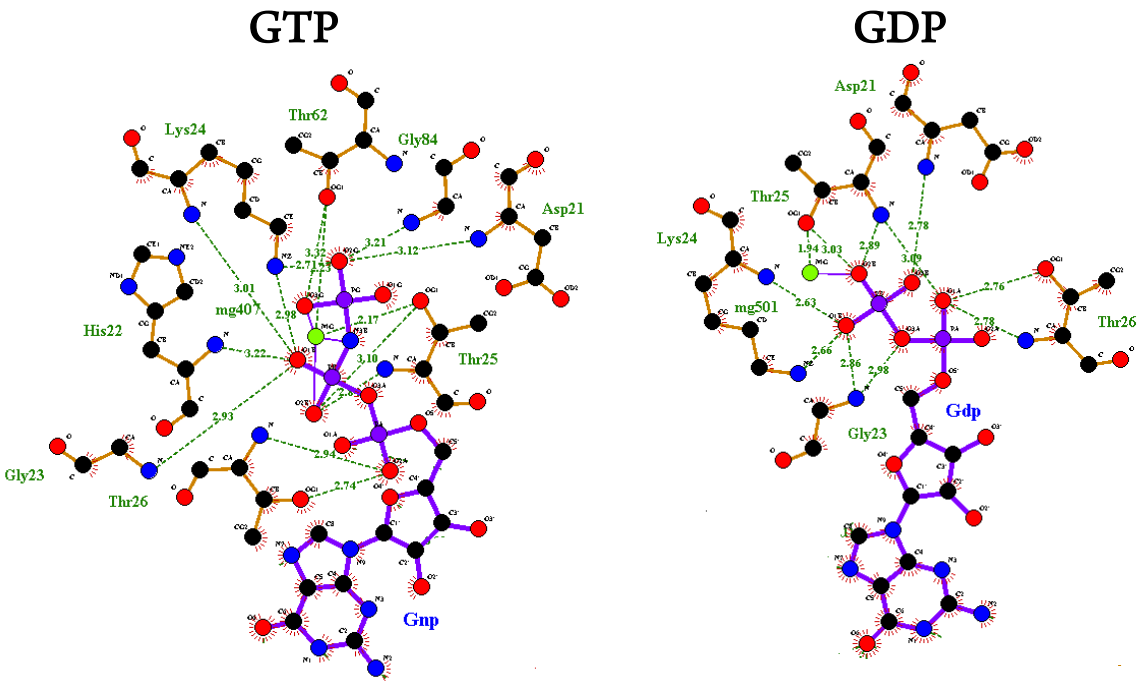

Figure A1.1 LIGPLOT view of EF-Tu interactions with GTP and GDP. (A) Coordinating residues of the guanosine nucleotide, water was not included in ligplot to avoid any bias from unresolved water molecules do to the differences in resolution of 1EFT (2.5Å) and 1EFC (2.05Å). (Wallace, Laskowski, & Thornton, 1995). (B) The number of water molecules within 3Å of the respective nucleotide during 100ns of simulation time.

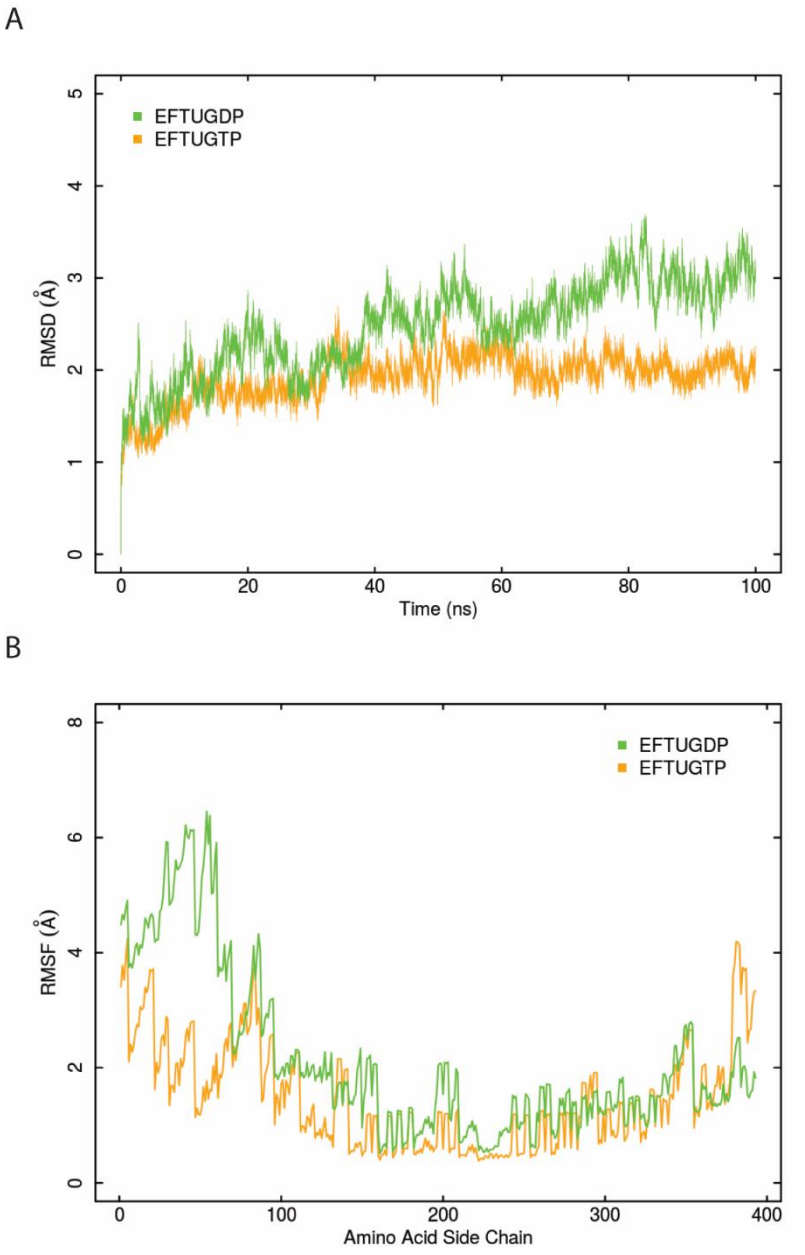

Figure A1.2. EF-Tu simulation deviations and flexibility (A) Root Mean Square Deviation (RMSD) and (B) Side chain Root Mean Square Fluctuation (RMSF) of the 100ns EF-Tu•GTP and EF-Tu•GDP simulations.

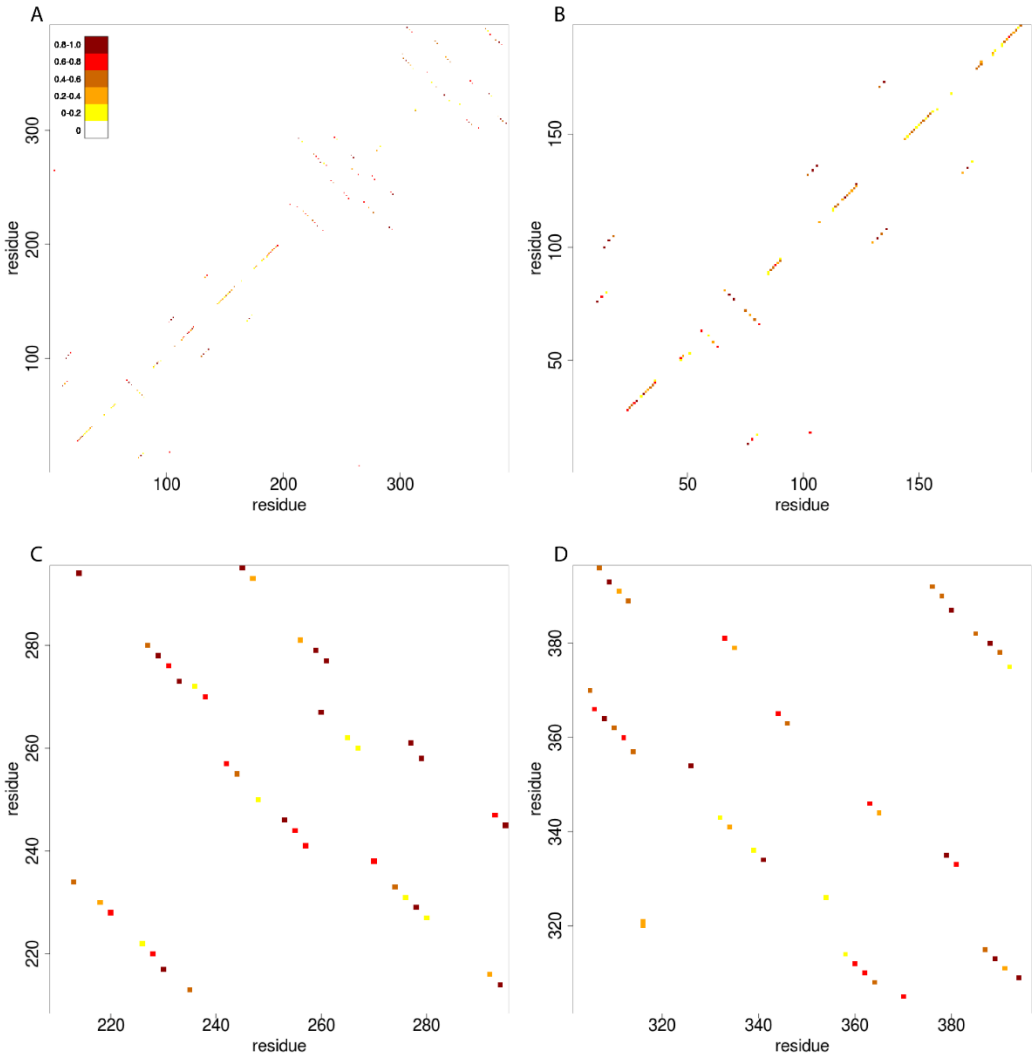

Figure A1.3. Hydrogen bonding network of EF-Tu•GDP. Hydrogen bonds were defined as Carboxyl O or Amide N-H of the peptide backbone that were in 3.0Å and within 60° of each other. Hydrogen bonding network of (A) EF-Tu•GDP, (B) domain I, (C) domain II, and (D) domain III. α-helices and β-strands are represented as consecutive hydrogen bonds along the bottom left to top right or top left to bottom right diagonals respectively

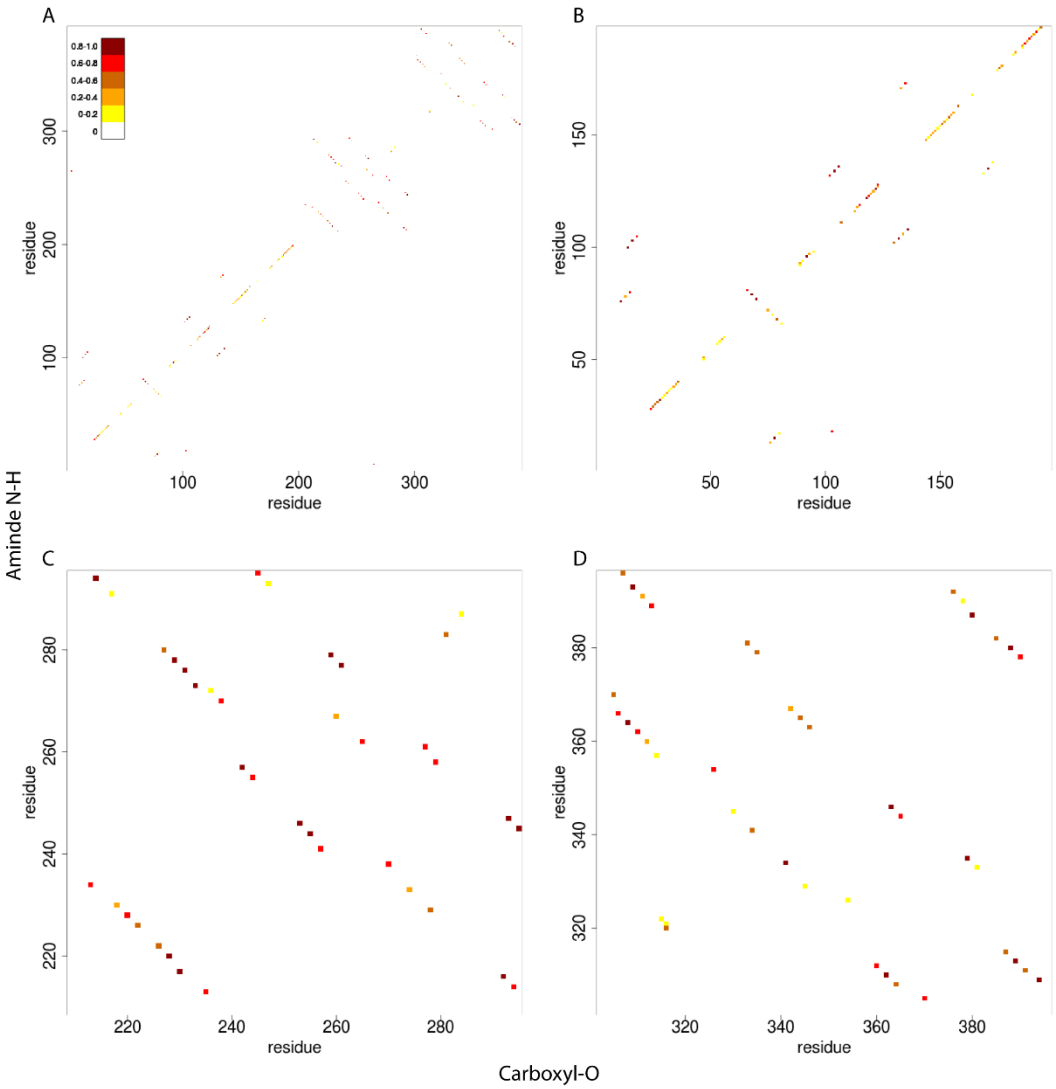

Figure A1.4. Hydrogen bonding network of EF-Tu•GTP. Hydrogen bonds were defined as Carboxyl O or Amide N-H of the peptide backbone that were in 3.0Å and within 60° of each other. Hydrogen bonding network of (A) EF-Tu•GTP, (B) domain I, (C) domain II, and (D) domain III. α-helices and β-strands are represented as consecutive hydrogen bonds along the bottom left to top right or top left to bottom right diagonals respectively

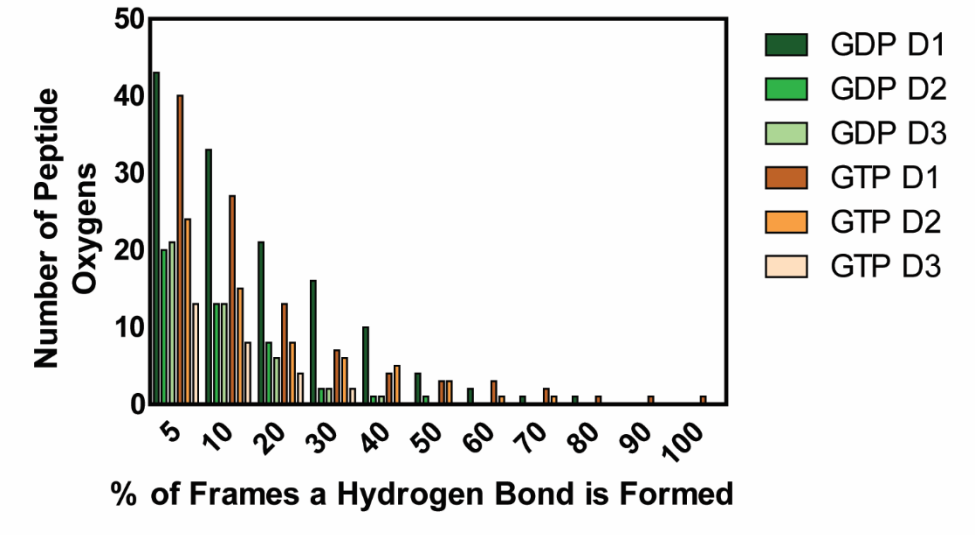

Figure A1.5. Number of backbone oxygens that are involved in hydrogen bonds in the EF-Tu•GTP and EF-Tu•GDP 100ns simulations separated into each domain.

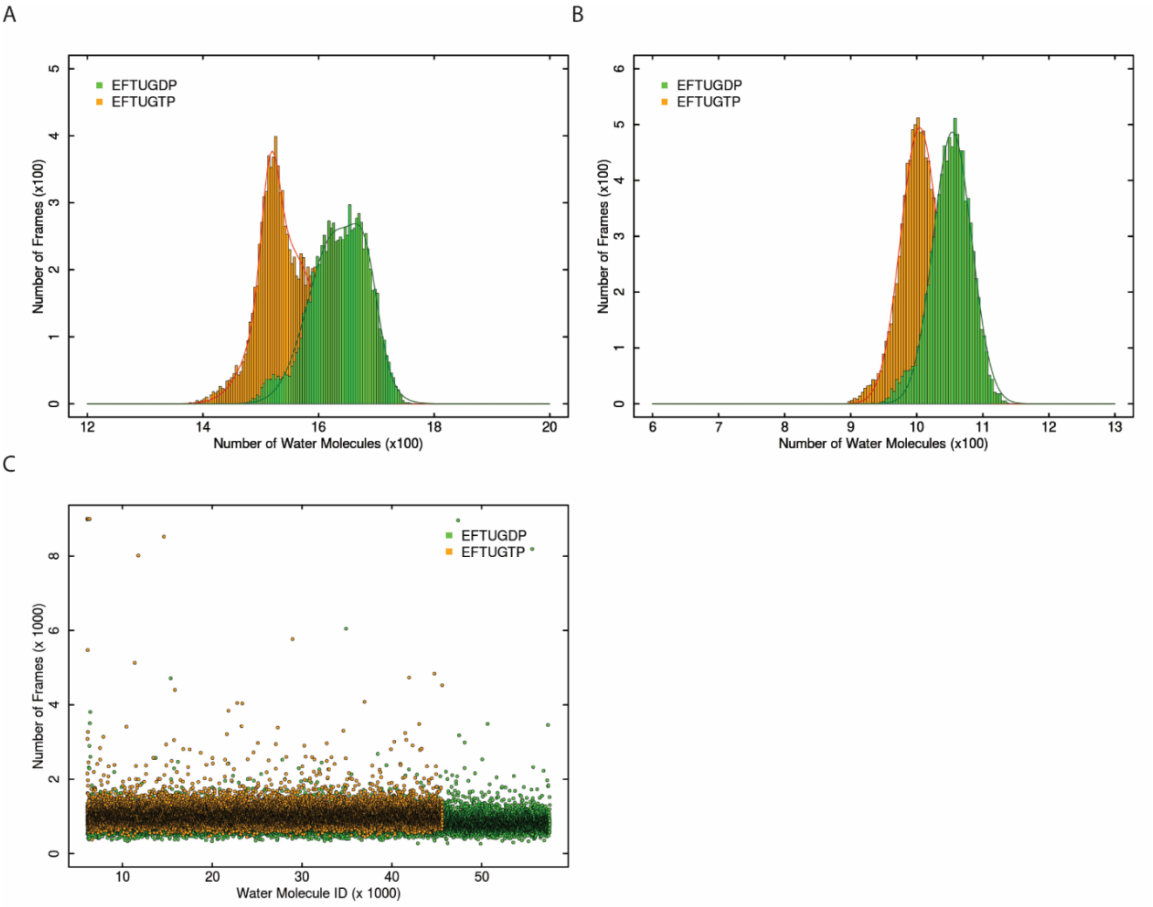

Figure A1.6 Water coordination of EF-Tu•GTP and EF-Tu•GDP during 100ns of simulation. (A) Water within 4.0 Å of EF-Tu (EF-Tu•GTP mean-1517 ± 16 and 1550 ± 50; EF-Tu•GDP mean-1628 ± 79 and 1682 ± 22). (B) Water within 3.0 Å of EF-Tu (EF-Tu•GTP mean – 1004 ± 29; EF-Tu•GDP mean – 1054 ± 29). (C) Residency times of water molecules in the EF-Tu simulations.

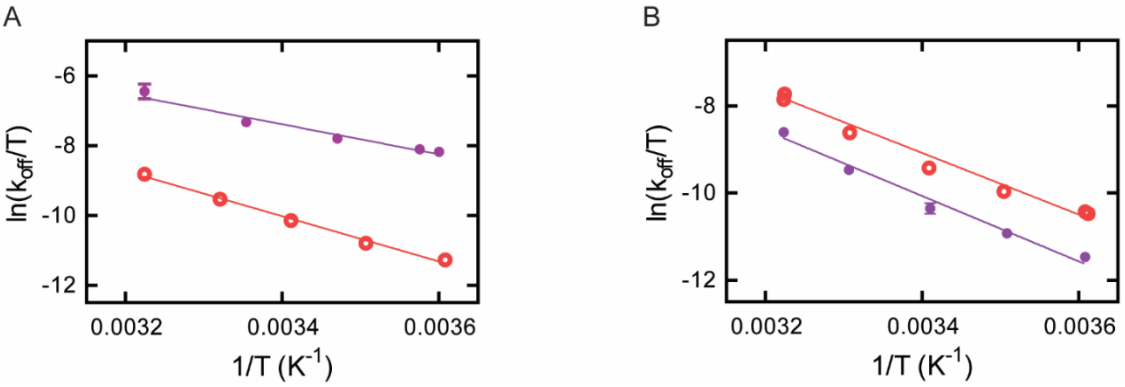

Figure A1.7. Eyring plot of nucleotide dissociation for EF-Tu variants H22G and M112L. (A) GTP and (B) GDP dissociation at temperatures ranging from 4°C to 37°C, M112L – purple (closed circle), H22G – red (open circle).

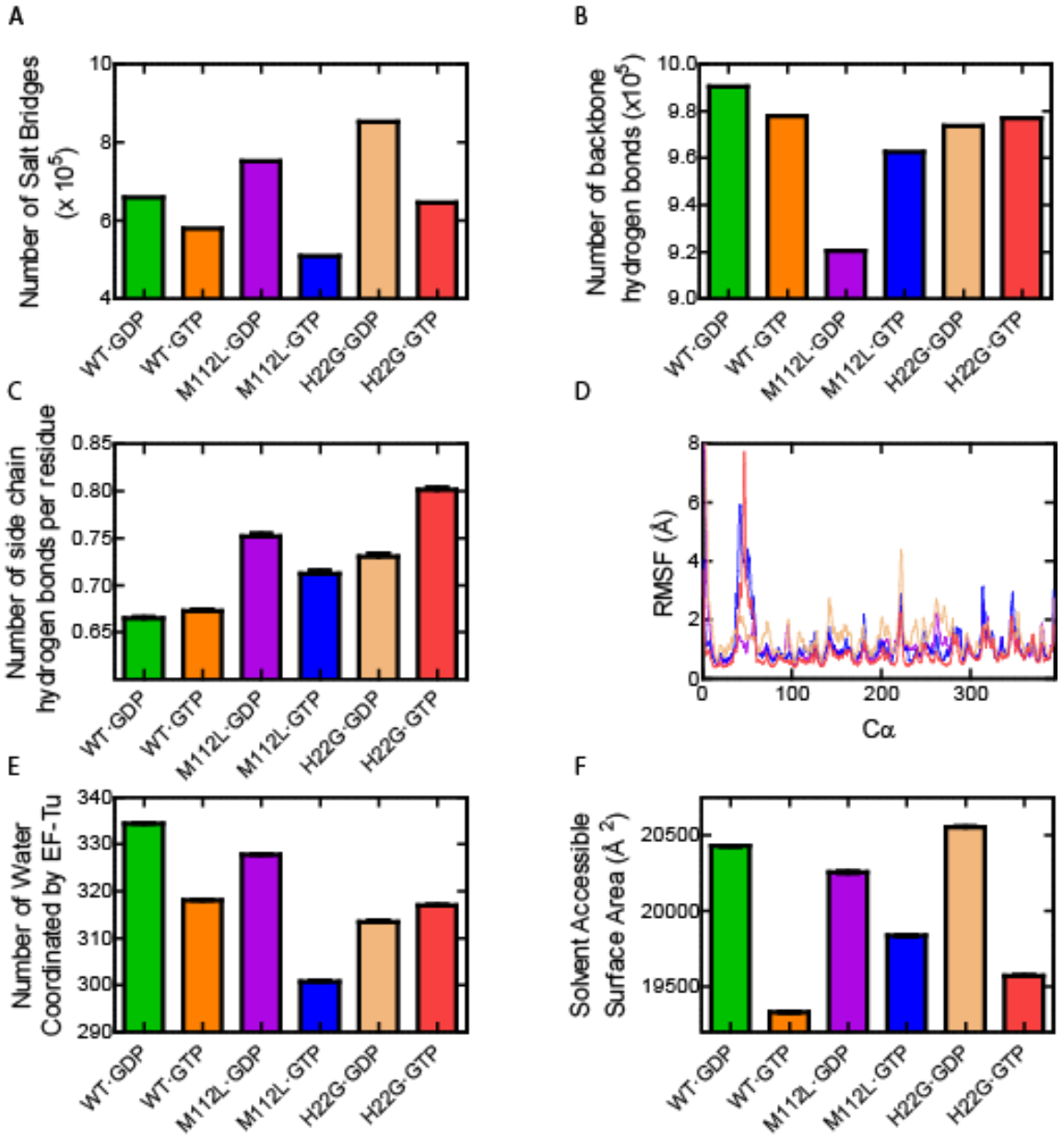

Figure A1.8. Analysis of 100ns EF-Tu H22G and M112L MD simulations. Enthalpic contributions to EF-Tu measured as number of (A) salt bridges, (B) backbone hydrogen bonds, and (C) sidechain hydrogen bonds in 100ns of simulation. Entropic contributions ot EF-Tu measured as (D) RMSF, (E) Number of water coordinate by EF-Tu, and (F) Solvent accessible surface area of EF-Tu. EF-Tu•GDP – green, EF-Tu•GTP – orange, M112L•GDP - purple, M112L•GTP – blue, H22G•GDP – beige, and H22G•GTP – red.

Appendix 2

Supplemental Material for: Protein Characterization for Personalized Medicine: Unveiling the Dynamics of D2 Dopamine Receptor Activation

Table. A2.1 Relative activity and ligand affinity of D2R variants compared to wild type D2R as reported in Sung *et al.*(2016). D2R dependent activation of G_i was measured by transfecting HEK293 cells with wild type or variant D2R. After 24 hours cells were incubated with FLIPR membrane potential fluorescent dye (Excitation 530nm, Emission 565nm). Dopamine dependent G_i activation opens the TRPC4β channels leading to changes in cell membrane potential resulting in a FLIPR fluorescence increase. Fluorescence is compared to background levels in the absence of dopamine to determine dopamine dependent activation. K_i was determined by incubating 0.4μM [^{3}H]-spiperone and cold dopamine at various concentrations with D2R embedded in HEK293 cell membranes. K_i was determined by comparison of non-specific [^{3}H]-spiperone binding at each dopamine concentration compared to [^{3}H]-spiperone binding in the absence of dopamine.

Variant	Relative Activation by Dopamine	$K_{i\text{-variant}}/K_{i\text{-wt}}$ (μM)
C385M	1.3	N.D.
F110W	3	1.02
F202L	1.3	0.99
F202L/Y213I	2.4	1.07
I48T	4	1.00
I48T/F110W	1.6	0.99
I105K	1.8	1.01
I105K/I195F	2.2	1.01
I195F	1.6	1.02
L171P	4.5	0.87
L379F	0	0.97
L387C	1.5	1.04
M117F	1	0.99
M117F/L387C	1.3	0.97
M117F/Y199F	1.5	0.93
N124H	1	1.01
N124H/L379F	0.1	0.95
N124H/T205M	1.1	1.21
S193G	0.4	N.D.
S193G/C385M	0	N.D.
S409N	1.2	1.04
T205M	2.5	1.21
T205M/L379F	1.3	N.D.
V83L	1.5	N.D.
V83L/V91S	1.1	N.D.
V91S	2.8	N.D.
V152A	1.4	0.92
V152A/L171P	1.9	0.78
V191L	1.5	0.97
V191L/S409N	1.1	1.04
Y199F	6	0.94
Y213I	1.3	1.03

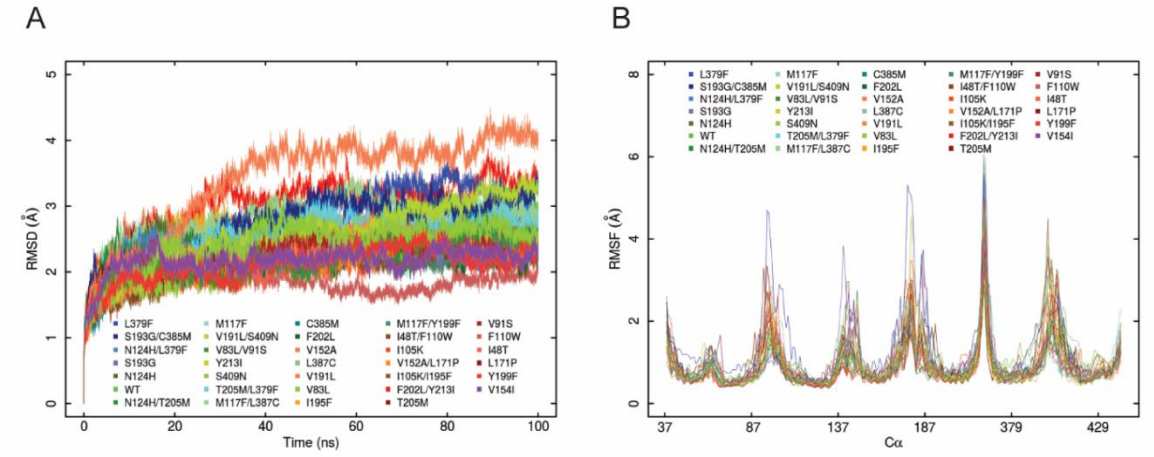

Figure A2.1. Stability and Dynamics of D2R simulations. (A) Root Mean Squared Deviation (RMSD) and (B) Root Mean Squared Fluctuation (RMSF) of D2R wt and variants.

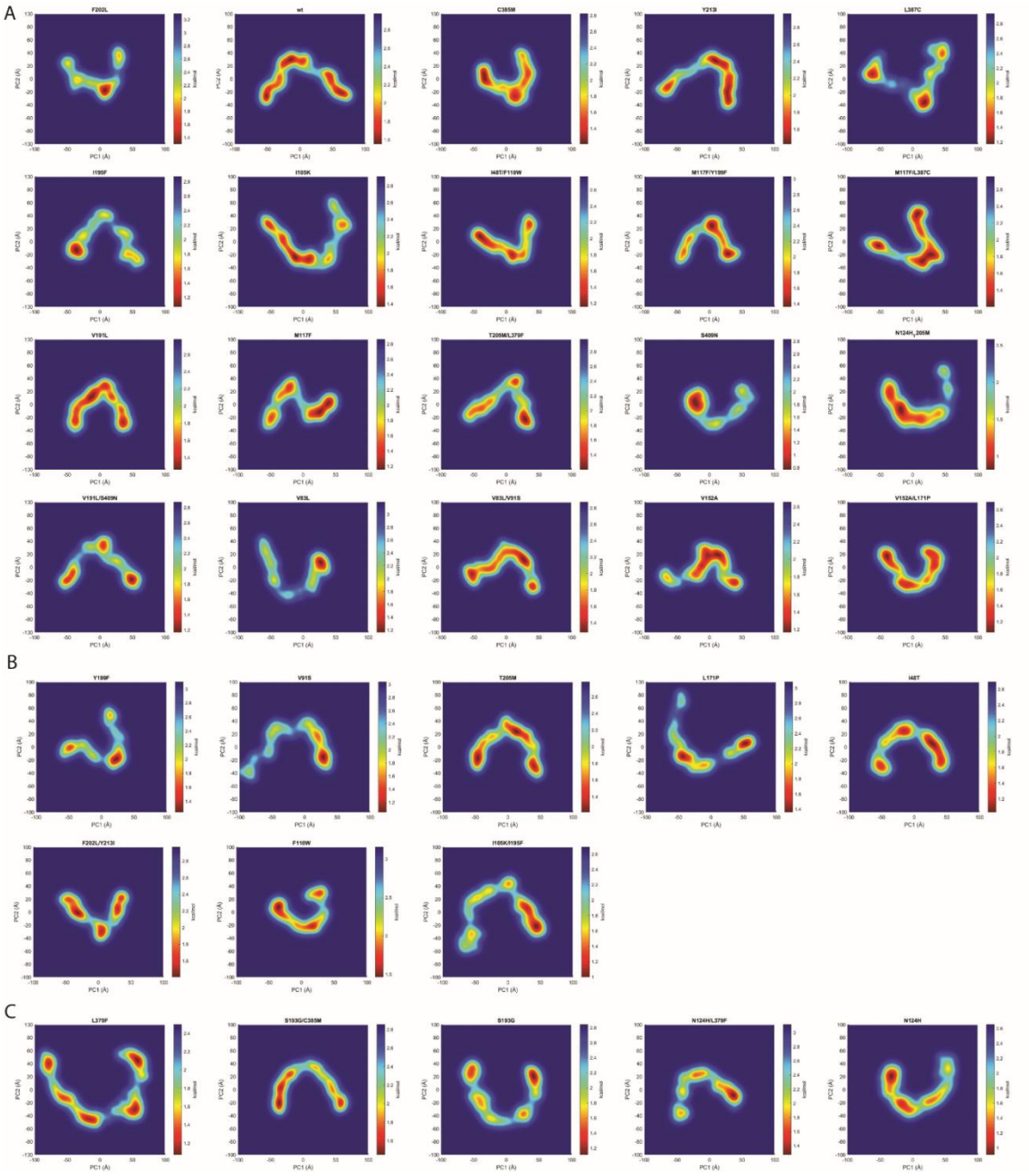

Figure A2.2. Principal Component Analysis (PCA) of wt and variant D2R. (A) Normal activity variants, (B) High activity variants, and (C) Low activity variants of D2R.

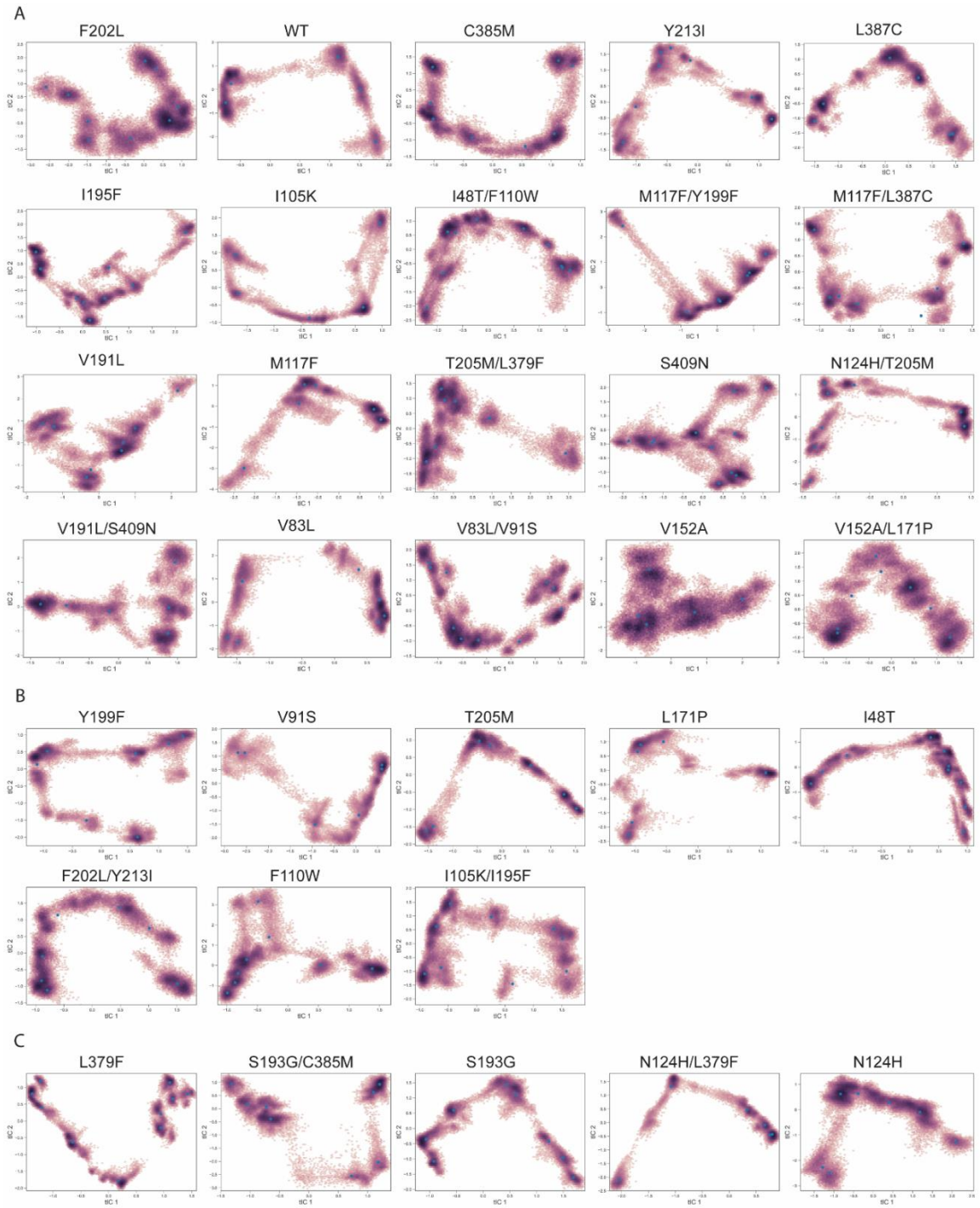

Figure A2.3. Time Independent Component Analysis (tICA) and kmeans clustering of wt and variant D2R. (A) Normal activity variants, (B) High activity variants, and (C) Low activity variants. Blue dots indicate a kmeans cluster.

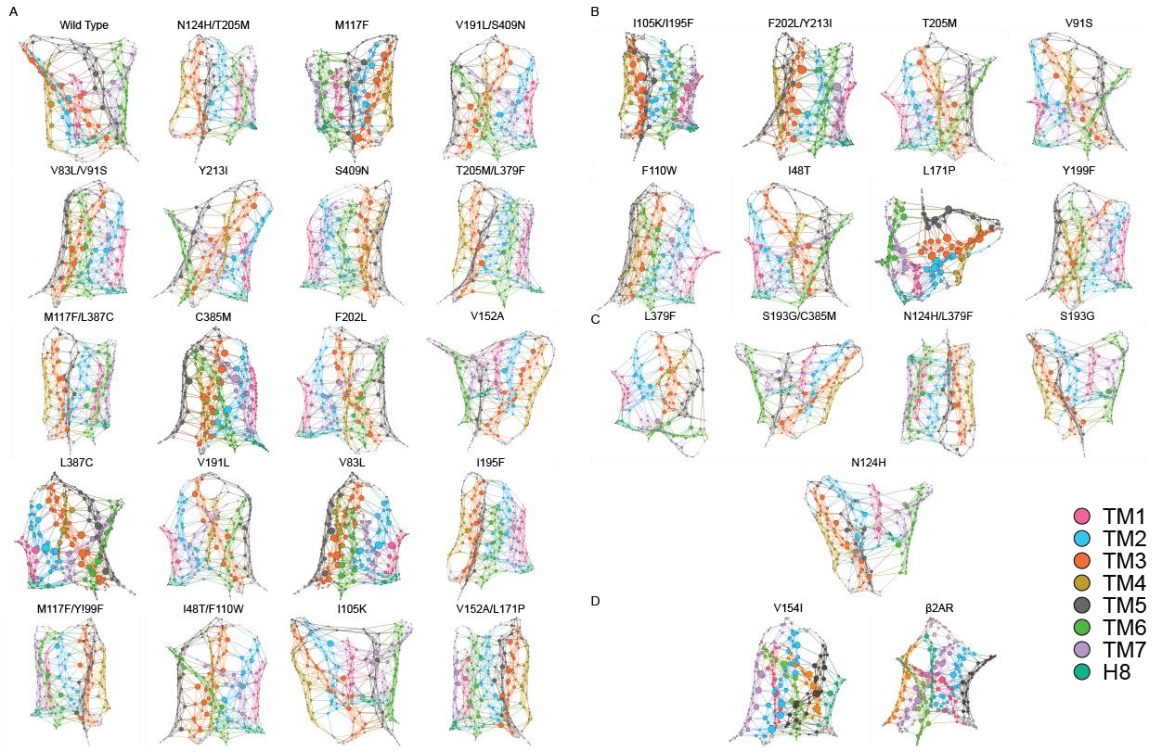

Figure A2.4. D2R correlated C_α Protein Structure Networks. (A) normal activity (B) high activity (C) low activity variants. (D) ccPSN for D2R Myoclonus dystonia mutation V154I and β2AR.

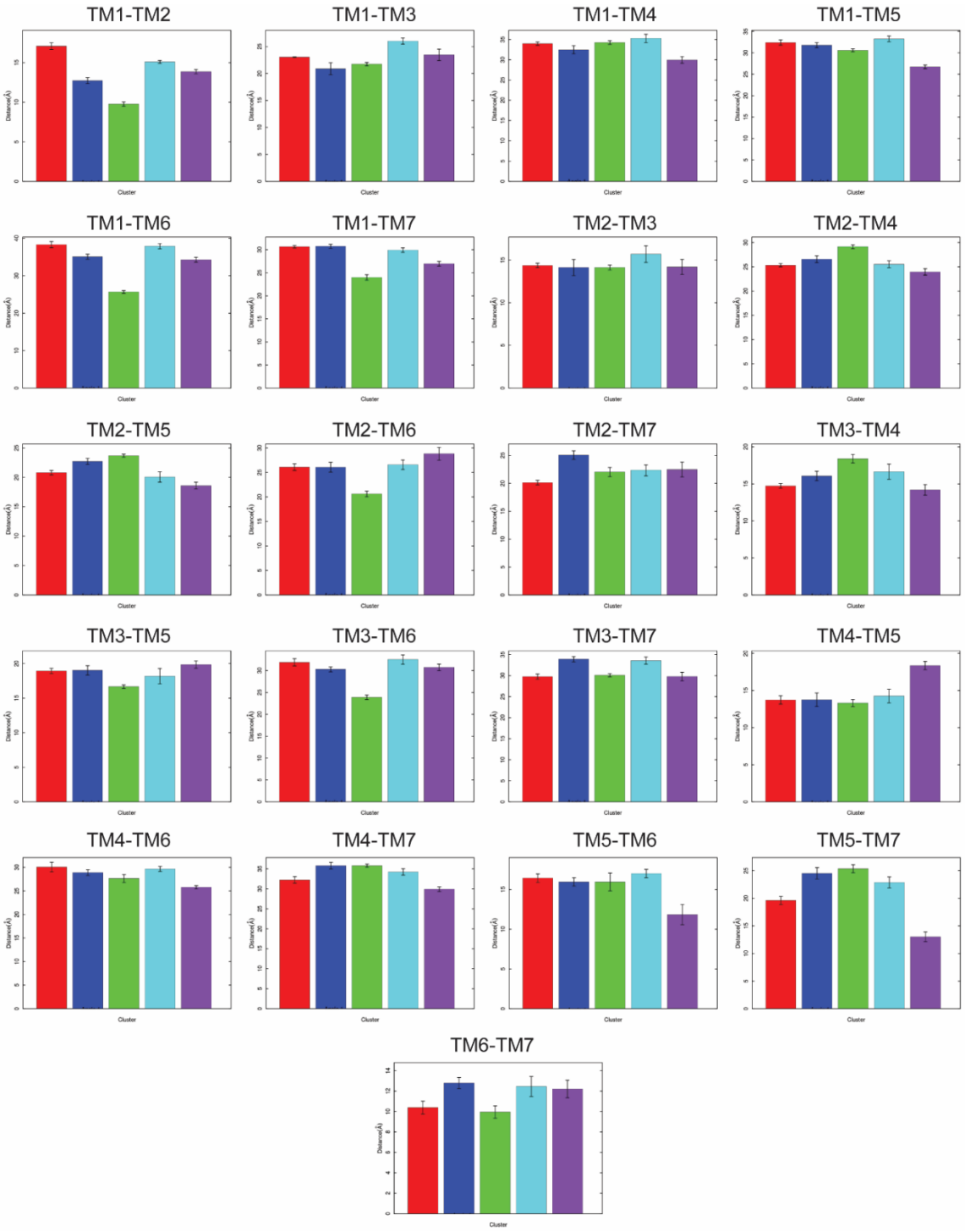

Figure A2.5. Extracellular TM helix Distances. Red – Cluster 1, Blue – Cluster 2, Green – Cluster 3, Cyan – Cluster 4, and Purpled – Cluster 5.

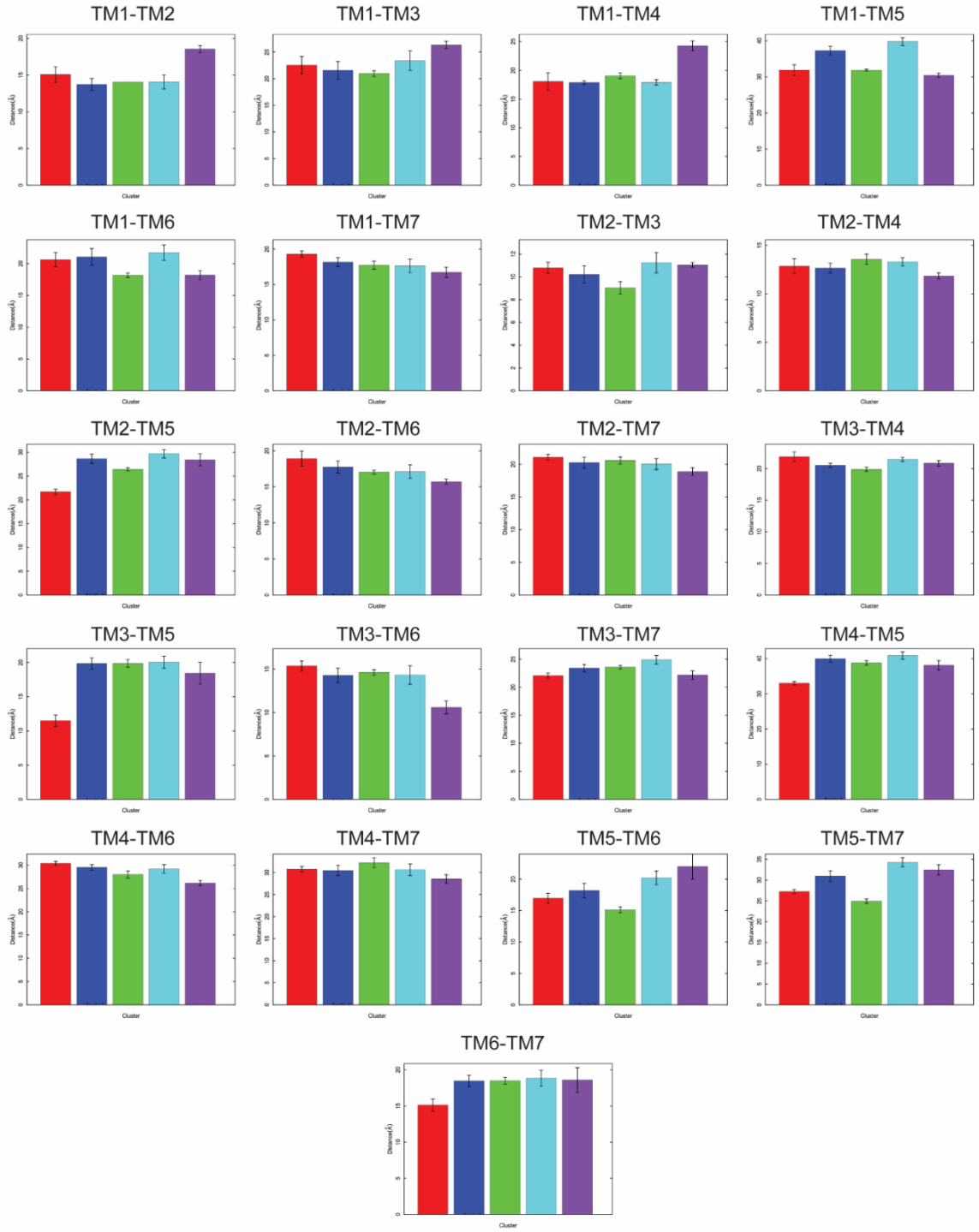

Figure A2.6. Extracellular TM helix Distances. Red – Cluster 1, Blue – Cluster 2, Green – Cluster 3, Cyan – Cluster 4, and Purpled – Cluster 5.

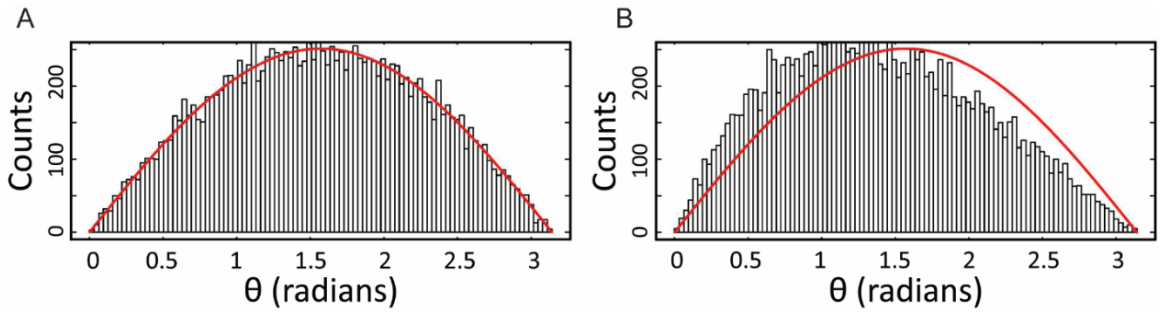

Figure A2.7. Representative distribution of θ. Histogram of the distribution of θ between the vectors of two amino acids whose Cα's (A) do not have significant correlation and (B) do have significant correlation. Red line indicates a random distribution.

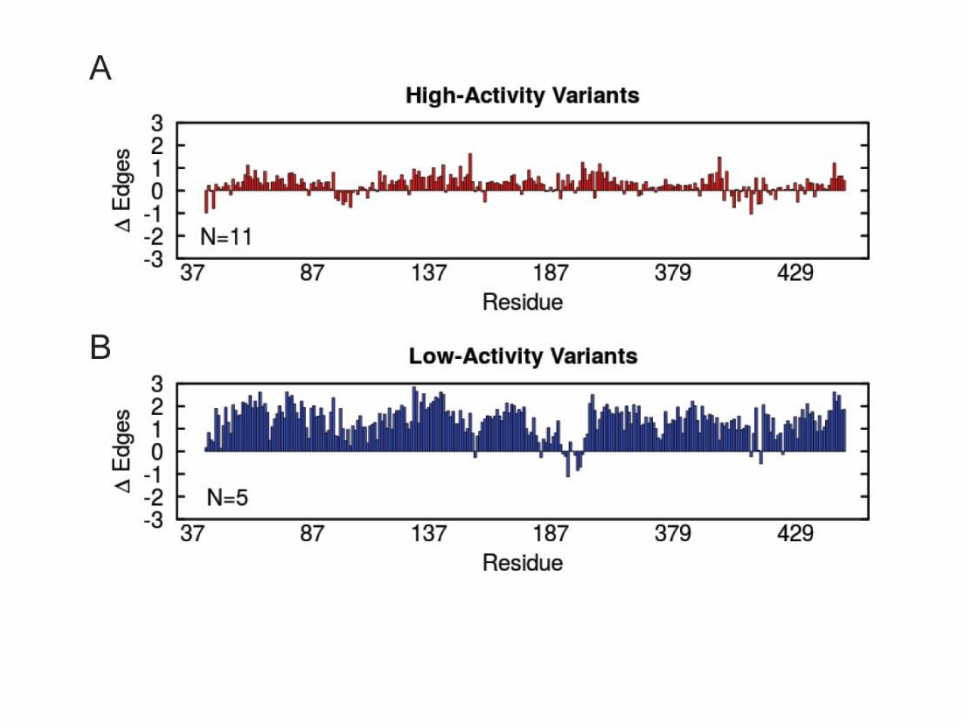

Figure A2.8. Differences in the connectivity of the networks. Average number of connections that each residue makes in the network of (A) high and (B) low activity variants in comparison to normal activity variants.

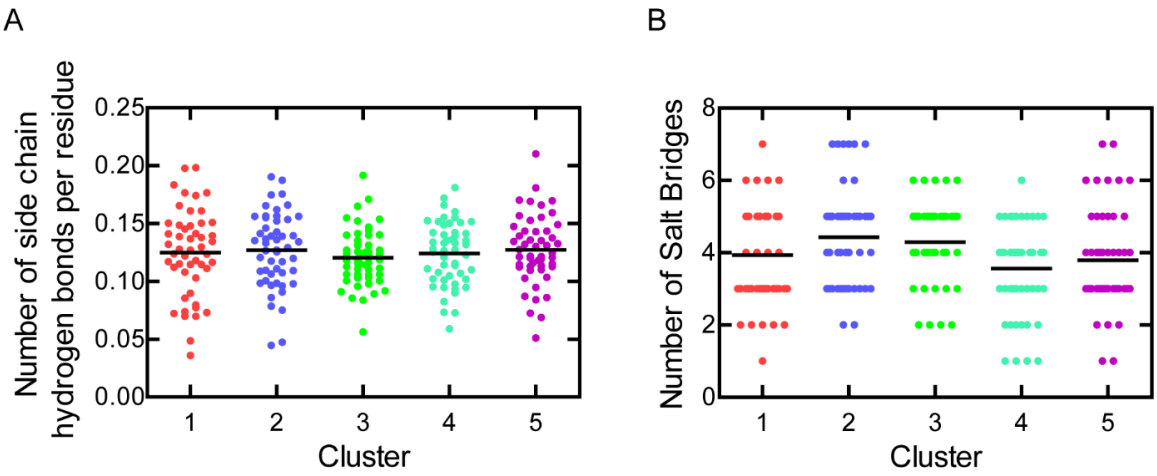

Figure A2.9. Enthalpy contributions to the clusters of D2R. (A) Number of hydrogen bonds per residue for each cluster (B) Number of salt bridges in D2R for each cluster.

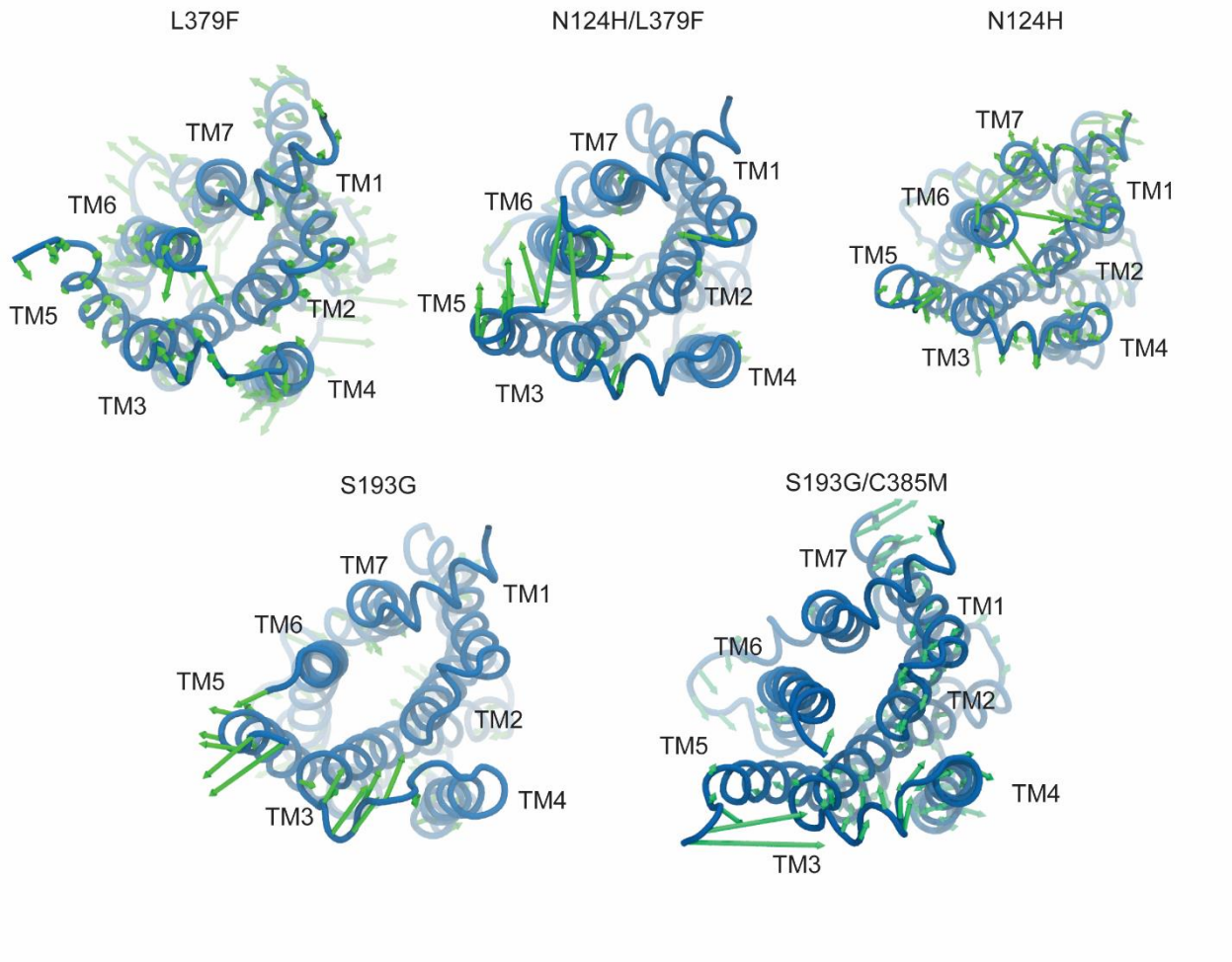

Figure A2.10. PC1 of low-activity D2R variants. Principal components are drawn in green if they are larger than 1Å movement.

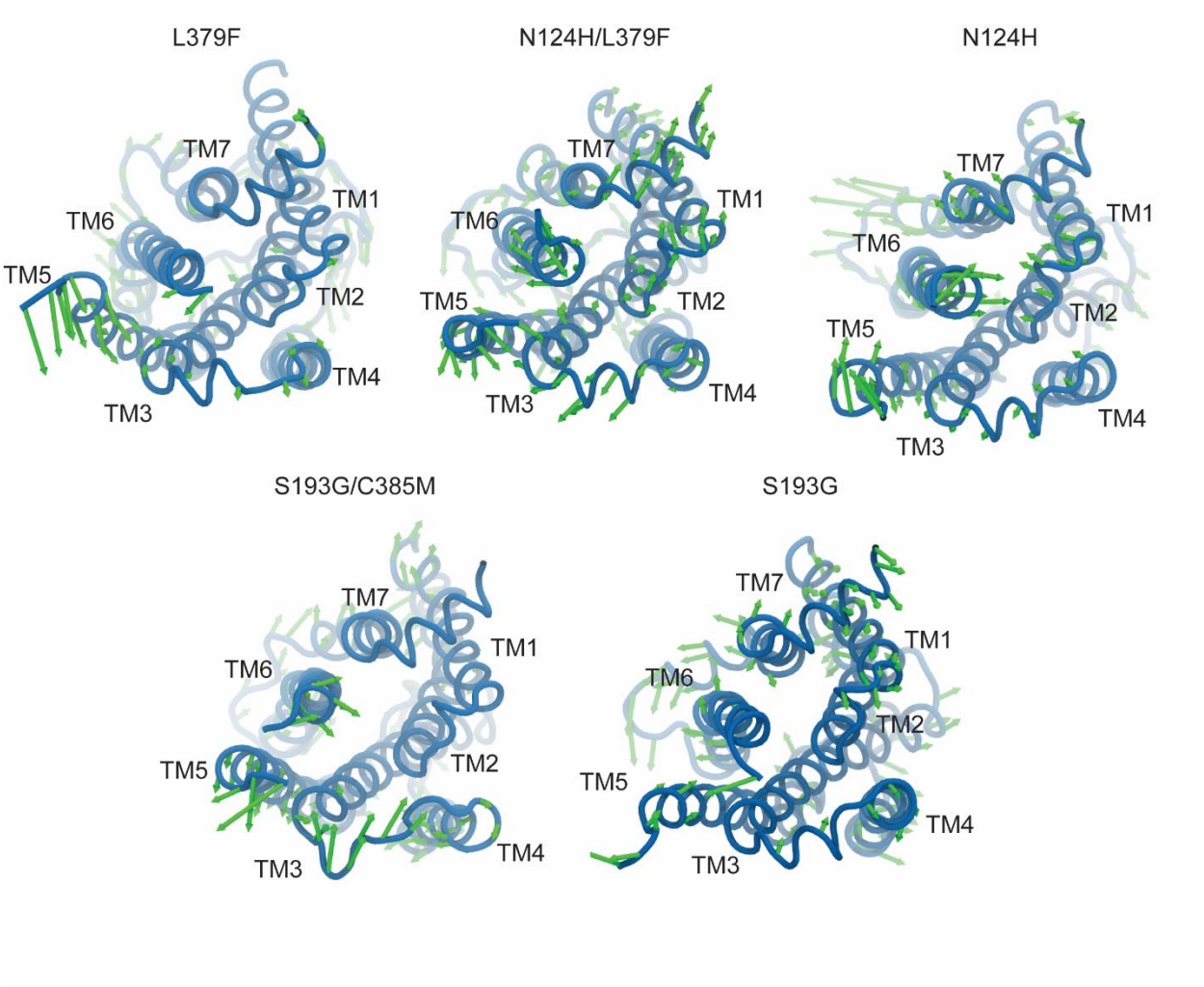

Figure A2.11. PC2 of low-activity D2R variants. Principal components are drawn in green if they are larger than 1Å movement.

Appendix 3

Supplemental Material for: Near-Cognate aminoacyl-tRNA Accommodation Proceeds through an Alternative Pathway

Supplemental Methods

Structure-based potential used in molecular simulations:

$$V = \sum_{bonds} K_r(r - r_0)^2 + \sum_{angles} K_\theta(\theta - \theta_0)^2 + \sum_{\substack{planar\ improper \\ dihedrals}} K_\chi(\chi - \chi_0)^2 + \sum_{\substack{backbone \\ dihedrals}} K_{\phi,BB} F_D(\phi) + \sum_{\substack{sidechain \\ dihedrals}} K_{\phi,SC} F_D(\phi) + \sum_{non-contacts} \varepsilon_{NC} \left(\frac{\sigma_r}{r}\right)^{12} + \sum_{non-contacts} \varepsilon_{NC} \left(\frac{\sigma_r}{r}\right)^{12} \quad \text{(eq A3.1)}$$

Table A3.1. Average number of time steps required for accommodation of the CCA end of A-site aa-tRNA and average distance between the A-site and P-site 3'-CCA ends (R_3).

	Number of time steps until accommodation ($x10^6$)		R_3 distance, post- accommodation(Å)	
	Cognate	Near-cognate	Cognate	Near-cognate
No Antibiotic	4.7 ± 2.1	4.6 ± 2.5	6.3 ± 0.3	9.6 ± 0.4
Gentamicin	2.5 ± 1.1	2.2 ± 1.0	6.9 ± 0.3	9.6 ± 0.4
Neomycin	2.5 ± 1.1	3.5 ± 2.3	6.9 ± 0.3	9.6 ± 0.3
Evernimicin	3.4 ± 1.2	2.5 ± 1.9	6.9 ± 0.3	9.6 ± 0.4
Hygromycin A	5.6 ± 3.1	2.7 ± 1.1	7.1 ± 0.3	9.8 ± 0.4

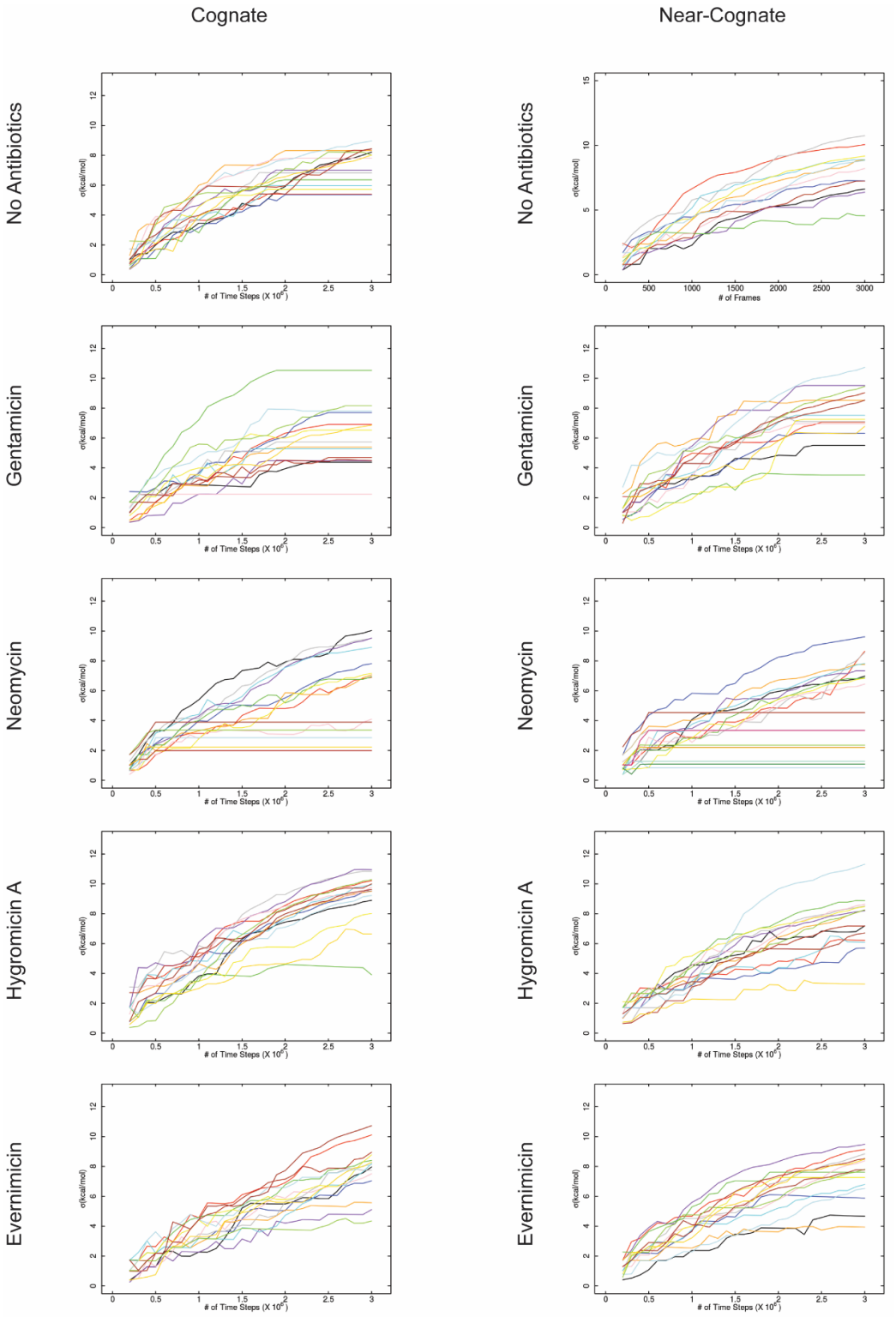

Figure A3.1. Convergence of aa-tRNA accommodation simulations. Convergence of structure-based simulations was determined by the time dependent deviations of the system $\sigma(t)$. Convergence was considered when the $\sigma(t)$ value reached a plateau value as described in Vaiana et al. (2005).

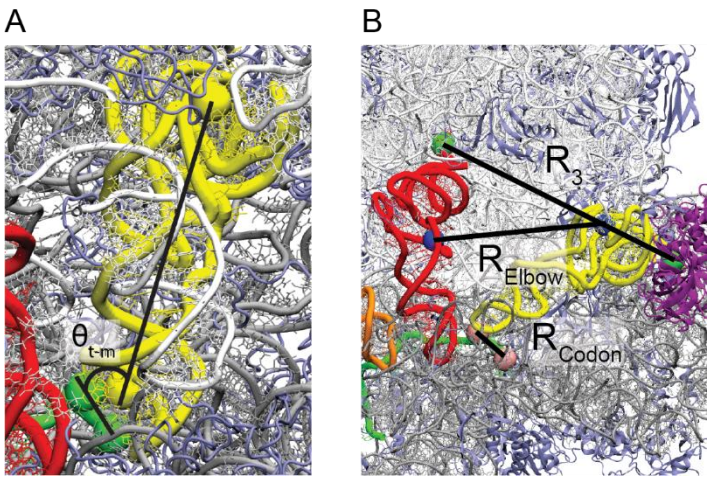

Figure A3.2. Description of the angles and distances used in calculations. (A) Measurement of $\theta_{t\text{-}m}$ angle between the codon vector of the mRNA (between the center of mass of residues 6 and 8) and between the vector v_t between the center of mass of the anticodon (residues 34 to 36) to the center of mass of U60. (B) Measurements for R_{Codon} (Distance between N1 of G in the wobble position on the mRNA and N3 of U34 in the tRNA), R_{Elbow} (Distance between O3' of U8 of the P-site tRNA and U60 of the A-site tRNA), R_3 (Distance between the center of mass of the A76 of the A-site and P-site tRNA).

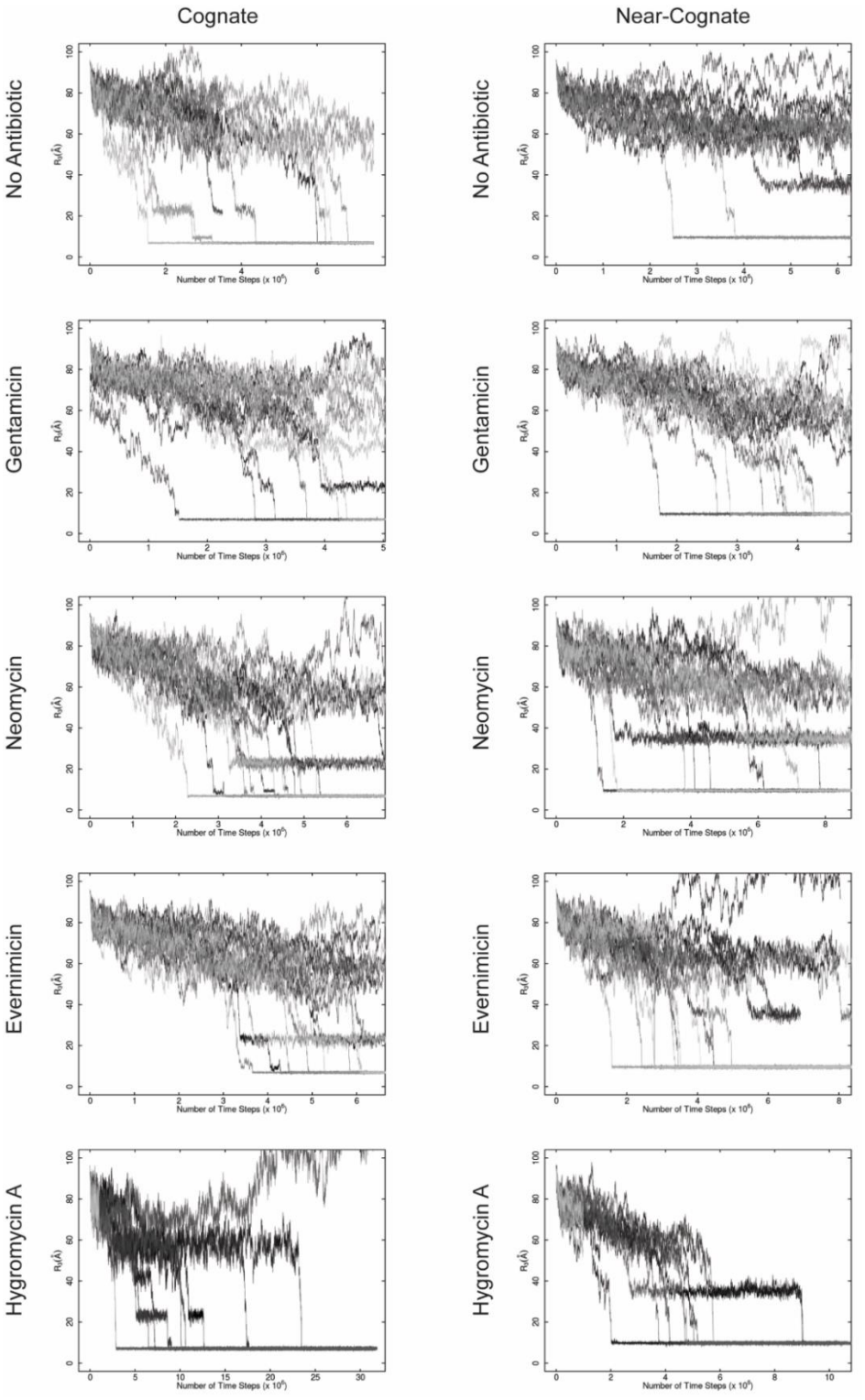

Figure A3.3. Time depdendence of R_3 during cognate and near-cognate accommodation in the presence and absence of antibiotics. Each of the model systems used for simulation (presence or absence of antibioitic) were simulated 20x, the different traces in gray scale represent a unique simulation.

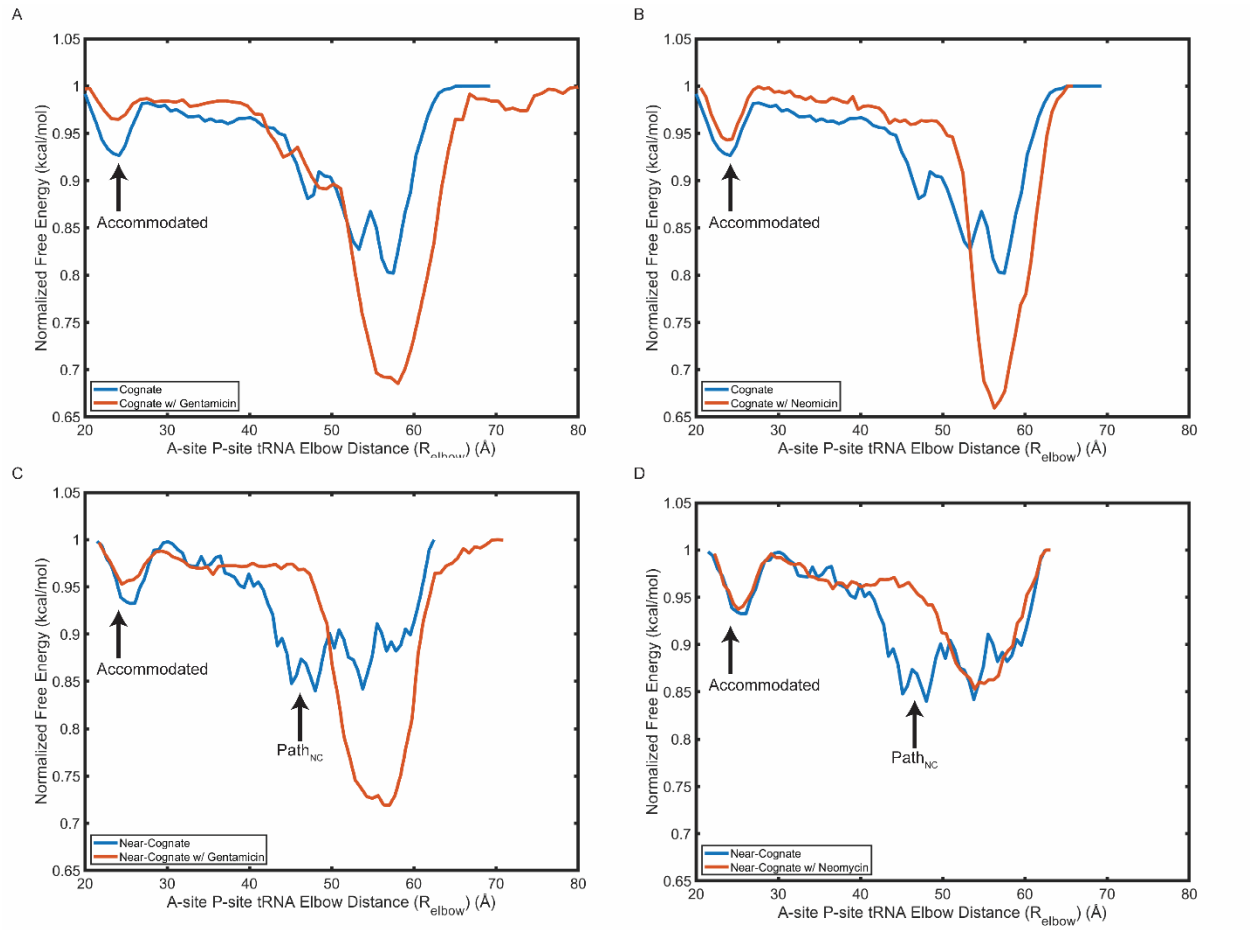

Figure A3.4. 1D free energy landscape of cognate and near-cognate aa-tRNA accommodation in the presence of gentamicin or neomycin. Cognate aa-tRNA accommodation in the presence and absence of (A) gentamicin or (B) neomycin. Near-cognate aa-tRNA accommodation in the presence and absence of (C) gentamicin or (D) neomycin. Antibiotics decrease the energy of the not accommodated state but have minimal effects on the accommodated state (~25Å). The presence of gentamicin or neomycin removes the energy minima at 45-50Å representing $Path_{NC}$.

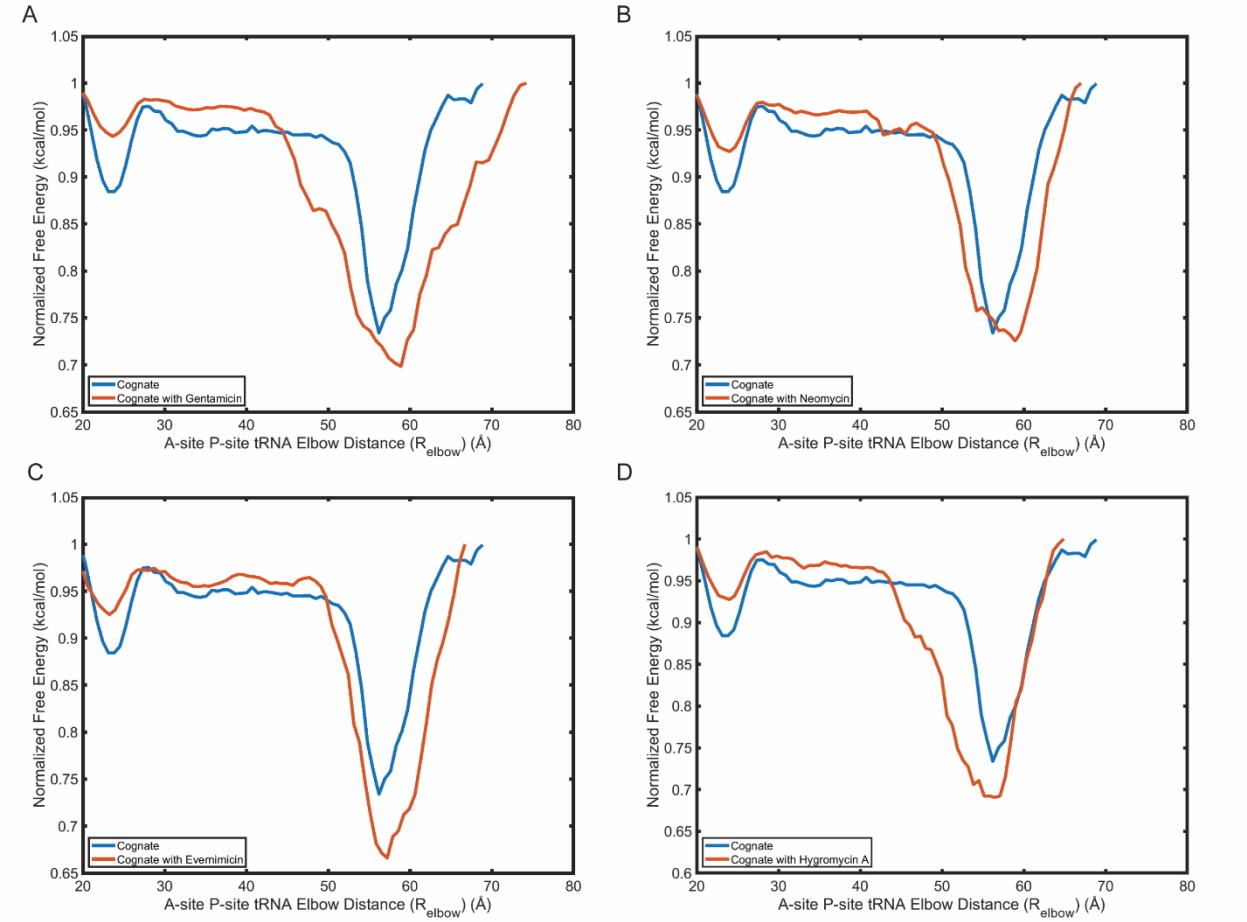

Figure A3.5. 1D free energy landscape of cognate aa-tRNA accommodation in the presence and absence of antibiotics. Cognate aa-tRNA accommodation in the presence and absence of (A) gentamicin, (B) neomycin, (C) evernimicin, or (D) Hygromycin A. Antibiotics decrease the energy of the A/A state (~25Å) and they increase the widths of the energy minima before the tRNA elbow begins to accommodate (~50-65Å).

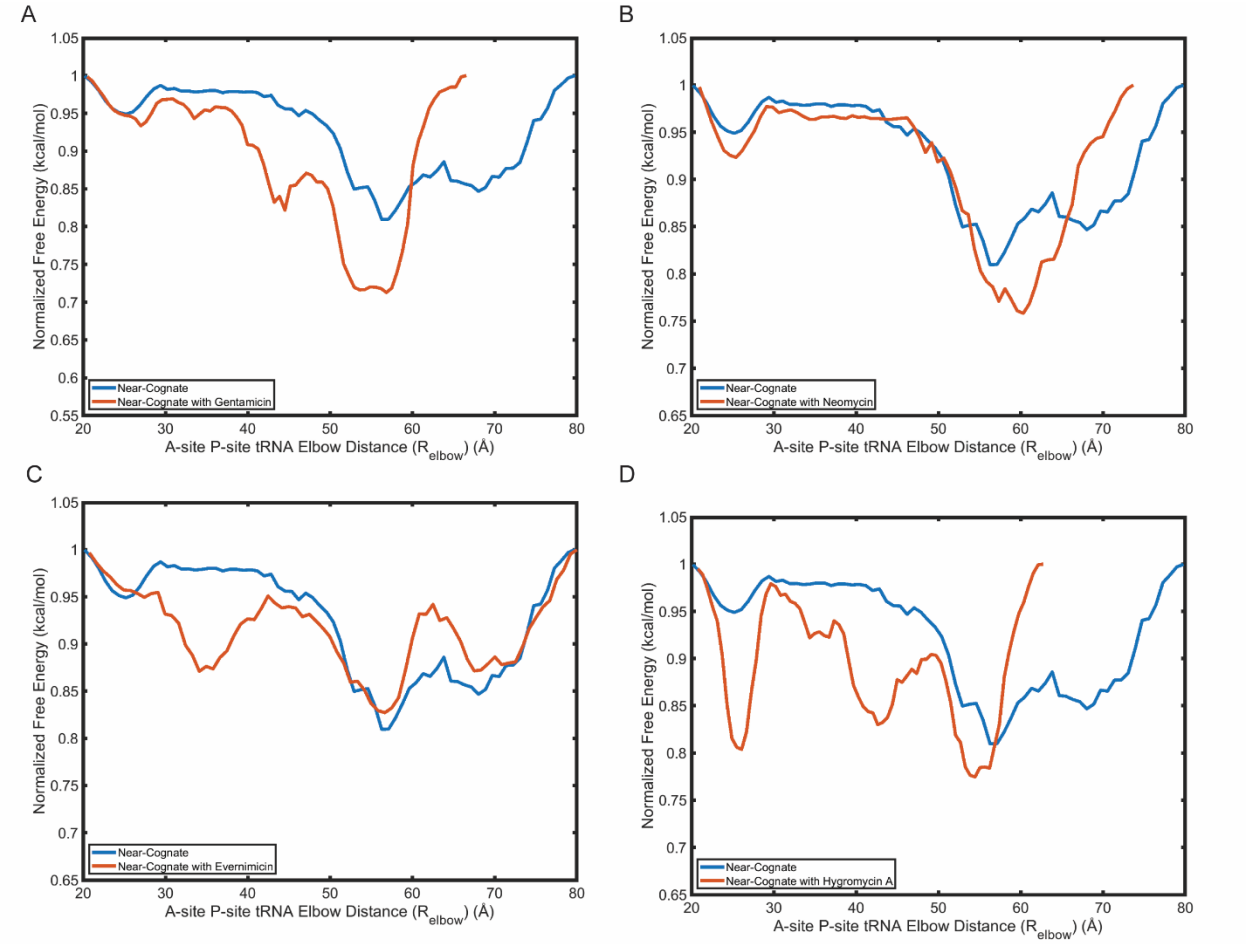

Figure A3.6. 1D free energy landscape of near-cognate aa-tRNA accommodation in the presence and absence of antibiotics. Near-cognate aa-tRNA accommodation in the presence and absence of (A) gentamicin, (B) neomycin, (C) evernimicin, or (D) hygromycin A. (A) Gentamicin decrease the free energy at an R_{elbow} of ~40-60Å indicating it decreases the barrier for accommodation. (B) Neomycin has minimal effects on the accommodation pathway but decreases the energy of the A/A state (~25 Å). (C) Evernimicin decreases free energy at a R_{elbow} of ~35 Å indicating the stalled tRNA in the tRNA channel. (D) Hygromycin A induces three energy minima at ~25 Å (A/A state), ~42 Å (tRNA channel), and ~55 Å (A/T state).

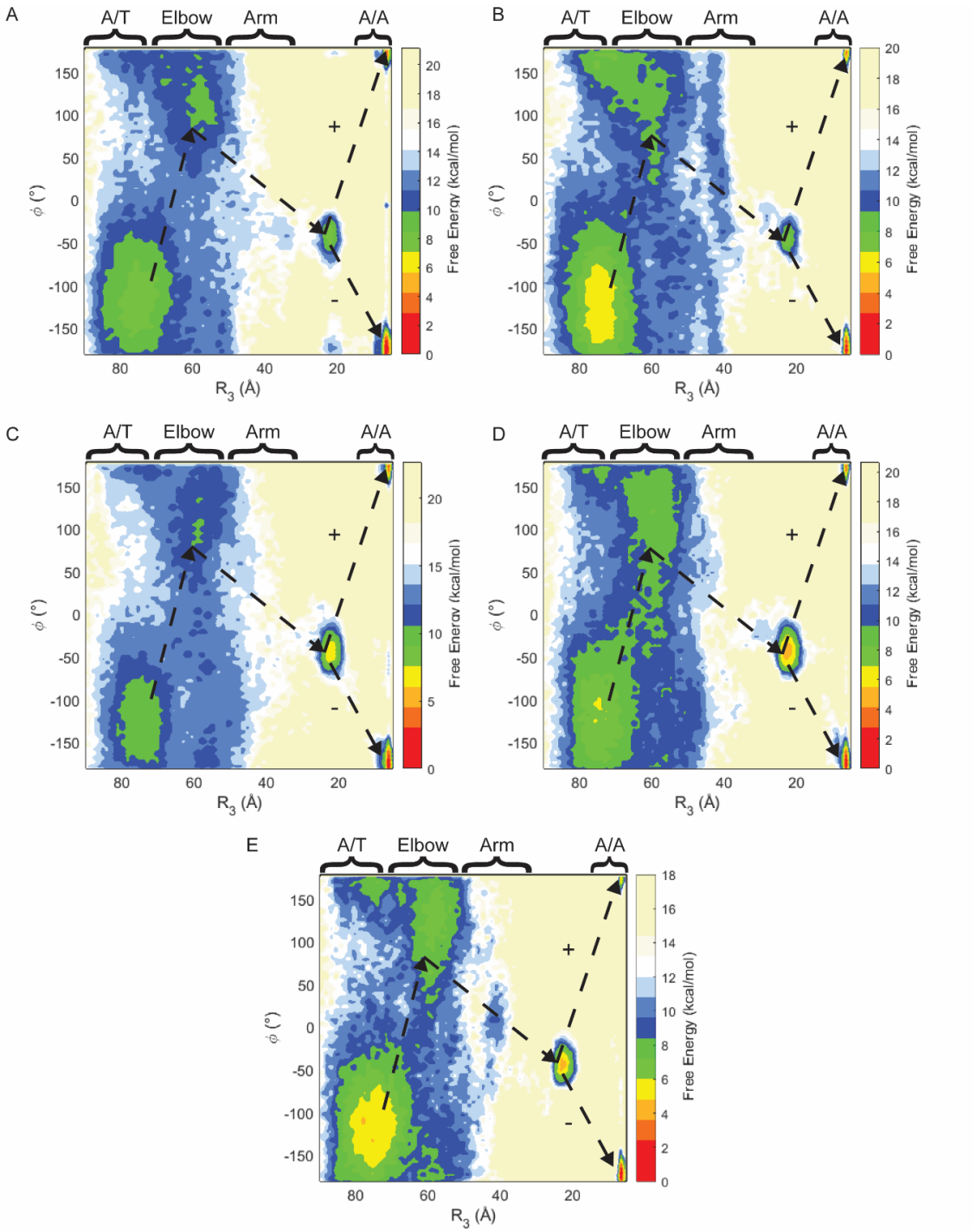

Figure A3.7. The free energy landscapes of cognate CCA end accommodation. Accommodation of the CCA end of the cognate aa-tRNA as determined by the two reaction coordinates R3 and φ for (A) no antibiotic and in the presence of (B) gentamicin, (C) neomycin, (D) evernimicin, and (E) hygromycin A. φ the angle between the O3' atoms of nucleotides 69, 71, and 73 and the O atom of the amino acid from Sanbonmatsu *et al*. 2005 and + and – paths from Whitford *et al.* (2010) (Sanbonmatsu, Joseph, & Tung, 2005; Whitford et al., 2010).

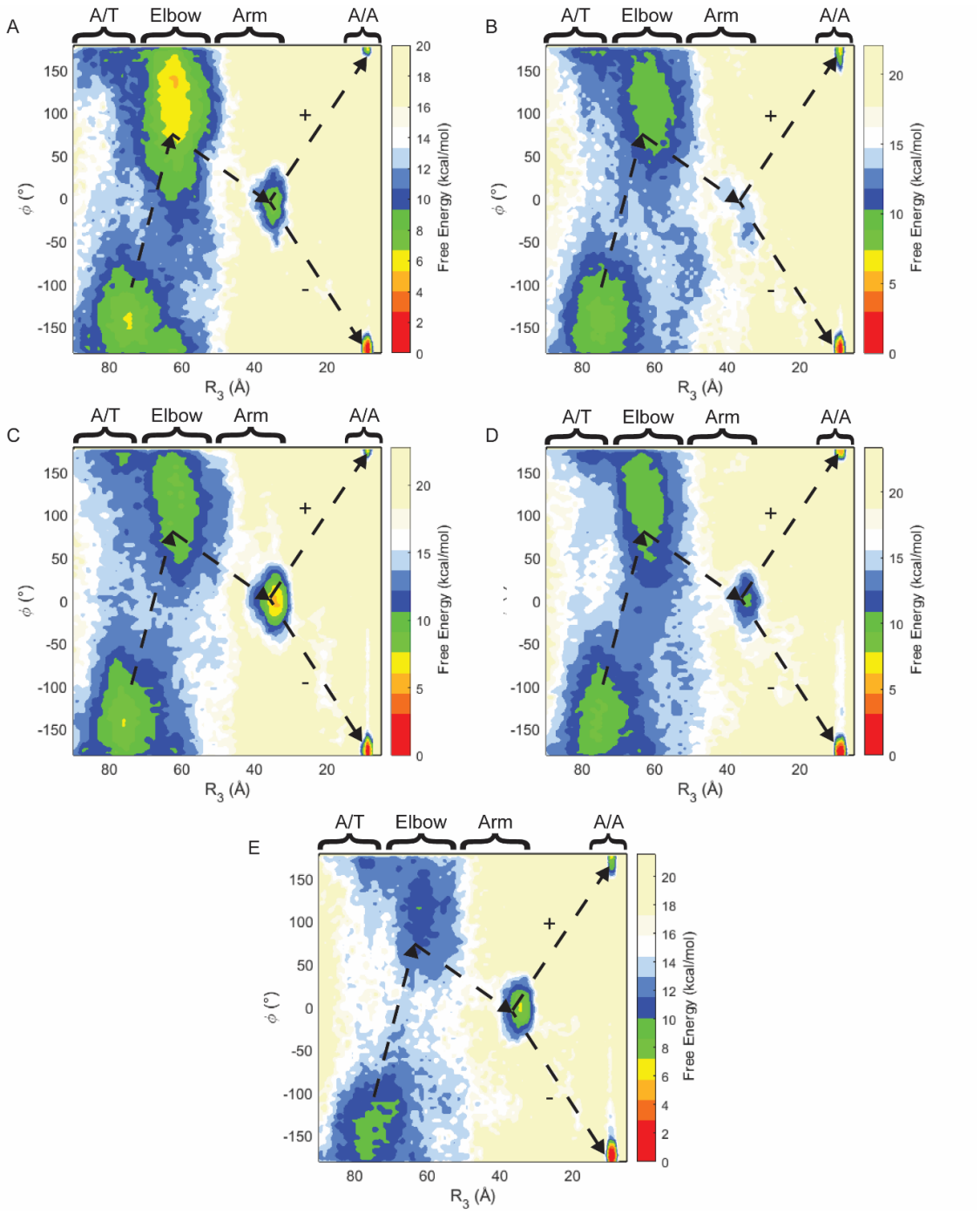

Figure A3.8. The free energy landscapes of near-cognate CCA end accommodation. Accommodation of the CCA end of the near-cognate aa-tRNA as determined by the two reaction coordinates R_3 and φ for (A) no antibiotic and in the presence of (B) gentamicin, (C) neomycin, (D) evernimicin, and (E) hygromycin A. φ the angle between the O3' atoms of nucleotides 69, 71, and 73 and the O atom of the amino acid from Sanbonmatsu *et al.* (2005) and + and – paths from Whitford *et al.* (2010) (Sanbonmatsu et al., 2005; Whitford et al., 2010).